PROMOTING THE APPLICATION OF ANAEROBIC DIGESTION TECHNOLOGY: MICROBIAL ELECTROLYSIS CELL (MEC) INTEGRATION AND STRUVITE PRECIPITATION

A THESIS SUBMITTED TO
THE GRADUATE SCHOOL OF NATURAL AND APPLIED SCIENCES
OF
MIDDLE EAST TECHNICAL UNIVERSITY

BY

FERİDE ECE KUTLAR

IN PARTIAL FULFILLMENT OF THE REQUIREMENTS
FOR
THE DEGREE OF MASTER OF SCIENCE
IN
ENVIRONMENTAL ENGINEERING

JUNE 2023

Approval of the thesis:

PROMOTING THE APPLICATION OF ANAEROBIC DIGESTION TECHNOLOGY: MICROBIAL ELECTROLYSIS CELL (MEC) INTEGRATION AND STRUVITE PRECIPITATION

submitted by **FERİDE ECE KUTLAR** in partial fulfillment of the requirements for the degree of **Master of Science** i**n Environmental Engineering, Middle East Technical University** by,

Prof. Dr. Halil Kalıpçılar
Dean, Graduate School of **Natural and Applied Sciences** _____

Prof. Dr. Bülent İçgen
Head of the Department, **Environmental Engineering** _____

Assist. Prof. Dr. Yasemin Dilşad Yılmazel Tokel
Supervisor, **Environmental Engineering, METU** _____

Examining Committee Members:

Prof. Dr. Ülkü Yetiş
Environmental Engineering, METU _____

Assist. Prof. Dr. Yasemin Dilşad Yılmazel Tokel
Environmental Engineering, METU _____

Prof. Dr. Ayşegül Aksoy
Environmental Engineering, METU _____

Prof. Dr. Tuba Hande Bayramoğlu
Environmental Engineering, METU _____

Assoc. Prof. Dr. Ulaş Tezel
Institute of Environmental Sciences, Boğaziçi University _____

Date: 16.06.2023

I hereby declare that all information in this document has been obtained and presented in accordance with academic rules and ethical conduct. I also declare that, as required by these rules and conduct, I have fully cited and referenced all material and results that are not original to this work.

Name Last name: Feride Ece Kutlar

Signature:

ABSTRACT

PROMOTING THE APPLICATION OF ANAEROBIC DIGESTION TECHNOLOGY: MICROBIAL ELECTROLYSIS CELL (MEC) INTEGRATION AND STRUVITE PRECIPITATION

Kutlar, Feride Ece
Master of Science, Environmental Engineering
Supervisor: Assist. Prof. Dr. Yasemin Dilşad Yılmazel Tokel

June 2023, 203 pages

Two novel technologies were studied to promote the application of anaerobic digestion (AD) in this thesis. AD was reconfigured with the microbial electrolysis cell (MEC). This thesis compared two methods for AD-MEC integrated system start-up: via the use of bioelectrodes (pre-biofilm formed in a controlled environment) vs. bare electrodes (without biofilm). Among all reactors, graphite-stainless steel bioelectrode AD-MECs fed with cattle manure at -0.95 V (vs. Ag/AgCl) cathode potential produced the highest CH_4 yield per gram volatile solids (VS), corresponding to 105% increase compared to conventional AD. Graphite cathode AD-MECs fed with cattle manure generated similar CH_4 productions in bioelectrode and bare electrode reactors resulting in 8-10% increase at -0.9 V (vs. Ag/AgCl) cathode potential and 45-51% increase at -1 V (vs. Ag/AgCl) cathode potential. When reactors were fed with wastewater biosolids, Bioelectrode, and pre-biofilm formed granular activated carbon (GAC) combination increased CH_4 production by 16% in comparison to the control. Overall, the methane production kinetics were enhanced with the implementation of AD-MECs. The results showed that the reactor

enhancements mainly depended on the cathode material and cathode potential. Archaeal community analysis confirmed the dominance of hydrogenotrophic methanogens on the cathode of graphite – graphite AD-MECs fed with cattle manure. The comparison of AD-MEC reactor performances indicated that pre-cultivation of biofilm on the electrodes in a controlled environment is not necessary and the use of bioelectrodes does not provide a significant advantage in the performance over bare electrodes.

As a post-treatment of AD effluents, struvite precipitation with sustainable additives was investigated in this thesis. Bone meal and waste magnesite powder were used as a replacement for pure P and Mg additives for struvite precipitation from cattle manure digestate. The important parameters and recovery efficiencies were determined via the Box-Behnken model. Under optimal conditions (pH = 9.0, Mg:N = 2.2, and P:N = 1.8), 97.8 ± 0.1% NH_4-N, 96.6 ± 0.31% PO_4-P, and 84.4 ± 0.9% Mg^{2+} were recovered. When the precipitated product was examined, X-ray diffraction showed only struvite crystals. The product purity was around 49%, which is relatively high when the use of wastes is considered. Heavy metals in the product were below regulatory limits for fertilizer application.

In summary, both technologies promoted the application of AD by providing selective benefits. The proposed processes have the potential to lower the impacts of climate change, reduce nutrient depletion impacts, and help achieve sustainable development goals. Next-generation biogas technology research should focus on commercializing these processes.

Keywords: Microbial Electrolysis Cells, Bioelectrodes, AD-MEC Integration, Industrial Symbiosis, Struvite Precipitation

ÖZ

ANAEROBİK ÇÜRÜTME TEKNOLOJİSİNİN UYGULANMASININ DESTEKLENMESİ: MİKROBİYAL ELEKTROLİZ HÜCRESİ (MEH) ENTEGRASYONU VE STRÜVİT ÇÖKELTİMİ

Kutlar, Feride Ece
Yüksek Lisans, Çevre Mühendisliği
Tez Yöneticisi: Dr. Öğr. Üyesi Yasemin Dilşad Yılmazel Tokel

Haziran 2023, 203 sayfa

Bu tezde anaerobik çürütme (AÇ) uygulamasını teşvik etmek için iki yeni teknoloji üzerinde çalışılmıştır. AÇ, mikrobiyal elektroliz hücresi (MEH) ile yeniden yapılandırılmıştır. Bu tez, AÇ-MEH entegre sisteminin başlatılması için iki yöntemi karşılaştırmıştır: biyoelektrotların (kontrollü bir ortamda önceden biyofilm oluşturulmuş) kullanımı ile bakir elektrotlar (biyofilmsiz). Tüm reaktörler arasında, -0,95 V (Ag/AgCl'ye kıyasla) katot potansiyelinde sığır gübresiyle beslenen grafit-paslanmaz çelik biyoelektrotlu AÇ-MEH'ler, gram uçucu katı madde (UKM) başına en yüksek CH_4 verimini üreterek geleneksel AÇ'ye kıyasla %105 artış sağlamıştır. Sığır gübresi ile beslenen grafit katotlu AÇ-MEH'ler biyoelektrot ve bakir elektrot reaktörlerinde benzer CH_4 üretimleri üreterek -0,9 V (Ag/AgCl'ye kıyasla) katot potansiyelinde %8-10 ve -1 V (Ag/AgCl'ye kıyasla) katot potansiyelinde %45-51 artış sağlamıştır. Reaktörler atık su biyokatıları ile beslendiğinde, Biyoelektrot ve ön biyofilm oluşturulmuş granüler aktif karbon (GAK) kombinasyonu CH_4 üretimini kontrole kıyasla %16 artırmıştır. Genel olarak, metan üretim kinetiği AÇ-MEH entegrasyonu ile geliştirilmiştir. Sonuçlar, CH_4 üretimindeki artışın esas olarak katot malzemesine ve katot potansiyeline bağlı olduğunu göstermiştir. Arkeal topluluk analizi, sığır gübresi ile beslenen grafit – grafit AÇ-MEH'lerin katodunda hidrojenotrofik metanojenlerin baskın olduğunu doğrulamıştır. AÇ-MEH reaktör

performanslarının karşılaştırılması, elektrotlar üzerindeki biyofilmin kontrollü bir ortamda önceden yetiştirilmesinin gerekli olmadığını ve biyoelektrot kullanımının bakir elektrotlara göre performansta önemli bir avantaj sağlamadığını göstermiştir.

Bu tezde, AÇ çıkışı için ileri arıtım olarak, sürdürülebilir katkı maddeleri ile strüvit çökeltilmesi araştırılmıştır. Kemik unu ve atık manyezit tozu, sığır gübresi çürütücü çıkış suyundan strüvit çökeltimi için saf P ve Mg katkı maddelerinin yerine kullanılmıştır. Önemli parametreler ve geri kazanım verimleri Box-Behnken modeli ile belirlenmiştir. Optimum koşullar altında (pH = 9.0, Mg:N = 2.2 ve P:N = 1.8), %97.8 ± 0.1 NH_4-N, %96.6 ± 0.31 PO_4-P ve %84.4 ± 0.9 Mg^{2+} geri kazanılmıştır. Çökeltilen ürün incelendiğinde, X-ışını kırınımında sadece strüvit kristalleri gözlemlenmiştir. Ürün saflığı %49 civarındadır ve atıkların kullanımı düşünüldüğünde bu oran oldukça yüksektir. Üründeki ağır metallerin ise gübre uygulaması için düzenleyici limitlerin altında olduğu görülmüştür.

Özetle, her iki teknoloji de seçici faydalar sağlayarak AÇ sisteminin uygulamasını teşvik etmiştir. Önerilen teknolojiler iklim değişikliğinin ve besin tükenmesi etkilerini azaltma, buna ek olarak sürdürülebilir kalkınma hedeflerine ulaşılmasına yardımcı olma potansiyeline sahiptir. Yeni nesil biyogaz araştırmaları bu teknolojilerin ticarileştirilmesine odaklanmalıdır.

Anahtar Kelimeler: Mikrobiyal Elektroliz Hücreleri, Biyoelektrotlar, AÇ-MEH Entegrasyonu, Endüstriyel Simbiyoz, Strüvit Çökeltme

To my beloved family

ACKNOWLEDGMENTS

The author would like to express her deep gratitude to her advisor, Assistant Professor Dr. Yasemin Dilşad Yılmazel Tokel, for all of her guidance, support, and wisdom throughout her studies.

The author would also like to Prof. Dr. Tuba Hande Ergüder Bayramoğlu for her suggestions and comments throughout the AD-MEC project.

The author would like to express her appreciation to Prof. Dr. Tuba Hande Ergüder Bayramoğlu, Prof. Dr. F. Dilek Sanin, and Prof. Dr. Bülent İçgen for allowing her to use the facilities of their laboratories.

This work is funded by the UK Royal Academy of Engineering Newton Fund Transforming Systems Through Partnerships Program (Project ID: TSP1283) and the Scientific and Technological Research Council of Turkey (TUBITAK) Priority Areas R&D Projects Support Program (Project ID: 218M854).

The author would like to give a special thanks to Amin Ghaderikia. It was thanks to him that I made progress in this adventure that started with a change of subject. His place and help have always been special. Thank you for being by my side.

The author would like to say a special thank you to İrem Şimşek. Her friendship and love gave me strength on this difficult path. I thank her for being with me from the very beginning. Mert Şanlı, Mehmet Yağcı, Berivan Tunca, Aykut Kaş, Yasin Odabaş, Berkan Öden, Elif Taştan, all of our research group BIOERG, and Aslı Onursal have been tremendously helpful through their suggestions, friendship, and encouragement.

I want to exclusively thank my parents and my sister for their everlasting love, encouragement, and for being extremely supportive throughout this journey.

TABLE OF CONTENTS

ABSTRACT v

ÖZ vii

ACKNOWLEDGMENTS x

TABLE OF CONTENTS xi

LIST OF TABLES xv

LIST OF FIGURES xvii

LIST OF ABBREVIATIONS xxi

CHAPTERS

1 INTRODUCTION 1

1.1 Aim of the Study 4

1.2 Scope of the Study 8

2 LITERATURE REVIEW 11

2.1 Anaerobic Digestion 11

2.1.1 Interspecies Electron Transfer 13

2.1.2 Limitations of AD 15

2.2 Bioelectrochemical Systems 17

2.2.1 Microbial Electrolysis Cell 18

2.2.2 Electromethanogenesis 20

2.2.3 Electron Transfer Mechanisms 21

2.3 Anaerobic Digestion Microbial Electrolysis Cell (AD-MEC) Integration 22

2.3.1 Substrate 31

2.3.2 Electrodes 31

2.3.3 Voltage application 33

2.3.4 Media 34
2.3.5 Microbial Community 34
2.3.6 Conductive Material Amendment 37
2.4 Nutrient Recovery 38
2.4.1 Ammonia Stripping 39
2.4.2 Ion Exchange and Adsorption 40
2.4.3 Membrane Filtration 40
2.4.4 Chemical Precipitation 41
2.5 Important Parameters for Struvite Precipitation 43
2.5.1 pH 43
2.5.2 Molar Ratio 44
2.5.3 Temperature 45
2.5.4 Presence of Competitive Ions 45
2.5.5 Reactor Configurations 47
2.5.6 Magnesium Sources 50
2.5.7 Phosphate Sources 53
3 MATERIALS AND METHODS 55
3.1 AD-MEC Integration 55
3.1.1 Inoculum, Substrate, and Media 55
3.1.2 Reactor Construction 59
3.1.3 Experimental Design and Reactor Operation 63
3.1.4 Electrochemical Data Processing 73
3.1.5 Calculations 74
3.1.6 Analytical Methods 76

3.1.7 Microbial Community Analysis 78
3.2 Struvite Precipitation 79
3.2.1 Preparation of the Biogas Plant Sample 79
3.2.2 Preparation of WMP and BM Solution 80
3.2.3 Experimental Design and Optimization 82
3.2.4 Struvite Precipitation Procedure 84
3.2.5 Analytical Methods 85
4 RESULTS AND DISCUSSION 89
4.1 AD-MEC 89
4.1.1 Set 1: Cattle Manure Fed AD-MEC Using Graphite – Graphite Electrodes 89
4.1.2 Set 2: Cattle Manure Fed AD-MEC Using Graphite – Stainless Steel Electrodes 107
4.1.3 Set 3: WBS Fed AD-MEC Using Graphite – Graphite Electrodes 120
4.1.4 Comparison of AD-MEC Sets 130
4.2 Struvite Precipitation 137
4.2.1 RSM for the Optimization of Struvite Crystallization Process 137
4.2.2 Response Surface Analysis 142
4.2.3 Verification of the Optimum Conditions 144
4.2.4 Product Purity and Characterization 145
4.2.5 Conclusion on Struvite Precipitation 148
5 CONCLUSIONS 151
6 RECOMMENDATIONS 153
REFERENCES 155

APPENDICES

A. Set 2 – Inoculum preparation and specific methanogenic activity of the seed 187

B. Example calculations 188

C. AD-MEC operation with 100 mM PBS media 189

D. Current density of the replicate AD-MEC reactors in Set 1 190

E. The modified Gompertz models of Set 1 191

F. H_2 partial pressure calculation 193

G. The current density of the replicates of AD-MEC reactors in Set 2 195

H. The modified Gompertz models for Set 2 198

I. The current density of the replicates of AD-MEC reactors in Set 3 199

J. The modified Gompertz models for Set 3 200

K. Estimations of regression coefficients and results of statistical tests 201

L. Comparison of the product heavy metal content with regulations 203

LIST OF TABLES

TABLES

Table 2.1. Summary of AD-MEC integration studies 26
Table 2.2 Microbial communities in AD-MEC studies 36
Table 2.3 Summary of conductive material amendment in CH_4 producing MECs and AD-MECs 38
Table 2.4. Possible precipitates 46
Table 3.1. Characterization of cattle manure and inoculum (AD seed) used in Set 1 56
Table 3.2. The composition of mineral and vitamin stock solutions 57
Table 3.3 The comparison of different media used in Set 1 57
Table 3.4 Characterization of cattle manure and inoculum (Lab-scale reactor seed) used in Set 2 58
Table 3.5 The characterization of WBS and inoculum (AD seed) used in Set 3 59
Table 3.6. Properties of the graphite 61
Table 3.7. Characterization of P-enriched digestate, raw WMP, and BM 81
Table 3.8 Box-Behnken experimental design 83
Table 4.1 Modified Gompertz kinetics of Set 1 98
Table 4.2 Kinetic parameters from the modified Gompertz model and VS removal for Set 2 115
Table 4.3 Kinetic parameters and VS removal of the Set 3 reactors at -0.9 V cathode potential 127
Table 4.4 CH_4 yields from all data sets of this study 131
Table 4.5 Theoretical calculations on AD-MEC for Set 1 (Cattle manure Gr-Gr) 134
Table 4.6 Theoretical calculations on AD-MEC for Set 2 (Cattle manure Gr-SS) 135
Table 4.7 Theoretical calculations on AD-MEC for Set 3 (WBS Gr-Gr) 136

Table 4.8 The Box-Behnken design, experimental and predicted results for the NH_4-N recovery, residual PO_4-P concentration, and residual concentration of the NH_4^+, PO_4^{3-} and Mg^{2+} 138
Table 4.9 ANOVA results for the NH_4-N, PO_4-P, and Mg^{2+} recovery 141
Table 4.10 Elemental composition of the product..... 148

LIST OF FIGURES

FIGURES

Figure 1.1. Aim of the study 5
Figure 2.1. Possible waste streams and benefits of the AD 11
Figure 2.2. AD steps 12
Figure 2.3. Electron transfer mechanisms in AD 14
Figure 2.4. Schematic of the MEC 19
Figure 2.5. Schematic of electromethanogenesis (CH_4-producing MECs) 20
Figure 2.6. Electron transfer mechanisms on cathode surface in CH_4 producing MECs. 22
Figure 2.7. Schematic of AD-MEC integrated system (adopted from (Q. Huang et al., 2020) 24
Figure 3.1. Summary of AD-MEC sets conducted in the thesis 55
Figure 3.2. Construction of double chamber MECs 59
Figure 3.3. Construction of single-chamber MECs 60
Figure 3.4. A) Reference electrode, B) salt bridge C) AD-MEC operation with a salt bridge 62
Figure 3.5. Potentiostats used during the operation of the reactors 62
Figure 3.6. Operation of reactors during A) cathode biofilm formation in double chamber MECs, B) anode biofilm formation on the anode in single chamber MECs 64
Figure 3.7. BioGAC formation and determination of BioGAC dosage to be used in Set 3 66
Figure 3.8. Anaerobic glovebox used in the experiments 67
Figure 3.9. Operation of the A) AD-MEC reactors and B) controls 67
Figure 3.10. The reactors operated in each cycle of Set 1 68
Figure 3.11. Schematic representation of the experimental design of Set 1 69
Figure 3.12. The reactors in each cycle of Set 2 70
Figure 3.13. The experimental design of Set 2 71

Figure 3.14. The reactors for AD-MEC operation in Set 3 72
Figure 3.15. The experimental design of Set 3 73
Figure 3.16. An example of a cyclic voltammogram curve 74
Figure 3.17. A) H_2, B) N_2, C) CH_4, and D) CO_2 gas calibration curve and equation 78
Figure 3.18. Acid dissolution procedure 80
Figure 3.19. A) BM, B) WMP, C) Protocol for preparing WMP and BM solutions 82
Figure 3.20. Struvite precipitation procedure 84
Figure 3.21. Mg^{2+} calibration curve 87
Figure 4.1. The cumulative CH_4 production during Set 1 cathode biofilm formation 90
Figure 4.2. CV analysis of cathode during Set 1 biofilm formation 90
Figure 4.3. Current generation during Set 1 anode biofilm formation 91
Figure 4.4. CV analysis of anode during Set 1 biofilm formation 91
Figure 4.5. Current density during AD-MEC operation 92
Figure 4.6. Cumulative A) CH_4 and B) H_2 production during 3 fed-batch cycles of Set 1 (cycle 1: no-PBS at -0.9 V, cycle 2: 5 mM PBS media at -0.9 V and cycle 3: 5 mM PBS media at -1 V) (Error bars represent standard deviations of triplicate reactors. The error bars may be smaller than the symbols) 94
Figure 4.7. Net CH_4 yield of the reactors in Set 1 95
Figure 4.8. CV of A) anode of bioelectrode, B) anode of bare electrode, C) cathode of bioelectrode, and D) cathode of bare electrode AD-MEC reactors at the end of biofilm formation (t=0), Cycle 1, Cycle 2, and Cycle 3 101
Figure 4.9. Set 1 - Relative abundance of archaeal communities at the genus level (The relative abundance of genus less than 3% of total composition was defined as others.) 102
Figure 4.10. Set 1 - Relative abundance of bacterial communities A) at the phylum level, B) at the genus level 105

Figure 4.11. A) CH_4 production, and B) H_2 production during cathode biofilm formation in Set 2 107
Figure 4.12. CV analyses during cathode biofilm formation in Set 2 108
Figure 4.13. A) Current density graph, and B) CV analyses during anode biofilm formation of Set 2 109
Figure 4.14. Cumulative A) CH_4 and B) H_2 production during AD-MEC operation in Set 3 111
Figure 4.15. Net CH_4 yield of the reactors in Set 2 113
Figure 4.16. Average current uptake graph during AD-MEC operation in Set 2 . 114
Figure 4.17. VS removal of the reactors 116
Figure 4.18. CV of the reactors at -0.9 V cathode potential, A) anode of Bare electrode, B) anode of Bioelectrode, C) cathode of Bare electrode, C) cathode of Bioelectrode reactors in Set 2 117
Figure 4.19. CV of the reactors at -0.95 V cathode potential, A) Anode of New_Bare electrode, B) anode of Bare electrode, C) cathode of New_Bare electrode, D) cathode of Bare electrode, E) anode of Bioelectrode, and F) cathode of Bioelectrode reactors in Set 2 119
Figure 4.20. Cumulative CH_4 production of the reactors during Test 1 (GAC) ... 120
Figure 4.21. Cumulative CH_4 production of the reactors during Test 2 (BioGAC) 121
Figure 4.22. Cumulative CH_4 production during cathode biofilm development in Set 3..... 122
Figure 4.23. CV during cathode biofilm development in Set 3 122
Figure 4.24. A) Current generation (Arrows represent new acetate injection.), B) CV during anode biofilm formation in Set 3..... 123
Figure 4.25. Cumulative A) CH_4, and B) H_2 production of reactors in Set 3..... 124
Figure 4.26. Net CH_4 yield of the reactors at -0.9 V cathode potential in Set 3... 126
Figure 4.27. Current uptake of the AD-MEC reactors during 2 cycles 126

Figure 4.28. CV plots for A) anode of Bare el, B) anode of Bare el-BioGAC, C) cathode of Bare el, D) cathode of Bare el-BioGAC, E) anode of Bioel-BioGAC, and F) cathode of Bioel-BioGAC at -0.9 V cathode potential in Set 3 129
Figure 4.29. Scatter diagram of predicted vs. experimental response values for the (A) NH_4-N recovery (B) PO_4-P recovery, and (C) Mg^{2+} recovery (%) 139
Figure 4.30. 3D surface and contour plots for NH_4-N (A)-(C), PO_4-P (D)-(F), and Mg^{2+} (G)-(I) showing the interaction of pH (8.0-9.0), Mg:N (1.5-2.3) and P:N (1.2-2.0) by fixing one factor at a time (pH = 8.5, Mg:N = 1.9, or P:N = 1.6) 143
Figure 4.31. The XRD results of the precipitates obtained from experimental runs compared with the peaks of reference struvite (JCPDS file No.15–0762) (Conditions are given as pH/Mg:N/P:N) 146
Figure 4.32. The XRD spectra and SEM images at 6000x magnification of the product under optimum condition (pH = 9.0, Mg:N = 2.2, P:N = 1.8) 147

LIST OF ABBREVIATIONS

ABBREVIATIONS

Abbreviation	Explanation
AAS	Atomic Absorption Spectroscopy
AC	Activated carbon
AD	Anaerobic digestion
AD-MEC	Anaerobic digestion-microbial electrolysis cell integration
ANOVA	Analysis of variance
BBD	Box-Behnken design
BES	Bioelectrochemical system
BM	Bone meal
COD	Chemical oxygen demand
Conv. AD	Conventional AD
CV	Cyclic voltammetry
DET	Direct electron transfer
DIET	Direct species electron transfer
EAM	Electrochemically active microorganisms
EPS	Extracellular polymeric substances
FBR	Fluidized bed reactor
GAC	Granular activated carbon
GC	Gas chromatography
Gr	Graphite
ICP-MS	Inductively Coupled Plasma – Mass Spectrometer
IET	Interspecies electron transfer
MAP	Magnesium ammonium phosphate
MEC	Microbial electrolysis cell
MF	Microfiltration
MFC	Microbial fuel cell
MR	Mg^{2+} recovery
NF	Nanofiltration
NR	NH_4-N recovery
OC	Open circuit
PBS	Phosphate buffer saline
PEM	Proton exchange membrane
PR	PO_4-P recovery
PS	Primary sludge
RO	Reverse osmosis
RSM	Response surface methodology
sCOD	Soluble chemical oxygen demand

SEM	Scanning electron microscopy
SHE	Standard hydrogen electrode
SRB	Sulfate-reducing bacteria
SS	Stainless steel mesh
STR	Stirred tank reactor
TCOD	Total chemical oxygen demand
TS	Total solids
UF	Ultrafiltration
VFA	Volatile fatty acids
VIF	Variable inflation factor
VS	Volatile solids
WAS	Waste activated sludge
WBS	Wastewater biosolids
WMP	Waste magnesite powder
XRD	X-Ray diffraction analysis

CHAPTER 1

INTRODUCTION

The finite nature of fossil fuel sources makes the development and improvement of sustainable energy resources crucial (Merlin Christy et al., 2014). Many issues with the economy and the environment have resulted from the primary energy source being fossil fuels (Adekunle & Okolie, 2015). In addition to an energy crisis, large quantities of waste created by today's societies pose a serious threat to ecosystems and the well-being of people and animals. Waste treatment and disposal procedures are employed to avoid and regulate this. Maximum safety, lowest environmental impact, and, wherever feasible, valorization of the waste and eventual recycling of the end products should always be the criteria for selecting the appropriate waste management approach (Holm-Nielsen et al., 2009). The anaerobic digestion (AD) process is an important option for sustainable energy and waste management, which will cut down the energy needs and may even offer an option to be a net energy producer (Holm-Nielsen et al., 2009). AD facilities may process a variety of organic materials, including household and commercial food waste, sewage from both municipal and industrial sources, agricultural waste, and livestock manures, to create energy on both small- and large-scale (WBA, 2019).

We have until 2030 before climate change becomes irreversible, according to the United Nations' IPCC Special Report of 2018 (IPCC, 2018). Governments are under increasing scrutiny to strengthen their climate policies, but we have a long way to go before we even come close to meeting the minimum requirements. Considering the worldwide potential for energy generation, greenhouse gas abatement, and nutrient recovery, AD is a crucial technique for combating climate change and many other challenges. In addition, AD technologies may be used to accomplish targets 2 (zero hunger), 3 (good health and well-being), 5 (gender equality), 6 (clean water and sanitation), 7 (affordable and clean energy), 9 (industry, innovation, and

infrastructure), 11 (sustainable cities and communities), 13 (climate action), and 15 (life on land) of the United Nations' Sustainable Development Goals (WBA, 2019). AD has the potential to reduce greenhouse gas (GHG) emissions from 3,290 to 4,360 Mt carbon dioxide (CO_2) eq., or 10-13% of the current GHG emissions due to decrease (WBA, 2019).

Worldwide, there are around 50 million micro-digesters, 132,000 small, medium, and large-scale digesters, and 700 biogas upgrading facilities. Germany (10,971 plants) and Italy (1,655 plants) are obviously in a leader position when it comes to the number of plants per European Union (EU) countries, followed by France, Switzerland, the United Kingdom, and Czechia, all of which have more than 500 plants each (EBA, 2018). However, there are only licensed 95 facilities in Turkey, which is quite low compared to EU countries (EPDK, 2022). This implies that Turkey has huge potential for biogas plants yet does not utilize this potential.

As AD allows the generation of clean energy from organic wastes, it is deemed economically and environmentally viable. Nonetheless, AD also has a few drawbacks, such as long start-up and hydraulic retention times, low organic conversion efficiency, unpredictable performance, an excess of nutrients in the effluent stream, and the development of scale on the equipment and post-digestion systems (Siciliano et al., 2020; Zakaria & Dhar, 2019). In this thesis, two novel approaches have been investigated to bolster well-established AD technology and make it more efficient and sustainable: anaerobic digestion-microbial electrolysis cell (AD-MEC) integration and struvite precipitation.

The long retention period, the low removal efficiency of organic compounds, and the low biomethane production rate of conventional AD frequently restrict its widespread utilization (Tomei et al., 2009). These limitations are typically linked to the slow growth of methanogenic microorganisms and the slow hydrolysis rates (Tomei et al., 2009). A relatively new technology, microbial electrolysis cells (MEC), has been developed to boost methane (CH_4) production using electro-active microorganisms (Yu et al., 2018a). When organic materials such as acetate are

oxidized by bacteria that are attached to the anode, the released electrons are delivered to the cathode where they can be converted into desired value-added products such as hydrogen (H_2) and CH_4 on the cathodic side. A minimal quantity of external energy is needed to overcome the thermodynamic barrier of the desired reaction (Zakaria & Dhar, 2019). When the obtained product is CH_4, the process is called electro-methanogenesis. Recently, AD and MEC technologies (AD-MEC) have been combined by introducing the electrodes into the AD system with the application of external voltage to overcome the limitations of conventional AD systems (Zakaria & Dhar, 2019). Several studies showed that CH_4 production yield, kinetics, and process stability can be increased with AD-MEC integration (Q. Huang et al., 2020; Zakaria & Dhar, 2019). Even though there are a number of studies available in the literature reporting positive impacts of the integration of AD-MEC systems compared to AD, the impact of biomass colonization on the electrodes has not been fully understood. Furthermore, the media composition, reactor design, and electrode materials, that favor AD-MEC systems based on the selected substrate are not identified.

Another shortcoming of AD systems is the high nutrient load effluent streams, especially for certain types of wastes such as animal manure and leachate. AD process is highly preferred to treat this kind of complex waste, yet their effluent stream is highly rich in nitrogen (N) and phosphorus (P) (Siciliano et al., 2020). The uncontrolled discharge of such streams with high N and P content is a serious environmental problem. For example, in the case of P overload in surface waters, N becomes a limiting factor for algae and aquatic plants, and N-fixing cyanobacteria start to grow excessively to restore the equilibrium (Daneshgar et al., 2018; Siciliano et al., 2020; Sondergaard et al., 2003). This excessive growth eventually leads to the accumulation of dead biomass in freshwater bodies diminishing dissolved oxygen content in the water column. Such impacts expressed under the term eutrophication may also cause harmful algal blooms, producing toxins that are risky for human health and the environment (Daneshgar et al., 2018; W. Zhang et al., 2018). Therefore, it is critical to offer viable alternatives for proper animal manure

management and promote sustainable agricultural activities, as these are among the major sources of nutrient pollution in the environment (Dadrasnia et al., 2021). On the other hand, N and P play a crucial role in food production and agriculture and are even required for preserving life as they are the building blocks of DNA (Kampen, 2014). N is present in the atmosphere, thus reachable via fixation, yet, phosphate rocks as P sources are non-renewable (Daneshgar et al., 2018; Sena et al., 2021). Currently, P is commonly extracted from mines, and the majority of the phosphate rock reserves are located in Morocco that is followed by the following countries in the order of abundance: Iraq, China, Algeria, Syria, Jordan, South Africa, the US, and Russia (de Ridder et al., 2012). This uneven spatial distribution of such a vital resource is a concern for many countries, including Turkey. Hence, over the past decade, there has been a lot of focus on recycling and recovering N and P from anaerobic digestion residues of a variety of wastes (Siciliano et al., 2020). Struvite (magnesium ammonium phosphate (MAP), $MgNH_4PO_4.6H_2O$) precipitation is a promising nutrient recovery approach that has been commonly applied to a variety of streams such as anaerobically digested poultry manure (Yilmazel & Demirer, 2011), urine (Sakthivel et al., 2012), leachate (H. Huang et al., 2014), swine manure (Ryu et al., 2020). Further, with this process, simultaneous N and P recovery is possible, and the product can be used as fertilizer and fire retardant barrier (Yetilmezsoy et al., 2020). Several large-scale struvite precipitation facilities may be found in various parts of the world (Desmidt et al., 2015). They are, nevertheless, relying heavily on pure chemicals. There is a gap in the literature about how to minimize operating costs while also increasing sustainability.

1.1 Aim of the Study

This thesis aimed to investigate the opportunities of promoting the AD process via studying two different promising applications: AD-MEC integration and struvite precipitation. In each one of these applications, research gaps were identified through

a detailed literature review and the experimental study was strategically designed to fill in the gaps. The summary of the aim of the study is given in Figure 1.1.

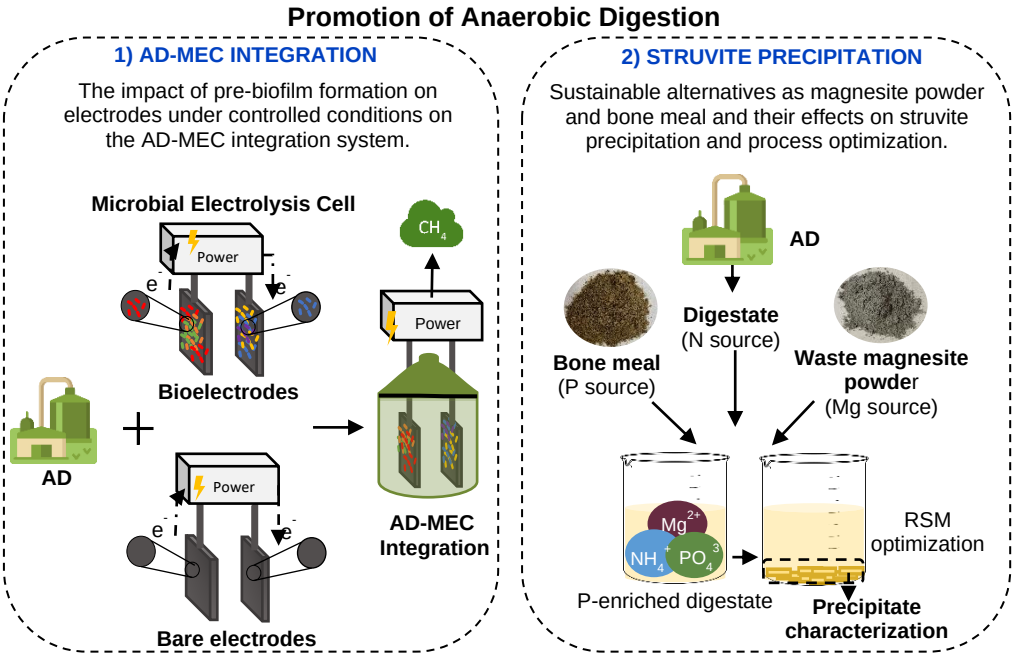

Figure 1.1. Aim of the study

1) AD-MEC integration

So far effective start-up strategies for AD-MEC systems have not been fully investigated. In this work, two different start-up strategies were investigated:

1. Starting with biofilm-developed electrodes in a highly controlled environment (bioelectrodes): This approach involves carefully monitoring and adjusting the biofilm growth before transferring the "bio"electrodes to the AD-MEC reactors. For preparation of bioelectrodes, under selected cathode/anode potentials, the anode and cathode biofilms were formed separately in a controlled environment. The bioelectrodes with the pre-formed biofilms are then transferred to the AD-MEC reactors once a stable and fully established biofilm has been formed.
2. Starting with bare electrodes (without biofilm): This method, as opposed to the first, involves putting bare electrodes into the AD-MEC reactors in their

bare form without any biofilms. In this approach, biofilm growth happens gradually and organically in an unregulated environment within the AD-MEC reactors. Over time, the microorganisms in the reactor gradually colonize and create biofilms on the electrode surfaces. This method depends on the reactor's natural microbial activity and community dynamics to start and grow the biofilms.

The purpose of this research was to evaluate the two approaches with regard to biofilm development, stability, and impact on methane generation as a whole. The study's primary objective was to see if the advantages of the first strategy's controlled environment were sufficient to warrant its adoption over the second.

In addition to biofilm formation, two different cathode materials and substrates were examined in the AD-MEC reactors. The study aimed to evaluate how these variations in cathode materials and substrates influence the overall performance, efficiency, and methane production of the AD-MEC systems. By analyzing the results, the objective was to gain insights into the optimal combination of cathode materials and substrates for maximizing the performance and energy recovery potential of AD-MEC systems.

2) Struvite precipitation

High amounts of magnesium and phosphate salts need to be added to obtain an effective N and P recovery through struvite precipitation from anaerobically digested wastes (H. Huang et al., 2014). This is due to the relatively higher abundance of N ions than other struvite-forming ions (Mg and P) in such waste streams. The external addition of such ions in the form of pure chemicals such as MgO or H_3PO_4 is costly and risks the financial sustainability of the process (T. Zhang et al., 2009). Therefore, sustainable replacements of pure chemicals such as MgO, $MgCl_2.6H_2O$, and H_3PO_4 (Le Corre et al., 2009) have been explored to develop an economically viable and environmentally friendly struvite precipitation process (Siciliano et al., 2020). On the other hand, foreign ions—those other than Mg^{2+}, PO_4^{3-}, and NH_4^+ can be present

during the precipitation of struvite due to the variety of wastewater sources. Ca^{2+} (the most common one), K^{+}, CO_3^{2-}, SO_4^{2-}, Cu^{2+}, Zn^{2+}, and Al^{3+} are typical foreign ions found in wastewater streams (B. Li et al., 2016). These ions may impact the rate of reaction, the effectiveness of recovery, the morphology, and the purity of the final product (Acelas et al., 2015; B. Li et al., 2016). Hence, the presence of such foreign ions is a critical factor during the choice of sustainable replacements of pure chemicals to be used in the struvite precipitation process. In this study, the use of such alternative sustainable replacements named waste magnesite powder (WMP) and bone meal (BM) was used in the struvite precipitation process as Mg and P sources, respectively. WMP is generated during the processing of magnesite ($MgCO_3$) to produce magnesium oxide (MgO) (Al-Mallahi et al., 2020). In Turkey, approximately 13 – 25% of WMP is produced, and since WMP is composed of very fine particles (~60 μm particle size), its disposal is problematic (Al-Mallahi et al., 2020). Besides, there is no known utilization of this waste material in Turkey (Al-Mallahi et al., 2020; Erdogan, 2013). BM, on the other hand, is a by-product of the meat industry that is produced by cooking and fat-removing mammal corpses and then drying and crushing them (Cascarosa et al., 2012). Contrary to the majority of naturally occurring phosphate ores, BM is devoid of heavy metals; hence, when used for the struvite precipitation process the obtained struvite product may even be more suitable as fertilizer (Deydier et al., 2005). More than 3.5 million tons of annual BM are produced in the European Union (Coutand et al., 2008). In the case of Turkey, estimated BM production equals 400,000 tons per year based on the annual number of slaughtered cattle (Ahiler Development Agency, 2021; TURKSTAT, 2022). Yet, only around 37% (~150,000 tons) of this total estimated amount has a beneficial use as chicken feed (TURKSTAT, 2022). Therefore, both BM and WMP have a long-term potential as sustainable P and Mg sources for struvite precipitation. In the literature, in different studies WMP and BM have been used separately to replace pure chemical additives in the struvite precipitation process (Al-Mallahi et al., 2020; Siciliano, 2016). Yet, to the best of the authors' knowledge, this is the first study that combines BM and WMP for struvite precipitation from biogas plant effluents. This

study aims to offer a sustainable process for struvite precipitation that provides a powerful example of “industrial symbiosis” that links meat production, magnesite processing, and biogas industries for resource recovery. The proposed concept enables a circular economy since the value-added product, struvite, can be employed as a slow-releasing fertilizer. This process may promote the AD process by providing a solution to the high nutrient load effluent management problem.

1.2 Scope of the Study

The experimental work of this thesis consists of two major parts: AD-MEC integration and struvite precipitation.

AD-MEC integration: In the experiments two different organic feedstocks, namely cattle manure and wastewater biosolids (WBS) were used. In the AD-MEC reactors, two different cathode electrode materials, namely graphite block and stainless-steel mesh (SS) were tested with varying cathode potentials. In total three experimental sets were performed:

- Set 1. Graphite anode – graphite cathode AD-MEC fed with cattle manure
- Set 2. Graphite anode – SS cathode AD-MEC fed with cattle manure
- Set 3. Graphite anode – graphite cathode AD-MEC fed with WBS

In the experiments, the initial and final volatile solids (VS) were measured to assess the extent of organic matter degradation throughout the AD-MEC operation. Cyclic voltammetry (CV) analyses were carried out to monitor the electroactivity of the biofilm on the electrodes. At the end of the AD-MEC operation, community analyses were conducted to characterize the microbial populations present and evaluate their diversity and abundance. Furthermore, the uptake of electric current was continuously monitored to quantify the performance of the AD-MEC system in terms of electron transfer efficiency. By employing these measurements and analyses, a comprehensive understanding of the system's organic matter degradation, microbial community dynamics, and electrochemical performance was obtained.

Struvite precipitation: Batch experiments were conducted to find the optimum nutrient recovery conditions from a cattle manure-fed biogas plant effluent. For the experiments, Box-Behnken Design (BBD) was used to define the optimum levels of significant process parameters to maximize PO_4-P, $Mg^{2+,}$ and NH_4-N recoveries. 45 runs were carried out with BBD and the optimum condition was defined by modeling the results. The optimum condition was performed, and precipitate characterization was performed by using X-ray diffraction (XRD), scanning electron microscopy (SEM), and elemental analyses.

CHAPTER 2

LITERATURE REVIEW

2.1 Anaerobic Digestion

AD is a well-established technology applied to process wastewater sludge and other organic materials such as manure, food waste, and crops in a sustainable way. AD has gained complete acceptance as a tried-and-true and even preferred approach for these wastes (Adekunle & Okolie, 2015). The major advantage of AD is biogas production which is rich in CH_4. Produced biogas can be used as heat and electricity for use in engines, microturbines, and fuel cells. Moreover, after biogas purification, CH_4 can be used as fuel and gas grid (Molino et al., 2013). Digestate, which has a liquid and solid portion, is the residual material remaining after the digestion process. Digestate is typically divided into liquid and solid components, which are handled differently (M. E. Lee et al., 2021). Digestate can be used for a variety of advantageous purposes, such as animal bedding, and nutrient-rich fertilizer (M. E. Lee et al., 2021). Possible waste streams and benefits of the AD are summarized in Figure 2.1.

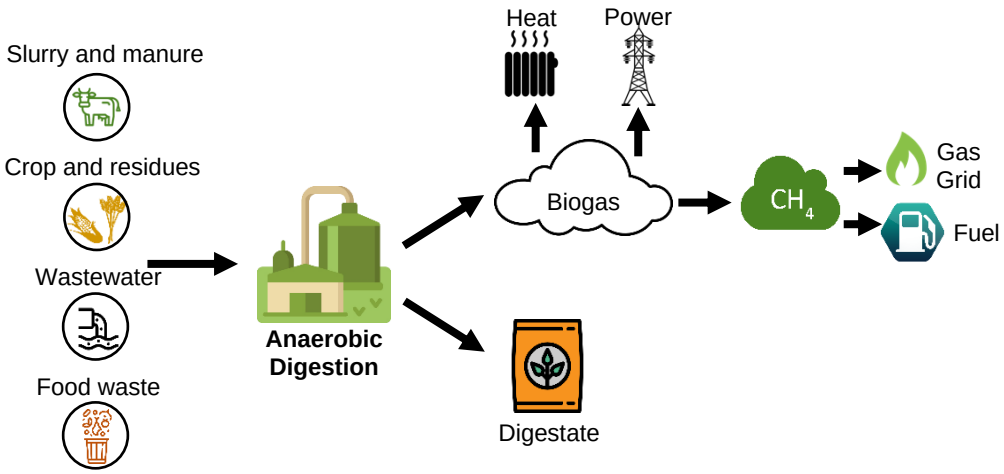

Figure 2.1. Possible waste streams and benefits of the AD

AD is a complex process in which various microorganisms actively participate (Molino et al., 2013). Moreover, each step has different rates. The steps of the AD are summarized in Figure 2.2.

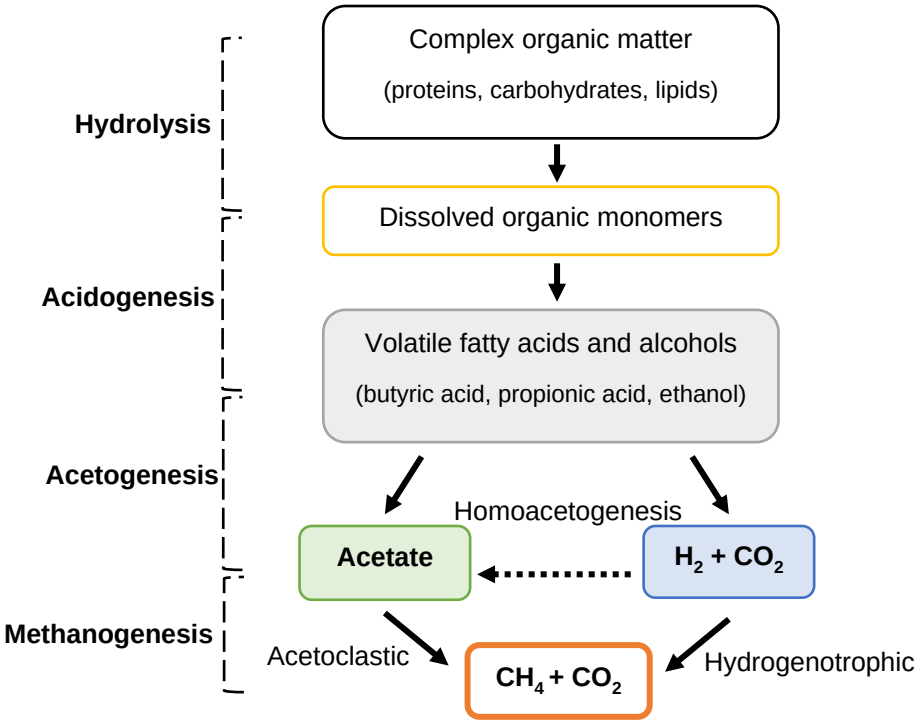

Figure 2.2. AD steps

Step 1 – Hydrolysis: The first step is the breakdown of complex organic polymers into simple, soluble monomers by extracellular enzymes (such as cellulase, amylase, protease, and lipase) generated by hydrolytic bacteria.

Step 2 – Acidogenesis: Acidogens (fermentative bacteria) transform the tiny molecules left behind after hydrolysis into a combination of volatile fatty acids (VFAs) such acetic acid, propionic acid, and butyric acid as well as other byproducts like H_2 and carbon dioxide (CO_2).

Step 3 – Acetogenesis: Here VFAs are further transformed by acetogenic bacteria into acetate, CO_2, and/or H_2.

Step 4 – Methanogenesis: It is the last step of the anaerobic process and produces the substrate for methanogenesis. There are two possible pathways for producing CH_4:

acetoclastic and hydrogenotrophic. Around 60-65% of the CH_4 is produced from the acetoclastic pathway (Kotsyurbenko et al., 2004). Long-known hydrogenotrophic methanogens can be found in some quantity in each microbial culture discovered in anaerobic fermenters. Since they convert H_2 and CO_2 to CH_4 and keep the H_2 concentration at a level that allows stable acetogenesis to occur as a result of the activity of syntrophic acetogenic microorganisms, which are extremely sensitive to higher H_2 concentrations (Kotsyurbenko et al., 2004). Therefore, hydrogenotrophic methanogen activity is crucial for the stability of the entire process. As methanogens are less tolerant to pH changes, maintaining methanogen development in the AD process is necessary for CH_4 generation. The pH range between 6.5 and 7.5 is ideal for the development of methanogens (Ray et al., 2023). Methanogens are unfavorably impacted by an extra buildup of intermediate metabolites such as VFAs, which lowers CH_4 synthesis. The variety of mesophilic or thermophilic microbes found in the AD system may affect the temperatures needed for the growth of methanogens. Another important element that may limit the methanogenesis process is mass transfer. These parameters affect the performance of the AD process.

The effectiveness of the bioconversion process depends on the balance between the various phases, which can be affected by a variety of variables. Although the underlying principle of AD has been known for many years, a lot of current research is focused on improving AD.

2.1.1 Interspecies Electron Transfer

The basis for a functional AD system is the syntrophic interactions between bacteria and methanogens. The AD microorganisms exchange electrons for energy, often by the transfer of tiny, soluble chemical molecules that serve as electron shuttles, such as H_2 or formate (Figure 2.3A) (Martins et al., 2018). These microbes have diverse but complementary metabolic capacities. Interspecies H_2/formate transfer pathway is crucial because the ability of the microbial communities to sustain a low H_2 partial pressure affects the overall thermodynamics. Diffusion restrictions between

anaerobic bacteria and methanogenic archaea can therefore constitute significant bottlenecks in the anaerobic conversion process (Martins et al., 2018).

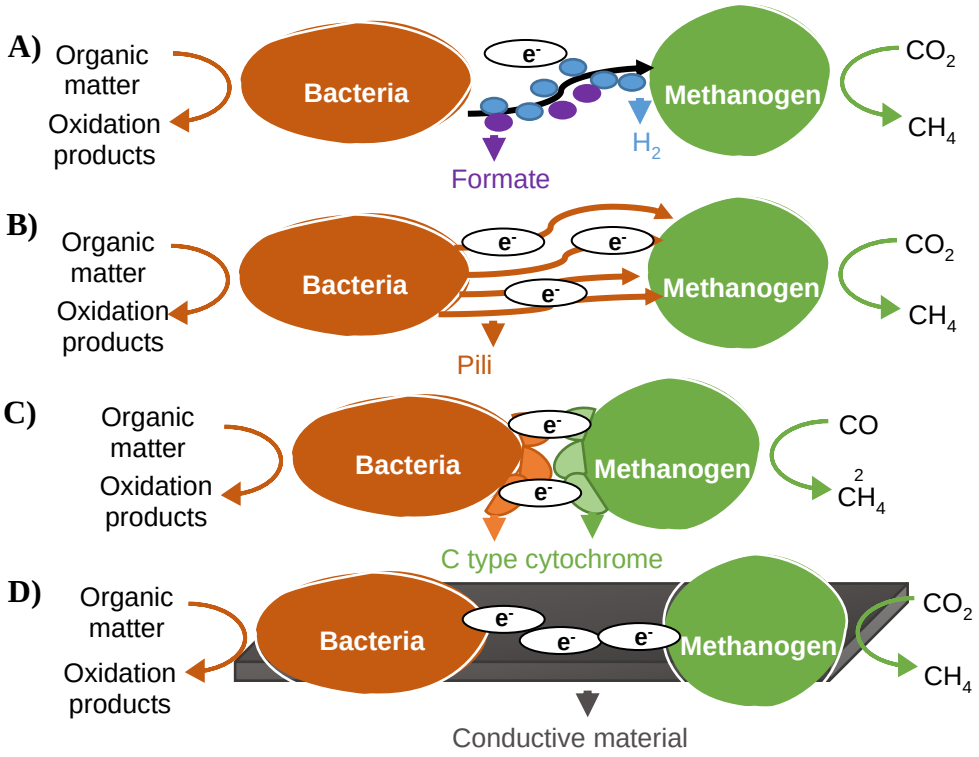

Figure 2.3. Electron transfer mechanisms in AD

It has also been observed that direct interspecies electron transfer (DIET) can occur through cytochrome, conductive-pili, and cell appendages on the cell membrane. DIET demonstrated better electron transfer efficiency than interspecies H_2/formate transfer (Cruz Viggi et al., 2014) (Figure 2.3B and Figure 2.3C). According to recent research, interspecies electron transfer (IET) may also be carried out directly between bacteria and methanogenic archaea or with the help of conductive materials, which may be a more energy-efficient method and increase the pace of methanogenesis (Kutlar et al., 2022) (Figure 2.3D). Microorganisms that can donate or uptake electrons to/from solid-state materials such as conductive materials are called electrochemically active microorganisms (EAM) (Cheng et al., 2009).

EAMs are present in electro-active biofilms, which may also harbor electrochemically inactive microorganisms (Borole et al., 2011). The latter may serve a variety of roles in the microbial community, including the decomposition of complex organics through processes such as fermentation or the utilization of other electron acceptors/donors (Borole et al., 2011). EAMs can be categorized into two distinct groups the first group is also known as exoelectrogens (transmit electrons to the outside of the cell) and the second group is known as electrotrophs (accepting electrons from outside of the cell) (Logan, 2009).

It was possible to demonstrate DIET only in co-cultures of exoelectogenic bacteria, namely *Geobacter* species, particularly in co-cultures of *Geobacter metallireducens* with *Methanosaeta harundinacea* or *Methanosarcina barkeri* (Lovley, 2017; Stams & Plugge, 2009). Moreover, all syntrophic bacteria or archaea are not exoelectrogenic or electrotrophic microorganisms, and not capable of DIET (Martins et al., 2018).

Besides these facts, several studies in the last five years have documented an increase in the production of CH_4 in anaerobic reactors that have added conductive materials, including metal-based materials such as magnetite, and carbon-based materials such as granular activated carbon (GAC), carbon nanotubes (CNT), and biochar and so on (Kutlar et al., 2022). These conductive materials have a wide surface area, strong adsorption capacity, and high electric conductivity in general (Kutlar et al., 2022). The addition of conductive materials into the AD process has some advantages as an increase in CH_4 yield, production rate, and stability, and a decrease in VFA accumulation, and lag time (Kutlar et al., 2022).

2.1.2 Limitations of AD

The kinetics of the slowest stage often dictates the kinetics of the whole bioprocess in such complicated bioprocesses as AD. Intermediates (mostly VFAs) from the degredation of complex compounds might build up inside the digester if the kinetics

of these processes are out of balance, which can cause process instability and decreased CH_4 production (Tomei et al., 2009). According to the properties of the substrates, methanogenesis or hydrolysis may be rate-limiting (Tomei et al., 2009). When digesters are supplied with complex feedstocks that mostly consist of particulate organics, the process is often constrained by the rate of the hysrolysis (Tomei et al., 2009). In contrast, the process of methanogenesis that occurs during the digestion of simple substrates may also be rate-limited (Tomei et al., 2009). To achieve consistent functioning and better CH_4 output, a balanced microbial community must be developed. The main limitations of AD can be summarized (Kofina et al., 2007; Le Corre et al., 2009; L. Zhao et al., 2021):

- Partial degradation of the organic chemicals in the waste.
- The reaction's slow rate necessitates a large-capacity digester, which is more expensive.
- It is less cost-effective because of the additional CO_2, H_2S, and moisture present in addition to the CH_4.
- The resultant sludge produces secondary contamination due to the presence of hazardous undegraded volatile and non-volatile materials (heavy metals) for agro-industrial waste
- The liquid part of the digestate has high nutrient content, which causes discharge problems.
- Scaling is caused by ions in the effluent, which can accumulate on the walls of AD and post-digestion systems as well as inside pipelines and heat exchangers. It results in a significant level of downtime, a reduction in hydraulic capacity, a limitation of flow, a loss of efficiency, and a rise in pumping and maintenance costs.

In this thesis, two developing technologies have been examined as a means of overcoming some of these constraints. The AD-MEC system was studied as a means of enhancing AD technology and making it a more efficient process in terms of yield and rate. Struvite precipitation was examined as a post-treatment to efficiently utilize

digester effluent in order to support the AD system. These two promising techniques have been investigated in an effort to advance current AD technology and make it more feasible and effective.

2.2 Bioelectrochemical Systems

For the generation of energy from wastewater, bioelectrochemical wastewater treatment has emerged as a potentially promising method. Using electrochemically active microorganisms is the basis of bioelectrochemical wastewater treatment. Extracellular electron transfer (EET) is a capability of active microorganisms that allows them to transport electrons to an electrode (anode) while oxidizing (and hence eliminating) the organic compounds in wastewater (Logan & Regan, 2006). The electrode is known as a microbial bioanode because the microorganisms act as a catalyst for the electrochemical oxidation of the organic substance. By electrically linking a microbial bioanode to a counter electrode (cathode) that conducts a reduction process, wastewater can be treated bioelectrochemically (Cheng et al., 2009). The electrode reactions may take place and the electrons can go from the anode to the cathode because of this electrical connection between the anode and cathode (i.e. electrical current can flow). The required operation of the bioelectrochemical system (BES) is determined by the Gibbs free energy change of the entire reaction. Electrical energy may be generated when the total reaction's Gibbs free energy change is negative, and the BES is then used as a microbial fuel cell (MFC) (Logan & Regan, 2006). On the other hand, when the entire reaction's Gibbs free energy change is positive, electrical energy must be used, and the BES is used as a microbial electrolysis cell (MEC) (Rozendal et al., 2008). EAMs play a significant role in BES systems. According to the desired product, EAMs form biofilm on the anode or both anode and cathode.

2.2.1 Microbial Electrolysis Cell

MECs have the potential to play a significant role in the design of future waste bioenergy facilities due to their ability to simultaneously treat waste and generate renewable energy, high energy efficiency, versatility in waste inputs, and provide resource recovery (Kadier et al., 2020). Figure 2.4 shows the schematic representation of the MEC system. The anode, cathode, membrane, and power supply are the four main parts of a MEC. By placing exoelectrogenic microorganisms on the anode of a MEC system, biodegradable substrates (organic matter) in wastewater are oxidized and electrons are transferred to the anode while the released protons (H^+) move to the cathode side. Then, on the cathode surface, abiotic hydrogen production takes place abiotically via a hydrogen evolution reaction (Logan et al., 2008).

Anode and cathode electrochemical reactions are described by the following equations (Varanasi et al., 2018):

At anode: (acetate is shown as an example organic compound)

$$CH_3COO^- + 4H_2O \rightarrow 2HCO_3^- + 9H^+ + 8e^- \quad \text{(Eq. 2.1)}$$

At cathode: (hydrogen evolution reaction)

$$8H^+ + 8e^- \rightarrow 4H_2 \ (E = -0.41 \text{ V vs. SHE}) \quad \text{(Eq. 2.2)}$$

Microbial electrolysis is endothermic (positive Gibbs free energy, negative cell voltage); hence it requires a very low partial pressure of H_2 to proceed spontaneously. Cathode H_2 production necessitates the application of a small voltage between the electrodes to "force" current generation. A tiny solar panel, low-grade heat, or MFCs can provide the necessary applied voltage (0.2-0.8 V), which is substantially lower than that required for conventional water electrolysis (1.8-3.5 V) (Kadier et al., 2016). As water electrolysis is currently used on full-scale plants for hydrogen production, bioelectrochemical hydrogen production in MECs can be accepted as a comparatively low-energy demand process (Y. Zhang & Angelidaki, 2014). Here,

organic matter's chemical energy stores bridge the gap between microbiological and pure electrochemical electrolysis. In addition to H_2, similar processes have been used to produce a wide variety of inorganic and organic compounds such as methane, ethanol, formic acid, and hydrogen peroxide (Y. Zhang & Angelidaki, 2014).

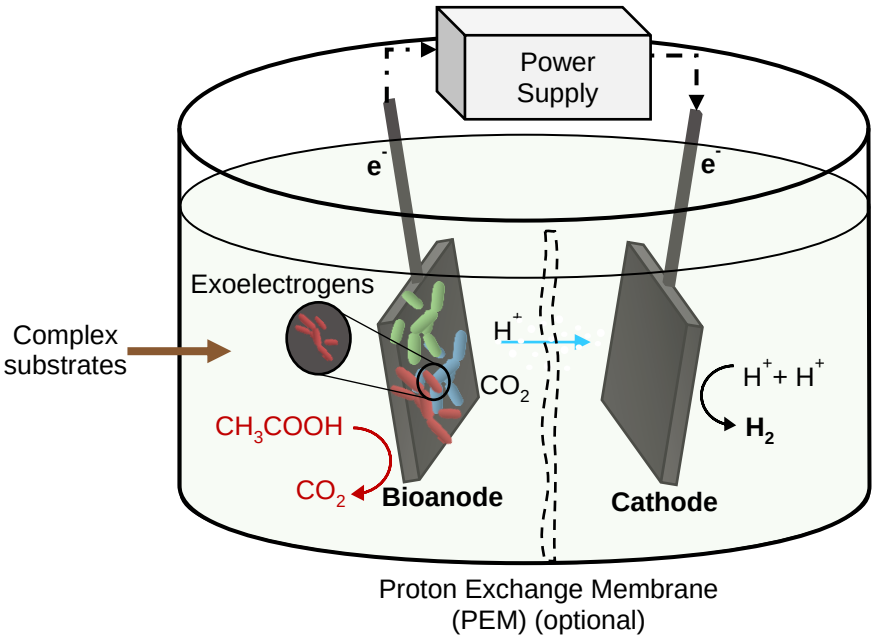

Figure 2.4. Schematic of the MEC

MEC may have either a single chamber or a double chamber design. When there are two independent compartments, they are separated by a membrane (typically a proton exchange membrane is used). In order to maintain high H_2 concentrations and prevent H_2 consumption by bacteria in the anode chamber, membranes have also been utilized in MECs. Nevertheless, even with the use of a membrane, the H_2 gas generated at the cathode can be contaminated by gases (such as CO_2) produced at the anode, as has been pointed out in the literature (Cheng & Logan, 2007). H_2 can still diffuse back into the anode chamber even when a membrane is present (Ditzig et al., 2007). Moreover, membranes can cause significant pH variations between the anode and cathode chambers, as well as impede proton transfer between the electrodes (Call & Logan, 2008). Also, the membrane increases the cost of the process. Due to these reasons, membraneless MECs have been developed called single chamber MECs.

2.2.2 Electromethanogenesis

During the H_2 production, in earlier studies, CH_4 has often been discovered in the MECs as a result of the growth of methanogens (Y. Zhang & Angelidaki, 2014). An unanticipated result of methanogen presence in H_2-producing MECs is a reduction in H_2 generation. Therefore, methanogen development in MECs has been inhibited by a number of methods such as explosion into the air and using specific inhibitors ($CHCl_3$, 2-BES, CH_3F, Na_2MoO_4, etc.,) (Karthikeyan et al., 2017; Y. Zhang & Angelidaki, 2014). Most of the approaches, however, are either inefficient or costly. However, direct CH_4 synthesis in MECs has various benefits over methanogen inhibition. Thus, CH_4-producing MECs have been developed.

CH_4 production by CO_2 reduction at a reduced energy input is possible with the use of cathode-attached methanogens (Siegert et al., 2015). The term "electro-methanogenesis" has been used to describe this novel approach to methanogenesis. The schematic of the process is given in Figure 2.5.

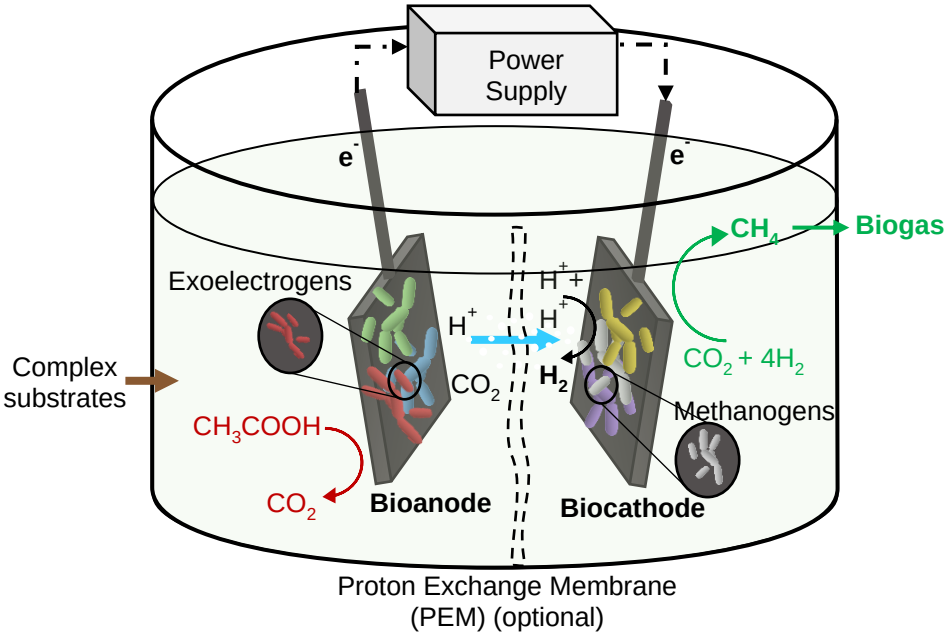

Figure 2.5. Schematic of electromethanogenesis (CH_4-producing MECs)

Anode and cathode electrochemical reactions in an electromethanogenic MEC are described by the following equations (Varanasi et al., 2018):

At anode: $CH_3COO^- + 4H_2O \rightarrow 2HCO_3^- + 9H^+ + 8e^-$ (Eq. 2.3)

At cathode:

Direct electromethanogenesis:

$CO_2 + 8H^+ + 8e^- \rightarrow CH_4 + 2H_2O$ (E = -0.244 V vs. SHE) (Eq. 2.4)

Indirect electromethanogenesis:

$8H^+ + 8e^- \rightarrow 4H_2$ (E = -0.41 V vs. SHE) (Eq. 2.5)

$CO_2 + 4H_2 \rightarrow CH_4 + 2H_2O$ (Eq. 2.6)

The configuration of CH_4-producing MECs is similar to H_2-producing MECs, except for the presence of a biocathode. In H_2-producing MECs, cathode, and H_2 production is abiotic. On the other hand, in CH_4-producing MECs methanogens are attached to the cathode surface (hence called biocathode) as shown in Figure 2.5.

2.2.3 Electron Transfer Mechanisms

In these systems, EAMs play a crucial role in facilitating effective electron transfer and optimizing current densities and energy efficiency. For this reason, optimizing the electron transfer activity of EAMs to the electrode or vice versa, as well as enhancing their metabolic efficiency, are top priorities for BES development. Two possible electron transfer mechanisms are possible during electromethanogenesis in MECs: direct or indirect electron transfer (Figure 2.6).

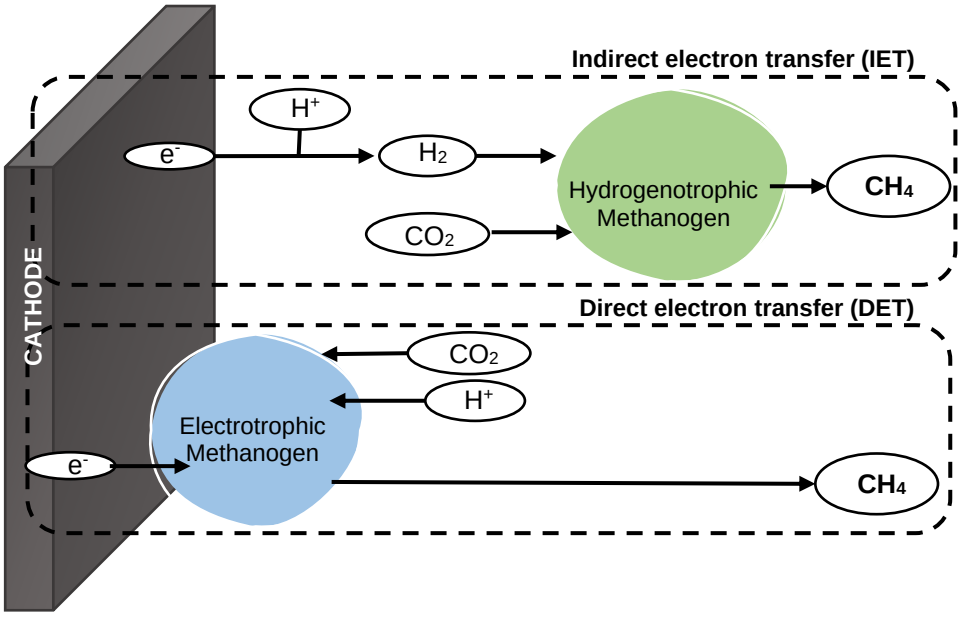

Figure 2.6. Electron transfer mechanisms on cathode surface in CH_4 producing MECs.

Direct electron transfer (DET) involves the uptake of electrons directly from the cathode, whereas mediated or indirect electron transfer (IET) involves the production of H_2 and other chemicals like acetate and formate that are then mixed with CO_2 to generate CH_4 (Figure 2.6) (Pawar et al., 2020). Direct DET for CH_4 synthesis is an efficient use of energy since the energy needed to drive the reactions is lower than that necessary for the IET as seen in Eq. 2.4 and 2.6. In CH_4-producing MECs, CH_4 is generated using a low voltage (0.2 to 0.8 V). However, because of the losses in the MECs more than 0.4 V is typically applied to the cells, and through such kind of voltage application it is possible to produce both H_2 and CH_4. This is why it is still not fully understood. which electron transfer path (direct or indirect) is used direct (Pawar et al., 2020).

2.3 Anaerobic Digestion Microbial Electrolysis Cell (AD-MEC) Integration

The electromethanogenesis can be integrated with conventional anaerobic digesters by introducing a pair of electrodes and external energy (Zakaria & Dhar, 2019).

These systems are called integrated AD-MEC processes. The findings from several research studies showed that AD-MEC systems were capable of resolving some of the issues that are troubling conventional digesters (Q. Huang et al., 2020). With the hydrolysis and fermentation process, simple organic acids are formed, which are then oxidized by certain electroactive bacteria in integrated AD-MEC systems.

CH_4 is produced via four pathways as seen in Figure 2.7.

1) Conventional acetoclastic methanogenesis.

2) Electromethanogenesis: electrotrophic methanogens directly use CO_2, protons (H^+), and electrons (e^-) to generate CH_4 ($CO_2 + 8H^+ + 8e^- \rightarrow CH_4 + 2H_2O$ (E = -0.244 V vs. SHE)).

3) Reduction of H^+ to H_2 gas by abiotic cathodic electrochemical H_2 evolution reaction ($8H^+ + 8e^- \rightarrow 4H_2$ (E = -0.41 V vs. SHE)), then H_2 is utilized by hydrogenotrophic methanogens.

4) Hydrogenotrophic methanogens utilize the H_2 produced by syntrophic fermenting microorganisms. (Conventional hydrogenotrophic methanogenesis).

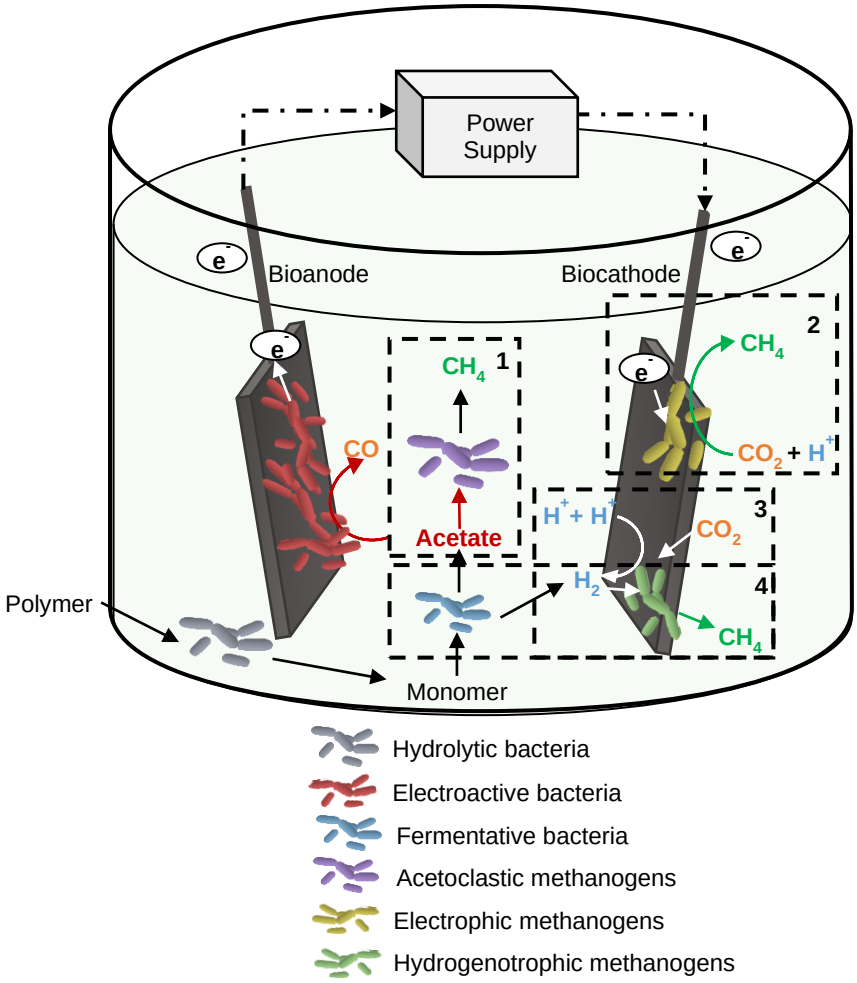

Figure 2.7. Schematic of AD-MEC integrated system (adopted from (Q. Huang et al., 2020)

The contribution of the reactions at the cathode (2 and 3) is determined by cathode potential. Moreover, energy loses including electrode overpotential and internal resistances must be considered while applying energy supply (Q. Huang et al., 2020). Generally, energy is applied more than needed theoretically (Q. Huang et al., 2020). Acetoclastic methanogens could be outcompeted by electroactive bacteria on the anode surface due to slow-growing kinetics and competition for the same substrate, acetate (Figure 2.7). Thus, this could enhance pathways 3 and 4. In particular, hydrogenotrophic methanogens might be enhanced since they are more resistant to ammonia inhibition and low temperature (Florentino et al., 2019). AD-MEC systems

may therefore provide kinetically and thermodynamically advantageous conditions for enhanced methanogenic productivity.

AD-MEC systems have recently received interest due to their potential to improve AD performance. An overview of AD-MEC studies is summarized in Table 2.1.

Table 2.1. Summary of AD-MEC integration studies

Substrate (con.)	Operating Mode	V (L)	T (°C)	Anode material	Cathode material	Voltage (V)	CH_4 production	Max. Current	Ref
Acetate (COD 0.8 g/L)	Fed batch	0.25	55	Plain carbon cloth	Plain carbon cloth	0.4, 0.7, 08	1103 mmol/m2./d at 0.8 V	NA	(Fu et al., 2015)
Acetate (COD 10 g/L)	Fed batch	0.23	25	Carbon felt	Stainless steel	1	225.5 mL/g COD	166.7A/m^3	Yin et al. 2016
Acetate (COD 10 g/L)	Fed batch	0.23	25	Carbon felt	Stainless steel	1	272 mL/g COD	304 A/m^3	Yin et al. 2016
Acetate (COD 10 g/L)	Fed batch	0.23	25	Carbon felt	Stainless-steel	1	360mL/g COD	304 A/m^3	Yin et al. 2016
Acetate (COD 3 g/L)	Continuous	1	25	Graphite rod	Graphite rod	E_{anode} -0.25, -0.3, -0.35 -0.4 V vs Ag/AgCl	77.7 mL/h at -0.25 V vs Ag/ AgCl	0.47 A at -0.25 V vs Ag/ AgCl	(Z. Zhao et al., 2014)
Glucose (1560 mmol e^-)	Fed batch	0.35	55	Graphite rod	Graphite rod	$E_{cathode}$ -0.8, -1.1, -1.3 V vs Ag/AgCl	0.6 L/L/d at -1 V vs Ag/AgCl	- 20 mA at -1.2 V vs Ag/AgCl	(Lin et al., 2017)
Glucose (COD 1 g/L)	Fed batch	0.8	35	Reticulated vitreous carbon	Reticulated vitreous carbon	0.3, 0.6	0.011 L/Ld at 0.3 v	0.122 A/m^2 at 0.6 V	(Gajaraj et al., 2017)
Glucose (COD 2 g/L)	Batch	0.27	3.5	Carbon fiber brush	Carbon fiber brush	0.5, 0.7, 1, 1.5	408 mL/g COD at 1 V	19.04 A/m^3 at 1 V	(Choi et al., 2017)
Glucose (COD 3 g/L)	Semi-batch	0.75	35	Graphite fiber	Graphite fiber	0.3	322.9 mL/g COD	2.65 mA	(Q. Feng et al., 2016)

Table 2.1. Summary of AD-MEC integration studies (continued)

Substrate (con.)	Operating Mode	V (L)	T (°C)	Anode material	Cathode material	Voltage (V)	CH_4 production	Max. Current	Ref
Glucose (COD 7 g/L)	Semi-continuous	1	35	Graphite rod	Graphite rod	1	248 mL/h	51 A/m^2	(Y. Li et al., 2016)
Mixed acids (each 0.5 g/L)	Fed batch	0.2	35	Graphite felt	Carbon paper	0.5	84 mL	N/A	(Luo et al., 2016)
Artificial beer brewery wastewater (COD 1 g/L)	Fed batch	0.7	35	Graphite fiber brush	Stacked of 2 layers stainless-steel mesh	0.5, 0.7, 0 9	100 mL/g COD at 0.9 V	8.4 mA at 0.9 V	(Z. Guo et al., 2017)
Artificial beer brewery wastewater (COD 1 g/L)	Fed batch	0.7	35	Graphite fiber brush	Stacked of 5 layers stainless-steel mesh	0.5, 0.7, 0 9	145 mL/g COD at 0.9V	12.9mA at 0.9 V	(Z. Guo et al., 2017)
Artificial beer brewery wastewater (COD 1 g/L)	Fed batch	0.7	35	Graphite fiber brush	Stacked Of 8 layers stainless-steel	0.5, 0.7, 0 9	260 mL/g COD at 0.9 V	12.6mA at 0.9 V	(Z. Guo et al., 2017)
Molasses (44.7 g/L)	Fed batch	0.8	34	Carbon felt	Carbon felt	0.5	65.5 mL/L/d	3.36 A/m^2	De Vrieze et al. 2014
Molasses (44.7 g/L)	Fed batch	0.08	34	Carbon felt	Carbon felt	1	127.5 mL/L/d	6.78 A/m^2	De Vrieze et al. 2014
E. densa harvested from domestic wastewater & lake water (TS 50 g/L)	Semi-continuous	0.8	35	Pair of Ti/RuO2 mesh plates	Pair of Ti/RuO2 mesh plates	0.4, 0.6, 0.8, 1	248 mL/L.d at 1 V	8.9 mA at 0.8 V	(Zhen et al., 2016)
Food waste (VS 49000 mg/L)	Batch	0.9	35	Graphite plate	SS	0.9	0.59 m^3/m^3 /day (total gas)	1.35 A/m^2	(Hassanein et al., 2017)

Table 2.1. Summary of AD-MEC integration studies (continued)

Substrate (con.)	Operating Mode	V (L)	T (°C)	Anode material	Cathode material	Voltage (V)	CH_4 production	Max. Current	Ref
Food waste (TCOD 60.3 g/L)	SBR	0.2	35	Graphite carbon mesh	Graphite carbon mesh	0.3	17 L/d	N/A	(J. Park et al., 2018)
Leachate (15.9 gCOD/L feed)	Batch	0.5	35	Graphite rod	Graphite rod	0.7	>33 mmol CH4	N/A	(Gao et al., 2017)
Raw sludge (TCOD 114.2 g/L)	Fed batch	2	35	Pair Of Fe tube	Graphite pillar	0.3, 0.6	170.2 L/kg VSS at 0.3 V	4.3 A/m^3	(Y. Feng et al., 2015)
Raw sludge (VS 29.7 g/L, COD 685 g/L)	Fed batch	1	35	Activated carbon fiber textile	mesh Activated carbon fiber textile	0.3-1.5	140.9 L/kg VS at 0.6 V	2.55 A/m^2 at 1.2 V	(Chen et al., 2016)
Raw sludge (VSS 17.1 g/L, TCOD 29.2 g/L)	Fed batch	2.5	30-40	Graphite felt	Graphite felt	0.3	1.11 m3/m3 at 35 'C	1.63 A/m^3 at 35 'C	(Ahn et al., 2017)
Sewage sludge (TCOD 32-47 g/L)	Batch	12	25	Graphite fiber	Graphite fiber	0.3, 0.5, 07	370mL/L.d at 0.3 V	392 mA/m^3 at 0.7 V	(Q. Feng et al., 2016)
Waste activated sludge (COD 10 g/L)	Fed batch	0.8	35	Reticulated vitreous	Reticulated vitreous carbon	0.3, 0.6	0.020 L/L.d at 0.3 & 0.6 V	0.067 A/m^2 at 0.3 V	(Gajaraj et al., 2017)
Waste activated sludge (VSS 14 g/L, TSS 20 g/L)	Fed batch	0.5	23	Graphite brush	Carbon cloth	0.8	138 mL/L reactor.d	11.8 mA	(W. Liu et al., 2016)
Waste activated sludge (VSS 28g/L, TSS 101 g/L)	Continuous	0.5	37	Graphite brush	Graphite rod	0.8	884.7 mL	0.0134 A/m^2	(Z. Zhao, Zhang, Ma, et al., 2016)

Table 2.1. Summary of AD-MEC integration studies (continued)

Substrate (con.)	Operating Mode	V (L)	T (°C)	Anode material	Cathode material	Voltage (V)	CH_4 production	Max. Current	Ref
Waste activated sludge (VSS 41 g/L)	Fed batch	0.5	37	Graphite brush	Graphite rod	0.6	2998.4 mL	0.35 A/m^2	(Z. Zhao et al., 2015)
Waste activated sludge (VSS 43 g/L, TSS 101 g/L)	Fed batch	0.5	37	Graphite brush	Graphite rod	0.6	230 mL/d	NA	(Z. Zhao, Zhang, Quan, et al., 2016)
Waste activated sludge (VSS 5.20 g/L, COD 7.89 g/L)	Continuous fed-batch	0.18	22.5	Carbon fiber brushes	Stainless-steel mesh	1.2	25.6 mL/d	15-25 a/m^3	(Asztalos & Kim, 2015)
Waste activated sludge (VSS, 30 g/L, TSS 45 g/L)	Fed batch	4	35	Carbon felt tube	Graphite pillar	0.6	1363.4 mL	0.1 A/m^2	(Z. Zhao, Zhang, Ma, et al., 2016)
Waste activated sludge (VSS 2.8 g/L)	Batch	0.52	25	Carbon brush	SS mesh	1	330 (mL/g VSS)	8 mA	(Hou et al., 2020)
Waste activated sludge (VSS 6.02 g/L)	Batch	0.18	37	Ti/Ru mesh plates	Ti/Ru mesh plates	1.8	200 (mL/g VSS)	-	(Xiao et al., 2018)
Waste activated sludge (VSS 14 g/L)	Batch	0.69	20–25	Carbon brush	Carbon cloth	0.8	115 (mL/g VSS)	-	(Bao et al., 2020)
Waste activated sludge (VSS 14 g/L)	Batch	0.55	20	Graphite brush	Carbon cloth	0.8	111 (mL/g VSS)	3.5 mA at peak	(Cai, Liu, et al., 2016)
Waste activated sludge (VSS 16 g/L)	Batch	0.3 for each chamber	37	Carbon brush	Carbon brush	0.8	157 (mL/g VSS)	0.6 mA average	(H. Wang et al., 2021)

Table 2.1. Summary of AD-MEC integration studies (continued)

Substrate (con.)	Operating Mode	V (L)	T (ºC)	Anode material	Cathode material	Voltage (V)	CH_4 production	Max. Current	Ref
Cattle Manure + Aloe Peel Waste	Batch	0.3	36	Graphite rod	Graphite rod	0.6	226.84 N mL/g VS	5.31 A/m^2 peak	(Xing et al., 2021)
Cow Dung (TS 5000 mg/L)	Batch	0.6	20	Graphite	SS	1	39 and 133 % increase compared with AD	-	(Jiao et al., 2022)
Dairy manure (VS 47000 mg/L)	Continuous	8	35	Graphite plate	SS cylinder	1.2	23.6 L on MEC and 10.9 L CH_4 on AD	7.4 A/m^2	(Hassanein et al., 2020)
Pig Slurry (16.37 g/L)	Continuous	0.5 anode, 0.265 cathode chamber	23	Carbon felt	Granular graphite	$E_{cathode}$ at -1 V vs Ag/AgCl	79 L CH_4/m^3 /d	average 0.4 A/m^2 (first 30 days) , then 4.5 A/m^2 at peak (average of 1.5 A/m^2)	(Cerrillo et al., 2018)
Swine manure	Batch	0.5	25, 35, 45	Graphite felt	Graphite felt	0.1, 0.3, 0.5, 0.7, and 0.9	0.64 m^3-CH_4/ kg-VS at 35C and 0.7 V. 25–30% higher than those of the conventional AD.	-	(J. Yu et al., 2019)

2.3.1 Substrate

Different substrates have been investigated in AD-MEC integrated system (Table 2.1). Among the studies, simple substrates have been widely investigated in the early years of AD-MEC studies (Zakaria & Dhar, 2019). Since hydrolysis of the complex substrates can be a limiting step for AD, using simple substrates such as acetate, glucose is an option for understanding the system. Among complex substrates, sludge from wastewater treatment plants such as waste activated sludge, and sewage sludge has the highest number of studies. Extracellular polymeric substances (EPS) and intracellular substances constitute the majority of organics of WAS (Zhen et al., 2015). Nevertheless, the complicated structure of EPS and strong cell wall results in a prolonged AD period and inefficient CH_4 generation (Zhen et al., 2015). Therefore, different pretreatment methods have been applied to the WAS to promote hydrolysis. Wang et al. (X. T. Wang et al., 2022) summarized the possible pretreatment methods and CH_4 production with AD-MEC integration. Animal waste, such as pig slurry or dairy manure, may contain recalcitrant components such as cellulose, hemicellulose, and lignin, which results in hindering the hydrolysis of cattle manure in AD (Y. Li et al., 2021; Nasir et al., 2012). Especially, lignin may only be degraded to a limited degree (Alvarez & Lidén, 2009). Moreover, animal manure typically has a high concentration of ammonia, which might hinder methane production (Yenigün & Demirel, 2013). Recent studies have demonstrated that the application of conductive materials and bioelectrochemical systems can mitigate the inhibition effect and increase the system's stability resulting from various substrates such as animal manure, industrial waste, etc. (Kutlar et al., 2022; X. T. Wang et al., 2022).

2.3.2 Electrodes

Table 2.1 shows that carbon-based cathodes have been widely employed in AD-MEC research, while metal-based cathodes have been used in just a limited number of studies. Due to the diverse system configurations, substrates, inoculums, and

operational parameters used in most of these studies, it is impossible to compare and remark on an ideal material for the cathode for electro-methanogenesis. Careful selection of cathode materials would be required to reduce cathodic overpotential and obtain a satisfactory CH_4 production rate, as demonstrated by a handful of systematic studies that compared various electrode materials under identical operating conditions. (Siegert, Yates, et al., 2014). Electrode materials with a high overpotential may result in a decrease in the transfer of electrons activity, accordingly requiring more energy supply. (Zhen et al., 2016). Moreover, the cost must be considered for the selection of the electrode material for AD-MEC systems. For example, Siegert et al. (2014) investigated different cathode materials as metal powders of stainless steel or nickel; iron mineral coatings of ferrihydrite, magnetite, or iron sulfide; MoS_2; and carbon- based materials that included plain graphite blocks, blocks coated with carbon black powder, and carbon fiber brushes during electromethanogenesis. Among them excluding platinum, the carbon brushes showed the best performance in terms of overall CH_4 production rates (Siegert, Yates, et al., 2014). In addition to the material of the electrode, the surface area of the electrode is another important feature. When attempting to commercialize or scale-up up a microbial electrochemical system, one of the most crucial factors to consider is the reactor volume needed for the electrodes (Siegert, Yates, et al., 2014). Theoretically, the electrochemical efficiency of an electrode may be improved by increasing its surface area, which lowers its over-potential. Moreover, as surface area increases biofilm attachment may also increase (Martins et al., 2018). Further, cathode to anode ratio can be another important consideration that can further increase CH_4 production in BESs. Guo et al. (2017) evaluated the influence of varying ratios of cathode to anode surface area on methane production. At 0.5 V, high cathode to anode ratio did not have an impact on the CH_4 generation rate, but at higher voltages, it steadily increased (0.7–0.9 V) (Z. Guo et al., 2017). Nevertheless, COD removal efficiencies were practically constant in varied settings, stressing that the inferior cathodic reaction largely reduced CH_4 output since the surface area of the cathode was insufficient to keep methanogens.

2.3.3 Voltage application

Among the parameters affecting the operation of the AD-MEC, voltage application is a parameter that directly changes the system. The feasibility of the process is significantly affected by this operational parameter. Therefore, it has been widely investigated in AD-MEC systems (Table 2.1). There are two possible voltage application ways as power supply or potentiostat. Potentiostat provides a controlled system by adjusting the potential of the working electrode. Contrarily, the power source provides a constant voltage across the gap between the working and counter electrodes. Even yet, due to the uneven dispersion of supplied potential inside a large electrode, using a potentiostat may not be a viable option for large-scale applications (Zakaria & Ranjan Dhar, 2021). Furthermore, the cost of implementing potentiostat-controlled systems for large-scale reactors is a significant concern. The voltage range varied significantly among the studies (Table 2.1). The necessary applied voltage is 0.2-0.8 V (Kadier et al., 2016). The conventional water electrolysis process requires 1.8-3.5 V (Kadier et al., 2016). Thus, high-voltage applications are not feasible.

The optimum voltage could change with electrode configuration, substrate, internal resistances in the system, and media (Q. Huang et al., 2020). Consequently, the optimum voltage should be determined with respect to each specific case. For example, Chen et al. (Chen et al., 2016) investigated the effect of voltage on AD of WAS. All applied voltages other than 0.9 V were able to increase CH_4 production and VS removal efficiency, with the optimal applied voltage for CH_4 production being 0.6 V, which is 76.2% greater than the control group (Chen et al., 2016). H_2 accumulated in the system as the voltage was raised from 0.9 V to 1.5 V (Chen et al., 2016). Moreover, Liu et al. (D. Liu et al., 2017) investigated different cathode potentials (−1.3, −1.1, and −0.8 V) on the CH_4 production rate. The highest CH_4 production rate was achieved at the most negative potential and at – 0.8 V cathode potential, the CH_4 production rate was significantly lower than others.

2.3.4 Media

There is a gap in the literature about the optimization of process conditions (*i.e.* voltage, buffer solution) and identification of microbial communities that perform electron transfer in AD-MECs. Buffer solutions, mostly phosphate buffer saline (PBS), have been used in MFC and MEC systems to provide pH balance, high conductivity, and reduction in solution resistance (Ahn & Logan, 2013; F. Guo et al., 2021; Liang et al., 2015). Although the effect of PBS has been investigated well for MFC and MEC systems, the impact of the presence/absence of buffer solutions on AD-MEC systems is still not exactly known. For example, the effect of 50 mM PBS media usage in AD-MEC treating waste activated sludge (WAS) was investigated (X. J. Xu et al., 2020). The presence of PBS increased CH_4 production by 1.4-fold compared to PBS under 0.8 V. Contradictory to this result, Sanli (2022) revealed that 50 mM PBS may inhibit the AD process treating WAS due to high orto-phosphate concentration. Moreover, Ghaderikia (2022) showed that 100 mM PBS inhibited the AD-MEC system severely when the system was fed with cattle manure and decreased the rate of the process significantly. However, the current generation was high compared to a different salt media indicating that although the system had a proper electron transfer with PBS media, PBS affected the AD process negatively (Gharerikia, 2022).

2.3.5 Microbial Community

The process of electro-methanogenesis involves intricate interactions between microorganisms. Clarifying the functions of various microorganisms in AD-MEC systems may require an understanding of the spatial organization of the functioning community. Biofilms on anode and cathode surfaces contain different types of archaea and bacteria species. Bacteria's faster growth rate makes them ubiquitous throughout the system, while archaea are more concentrated at the cathode than at the anode and reactor content (suspension) (Cai, Han, et al., 2016). The distribution

of microbes has only been fully characterized in a few studies. The majority of the electroactive bacteria were found to reside on the anode, rather than the cathode or in suspension (D. Liu et al., 2016). Hydrolytic/fermentative bacteria including *Cloacamonas, Bifidobacterium,* and *Pseudomonas* were often the most abundant in suspended sludge (Zakaria & Dhar, 2019). Hydrogenotrophic methanogens were the most common kind of archaeal community found in cathode biofilms and suspension (Zakaria & Dhar, 2019).

2.3.5.1 Archaeal Community

The integration of AD-MEC may enhance the abundance of fast-growing hydrogenotrophic methanogens, including *Methanobacterium*, M*ethanocorpusculum,* and *Methanoculleus* (Table 2.2). Cathodic H_2 may increase the abundance of hydrogenotrophic methanogens on cathode surface (Cheng et al., 2009). Additionally, due to their fast growth kinetics, certain exoelectrogens can outcompete acetoclastic methanogens, since both of the microorganisms use acetate (Cai, Liu, et al., 2016). Furthermore, hydrogenotrophic methanogens are more resistant than acetoclastic methanogens (Florentino et al., 2019). Hence, the increase in the abundance of hydrogenotrophic methanogens in AD-MEC systems should help maintain system stability under adverse metabolic circumstances. In addition, methanogens are capable of directly receiving electrons from conductive materials, such as *Methanosaeta,* and *Methanosarcina* via DIET (Kutlar et al., 2022). These methanogens can establish more effective syntrophic cooperation with syntrophic fermentative bacteria, thereby mitigating the risk of organic acid accumulation in digesters with high organic loading (Kutlar et al., 2022).

Table 2.2 Microbial communities in AD-MEC studies

Substrate	Dominant microorganisms		Ref
	Bacteria	**Archaea**	
WAS	*Geobacter*	*Methanobacterium*	(Cai, Liu, et al., 2016)
WAS	*Geobacter*	*Methanocorpusculum*	(Sun et al., 2015)
WAS	*Levilinea*	*Methanosaeta*	(Z. Zhao, Zhang, Quan, et al., 2016)
Sludge fermentative liquid	*Geobacter*	*Methanobacterium*	(W. Liu et al., 2016)
Sewage sludge	*Caprothermobacter*	*Methanoculleus*	(Sasaki et al., 2013)
WAS	*Acinetobacter* (0.3 V) *Pseudomonas* (0.6 V, 1.2 V, 1.5 V) *Proteiniclasticum* (0.9 V)	*Methanosaeta* (0.3 V) *Methanoregula* (0.6 V, 0.9 V, 1.2 V, 1.5 V)	(Chen et al., 2016)
Synthetic medium	*Arcobacter*	*Methanospirillum*	(Bo et al., 2014)
Food waste	*Clostridia (class)*	*Methanosarcina*	(J. Park et al., 2018)
Incineration leachate	*Desulfuromondales*	*Methanobacterium*	(Gao et al., 2017)
Table olive brine processing wastewater	*Desulfuromondales*	*Methanoplanus*	(Marone et al., 2016)

2.3.5.2 Bacterial Community

Table 2.3 shows that different types of electroactive bacteria on the anode might be enriched by combining AD with MEC. Several investigations have shown that electroactive *Geobacter* species predominate in AD-MEC systems (Cai, Han, et al., 2016; W. Liu et al., 2016; Sun et al., 2015). Notably, most electroactive bacteria (such as *Geobacter*) have restricted metabolic flexibility and do not have ability to metabolize complex fermentable organics (Logan, 2009). *Pseudomonas* and *Desulfuromondales* species, on the other hand, are not only electroactive but can degrade aromatic molecules and other complex hydrocarbons as well (Gao et al., 2017). Yet, in AD-MEC systems, a wide variety of fermentative bacteria play a pivotal role in the breakdown of fermentable organics (J. Hao & Wang, 2015).

The relative abundance of fermentative bacteria may increase, which may help speed up the breakdown of complex organics (Chen et al., 2016). A predominancy of fermentative bacteria (*Bacteroides, Anaerolinea, Aminobacterium, and Aminomonas*) that degrade carbohydrates and proteins was also observed (Z. Zhao, Zhang, Ma, et al., 2016). In addition, studies have shown an increase in *Syntrophomonas* and *Syntrophobacter* (Gao et al., 2017). It was discussed that hydrogenotrophic methanogens predominate in AD-MEC systems. Hydrogenotrophic methanogens' high rate of H_2 consumption keeps the partial pressure of H_2 gas low, creating an environment where fermentative bacteria may thrive (Sasaki et al., 2013). Hence, their syntrophic interactions may allow AD-MEC systems to convert complicated feedstocks rapidly and increase in CH_4 production rate.

2.3.6 Conductive Material Amendment

It has been demonstrated that adding conductive materials such as GAC, PAC, or magnetite to MEC and AD-MEC increases CH_4 production, as reported in Table 2.3. LaBarge et al. (2017) improved the performance of their MEC by adding GAC pre-acclimated with methanol/ H_2, which reduced the start-up time and boosted the CH_4 production rate. The establishment of DIET pathways in AD-MEC may be one mechanism related to the enhanced performance generated by the conductive additives. CH_4 generation in AD-MEC was mostly from bulk solution rather than electrode surfaces, therefore adding conductive materials to the reactor to promote DIET acting on electroactive microorganisms might be a feasible improvement technique (An et al., 2020).

Table 2.3 Summary of conductive material amendment in CH_4 producing MECs and AD-MECs

Conductive material	Dosage	Substrate	T (ºC)	Voltage (V)	↑ in CH_4 production	Ref
Pre-acclimated GAC	-	CO_2	31	-0.6 (cathode, vs. SHE)	Start-up time ↓	(LaBarge et al., 2017b)
AC	3 g/L	Lignite	35	0.33	3.3%	(Piao et al., 2019)
AC	3 g/L	Lignite	35	0.67	26.7%	(Piao et al., 2019)
Biochar	1 g/g DM	WAS	55	0.6	44.4%	(C. Yin et al., 2019)
Nitrate	1 g/L	WAS	35	0.8	8.9%	(Peng et al., 2019)
Pre-acclimated GAC	5 g/L	Synthetic wastewater	35	0.5	34%	(Xu et al., 2019)
Pre-acclimated PAC	5 g/L	Synthetic wastewater	35	0.5	32%	(Xu et al., 2019)
AC	1 g/L	Glucose	35	0.5	5.8%	(Feng et al., 2020)
Magnetite	20mM	Glucose	35	0.8	12.9%	(Vu et al., 2020)
Magnetite	20mM	Dairy wastewater	35	0.6	288%	(Baek et al., 2020)
CBC*	0.15% (w.)	Cow manure and aloe peel waste	36	0.6	120.68%	(Xing et al., 2021)

*Coconut-shell-derived bio-based carbon

2.4 Nutrient Recovery

For bio-energy production, organic biodegradable waste valorization, and possible recovery of rich nutrient resources, which are concentrated in the residual (mineralized) digestate, AD of sewage sludge, organic biological waste (crop leftovers and other food waste), and animal manure is one of the most efficient and ecologically beneficial processes (Vaneeckhaute et al., 2017). Because these digestates cannot or only sparingly be returned to agricultural land in their basic unprocessed form, further sustainable development of this technology is now restricted, especially in high-nutrient locations. Legislative restrictions (low nitrogen (N) and phosphorus (P) fertilization levels within the context of environmental regulation), as well as logistical (high transport and storage costs due to volume), are

the primary causes of this technological hurdle. Hence, digestate must undergo further processing to concentrate and recover the nutrients as high-quality end-products, so avoiding the problems associated with direct application. Sustainability in the collection and recycling of nutrients from digestate is a problem for AD plants. To put it another way, the current 'waste' problem may be converted into an economic opportunity by both satisfying regulatory drivers and creating an internal income stream.

About all the nutrients in an AD system are found in the liquid and solid phases. Most of the total N is converted to ammonium and free ammonia by anaerobic hydrolysis and fermentation (Shi et al., 2018). Phosphorus in solution is often found in the form of orthophosphate, which is strongly pH dependent. Around 90% of the P in the digestate precipitates out with the metals, leaving just 10% in the solution (Shi et al., 2018). The possible removal and recovery technologies are summarized in the following sections.

2.4.1 Ammonia Stripping

Steam or air is supplied into stripping towers via compressors, while digestate flows in the opposite direction, releasing NH_3 from the liquid to the gas phase (Shi et al., 2018). NH_3 removal from digestate has been used worldwide from lab-scale to full-scale. Nine to ten US full-scale stripping facilities recover NH_3 from digested sludge. Germany has 15 stripping plants by 2015 (Zarebska et al., 2015). NH_4^+ concentration, temperature, pH, retention duration, and gas and liquid flow rates in stripping towers determine NH_3 stripping efficiency. High pH, temperature, air flow, and NH_4^+ concentration would help the NH_4^+/NH_3 equilibrium move toward NH_3. Practical plants add alkali such as lime which is cheap and widely utilized (Shi et al., 2018). Unfortunately, large lime dosages cost a lot. Moreover, pH increases digestate metal precipitation. NH_3 stripping is also complicated by digestate heating, which demands a lot of energy. Most importantly, ammonia stripping only removes N, not recovers it.

2.4.2 Ion Exchange and Adsorption

Ion exchange and adsorption use sorbents in a column bed to remove target molecules like PO_4^{3-} or NH_4^+ from the feed solution. Ionic forces promote ion-exchange, while intermolecular forces cause adsorption. Zeolites and resins can support both processes. Zeolites are the most researched adsorbents. Their enormous holes and negative charges readily absorb cations. After application, zeolites may release NH_4^+ into the soil. Zeolites remove and recover NH_4^+ from digestate in several investigations.

Ion exchange and adsorption are difficult processes. Particle removal is important because suspended particles and precipitates can obstruct sorbent material cavities. Zeolites may also adsorb metals like Mg^{2+} and Ca^{2+}, which compete with the target NH_4^+ and PO_4^{3-} ions. Zarebska et al. (2015) examined zeolite adsorption, NH_3 stripping, and struvite production chemical costs. Zeolites require more chemicals than lime and MgO, hence their chemical cost was greater. Ion exchange and adsorption are straightforward to operate, which may save energy and labor costs (Vaneeckhaute et al., 2017).

2.4.3 Membrane Filtration

Pressure-driven membrane filtration, microfiltration (MF), ultrafiltration (UF), nanofiltration (NF), or reverse osmosis (RO), is a wastewater treatment method. Nevertheless, digestate, manure, and sludge treatment have not yet shown promise in the case of membrane technology (Vaneeckhaute et al., 2017). Due to high operational expenses, few full-scale manure and digestate processing plants have launched commercial pilots (Vaneeckhaute et al., 2017). Particles bigger than 0.1-1 µm can be eliminated by MF, whereas those between 0.01-0.2 µm are retained by UF (colloids) (Zarebska et al., 2015). Both MF and UF can utilize either a ceramic membrane or a polymeric membrane Zarebska et al., 2015). MF and UF are thought to be ineffective in removing dissolved compounds. Hence, following MF or UF

separation, a liquid fraction rich in NH_4-N and a solid fraction high in P can be harvested. Water is readily diffused during nanofiltration (NF) and reverse osmosis (RO), but salts and organic materials are retained. These systems can be used for the aim of reusing water on farms, such as in the flushing of animal pens and for agricultural irrigation (Hjorth et al., 2009). Meanwhile, the volume reduction makes it possible to concentrate the ions in the feed solution. Results of a study showed that RO can concentrate NH_4-N to concentrations of 7-10 g/L, with a retention efficiency of up to 99.8 percent (Ledda et al., 2013). According to Gerardo et al. (2015), the separation efficiency of NH_4-N in NF was only 5-23%, whereas the efficiency of P is 97- 98%. However, it should be noted that the pressure need for NF is lower than RO. The biggest problems associated with membrane technology are membrane blockage and fouling, which need a lot of chemicals and energy (Ledda et al., 2013).

2.4.4 Chemical Precipitation

P recovery can be achieved by a variety of methods, such as adsorption (Rout et al., 2017), metal ion precipitation (N. Xu et al., 2014), and reverse osmosis (Luo et al., 2016). However, these methods produce dense sludge, treatment of which is expensive, thus may only temporarily solve the problem without providing a sustainable solution. Therefore, there is a need for a sustainable and economically viable nutrient recovery process. It is generally accepted that P may be recovered from the liquid phase by crystallization procedures as either magnesium ammonium phosphate hexahydrate (also known as struvite), a slow-release fertilizer, or calcium phosphates, which resemble phosphate rocks (Desmidt et al., 2015). K-struvite is another kind of struvite ($KMgPO_4.6H_2O$). The main difference between K-struvite and struvite ($MgNH_4PO_4.6H_2O$) is the substitution of a smaller K^+ ion for the larger NH_4^+ ion.

Struvite (magnesium ammonium phosphate (MAP), $MgNH_4PO_4.6H_2O$) precipitation is a promising nutrient recovery approach that has been commonly applied to a variety of streams such as anaerobically digested poultry manure

(Yilmazel & Demirer, 2011), urine (Sakthivel et al., 2012), leachate (H. Huang et al., 2014), swine manure (Ryu et al., 2020). Further, with this process, simultaneous N and P recovery is possible, and the product can be used as fertilizer, a fire-retardant barrier on the flammability of cotton fabric and wooden plates (Yetilmezsoy et al., 2020).

Struvite is a white insoluble crystalline substance, and its precipitation occurs when the concentrations of ammonium, magnesium, and phosphate exceed the solubility product under alkaline conditions (Fattah et al., 2008; H. Huang et al., 2014). Struvite precipitation takes place according to the reaction (1) where n = 0, 1, or 2 (S. Li et al., 2020):

$$Mg^{2+} + H_nPO_4^{n-3} + NH_4^+ + 6H_2O \rightarrow MgNH_4PO_4.6H_2O \downarrow + nH^+ \quad \text{(Eq. 2.7)}$$

The occurrence and development of struvite are based on two stages: nucleation and crystal growth (Le Corre et al., 2009). Nucleation is a stage in that crystal birth occurs in liquid media (Le Corre et al., 2009). Ions are combined and form struvite embryos, which is the first state of crystals. After nucleation, crystal growth occurs, and crystals are developed until equilibrium (Le Corre et al., 2009). As follows, the final form and the size of crystals are established according to the kinetics. The time passes through the mixing of the solution of precipitant ions, and the first measured crystal is called induction time. To achieve precipitation of struvite, supersaturation should be maintained in the solution. Supersaturation is a driving force and prerequisite for crystallization on an industrial scale.

High amounts of magnesium and phosphate salts need to be added to obtain an effective N and P recovery through struvite precipitation from anaerobically digested wastes (H. Huang et al., 2014). This is due to the relatively higher abundance of N ions than other struvite-forming ions (Mg and P) in such waste streams. The external addition of such ions in the form of pure chemicals such as MgO or H_3PO_4 is costly and risks the process's financial sustainability (T. Zhang et al., 2009). Therefore, sustainable replacements of pure chemicals are explored to develop an economically viable and environmentally friendly struvite precipitation process. There have been

pilot-scale and full-scale applications of the method for treating crude digestate and wastewater (digested) sludge and manure, respectively.

2.5 Important Parameters for Struvite Precipitation

Thermodynamic instability characterizes struvite precipitation; however, the process may be stabilized by nucleation and crystal growth (Desmidt et al., 2015). In addition, physicochemical process factors including pH, molar ratio, presence of other ions, and temperature have a significant role in crystallization. These variables are associated with the waste stream and treatment method employed during struvite precipitation. The system's efficiency can be maximized, and the recovered struvite can be used as a product if these factors are addressed.

2.5.1 pH

Mg^{2+}, NH_4^+, and PO_4^{3-} concentrations must be higher than the solubility product (K_{sp}) for struvite to occur. Magnesium, ammonium, and phosphorus species and their availability are determined by pH (Le Corre et al., 2009). Formation and precipitation of struvite are greatly influenced by pH since the its speciation components depends on pH.

In contrast to its solubility under acidic conditions, struvite is insoluble in alkaline ones (Ariyanto et al., 2014). This means that the pH of the solution is used to regulate the precipitation process. Typically, a pH of 7–11 is needed for struvite precipitation (Le Corre et al., 2009). Researchers have reported a range of values for the optimal pH for struvite, ranging from 8.0 to 10.7 (J. Wang et al., 2005). After pH 9, it is reported that the purity of the struvite decreases (X. Hao et al., 2013). Moreover, after pH 9, ammonia stripping occurs; hence available NH_4^+ for the precipitation decreases (Le Corre et al., 2009). The process of struvite precipitation involves several interconnected variables. As a result, just the pH impact may be puzzling. For each specific waste and additive, pH should be optimized.

Generally, AD effluents have natural pH (Siciliano et al., 2020). To increase the pH to a desired level, the supplementation of alkaline compounds is needed. NaOH is a commonly used chemical for pH increase (Siciliano et al., 2020). Considering the operational cost, the alkali addition must be considered.

2.5.2 Molar Ratio

When there are equal amounts of Mg^{2+}, NH_4^+, and PO_4^{3-} in a solution, struvite nucleation occurs. Hence, the development of struvite crystals relies heavily on the accessibility of the three components. The actual effluents typically have substantially different molar concentrations of Mg^{2+}, NH_4^+, and PO_4^{3-} ions than those found in laboratory samples. For instance, many wastewaters have more ammonium relative to the other struvite elements in terms of molar quantities (Siciliano et al., 2020). The contrast is most pronounced in AD products like leachate and digestate. The cost of struvite precipitation, which is used to remove phosphorus and ammonium from their contexts, rises because reagents of magnesium and phosphorus must be added to achieve the stoichiometric molar ratios. In this scenario, the effectiveness of the process is proportional to the molar ratios of the three elements, nitrogen, magnesium, and phosphorus. Struvite precipitation designed for phosphorus removal and recovery is a more environmentally friendly option. However, N can also cause environmental problems and struvite precipitation can achieve both removal and recovery of N and P. Moreover, by increasing molar ratios, obtained product can be maximized, meaning that end-product benefits and value can be increased. The cost is an important parameter to think about while increasing molar ratios with additives. However, these additives can be by-products or wastes so that the operational cost can be minimized.

Due to the presence of competitive ions in real wastewater, such as Ca^{2+}, Na^+, K^+, Al^{3+}, Fe^{3+}, etc., which may react with Mg^{2+} and PO_4^{3-} ions to reduce their availability for struvite, the reagents should be overdosed in comparison to the theoretical value, even though the molar amounts needed for struvite precipitation are the same (Le

Corre et al., 2009). Since the optimal molar ratios vary so greatly on the chemical-physical features of wastewater, they must be evaluated on a case-by-case basis. Dosages can also change based on the specific chemicals used as magnesium and phosphorus sources.

2.5.3 Temperature

Compared to pH or the presence of other ions, temperature has less of an impact on the precipitation of struvite. Nonetheless, it may have an impact on crystal shape or solubility (Le Corre et al., 2009). Aage et al. (1997) showed that as the temperature rises, struvite becomes more soluble. The influence of various temperatures (20°C to 30°C) on struvite precipitation was examined by Ariyanto et al. (2014). The pace at which struvite crystals grew increased along with the temperature. Struvite precipitation often takes place between 25 and 35 °C (Ariyanto et al., 2014). Moreover, ionic activities and the supersaturation coefficient have been reported to increase as the temperature rises from 14 °C to 35 °C, decreasing the efficiency of crystal formation by more than 30% (Ben Moussa et al., 2011). The chemical structure of the solution has a significant impact on the solubility of the struvite in combination with temperature. In essence, various research examined the relationship between the solubility of struvite and the properties of the wastewater where the precipitation takes place (Siciliano et al., 2020).

2.5.4 Presence of Competitive Ions

The struvite precipitation process is complicated by the presence of various ions in the influence stream and additives. There are a few potential ways in which these ions might influence the struvite precipitation process. It has been shown that waste streams may contain the ions $Ca^{2+,}$ Cu^{2+}, Zn^{2+}, Al^{3+}, CO_3^{2-}, and SO_4^{2-} (Li et al., 2016). According to physicochemical factors, these ions can precipitate instead of struvite. Table 2.4 lists several possible precipitates that may form. The pace of a reaction, its

efficiency, the purity of a crystal, and even its form can all be altered by these factors (Li et al., 2016).

There may be competition for ammonium in the synthesis of struvite compounds from mono-valent ions like Na^+ and K^+, leading to the creation of $MgNaPO_4$ and $MgKPO_4$ rather than MAP (Siciliano et al., 2020). Since influent contained high Na^+ ions, Na salts were observed in the product (Siciliano, 2016). cPotassium salts, including $MgKPO_4$, have been found in the recovered solid of the MAP precipitation procedure in various studies (Di Iaconi et al., 2010). Some research, however, claims that high concentrations of $NH4^+$ are necessary for $MgKPO_4$ synthesis (Pastor et al., 2010).

Table 2.4. Possible precipitates

Name	**Formula**
Struvite	$MgNH_4PO_4.6H_2O$
K-Struvite	$MgKPO_4$
Newberyite	$MgHPO_4.3H_2O$
Bobierrite	$Mg_3(PO_4)_2.8H_2O$
Trimagnesium phosphate	$Mg_3(PO_4)_2.22H_2O$
Hydroxyapatite	$Ca_5(PO_4)_3(OH)$
Whitlockite	$Ca_3(PO_4)_2$
Oactacalcium phosphate	$Ca_8(HPO_4)_2(PO_4)_5.5H_2O$
Monenite	$CaHPO_4$
Brushite	$CaHPO_4.2H_2O$
Calcium carbonate	$CaCO_3$
Calcium hydroxide	$Ca(OH)_2$
Brucite	$Mg(OH)_2$
Magnesium carbonate	$MgCO_3$
Magnesium bicarbonate	$Mg(HCO_3)_2$
Ammonium bicarbonate	NH_4HCO_3

Very high levels of alkalinity can also prevent struvite from forming. In particular, HCO_3 and CO_3^{2-} may lead to the development of $MgCO_3$, $Mg(HCO_3)_2$, and NH_4HCO_3 (H. Huang et al., 2017). This decreases the availability of these two elements, which are necessary during struvite precipitation. Furthermore, the presence of Ca^{2+} ions have a major negative influence on MAP precipitation. Struvite

nucleation can be blocked by high calcium levels in the solution (B. Li et al., 2016). Moreover, apatite and hydroxyapatite can be formed by the interaction of calcium ions with orthophosphate. These processes deplete the solution of phosphate ions, lowering the potential for struvite to develop. Even though struvite can precipitate with high Ca^{2+} concentration, the product purity declines (Hao et al., 2013). Important considerations include the possibility that the product's shape and size will be affected by the presence of other ions. When used as fertilizer, the quality of the product must be ensured at a desired level. Li et al. (2016) showed that a Ca:Mg ratio of less than 0.5 is necessary for practical operation for struvite precipitation. Interference with the struvite precipitation can be avoided by pretreating Ca-rich waste streams, such as dairy industry effluent, before the precipitation. Product value and process capital and operating expenses should both be factored into any economic evaluation.

2.5.5 Reactor Configurations

2.5.5.1 Stirred Tank Reactors

Lab experiments often make use of stirred tank reactors (STR) (Siciliano et al., 2020). From a design standpoint, they are incredibly straightforward units that just need a mixing system to homogenize the components, and regulating the operating parameters (Aguado et al., 2019). The generation of struvite is influenced by the internal mixing conditions of the reactor (Stratful et al., 2004). If the solution and solid phases are mixed well enough, more ions will be transferred from the solution to the solid phase, facilitating the nucleation and development of the crystals. In research using both synthetic and actual urine samples, Liu et al. (X. Liu et al., 2014) found that an increase in mixing energy from 160 to 240 rpm improved struvite crystal precipitation efficiency by 33%. Moreover, insufficient stirring energy raises local solution oversaturation, which in turn encourages the regional production of new struvite crystals without fostering their expansion. As a result, the rate at which

crystals develop in a reactor rises in response to increased turbulence (Le Corre et al., 2009). At a certain mixing speed, however, the benefits to crystal development and morphology no longer exist (X. Liu et al., 2014). In fact, struvite crystal formation was found to be limited at velocities over 500 rpm (Stratful et al., 2004).

The mixed reactors can function either continuously or in batches. The production and precipitation of struvite take place in the same apparatus in a batch reactor, which operates according to a sequence of stages. The precipitation stage, on the other hand, is handled in a different unit from the struvite synthesis in a continuous reactor. The generation of struvite can be controlled more easily and efficiently in stirred tank reactors than in other technologies, which is why they are widely used. In particular, STRs don't have the flow control issues that plague fluidized bed reactors (FBRs), nor do they introduce plant complications (Iqbal et al., 2008). Furthermore, STR may be employed in either batch or continuous settings without any difficulty. cIn addition, the hydraulic reaction period may be brought down, resulting in excellent process performance (Siciliano et al., 2020).

2.5.5.2 Fluidized Bed Reactors

In the conventional arrangement, the fluidized bed reactors (FBR) have a central body with a mostly longitudinal development, which is where crystal nucleation and growth occur (Ohlinger et al., 2014). Typically, the chemicals required for struvite nucleation and the waste stream are fed from the base of the reactor. The liquid drains from the reactor's top to another clarifier, where some portion is recycled back down to the reactor (Bhuiyan et al., 2008). The effluent and suspended struvite crystals are recirculated from the top to the bottom of the reaction tank in some designs. The recirculation flowrate is very sensitive to the features of the reactor and the kind of wastewater being treated (Siciliano et al., 2020). The nucleation of struvite crystals originates in the main part of the FBR, either through interactions with other struvite particles or with seeding inert elements comprising the fluidized bed (Battistoni et al., 2005). Either aeration or a sufficiently high recirculation flow rate will ensure

that the particles in the reactor are fluidized (Battistoni et al., 2005). In addition to bed fluidization, air insufflation also promotes pH rise, therefore less alkaline chemicals are needed to achieve pH values favorable for struvite nucleation (Battistoni et al., 2005). Le Corre et al. (2007) were able to remove up to 80% of phosphorus in a batch FBR laboratory pilot plant.

In some of the studies, FBR was constructed from a series of zones whose diameters gradually increased (Fattah et al., 2008). As fluidized particles undergo a change in diameter, turbulent eddies form above each transition zone, facilitating proper mixing and size classification (Rahaman et al., 2014). For example, phosphate removals of 75-85% were reported at upflow velocities of 400-410 cm/min (Bhuiyan et al., 2008). Fattah et al. (2008) found that at pH 7.5, the reactor with the increasing diameter removed more than 90% of the phosphate.

Fluidized bed reactors accelerate struvite crystal formation (Le Corre et al., 2009). In FBR, MAP particle dimensions grow over time, although numerous modalities (seed inert substance, metallic meshes, internal seeds recycling, etc.) might restrict fine particle generation (B. Li et al., 2019). Moreover, FBR requires more management than stirred tank reactors. Controlling bed fluidization and fine particle recycling flows could be problematic. Also, high flow rates cause high energy usage.

2.5.5.3 Bioelectrochemical Systems

BES might also help recover nutrients via struvite (Cusick & Logan, 2012). Both MFCs and MECs can be used for struvite precipitation. Compared to STR and FBR reactors, BES systems have been developed recently. No full-scale or pilot-scale applications have been constructed. Chemical addition, CO_2 stripping, or electrolysis can regulate struvite recovery from waste streams. Most struvite recovery research involves increasing solution pH using chemical bases (NaOH, $Mg(OH)^2$, $Ca(OH)^2$) and removing CO_2 with aeration (Siciliano et al., 2020). These procedures cost $140–460 per struvite ton (Cusick & Logan, 2012). Chemical bases can make up

97% of struvite precipitation costs (Jaffer et al., 2002). Minimizing operational expenses might turn recovered struvite into money.

MECs can offer a high local pH to induce struvite precipitation on the cathode without base chemicals (Almatouq & Babatunde, 2017). Many MEC studies have employed high local pH to precipitate harmful heavy metals and struvite crystals without base chemicals (Cusick & Logan, 2012). Moreover, MECs can produce H_2 as an additional benefit.

Phosphorus recovery in the form of struvite was studied by Cusick and Logan (2012) via a single-chamber MEC. All of the cathodes were stainless steel, either 304 mesh or flat plates (Cusick & Logan, 2012). The removal of phosphorus varied between 20% and 40%, with more removal achieved with mesh cathodes than with flat plates (Cusick & Logan, 2012). While alternative techniques for forming struvite need far more energy, with only 0.2-0.3 Wh/L, they were able to reduce the phosphate concentration in the digestate supernatant by 70%-85% (Cusick et al., 2014). Moreover, Almatouq and Babatunde (2017) used a double-chamber electrolytic microbial cell to remove 95% of the phosphorus from synthetic wastewater. The phosphorus was removed as struvite. With a voltage of 1.1 V, maximum H_2 production rate was 0.28 m^3H_2/m^3d. Although BES shows promising results, their widespread use in industry is still some distance off; hence, more research is required.

2.5.6 Magnesium Sources

Magnesium and, if ammonium need to be eliminated, phosphorus compounds, are essential to the struvite precipitation processes, as mentioned. The efficiency of a process is profoundly affected by the selection of the reagents to be used. Indeed, the reagents ought to be efficient, user-friendly, and free of substances that might impede the struvite nucleation procedure. In addition, determining the efficacy of

unconventional reagents at a low cost is crucial to reducing the treatment's financial burden (Xavier et al., 2014).

The treatment for MAP precipitation often involves the use of pure reagents such as $MgSO_4$, $MgCl_2.6H_2O$ and MgO (Siciliano et al., 2020). Several of these salts, including magnesium sulfate ($MgSO_4$) and magnesium chloride ($MgCl_2$), are advantageous because they are extremely soluble, allowing for the recovery of a precipitate with a high purity degree (Uysal et al., 2010).

Recently, researchers have been focusing on low-cost and sustainable magnesium sources. Several substances, including wood-ash (Sakthivel et al., 2012), salt water (B. Liu et al., 2013; X. Liu et al., 2014; Rubio-Rincón et al., 2014), seawater bittern (S. I. Lee et al., 2003; Siciliano & De Rosa, 2014), magnesite (Gunay et al., 2008; H. Huang et al., 2014; Krähenbühl et al., 2016; Quintana et al., 2004)., and waste magnesite powder (Al-Mallahi et al., 2020; Astals et al., 2021; Chimenos et al., 2003; Quintana et al., 2004; Romero-Güiza et al., 2015) have been tested.

- **Wood ash:** Intending to encourage the precipitation of struvite, Sakthivel et al. (2012) looked into the viability of using wood combustion ashes as a magnesium source. 87% of entering phosphorus was eliminated when wood ashes were added to the urine, although hydroxyapatite formation was still the primary byproduct (Sakthivel et al., 2012). Moreover, the recovered precipitate may not comply with the regulations for fertilizers because of the significant content of metal compounds in combustion ashes.
- **Salt water:** The magnesium in seawater, at around 146 kg Mg^{2+}/m^3, may be used to precipitate struvite at a reasonable cost (X. Liu et al., 2014). Recovery of phosphorus by MAP production from isolated human urine was investigated by Rubio-Rincón et al. (2014). At a Mg:P molar ratio of 3.3:1, 99% of the phosphorus was removed from the seawater in about 10 minutes when it was combined with either non-hydrolyzed or hydrolyzed urine (Rubio-Rincón et al., 2014). In other studies, fine crystal formation and co-

precipitation of calcite together with struvite were found due to the usage of saltwater (B. Liu et al., 2013; X. Liu et al., 2014).

- **Seawater bittern:** The bittern found in seawater is a byproduct of the production of sea salt and consists primarily of $MgCl_2$ with trace quantities of other inorganic chemicals. It might be a viable low-cost source of magnesium because its Mg^{2+} level is much greater than that of seawater (S. I. Lee et al., 2003). By adding bittern to a synthetic solution, phosphorus levels were reduced to the same extent as when using $MgCl_2$ or saltwater as a magnesium ions source (H. Huang et al., 2014). For the elimination of NH_4^+ from leachates and digestate of calf dung, Siciliano et al. (2014) discovered that seawater bittern may be employed effectively.
- **Magnesite ($MgCO_3$):** It is a common mineral rock; however, it requires proper pretreatments due to its limited solubility in water. Magnesite was employed to test the efficacy of ammonium removal from landfill leachate (Gunay et al., 2008). Specifically, HCl was used to prepare the magnesite such that a significant amount of magnesium could be extracted as a solution. 91% of the ammonium was recovered as struvite (Gunay et al., 2008). The use of $MgCO_3$ rather than $MgCl_2$ was estimated to reduce process costs by 18.3% (Gunay et al., 2008). Unfortunately, a sizable amount of HCl was needed to completely dissolve the magnesium in the magnesite. Further research has shown that by calcining magnesite at high temperatures, a by-product may be created that is rich in MgO and can be used as a magnesium source (H. Huang et al., 2014; Krähenbühl et al., 2016; Quintana et al., 2004). In the struvite precipitation procedure, Quintana et al. (Quintana et al., 2004) found that BMP derived from magnesite calcination performed far worse than pure MgO. Justification for this may be found in the fact that the amount of Mg^{2+} accessible in BMP is less than that in pure MgO (H. Huang et al., 2014; Krähenbühl et al., 2016; Quintana et al., 2004).
- **Waste magnesite powder:** A trace quantity of dust is produced and transported by the exhaust gas during the kiln processing of magnesite. Then,

an electrostatic precipitator is used to get rid of the dust called waste magnesite powder (WMP). Chimenos et al. (2003) used WMP to precipitate struvite from cochineal insect effluent. It was shown that WMP could extract phosphorus as struvite, but it took 6.5 times more compared to pure MgO (Chimenos et al., 2003). Moreover, Quintana et al. (Quintana et al., 2004) demonstrated that WMP precipitates struvite over time due to phosphate loss. WMP was less reactive than pure MgO, hence removal process took longer. Boosting WMP reactivity reduces reaction time. Al-Mallahi et al. (2020) investigated the effect of calcination of WMP on P recovery. It was determined that 1 g/L of calcined WMP and a reaction time of 2 hours were optimal precipitation conditions for the liquid fraction digestate(Al-Mallahi et al., 2020). WMP was calcinated at 900ºC for 0.25 h, resulting in a 96% reduction in phosphorus for the synthetic solution and a 75% reduction for the actual digestate (Al-Mallahi et al., 2020). Moreover, Romero-Güiza et al. (Romero-Güiza et al., 2015) and Astals et al. (2021) investigated the stabilizing agent as the magnesium phosphate resulting from pre- mixing MgO and phosphoric acid on struvite precipitation. Experimental results demonstrated that this reagent caused the precipitation of the magnesium phosphate mineral phase (bobierrite or newberyite). For, Newberyite-rich sample NH4-N removal was 66–73% from pig manure (Astals et al., 2021).

2.5.7 Phosphate Sources

P-based chemicals are typically H_3PO_4 and phosphate salts like Na_3PO_4, Na_2HPO_3, and NaH_2PO_4 for struvite precipitation (Siciliano et al., 2020). These chemicals allow highly pure struvite and extremely efficient ammonium removal rates. Unfortunately, using pure reagents consumes natural P resources and drives up the cost of the process (Siciliano et al., 2020). Hence, it's important to find inexpensive and non-traditional phosphorus sources that can be used in the struvite precipitation

process. The usage of P by-products has received very little attention in the scientific community thus far.

Huang et al. (2014) used waste phosphoric acid to remove NH_4^+ from landfill leachate using phosphorus. At pH 9 and Mg:P:N ratio of 1.2:1:1, ammonium removal was comparable to pure phosphate salts. By pairing H_3PO_4 waste with low-cost MgO as the magnesium supply and alkali compound for pH adjustment, the NH_4^+ removal was 83% (H. Huang et al., 2014). On the other hand, Al^{3+} in phosphoric acid waste competed for phosphate ions, hindering struvite production (H. Huang et al., 2014). Moreover, bone meal, a byproduct of meat waste thermal treatment, was employed as a low-cost phosphate source for MAP precipitation (Siciliano, 2016; Siciliano et al., 2013; Siciliano & De Rosa, 2014). This by-product is seldom used as a fertilizer in Europe and is mainly landfilled (Coutand et al., 2008; Deydier et al., 2005). Hence, using bone meal for struvite precipitation is profitable because it recovers its P content and produces a more valuable chemical containing PO_4^{3-} and NH_4^+. NH_4^+ was recovered from methanogenic landfill leachates and calf dung digestates using bone meal and seawater bittern as PO_4^{3-} and Mg^{2+} sources, respectively (Siciliano, 2016; Siciliano et al., 2013; Siciliano & De Rosa, 2014). The bone meal was carefully combined in sulfuric acid solutions to dissolve its phosphorus content (Siciliano, 2016). H_2SO_4 limited bone meal calcium breakdown, which generally remained insoluble as $CaSO_4$ (Siciliano, 2016). By combining bone meal with seawater bittern, 95% of NH_4^+ and 99% of PO_4-P added were eliminated from landfill leachate (Siciliano, 2016). Using the same reactants, digestates of calf dung reduced NH_4^+ by 90% and recovered PO_4-P by 99% at pH 9 and Mg:P:N = 1.3:1.3:1 (Siciliano & De Rosa, 2014). Moreover, Darwish et al. (2017) discovered the greatest phosphorus content in waste fish bone ash. Wastewater treatment yielded high-purity MAP and 90% ammonium abatement (Darwish et al., 2017).

CHAPTER 3

MATERIALS AND METHODS

3.1 AD-MEC Integration

There were in total of three AD-MEC sets in this thesis. The summary of three AD-MEC sets conducted in the thesis is presented in Figure 3.1.

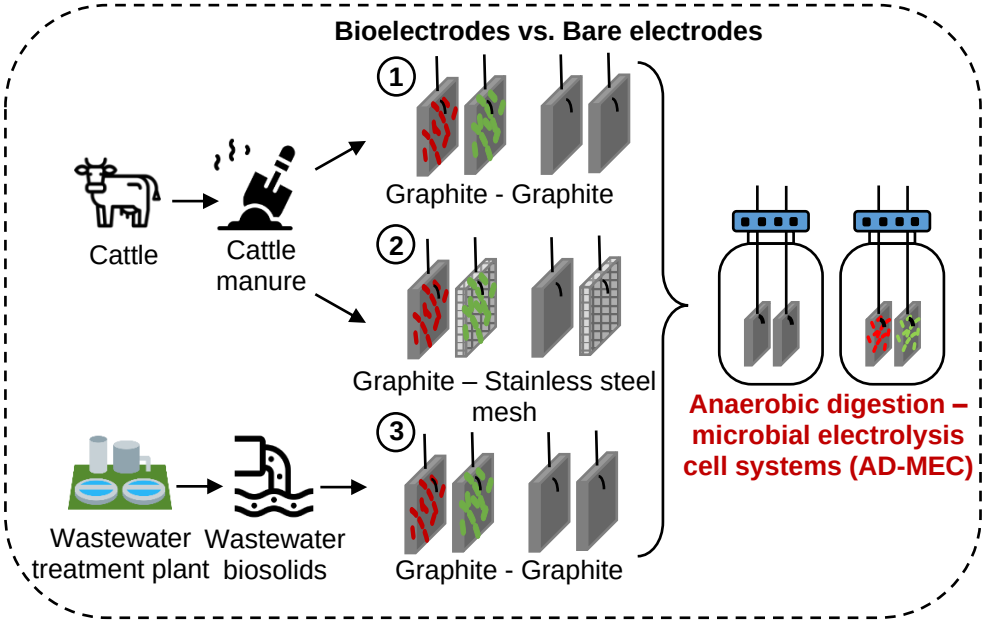

Figure 3.1. Summary of AD-MEC sets conducted in the thesis

3.1.1 Inoculum, Substrate, and Media

3.1.1.1 Set 1: Cattle Manure Fed AD-MEC Using Graphite – Graphite Electrodes

Cattle manure was collected from the feed tank of a full-scale anaerobic digester treating cattle manure in Ankara, Turkey. The raw cattle manure was blended for 15

minutes for homogenization. Inoculum sludge was collected from a mesophilic anaerobic digester of a municipal wastewater treatment plant in Eskisehir, Turkey. The samples were stored at 4 ºC until use. Characteristics of the samples are presented in Table 3.1.

Table 3.1. Characterization of cattle manure and inoculum (AD seed) used in Set 1

Parameters	**Cattle manure**	**Inoculum**
COD (mg/L)	146,800 ± 3,100	13,000 ± 8
sCOD/TCOD (%)	15.1 ± 0.8	3.9 ± 0.2
TS (mg/L)	124,000 ± 1,400	34,000 ± 6
VS (% of TS)	78 ± 0.04	56 ± 0.1
pH	7.84	7.55

Three different media compositions were used in the study: 100 mM PBS, no-PBS, and 5 mM PBS media. 100 mM PBS media contained $NaH_2PO_4 \times H_2O$ 9.94 g/L, $Na_2HPO_4 \times H_2O$ 5.5 g/L, NH_4Cl 310 mg/L, KCl 130 mg/L, $NaHCO_3$ 2.5 g/L, 81.2 mL/L of mineral and 26 mL/L vitamin solutions (Siegert, Li, et al., 2014). The composition of the mineral and vitamin solutions is given in Table 3.2. Phosphate compounds were eliminated from the media and named "No-PBS" (containing NH_4Cl 310 mg/L, KCl 130 mg/L), which contained the same amounts of $NaHCO_3$, minerals, and vitamins. By adding electrolytes as phosphate compounds, NaCl and doubled $NaHCO_3$, 5 mM PBS media (containing $NaH_2PO_4 \times H_2O$ 0.53 g/L, $Na_2HPO_4 \times H_2O$ 0.23 g/L, NH_4Cl 310 mg/L, KCl 130 mg/L, NaCl 1 g/L, $NaHCO_3$ 5 g/L) was prepared. The mineral and vitamin solutions were the same for all types of media (Siegert, Yates, et al., 2014). The comparison between different media used in Set 1 is given in Table 3.3. PBS and mineral solution mixture were sparged and purged for 40 minutes with N_2 and autoclaved. It was cooled down with a flow of N_2. Separately sterilized anaerobic vitamin and bicarbonate solutions were added in an anaerobic glovebox (Plas Labs 818-GB, MI, USA). The medium used for all experiments was prepared as a 6.5X stock solution.

Table 3.2. The composition of mineral and vitamin stock solutions

Mineral Solution (g/L)	**Vitamin Solution (g/L)**
Nitrilotriacetic Acid: 1.5	Pyridoxine-HCl: 0.0625
$MgSO_4.7H_2O$: 3.0	Thiamine-HCl: 0.03125
NaCl: 1	Riboflavin: 0.03125
$MnSO_4.2H_2O$: 0.5	Nicotinic Acid: 0.03125
$NiCl_2.6H_2O$: 0.2	Calcium Pantothenate: 0.03125
$FeSO_4.7H_2O$: 0.1	Vitamin B12: 0.03125
$CoCl_2$: 0.1	p-Aminobenzoic Acid: 0.03125
$CaCl_2.2H_2O$: 0.1	Lipoic (Thioctic) Acid: 0.03125
$ZnSO_4$: 0.1	Biotin: 0.0125
$CuSO_4.5H_2O$: 0.01	Folic Acid: 0.0125
$AlK(SO_4)_2$: 0.01	
H_3BO_3: 0.01	
$Na_2MoO_4.2H_2O$: 0.01	
Na_2SeO_3: 0.01	
Na_2WO_4: 0.01	

Table 3.3 The comparison of different media used in Set 1

Salt solution composition	**100 mM PBS**	**No-PBS**	**5 mM PBS**
NH_4Cl (g/L)	0.31	0.31	0.31
KCl (g/L)	0.13	0.13	0.13
$NaH_2PO_4x2H_2O$ (g/L)	11.24	-	0.6
Na_2HPO_4 (g/L)	4.88	-	0.2
NaCl (g/L)	-	-	1
Sodium bicarbonate (g/L)	2.5	2.5	5
Conductivity (mS/cm)	4.4	1.1	2.6

3.1.1.2 Set 2: Cattle Manure Fed AD-MEC Using Graphite – Stainless Steel Electrodes

As the experimental sets were conducted at different times fresh cattle manure was collected before each set and characterization was performed similarly (Table 3.4). In this set, the inoculum was collected from the effluent of a lab-scale mesophilic AD treating cattle manure in the presence of 5 mM PBS media. Details and activities about the continuously operated lab-scale reactor are given in Appendix A. Before

the use of this seed, a specific methanogenic activity assay (SMA) has been conducted as described below:

Two serum bottles with a total volume of 110 mL were split to serve as the control and test with the duplicate operation. A known quantity of acetic acid (COD concentration of 3000 mg/L in the reactor), 30 mL of seed, 10 mL of 5 mM PBS media, and 25 mL of deionized water were added to the reactors. To achieve the same active volume, all other variables were held constant in the control reactors while deionized water was introduced in place of acetic acid. Estimates of the activity are expressed as a ratio of actual to hypothetical methane output. The seed was deemed appropriate for use in the reactors if the inoculum's activity was more than 70%.

In Set 2, 5 mM PBS media was used in Set 2 (See Table 3.3 for composition).

Table 3.4 Characterization of cattle manure and inoculum (Lab-scale reactor seed) used in Set 2

Parameters	**Cattle manure**	**Inoculum**
TS (mg/L)	103,000 ± 600	78,500 ± 600
VS (% of TS)	78 ± 0.06	65 ± 0.4
pH	7.8	7.8

3.1.1.3 Set 3: WBS Fed AD-MEC Using Graphite – Graphite Electrodes

Primary sludge (PS) and waste activated sludge (WAS) were obtained from the primary and secondary sedimentation tanks of a municipal treatment plant in Eskişehir, Turkey. PS and WAS were mixed at a 30:70 ratio (v:v), and the mixture is named WBS. Inoculum was collected from the digester of the same wastewater treatment plant in Eskisehir, Turkey as in Set 1. The samples were stored at 4 ºC until use. Characteristics of the samples are presented in Table 3.5. Similar to Set 2, 5 mM PBS media was used during biofilm formation and AD-MEC operation stage.

Table 3.5 The characterization of WBS and inoculum (AD seed) used in Set 3

Parameters	WBS	Inoculum
COD (mg/L)	33,500 ± 899	19,800 ± 98
TS (mg/L)	31,600 ± 500	33,300 ± 100
VS (% of TS)	59 ± 0.1	51 ± 0.2
pH	6.36	7.6

3.1.2 Reactor Construction

Two types of reactors were used in this study. H-shaped double chamber MECs of a total volume of 300 mL were used to develop cathode biofilms. The active volume in each compartment was 100 mL, while the headspace volume was 50 mL. The side-arms that connected the chambers had a length of 3.8 cm and an inner diameter of 2.4 cm (Figure 3.2). The chambers were separated with a Nafion 117 proton exchange membrane (PEM) and sealed with an o-ring. The PEM was pretreated by boiling in 3% H_2O_2 for 1 h, deionized water for 1 h, 0.5 M H_2SO_4 for 1 h, and then deionized water for 1 h. Chambers were held by a screw clamp.

Figure 3.2. Construction of double chamber MECs

Single chamber MECs with an active volume of 65 mL (total volume of 130 mL) were used for anode biofilm development and AD-MEC experiments. All reactor tops were sealed with neoprene stoppers held tight using polypropylene screw caps

with a 2.5 cm center hole (Figure 3.3). The stopper of the voltage-applied reactors had a center hole to hold a reference electrode.

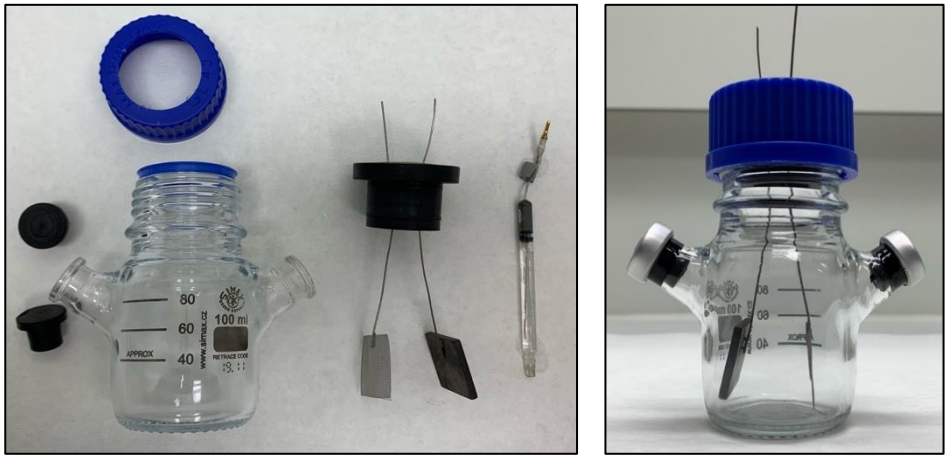

Figure 3.3. Construction of single-chamber MECs

Based on their unique qualities and attributes, graphite blocks and SS mesh were chosen as cathode materials for the methane generation experiment in AD-MEC systems.

Graphite block: Due to its great chemical stability and electrical conductivity, graphite is a good material for electrochemical processes. Even with modest current densities per unit area, cathodes built from these materials with high surface areas might facilitate overall efficient electron transmission (Siegert, Yates, et al., 2014. Additionally, methanogens attach well to carbon materials (Siegert, Yates, et al., 2014).

SS mesh: SS cathodes with high specific surface areas can reach performance comparable to carbon cathodes in MECs (Y. Zhang et al., 2010). Additionally, comparing SS to graphite block cathode, SS is more prone to undergo the hydrogen evolution reaction (Siegert, Yates, et al., 2014).

The study aims to evaluate the relative methane generation rates, efficiency, and system performance of the two cathode materials by comparing them. Insights into how cathode material affects the electrochemical reactions and microbiological

activities involved in methane generation are anticipated to emerge from the investigation. When employing SS as a cathode material, it might give insightful information on the hydrogen evolution process and its effect on methane generation.

In Set 1 and Set 3, both electrodes (anode and cathode) were 2.5x2.5x0.3 cm graphite plates (Eren Karbon Grafit San. Tic. Ltd. Sti, Istanbul, Turkey) with a total of 15.5 cm^2 surface area. Graphite blocks were Grade 2220 and characteristics are given in Table 3.6. The graphite plates were polished using sandpaper, sonicated, cleaned by soaking in 1 M HCl overnight, and rinsed. Titanium wires with a diameter of 1 cm and a length of 15 cm (Timed Metal, Kocaeli, Turkey) were used to connect the electrodes to the circuit.

Table 3.6. Properties of the graphite

Properties	**Values**
Density (gr/cm^3)	1,84
Porosity (%)	10
Bending Resistance (MPa)	57
Compressive Strength (MPa)	124
Particle size (cm)	0,0013
Resistivity μΩ.cm	1.140

In Set 2, graphite was used as the anode and SS was used as the cathode. The graphite anode was identical to the graphite used in Set 1 and Set 3. SS mesh was Type 304 with mesh size 60x60. SS mesh electrodes were connected to a SS wire (Type 304). SS mesh was cut as 2.5x2.5 cm.

All anode and cathode potentials were measured using Ag/AgCl reference electrodes (3 M NaCl, + 0.197 V vs. Standard H_2 electrode (SHE), RE-5B, BASi, U.S.A.) and reported as V vs. Ag/AgCl (Figure 3.4A). Since the Ag/AgCl reference electrodes used in the experimental setup are placed in sludge, clogging or contamination problems may occur at the tip from time to time. This leads to operational problems and setting the correct cathode potential becomes problematic. Therefore, it is necessary to refurbish the reference electrodes periodically. Refurbishment of reference electrodes was done as described by Siegert et al. (2014) by changing the

solution and the tip. Firstly, in Set 1 reference electrodes were directly inserted into the AD-MEC reactors however there were several problems during operation. Thus, the problem was solved by making glass materials called salt bridges. Set 2 and 3 were operated with salt bridges and reference electrodes were placed into these salt bridges. In this way, the reference electrodes were used longer, and overloading problems were eliminated. Images with salt bridges were given in Figure 3.4B. With a 3-electrode design, potentiostats (Interface 1010B, Gamry Instruments, U.S.A.) were employed to apply the desired potentials to the system, with either the anode or the cathode serving as the working electrode (Figure 3.5).

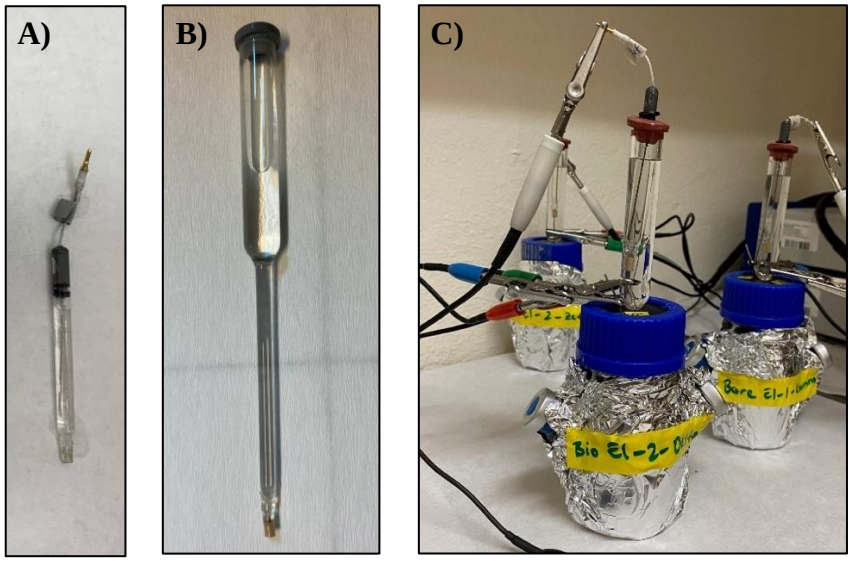

Figure 3.4. A) Reference electrode, B) salt bridge C) AD-MEC operation with a salt bridge

Figure 3.5. Potentiostats used during the operation of the reactors

3.1.3 Experimental Design and Reactor Operation

3.1.3.1 Biofilm Formation

All three experiments had two steps: biofilm formation and AD-MEC operation. In the first step, cathode and anode biofilms were developed simultaneously in different reactor set-ups. The details of cathodic and anodic biofilm development are described below. The bare electrodes that were colonized by the cathodic or anodic biofilm are named bioelectrodes throughout this thesis. These bioelectrodes were then carefully placed in the AD-MEC reactors.

Cathode Biofilm

Methanogens were enriched on the cathode in double chamber reactors under -0.9 V cathode potential. MECs were filled with 100 mM PBS media in Set 1, and 5 mM PBS media in Set 2 and Set 3. During the fed-batch operation of two-chamber MECs water electrolysis was performed in the anode chamber to eliminate any contamination to the cathode surface. Thus, the anode chamber was not inoculated. The cathode chamber was inoculated with AD seed and filled with fresh media containing $NaHCO_3$ as the sole carbon source. During the operation, CH_4 production in the cathode chamber was monitored. When the increase in CH_4 production was lower than 10% in two successive measurements, a new batch cycle was started. To start a new cycle, both chambers were filled with fresh media and some portion of the cathode chamber media (called catholyte) was left in the cathode chamber. 4 batch cycles were performed for cathode biofilm development in each Set. The details of the seed and volume ratio of catholyte left in the reactor are given below:

- Set 1: Cycle 1 started with 10% AD seed, Cycle 2 20% catholyte left, Cycle 3 10% catholyte left, and Cycle 4 10% catholyte left in the cathode chamber.
- Set 2: Cycle 1 started with 20% AD seed, Cycle 2 20% catholyte left, Cycle 3 20% catholyte left, and Cycle 4 0% catholyte left in the cathode chamber.

- Set 3: Cycle 1 started with 20% AD seed, Cycle 2 20% catholyte left, Cycle 3 20% catholyte left, and Cycle 4 0% catholyte left in the cathode chamber.

Anode Biofilm

In the case of anode biofilm formation, single-chamber MECs were used. The reactors were started with 10% AD seed and filled with 100 mM PBS media in Set 1-, and 5 mM PBS media in Set 2 and Set 3. 10 mM acetate was used as a carbon source as most exoelectrogens are capable of consuming acetate (Borole et al., 2009). To figure out which anode potential is suitable +0.4, +0.2, and 0 V anode potential were applied during biofilm formation in Set 1. Based on the tests conducted in Set 1, 0 V was selected for biofilm formation for all three sets (Set 1, Set 2, and Set 3). During biofilm development, current production was monitored continuously. When the current dropped below 0.3 mA, 10 mM acetate was injected into the reactors to start a new cycle.

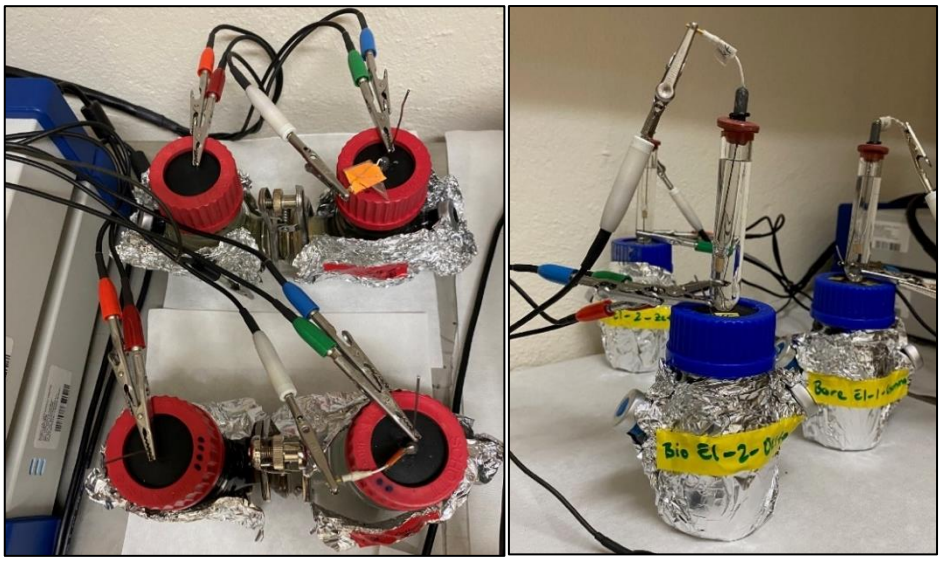

Figure 3.6. Operation of reactors during A) cathode biofilm formation in double chamber MECs, B) anode biofilm formation on the anode in single chamber MECs

Test 1: Biofilm formation on GAC particles

Our study team's simultaneous investigations showed that operating an AD-MEC with both a bare electrode and a bioelectrode fed with WBS did not significantly boost methane generation (Şanlı, 2022). As a result, conductive materials were added to the AD-MEC system to increase methane generation in the case of WBS usage in this thesis. GAC was chosen as a conductive material due to reports of improved methane generation yield and kinetics according to our group and the literature (Ghaderikia, 2022; Kutlar et al., 2022; Odabaş, 2022). The reason for adding GAC is to provide an advantage of surface area for microorganisms to attach. Moreover, the cathode was touched to the GAC particles as an extension of the electrode.

Firstly, a preliminary experimental study (Test 1) was carried out to create a biofilm on GACs and to decide on the GAC concentration in the reactor.

In the blank reactors, only the inoculum was used. Other reactors were fed with WBS. All reactors included 5 mM PBS media and inoculum. In this test, an anaerobic reactor fed with WBS was operated with 25, 35, and 45 g/L bare GACs (2.5 mm, extra pure, Merck, Germany) in accordance with the literature. GAC reactors contained additionally designated GAC concentrations. Conv. AD reactors did not contain any GAC of BioGAC. Single chamber MECs with an active volume of 65 mL (total volume of 130 mL) were used for this set. In test 1, the F/M ratio of all reactors was 1. Accordingly, the total VS in the reactors was 15200 ± 200 mg/L.

Test 2: Operation with BioGAC

After Test 1, the GAC particles collected from the reactors were named BioGAC. As a result of this operation, sludge inside the reactors containing BioGAC was carefully poured out in an anaerobic glovebox. BioGAC was rinsed two times gently with distilled water to remove any sludge that may potentially accumulate in it. Fresh substrate, inoculum culture, and media were then added to the reactor for Test 2. Similar to Test 1, F/M was set to 1 with a corresponding total VS of 14200 ± 300 mg/L. In the 2nd test, the BioGACs and control reactors were set up similarly to Test

1. The highest CH_4 production according to the concentration of BioGACs in this set was selected to use in the AD-MEC operation. A summary of the preliminary tests is given in Figure 3.7.

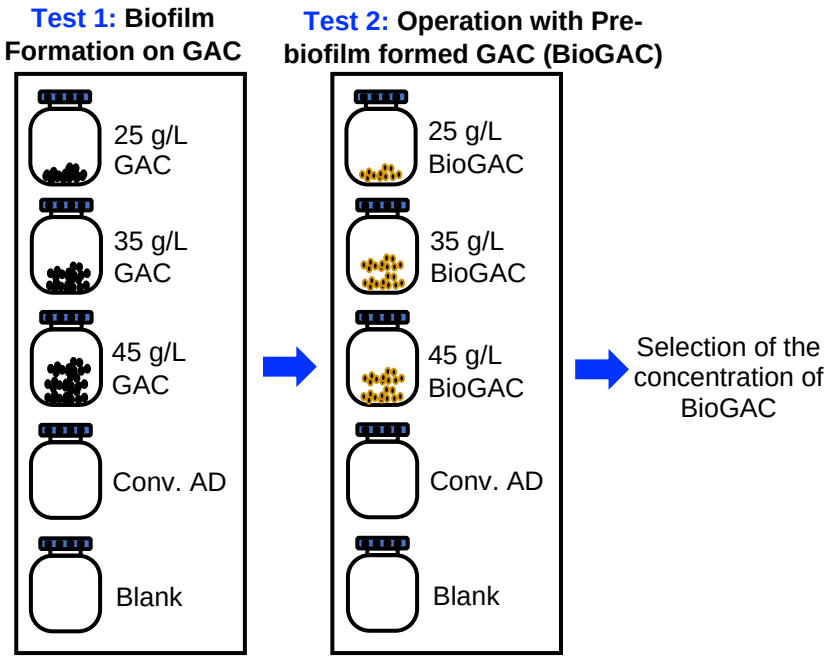

Figure 3.7. BioGAC formation and determination of BioGAC dosage to be used in Set 3

3.1.3.2 AD-MEC Operation

In each set of AD-MEC operations, there were multiple reactors along with some control reactors. The controls in each set will further be described yet each set includes Bioelectrode containing AD-MEC reactors. These are set by placing the bioelectrodes that were developed during the biofilm formation stage without touching the electrode surface into single chamber reactors in an anaerobic glovebox (Figure 3.8). These reactors were then called bioelectrode reactors. At the same time as a control, bare electrodes (without any biofilm) were placed in a single chamber reactor and these reactors were called bare electrode reactors.

Figure 3.8. Anaerobic glovebox used in the experiments

Set 1: Cattle Manure Fed AD-MEC Using Graphite – Graphite Electrodes

During AD-MEC operation, conventional AD (Conv AD, without any electrodes), open circuit control (OC) (only electrodes, but no applied voltage), and blank (only seed, without any electrodes) reactors were set to compare the effects of bioelectrochemical systems. The reactors operated in each cycle are given in Figure 3.9 and Figure 3.10.

Figure 3.9. Operation of the A) AD-MEC reactors and B) controls

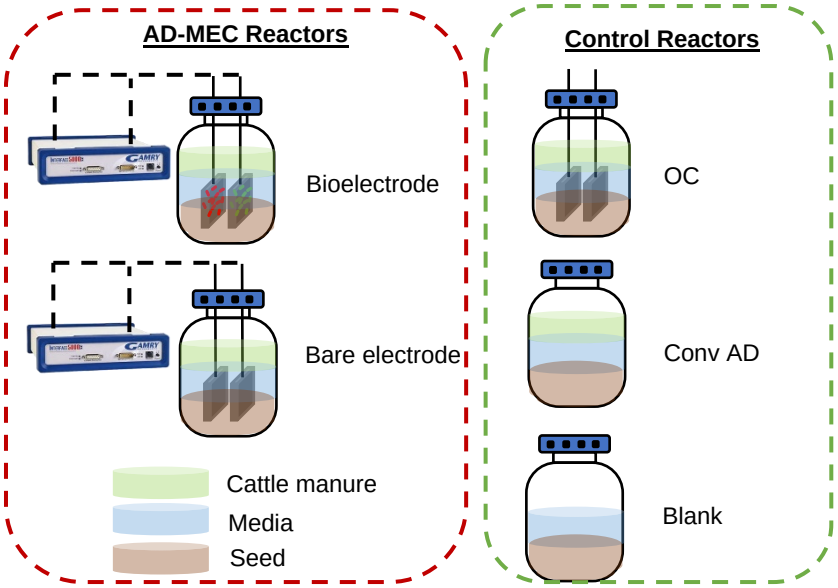

Figure 3.10. The reactors operated in each cycle of Set 1

The fed-batch operation was employed during the AD-MEC stage and in AD-MEC reactors cathode potential was set by using a potentiostat. Initially, the AD-MEC operation was started using 100 mM PBS media. However, as a result of significant inhibition, the reactors were emptied, and subsequently, the actual setup was restarted (See 4.1.1).

After restart, 3 fed-batch cycles were operated: (1) no-PBS media under -0.9 V cathode potential, (2) 5 mM PBS media under -0.9 V cathode potential, and (3) 5 mM PBS media under -1 V cathode potential. Electrodes of bioelectrode, bare electrode, and OC reactors were preserved during all cycles. The schematic representation of the experimental design is given in Figure 3.11. Cattle manure was used as substrate in all cycles. In the first cycle, AD seed was used as inoculum. At the second and third cycles, digestate obtained from the previous cycle was used as inoculum without adding any AD seed. Fresh media and fresh cattle manure were added to the reactors to start a new cycle. All experiments were performed in duplicates. However, in Cycle 3, the duplicate of bioelectrode and bare electrode were not given since an operational problem occurred due to the reference electrodes, and thus the replicate reactor was stopped. The pH was adjusted to 7.0 ± 0.1 at the

start of each cycle. All reactors were incubated at 35 ± 2 °C without shaking. All reactors were covered with aluminum foil to prevent light entrance. In Set 1, the F/M ratio of all reactors was 1. Accordingly, the total VS in the reactors was 19,000 ± 450 mg/L.

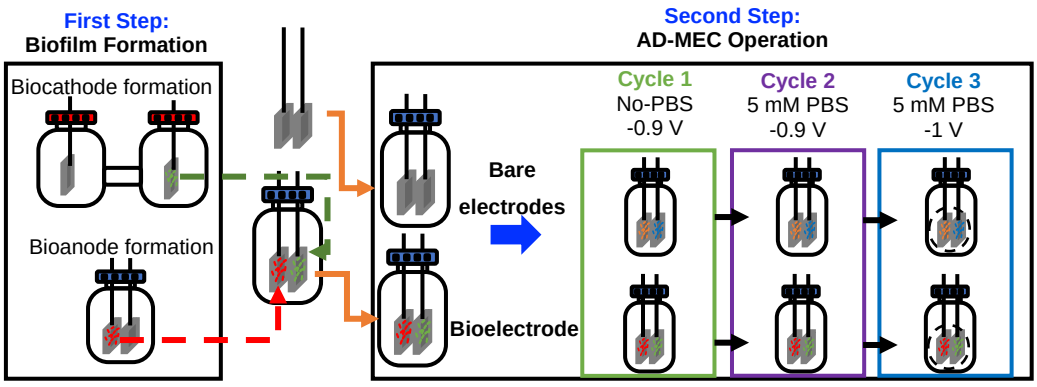

Figure 3.11. Schematic representation of the experimental design of Set 1

Set 2: Cattle Manure Fed AD-MEC Using Graphite – SS Mesh Electrodes

Similar to Set 1, biofilm-formed graphite anodes (bioanodes) and biofilm-formed SS mesh cathodes (biocathodes) were transferred to single-chamber reactors inside the anaerobic glovebox. Bare electrodes were also put into single-chamber reactors. 3 fed-batch cycles were completed in Set 2. In the first cycle, - 0.9 V cathode potential was applied. Each cycle had similar control reactors as in Set 1 (Figure 3.12).

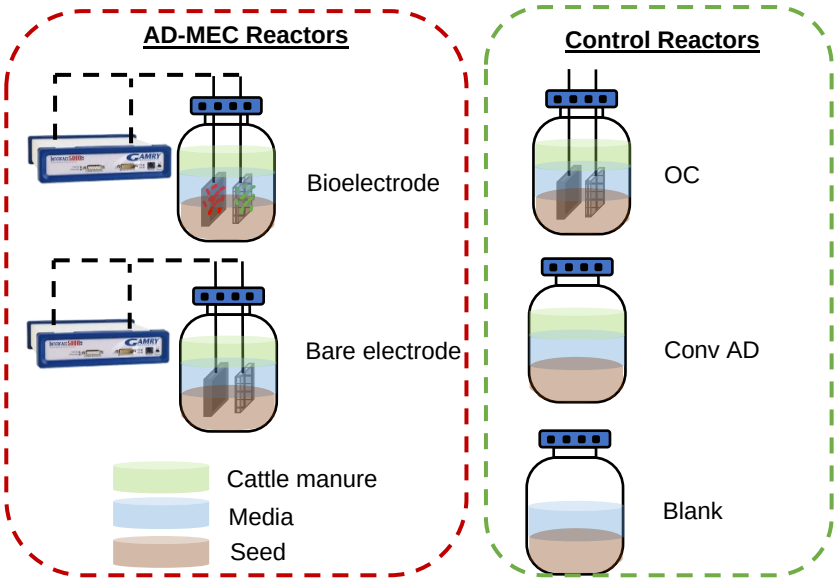

Figure 3.12. The reactors in each cycle of Set 2

After the first cycle, reactors were emptied and fresh cattle manure, seed, and media were put into reactors. The electrodes of Bioelectrode reactors and Bare electrode reactors were preserved for Cycle 2. But in Cycle 2, new bare electrode reactors were also set to investigate the effect of bare electrodes in different cathode potentials. This new reactor couple was called the New Bare electrode. In terms of the reactor types operated this is a major difference between Set 1 and Set 2. The original time zero bare electrode reactors had no biofilm at t = 0, but after Cycle 1, they had biofilm on the electrodes. Therefore, at the start of Cycle 2, new bare electrode-containing reactors were also operated. In Cycle 2, - 1 V cathode potential was applied. Moreover, in this set the electrodes of the OC were also changed with new bare electrodes in each cycle.

After Cycle 2, similarly, the reactors were emptied and filled with fresh cattle manure, seed, and media. The electrodes of Bioelectrode and Bare electrode reactors were preserved. Yet, the electrodes of the New Bare electrode reactors were replaced with bare ones. In Cycle 3, - 0.95 V cathode potential was applied. The summary of the experimental design of Set 2 is given in Figure 3.13. In Set 2, the F/M ratio of all reactors was 1. Accordingly, the total VS in the reactors was 16,000 ± 800 mg/L.

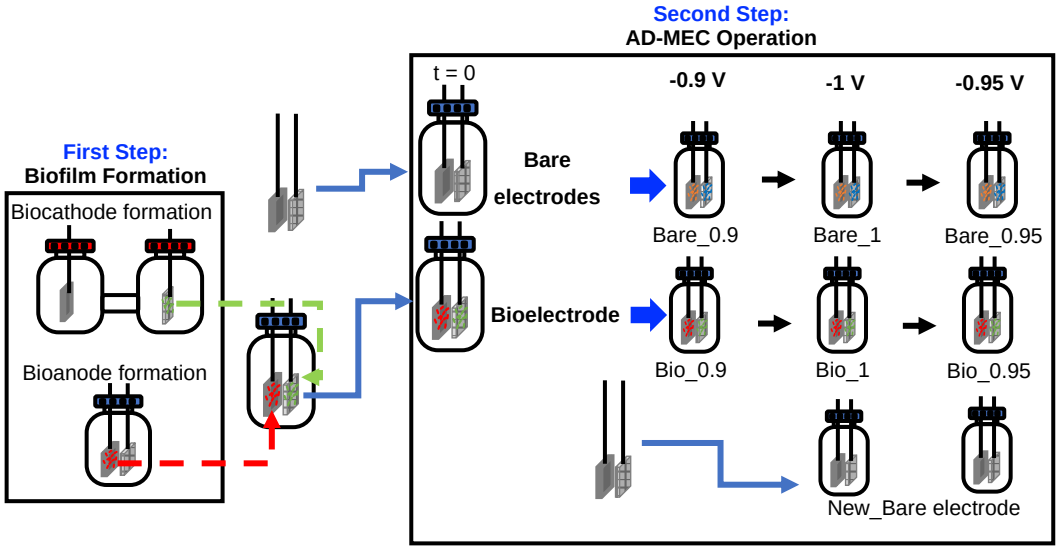

Figure 3.13. The experimental design of Set 2

Set 3: WBS Fed AD-MEC Using Graphite – Graphite Electrodes

As summarized earlier in this set there was BioGAC addition into some of the reactors in this set and WBS was used as substrate in this set. According to the results of the BioGAC dosage study (Test 1 and Test 2), the concentration of the BioGAC to be added to the reactors was selected as 35 g/L. BioGAC and bioelectrodes were transferred to the AD-MEC system prior to reactor operation. Similarly, bare electrodes were put into AD-MEC systems. In Set 3, the F/M ratio was kept at 1 and the total inlet VS was 12,500 ± 1000 mg/L. All the reactors were incubated at 35 ± 2 ºC without mixing. In this set, a constant cathode potential of -0.9 V and -1.0 V were applied for Cycle 1 and Cycle 2, respectively. The experimental design of the AD-MEC operation is given in Figure 3.14.

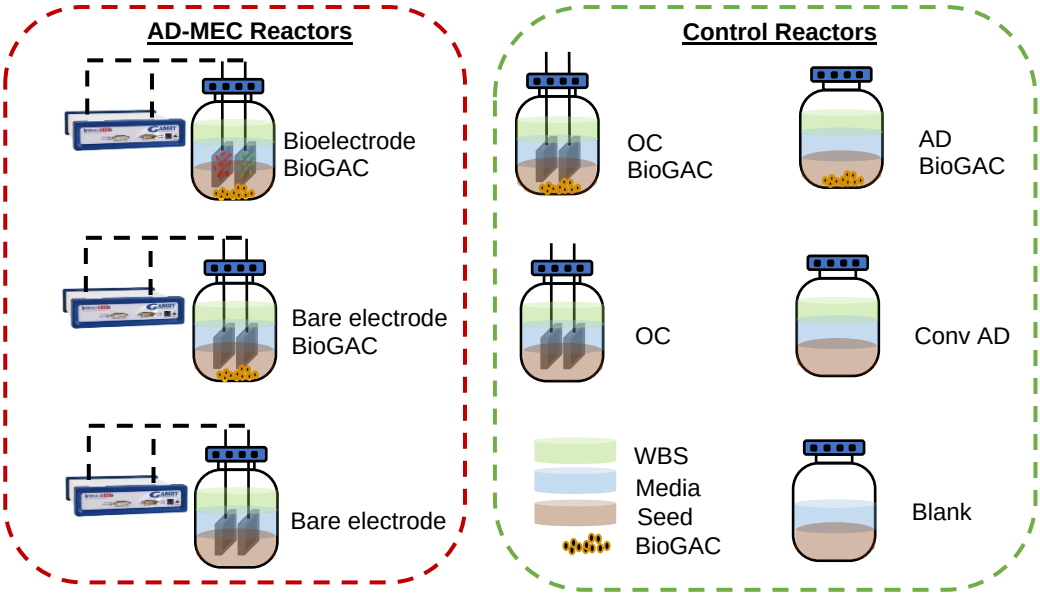

Figure 3.14. The reactors for AD-MEC operation in Set 3

Each cycle had the following reactors Bioelectrode-BioGAC, Bare electrode-BioGAC, and Bare electrode as AD-MEC reactors. As control reactors, OC-BioGAC, OC, Conv. AD-BioGAC, Conv. AD and Blank were set as seen in Figure 3.14.

After Cycle 1, the reactors were emptied and the reactors were filled again with fresh media, WBS, and inoculum to start Cycle 2. Bioelectrodes and BioGAC were preserved through Cycle 1 to Cycle 2. The electrodes of the Bare electrode-BioGAC and Bare electrode reactors were changed to new bare electrodes and fresh GAC after Cycle 1. The detailed experimental design of the set and control reactors is presented in Figure 3.15.

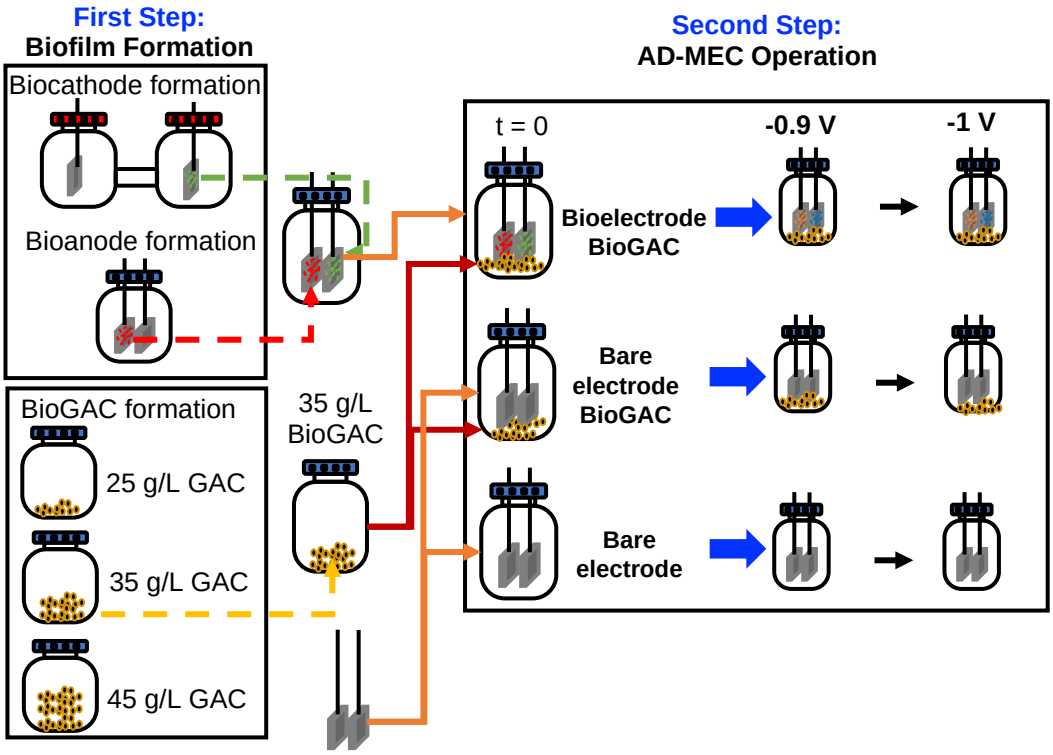

Figure 3.15. The experimental design of Set 3

3.1.4 Electrochemical Data Processing

The applied potential on the anode or cathode was set using chronoamperometry (CA) by a potentiostat, and the current production/uptake was monitored over the whole operation duration of the reactors. The data is recorded at 10 min intervals. CV analyses were performed to monitor the electroactivity of biofilms on the anodes and the cathodes. During CV the scan range was between -0.8 to 0 V vs. Ag/AgCl with a scan rate of 1 mV/S. CV was performed at t =0 (bare electrode), at the end of anode biofilm formation on bioanode, and end of each cycle of cathode biofilm formation on biocathode. For AD-MEC operation, CV analyses were performed for each cycle. An example of the CV is given in Figure 3.16. If no oxidation or reduction reaction occurs on the surface of the electrode, no peaks are expected in a CV curve (Harnisch & Freguia, 2012). If the CV is performed on the anode (the working electrode is the anode), an oxidative peak is expected to be observed. If CV

on the cathode is performed (the working electrode is the cathode), a reductive peak is expected to be observed in the presence of biofilm. As either anodic or cathodic activity increases on electrodes, the peak will be larger compared to bare electrodes. Thus, CV analysis is an important tool to observe the activity of the biofilm on the surface of the electrodes (Harnisch & Freguia, 2012).

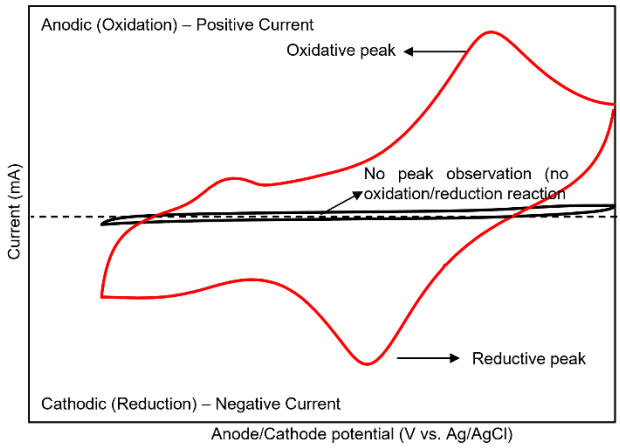

Figure 3.16. An example of a cyclic voltammogram curve

3.1.5 Calculations

Net CH_4 yield

The volumes of CH_4 and H_2 in the biogas were calculated with the syringe method as described by Filer et al. (2019). The net amount of CH_4 production was calculated by subtracting the cumulative CH_4 production of test reactors from the blank. controls. Moreover, net CH_4 yield was calculated by dividing net CH_4 production (mL) by the total mass of VS added (g) from the substrate. Similarly, H_2 yield was calculated as cumulative H_2 production (mL) divided by the mass of VS added (g) from the substrate.

CH_4 production kinetics

The modified Gompertz model (Eq. 3.1) was used to describe the kinetics of CH_4 production during AD-MEC operation (Baek, Saikaly, et al., 2021). Detailed calculation is given in Appendix B.

$$P = P_{\infty}.\exp\left\{-\exp\left[\frac{R_m.e}{P_{\infty}}(\lambda - t) + 1\right]\right\} \quad \text{(Eq. 3.1)}$$

where P_{∞} is the maximum CH_4 potential as mL/g VS, R_m is the maximum CH_4 production rate as mL/VS.d, λ is lag phase as d, e is Euler's constant (2.718).

Current density

Current density (J) (Eq. 3.2) was calculated as:

$$J = \frac{I}{A_{anode/cathode}} \quad \text{(Eq. 3.2)}$$

Where I is current and $A_{anode/cathode}$ is the total surface area of the anode or cathode.

Current to CH_4

Current to CH_4 is the theoretical calculation of how much CH_4 can be produced for a given current uptake.

The cumulative electric charge (meq_i) was calculated by integrating the current (A) over time and dividing it by Faraday's constant (F = 96485C/eq).

$$\text{Current to } CH_4 \text{ (mmol)} = \frac{\int_0^t Idt}{F*8} \quad \text{(Eq. 3.3)}$$

Where F is Faraday's constant (F = 96485C/eq). 8 is the number of electrons exchanged in the reaction ($CO_2 + 8e^- + 8H^+ \rightarrow CH_4 + 2H_2O$).

Volume of methane is then calculated using the ideal gas law:

$$CH_4 \text{ (mL)} = \frac{CH_4(\text{mmol})*0.08314*308*1000}{1.01325} \quad \text{(Eq. 3.4)}$$

Cathode Capture Efficiency (CCE, %)

Cathode Capture Efficiency (CCE, %) is the fraction of the flowing electric current diverted into a reduced product (methane and hydrogen) inside the cathodic chamber (Cristiani et al., 2021).

$$\mathrm{CCE} = \frac{\mathrm{meq}_{\mathrm{CH_4}} + \mathrm{meq}_{\mathrm{H_2}}}{\mathrm{meq_i}} \quad \text{(Eq. 3.5)}$$

The cumulative electric charge (meq_i) was calculated by integrating the current (mA) over time and dividing it by Faraday's constant (F = 96485C/eq).

$meq_{CH4} = rCH_4(mmol)*8$

$rCH_4 = \Delta CH_4 = CH_{4AD\text{-}MEC} - CH_{4OC}$

$meq_{H2} = rH_2(mmol)*2$

Removed VS to CH_4

$$\text{Removed COD (mg)} = \text{Removed VS (mg)} * \frac{\text{COD}}{\text{VS}}\ \text{ratio} \quad \text{(Eq. 3.6)}$$

The COD/VS ratio was 1.46 for Set 1, 1.86 for Set 2, and 1.48 for Set 3. The difference was due to different inoculum and substrates among different sets.

$$\text{Removed VS to } \mathrm{CH_4} = \text{Removed COD (mg)} * \frac{0.395\ \text{mL } \mathrm{CH_4}}{1\ \text{mg COD}} \quad \text{(Eq. 3.7)}$$

0.395 mL CH_4 is the theoretical conversion of 1 mg COD at 35°C (Raposo et al., 2011).

Organic Conversion Efficiency (OCE)

$$\text{Conversion Efficiency (OCE) (\%)} = \frac{\text{Actual } \mathrm{CH_4}\ \text{(mL)}}{\text{Theoretical Removed VS to } \mathrm{CH_4}\ \text{(mL)}} \quad \text{(Eq. 3.8)}$$

3.1.6 Analytical Methods

Standard methods were used to determine the total chemical oxygen demand (TCOD), soluble oxygen demand (sCOD), total solids (TS), and volatile solids (VS) of the samples (APHA et al., 2017). pH was measured with a portable pH meter

(Starter300, Ohaus, U.S.A.). Conductivity was measured with a portable conductivity meter (sensION 5, Hach, U.S.A.). Biogas production was measured with a water displacement device which comprises solution at pH 2. Biogas compositions were examined by gas chromatography (GC) (TRACE GC Ultra, Thermo Scientific, U.S.A.) by injecting 200 µL of the sample. The GC was configured with two series-connected columns (CP-Moliseve 5A and CP-Porabond Q). and a thermal conductivity detector (TCD). Helium was the carrier gas with a constant pressure of 100 kPa. Oven, injector, and detector temperatures were 35°C, 50°C, and 80°C, respectively.

Calibration curve for GC analysis

GC calibration curves were formed by the use of 5-point duplicate injections of the calibration gas. Calibration gas was composed of 50% H_2, 10% N_2, 10% CH_4, and 30% CO_2. Volumes ranging from 100 µL to 500 µL were injected into the GC. An example of the calibration curve for each gas is given in Figure 3.17. All the gas production data is given for 35 °C.

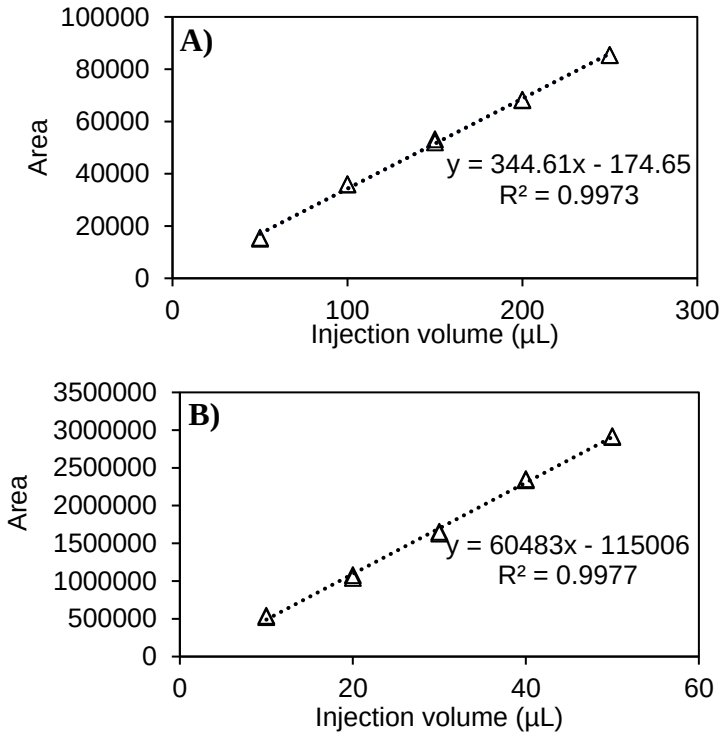

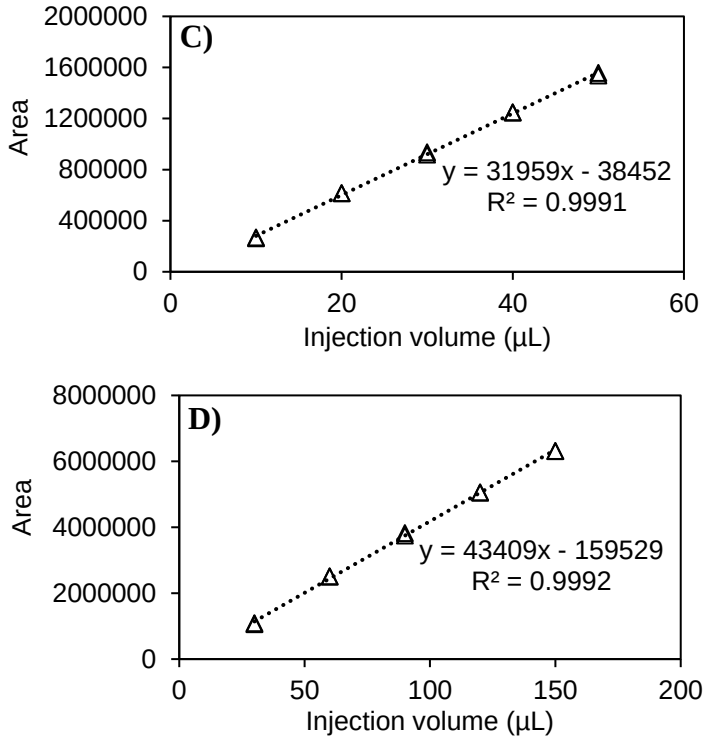

Figure 3.17. A) H_2, B) N_2, C) CH_4, and D) CO_2 gas calibration curve and equation

3.1.7 Microbial Community Analysis

Sample collection and DNA isolation

For Set 1, after Cycle 3 electrodes of all reactors and suspended of Conv. AD reactors were taken for DNA isolation. In a sterile laminar flow hood, biofilms were dried on the electrodes for about 10 minutes before being scraped off using a sterile scalpel. DNA extraction was performed following the manufacturer's protocol (GeneMATRIX Soil DNA Purification Kit, EURx, Poland). Gel electrophoresis and NanoPhotometer P-Class (Titertek-Berthold, Germany) were used to determine the quantities and to check the purity of the isolated DNA samples.

16S rRNA-based identification

Isolated DNA samples were then sent to the BM Laboratory Systems Company (Ankara, Turkey) where the metagenomic analysis was carried out. Briefly, for

microbial community analysis, the V3-V4 variable region of the bacterial and archaeal 16S rRNA genes (length: 464 bp) was employed. The primers used were 341F (5′-CCTAYGGGRBGCASCAG-3′) and 785R (5′-GGACTACNNGGGTATCTAAT-3′) for bacteria and archaea, respectively. PCR amplification was performed using the following thermal cycling profile: 95^{o}C for 3 minutes, 28 cycles of 95^{o}C for half a minute, 55^{o}C for half a minute, and 72^{o}C for a half minute, elongation at 72^{o}C for 5 mins in BM Laboratory Systems Company. On the Illumina Novaseq 6000 platform, high-throughput sequencing was carried out in compliance with the standard protocol. The analysis did not include reads with low-quality scores, unclear bases, or possible chimeric sequences. QIIME2 v2020.8 was used for the bioinformatics analysis at every stage. DNA sequence data were grouped into operational taxonomic units (OTUs) using q2-vsearch. By using the Silva database (http://www.arb-silva.de) to align sample sequences from each OTU, taxonomic identification was accomplished. Based on biodiversity, the general community structure of the bacterial and archaeal domains was identified. Alpha diversity was described using the Shannon, Chao1, phylogenetic, and observed richness diversity indexes. To evaluate the diversity between samples (beta diversity) based on the OTUs produced from each sample, the unweighted pair group method with the arithmetic mean (UPGMA) clustering technique was applied. The QIIME pipeline was used to process both the alpha and the beta diversity indexes.

3.2 Struvite Precipitation

3.2.1 Preparation of the Biogas Plant Sample

Biogas plant effluent sample was collected from a full-scale biogas plant treating cattle manure at mesophilic conditions in Polatli, Turkey. The preparation process is given in Figure 3.18 as described elsewhere (Yilmazel & Demirer, 2011).

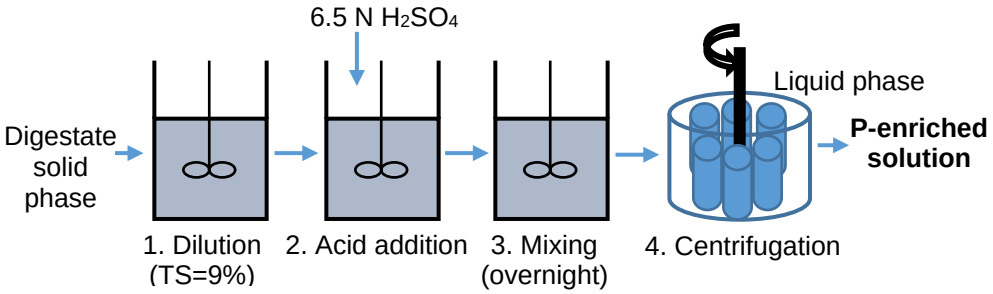

Figure 3.18. Acid dissolution procedure

The sample was centrifuged at 11,000 *g* for 15 minutes. Solid fraction (Total solids (TS) = 16%) was collected and diluted to TS of 9% to enable continuous mixing. The sample was then subjected to an acidic dissolution process to increase dissolved PO_4^{3-} concentration and maximize P recovery. Acidic dissolution was accomplished in three steps: (i) acid addition, (ii) mixing, and (iii) centrifugation, as described elsewhere (Yilmazel & Demirer, 2013). 6.5 N sulphuric acid (H_2SO_4) was added until pH was decreased to 2.0 ± 0.2. The mixture was continuously mixed overnight using a stirrer (Velp Scientifica, AREC, Italy). Finally, the sample was centrifuged at 11,000 *g* for 15 minutes to collect the supernatant. This liquid solution, P-enriched digestate, was characterized and kept at 4° C until use (Table 3.7).

3.2.2 Preparation of WMP and BM Solution

BM was collected from DSA Agri-food Products, Kirikkale, Turkey. WMP was obtained from KÜMAŞ Magnesite Inc. in Kütahya, Turkey. The characterizations of these raw materials are presented in Table 3.7.

Table 3.7. Characterization of P-enriched digestate, raw WMP, and BM

Parameters	P-enriched digestate	WMP	BM
PO_4-P (mg /L)	1100 ± 110 (35.5 ± 4 mM)	-	-
NH_4-N (mg/L)	1950 ± 180 (139 ± 13 mM)	-	-
K (mg/g)	2.0 ± 0.1 (51.2 ± 2 mM)	0.367 ± 0.02	2.5 ± 0.1
Mg (mg/g)	1.14 ± 0.05 (46.9 ± 2 mM)	270 ± 10	3.4 ± 0.1
Fe (mg/g)	1.06 ± 0.01 (18.9 ± 0.002 mM)	14.6 ± 0.2	n.d.
Na (mg/g)	0.90 ± 0.01 (39.1 ± 0.04 mM)	0.597 ± 0.01	6.2 ± 0.2
Ca (mg/g)	0.49 ± 0.01 (12.2 ± 0.05 mM)	6.6 ± 0.1	170 ± 10
P (mg/g)	-	n.d.	74 ± 2
Zn (mg/g)	0.033 ± 0.002 (0.5 ± 0.03 mM)	0.021 ± 0.001	n.d.
Al (mg/g)	0.013 ± 0.001(0.5 ± 0.04 mM)	0.720 ± 0.04	n.d.
Cu (mg/kg)	2.1 ± 0.1 (33 ± 1.6 µM)	15.1 ± 0.3	n.d.
Cr (mg/kg)	1.5 ± 0.1 (0.5 ± 1.9 µM)	286 ± 7	n.d.
Ni (mg/kg)	0.80 ± 0.03 (13.6 ± 0.5 µM)	668 ± 14	n.d.
Pb (mg/kg)	0.052 ± 0.002 (0.02 ± 0.01 µM)	11.5 ± 0.04	n.d.
Cd (mg/kg)	0.014 ± 0.001 (0.12 ± 0.009 µM)	0.67 ± 0.04	n.d.
n.d.: not detected, (-) indicates a parameter that was not measured			

The images of BM and WMP are given in Figure 3.19A-B. Like biogas plant effluent, an acidic dissolution process was applied to both raw materials for proper solubilization of magnesium and phosphate before experimental runs. The method was modified from Siciliano and De Rosa (Siciliano & De Rosa, 2014). Briefly, 60 grams of BM was dissolved in 150 mL 3 N H_2SO_4. In the case of WMP, 90 grams of solid WMP was dissolved into 100 mL 3 N H_2SO_4. H_2SO_4 was used to prevent the dissolution of calcium ions (Siciliano & De Rosa, 2014). The mixtures were mixed for 2 hours and centrifuged at 4,000 *g* for 15 minutes. The supernatant solutions obtained after centrifugation were used as liquid Mg and P sources in the experiments. The schematic of the dissolution process is given in Figure 3.19C. WMP solution contained 88 g/L Mg^{2+} (3.6 M) and BM solution contained 18 g/L PO_4– P (0.6 M) and 0.4 g/L NH_4-N (28 mM).

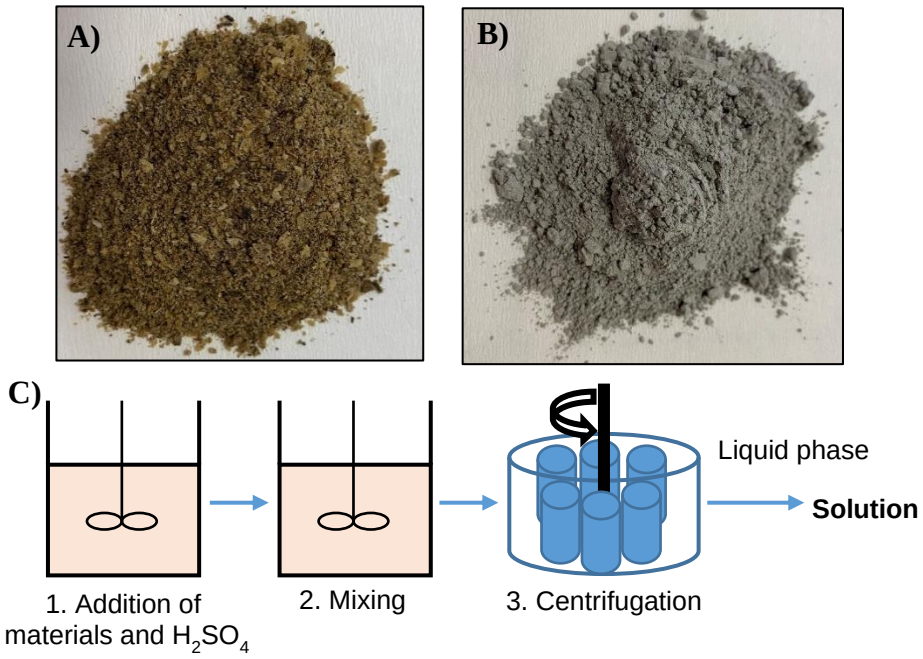

Figure 3.19. A) BM, B) WMP, C) Protocol for preparing WMP and BM solutions

3.2.3 Experimental Design and Optimization

This work used a statistical model to investigate the impacts of different factors on the performance parameters, such as the amounts of sustainable substitutes and the operation pH. BBD was selected as response surface methodology (RSM) since it can assess multiple factors with the smallest number of experimental trials possible (Engin et al., 2018). Most importantly, interactions between factors can be investigated via BBD (Engin et al., 2018). In the formation of struvite, pH is the driving force, and any change in the pH of the solution may affect struvite precipitation (Gunay et al., 2008). Besides, low pH values hinder struvite formation, and at high pH values, co-precipitates may be produced instead of struvite, which may cause a decline in ammonium recovery efficiency (Dogan et al., 2018; T. Zhang et al., 2009). Additionally, the struvite precipitation process is highly affected by the concentrations of Mg, P, and N (Dogan et al., 2018). Struvite precipitation occurs when molar concentrations of Mg^{+2}, NH_4, and PO_4^{-3} are equivalent, making their availability crucial (Le Corre et al., 2009; Siciliano et al., 2020). Although molar

amounts of the struvite-forming ions should be equal, the presence of competitive ions like Ca^{2+}, Na^{+}, and AI^{3+} from digestate, BM, and WMP can react with Mg^{+2} and PO_4^{-3} and cause a decline in the available ions to form struvite (Le Corre et al., 2009; Siciliano et al., 2020). Accordingly, the optimum molar ratios of the struvite-forming ions should be evaluated by considering the type of wastewater used. For these reasons, in this study, the BBD matrix was created (Table 3.8) using three factors: pH (*A*), Mg:N molar ratio (*B*), and P:N (*C*). Each factor was tested at three levels :- 1 denotes the low level, +1 represents the high level, and 0 shows the midpoint to evaluate experimental error (Polat & Sayan, 2019). Researchers have reported a range of values for the optimal pH for struvite, ranging from 8.0 to 10.7 (J. Wang et al., 2005). Since after pH 9, the purity of the struvite decreases, the pH range was selected as 8 – 9 in this study (X. Hao et al., 2013). The amounts of Mg^{2+} and PO_4^{3-} ions available for the formation of struvite are decreased by the phosphorus and magnesium, which can result in the formation of additional magnesium and phosphate compounds (S. I. Lee et al., 2003). This is why the amount of phosphorus and magnesium exceeded the theoretical value required to obtain high recovery values (S. I. Lee et al., 2003). Therefore, to maximize ammonia recovery, Mg:N and P:N molar ratio was set to more than 1. The ranges of the factors were set as 8 – 9 for pH (A), 1.5 – 2.3 for Mg:N molar ratio (B), and 1.2 – 2 for P:N molar ratio (C). The responses were selected as NH_4-N, PO_4-P, and Mg^{2+} recovery. Recovery is calculated according to levels after the addition of sustainable substitutes. The experimental design is given in Table 3.8. For quality control experiments were run in triplicate, thus a total of 45 experiments were carried out.

Table 3.8 Box-Behnken experimental design

Factors	**Levels**		
	-1	0	+1
pH	8.0	8.5	9.0
Mg:N (molar ratio)	1.5	1.9	2.3
P:N (molar ratio)	1.2	1.6	2.0

A second-order polynomial reaction related to the NH_4-N recovery and the residual PO_4-P concentration is given in Equation (2) as follows:

$$\hat{Y}_{NR/PR/MR} = \beta 0 + \beta_1 A + \beta_2 B + \beta_3 C + \beta_4 A^2 + \beta_5 B^2 + \beta_6 C^2 + + \beta_7 AB + \beta_8 AC + \beta_9 BC \quad (2)$$

where $\hat{Y}_{NR}$ = predicted response for NH_4-N recovery $\hat{Y}_{RP}$ = predicted response for PO_4-P recovery, $\hat{Y}_{MR}$ = predicted response for Mg^{2+} recovery, β_0 = intercept, β_1, β_2, β_3 = linear coefficients, β_4, β_5, β_6 = squared coefficients, β_7, β_8 and β_9 = interaction coefficients and A, B and C = independent variables.

3.2.4 Struvite Precipitation Procedure

Four sequential steps were followed in the batch-type experiments: (i) addition of reagents, (ii) pH adjustment, (iii) settling, and (iv) filtration (Uysal et al., 2010; Yilmazel & Demirer, 2013). The steps are shown in Figure 3.20.

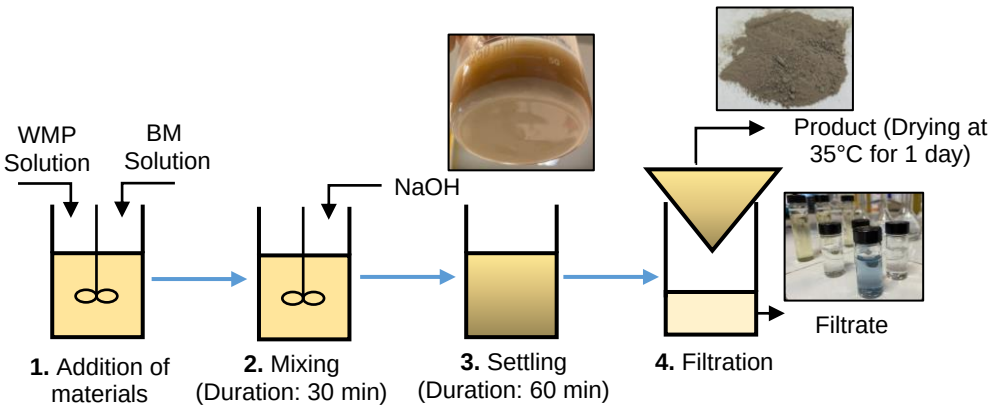

Figure 3.20. Struvite precipitation procedure

Each reactor contained 40 mL of P-enriched digestate sample. For each run, ammonium, and phosphate concentration of the P-enriched digestate sample was measured. To achieve the desired total molar concentration ratio of Mg:N:P in the reactor, the addition of WMP and BM solution to the digestate sample was calculated by taking into account the initial concentrations of these ions in the sample and were adjusted accordingly. pH was increased to the desired value using 10 N NaOH and mixed using a magnetic stirrer (Velp Scientifica, AREC, Italy). The pH of the

solution was measured continuously until a steady pH at the desired level was observed. After the pH value was stabilized (with a variation of ± 0.1), the equilibrium state was reached. After equilibrium, the reactors were kept mixed at 200 rpm for 30 minutes. All the runs were carried out at ambient laboratory temperature (~20 ◦C). The reactors were then settled for 1 hour to allow the separation of crystallized precipitate from bulk liquid. Finally, the reactor contents were filtrated through a folded coarse filter (ISOLAB, product code: 1.107.40.140) to separate the product from the liquid. The filtrate was subjected to Mg^{2+}, NH_4-N, and PO_4-P, measurements. The remaining part on the filter (product) was dried at a constant temperature room (35 ± 1 º C) for 24 h. The tare weight of the coarse filter and the weight of filter paper containing the product after drying was measured to calculate the amount of total precipitate. The product was manually separated from the filter paper. Since the product may contain different precipitates such as K-struvite, struvite, newberyite, brucite, calcium carbonate, and calcium hydroxide, the product was subjected to XRD and SEM analyzes (B. Li et al., 2016).

3.2.5 Analytical Methods

All samples were filtered using 0.45 µm filters to remove any suspended particles before analyses. The amino acid colorimetric method (Hach Method 8178) and the Nessler colorimetric method (Hach Method 8038) were used to quantify PO_4-P and NH_4-N concentration, respectively. A spectrophotometer was used for colorimetric methods (HACH, DR 2800). All metals and ions except Mg were measured with inductively coupled plasma mass spectrometry (ICP-MS) (Perkin Elmer, DRC II, USA) in METU-Central Laboratory, Turkey. Mg concentrations were measured following the procedures in the Standard Methods by using atomic absorption spectroscopy (Perkin Elmer, Aanalyst 400, USA). The pH was monitored with a portable pH meter (Ohaus, Starter300, USA).

XRD tests were carried out to explain the structural behavior of the powder samples to verify that the precipitate contains struvite. All the samples were examined using

a Rigaku Ultima IV X-ray diffractometer at METU Central Laboratory. During XRD, the scan range was set to 5-70°, and the duration time/scan speed was 1 deg/min. The morphologies of the precipitates were analyzed with Field Emission SEM (Quanta, 400F) at METU Central Laboratory.

Elemental analysis (C, H, N, S) was conducted with an elemental analyzer (LECO, CHNS-932 at METU Central Laboratory. Extracted Phosphorus (2% Citric Acid Soluble) in the effluent was analyzed using ICP-OES (TS EN 15959) at Çınar Environmental Laboratory Co. Other macro and micro elements were analyzed with ICP MS (TS EN ISO 17294) at Çınar Environmental Laboratory Co. Since struvite is the desired chemical, the product purity is determined by the proportion of struvite in the solid precipitate. The effectiveness of the product for end-use applications and the market price would therefore both be enhanced by high product purity. Unwanted particles may precipitate concurrently during struvite crystallization, influencing the struvite crystal development, due to the complexity of the digestate, WMP, and BM composition. Theoretical value elements for pure struvite are 9.9%, of Mg, 5.7% of N, and 12.6% of P (H. Huang et al., 2006). Since the only precipitate that contains N is struvite, purity was calculated as given in Eq. 3.3 (Cerrillo et al., 2015; Numviyimana et al., 2020).

$$\text{Purity}\ (\%) = \frac{n_{NH4-N}}{5.7} * 100 \qquad \text{(Eq. 3.3)}$$

Where $n_{NH4\text{-}N}$ is the molar ratio of N in the product. The theoretical molar ratio of N is 5.7 for struvite (H. Huang et al., 2006).

Calibration for AAS measurement

Before each measurement, calibration is performed in AAS analysis. Mg^{2+} standards were prepared as concentrations 0.1, 0.5, 1.0, and 1.5 mg Mg^{2+} /L. As calibration blank, deionized water was used. An example of a calibration curve is given in Figure 3.21.

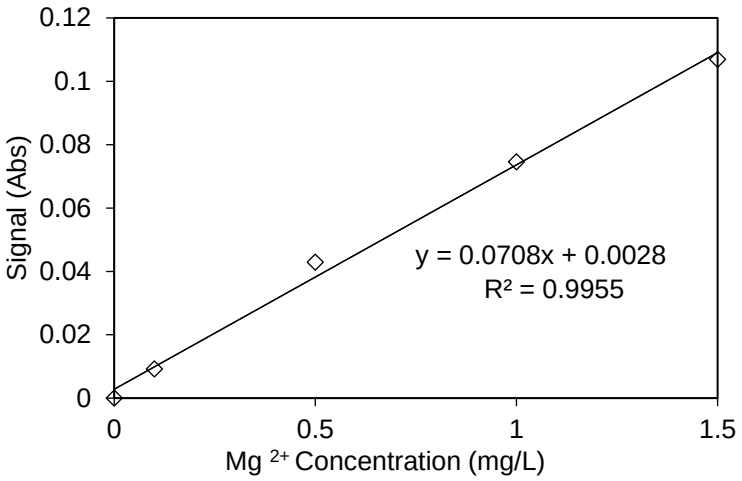

Figure 3.21. Mg^{2+} calibration curve

CHAPTER 4

RESULTS AND DISCUSSION

4.1 AD-MEC

4.1.1 Set 1: Cattle Manure Fed AD-MEC Using Graphite – Graphite Electrodes

4.1.1.1 Biofilm Formation

After the inoculation of the cathode chamber, cathode biofilm was formed with 4 cycles. A new cycle started when the daily increase in methane production dropped below 10%. 100 mM PBS medium was used for biofilm formation (Baek et al., 2017; Siegert, Li, et al., 2014). CH_4 production during biocathode development is given in Figure 4.1. Maximum CH_4 production was observed during Cycle 1 since 10% inoculum was present at that cycle. As the operation continued, CH_4 production stabilized at around 12 mL at the end of 47 days. Baek et al. (2017) investigated the development of biocathode with a similar configuration under -0.9 V vs. Ag/AgCl cathode potential during repeated cycles. To contrast to this study, CH_4 production in the first cycle was low compared to the following cycles. Reported CH_4 production rate was 46.2 – 384.3 mmol/m^2.d. In this study, the CH_4 production rate was 26 mmol/m^2.d which is lower than the reported rate. This deficiency may result from the differences in reactor configuration such as electrode and wire material, and inoculum. Biofilm formation was also confirmed with CV analysis as shown in Figure 4.2. At t=0, there was no reduction peak. After the first cycle, the reduction peak was clear indicating biofilm formation on the cathode surface.

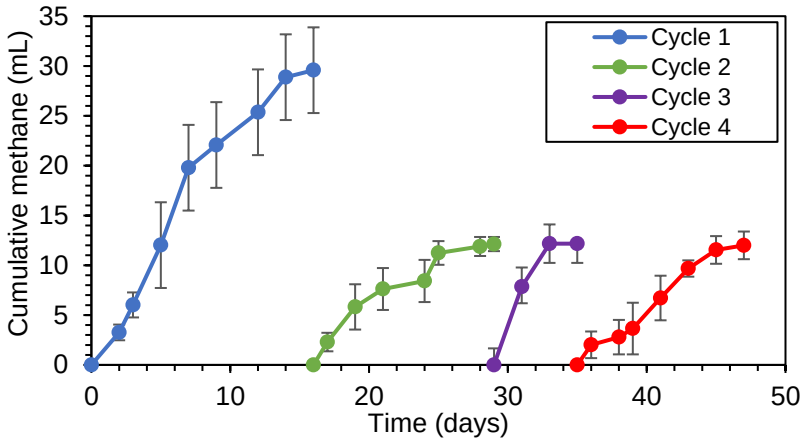

Figure 4.1. The cumulative CH_4 production during Set 1 cathode biofilm formation

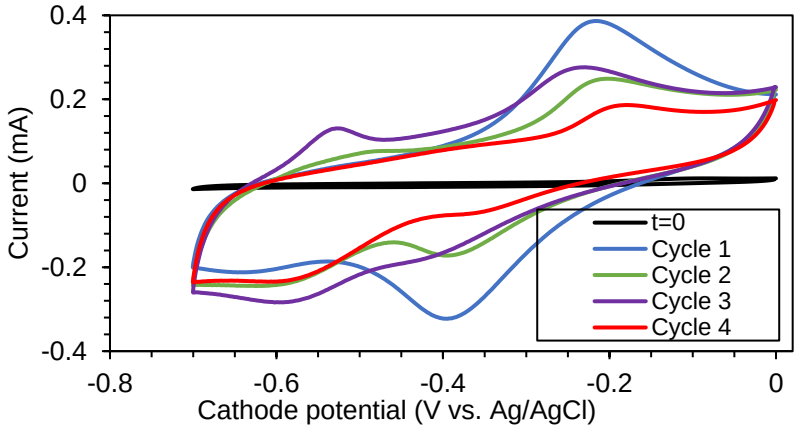

Figure 4.2. CV analysis of cathode during Set 1 biofilm formation

Anode biofilm formation was monitored by current production (Figure 4.3). Current generation at +0.4 and +0.2 V anode potential was not observed (data is not shown). The current was seen after switching the anode voltage to 0 V. Maximum current density was 0.63 ± 0.1 A/m^2 during biofilm formation. Cycle time was decreased during the operation to 2 days. Anode biofilm formation (18 days) was shorter than cathode biofilm formation (47 days) and this is expected because exoelectrogens on the anode grow at a faster rate than methanogens on the cathode. Biofilm formation via electrochemical activity on the anode was also monitored with CV (Figure 4.4). The oxidation reaction was observed on the anode which results from the attachment of exoelectrogenic bacteria to the surface of the anode.

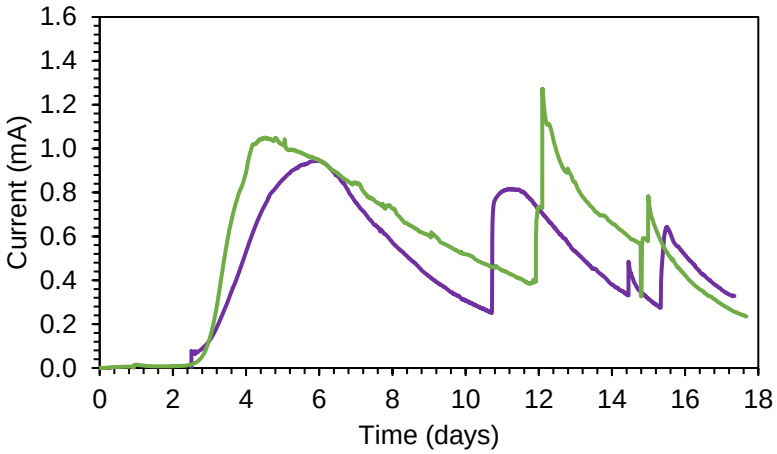

Figure 4.3. Current generation during Set 1 anode biofilm formation

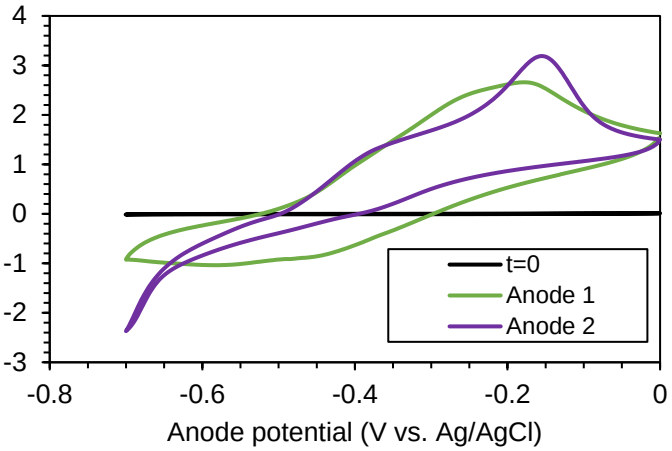

Figure 4.4. CV analysis of anode during Set 1 biofilm formation

4.1.1.2 Current Uptake

After biofilm formation, AD-MEC operation was started with 100 mM PBS media. Buffer solutions, mostly phosphate buffer saline, have been used in microbial fuel cell (MFC) and MEC systems to provide pH balance, high conductivity, and reduction in solution resistance (Ahn & Logan, 2013; F. Guo et al., 2021; Liang et al., 2015). The current and methane production data with 100 mM PBS is given in Appendix C. Significant inhibition was observed during operation. It was reported that high PBS concentrations containing PO_4-P may inhibit the AD process (Carliell-

Marquet & Wheatley, 2002; Mancipe-Jiménez et al., 2017; R. Wang et al., 2015). Especially, rate of the process may be affected severely. Therefore, the AD-MEC operation was restarted with no-PBS media.

Current uptake was monitored during 102 days of AD-MEC operation as seen in Figure 4.5. Replicates of the reactors are given in Appendix D. All current data reported as negative indicating cathodic current. Bioelectrode reactors had a maximum current density of -0.17 ± 0.11 A/m^2 and an average current density of -0.09 ± 0.07 A/m^2. The absence of PBS may have no effect on the current flowing through bioelectrode reactors since they were already colonized by biofilm at the beginning of this test. However, the current uptake in bare electrode reactors during Cycle 1 was almost zero (-0.0026 ± 0.002 A/m^2 average current density). It implies that biofilm could not develop on electrodes without PBS. The current was very low since there was no electron transfer. In the absence of PBS, low conductivity in the reactor and high internal resistance due to suspended sludge may limit electron transfer (Ahn & Logan, 2013). For example, in another work it is reported that the maximum power density was improved by 45% when the phosphate buffer concentration was increased from 50 to 100 mM, indicating enhanced electron transfer (Fan et al., 2007).

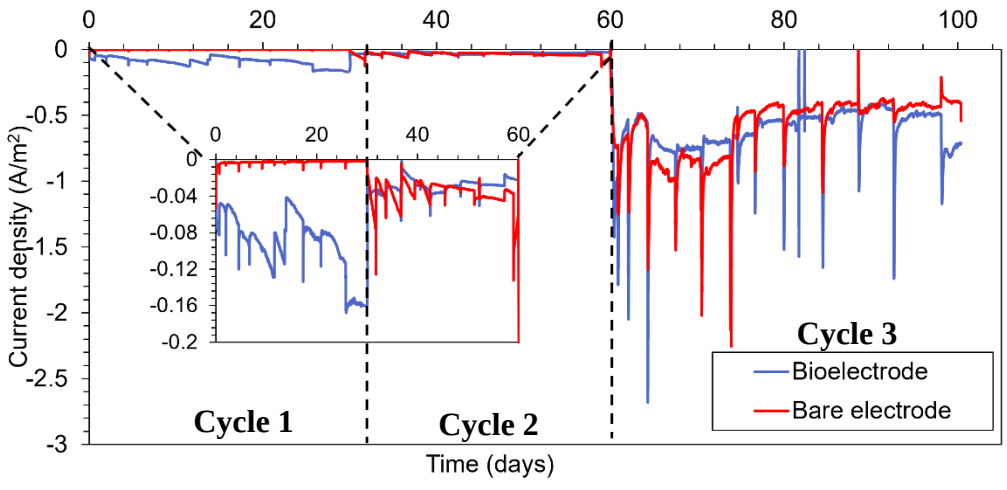

Figure 4.5. Current density during AD-MEC operation

Therefore, in the second cycle, electrolytes were added to the media to increase conductivity. Bicarbonate and NaCl addition was selected as electrolytes since several studies reported that they may substitute PBS (Ahn & Logan, 2013; Ambler & Logan, 2011; F. Guo et al., 2021). The conductivity of this new 5 mM PBS medium (2.6 mS/cm) was adjusted to be close to 100 mM PBS media (4.4 mS/cm) without any inhibition. When media was switched, bare electrode reactors started current uptake with a maximum current density of -0.15 ± 0.1 A/m^2 and an average current density of -0.04 ± 0.03 A/m^2 under the same cathode potential of -0.9 V vs. Ag/AgCl. During Cycle 2, as biofilm formed, the current uptake of bare electrode reactors had an increasing trend. Bioelectrode reactors had -0.09 ± 0.02 A/m^2 maximum-current density and -0.03 ± 0.03 A/m^2 average current density. After the media switch, which was adequate conditions for bare electrode biofilm growth, both reactors had matching current densities, showing that bioelectrode reactors had no benefit over bare electrode reactors in terms of current uptake.

When cathode potential increased to -1 V with 5 mM PBS media, current density increased significantly for the bare electrode (-2.25 A/m^2 maximum current density) and bioelectrode (-2.26 A/m^2 maximum current density) reactors compared to previous cycles. Bioelectrode and bare electrode reactors had comparable current uptake among operations of Cycle 3 like Cycle 2. Bioelectrode (-0.63 A/m^2) and bare electrode (-0.59 A/m^2) reactors both had similar average current densities. Few studies investigated applied cathode potential on AD-MEC systems (Cerrillo et al., 2018; Cristiani et al., 2021; W. Liu et al., 2016). Moreover, the current should be normalized to the surface of electrodes or reactor volume to compare data from different studies. Liu et al. (D. Liu et al., 2016) reported -10 mA/m^3 current density at 10°C under -0.9 V cathode potential, which is lower than the current densities recorded in our study (30 – 3846 mA/m^3 during Cycle 1 and Cycle 2 at -0.9 V cathode potential). These deviations could result from differences in feed, operation temperature, reactor volume to electrode surface area, and electrode material.

4.1.1.3 Methane and Hydrogen Production

VS normalized cumulative CH_4 productions are given in Figure 4.6. Net CH_4 yields are presented in Figure 4.7.

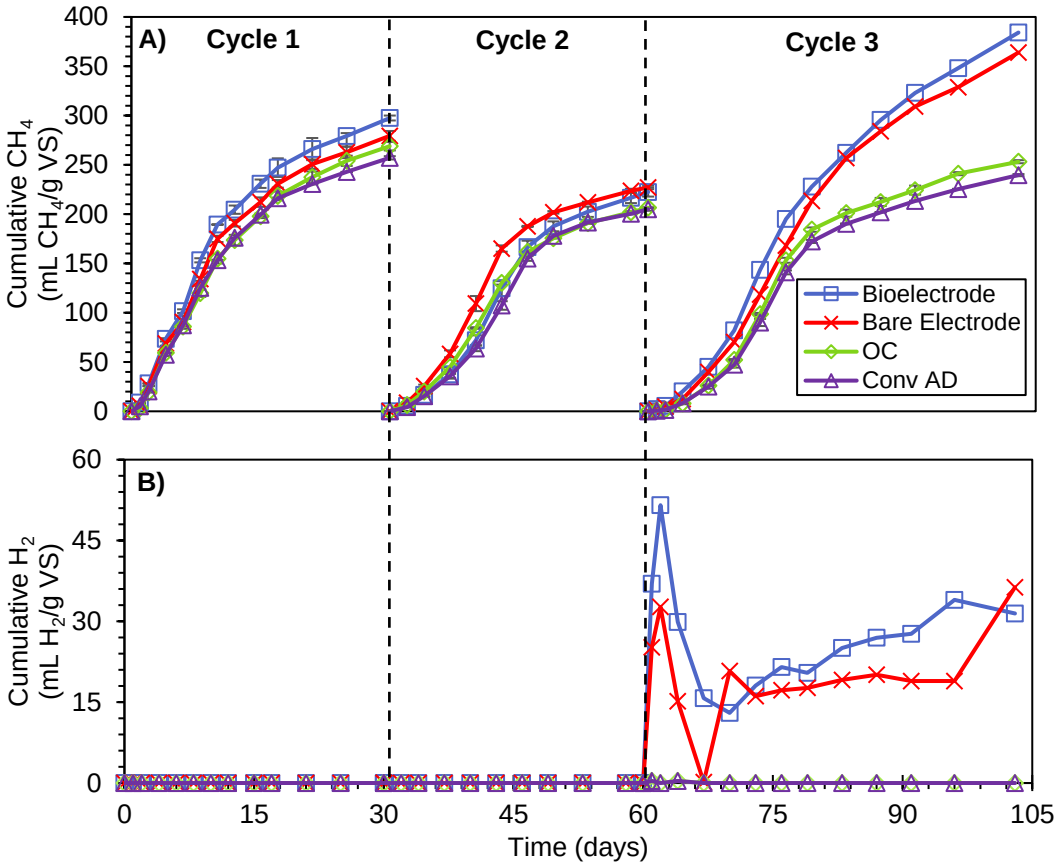

Figure 4.6. Cumulative A) CH_4 and B) H_2 production during 3 fed-batch cycles of Set 1 (cycle 1: no-PBS at -0.9 V, cycle 2: 5 mM PBS media at -0.9 V and cycle 3: 5 mM PBS media at -1 V) (Error bars represent standard deviations of triplicate reactors. The error bars may be smaller than the symbols)

In the first cycle, cumulative CH_4 production of Conv. AD was 257 ± 4, 205 ± 3, and 239 ± 2 mL CH_4/g VS for Cycles 1, 2, and 3, respectively. In each cycle, control reactors were set to compare AD-MEC implementation. This is because even conventional AD yields show variations from cycle to cycle depending on the media and the inoculum.

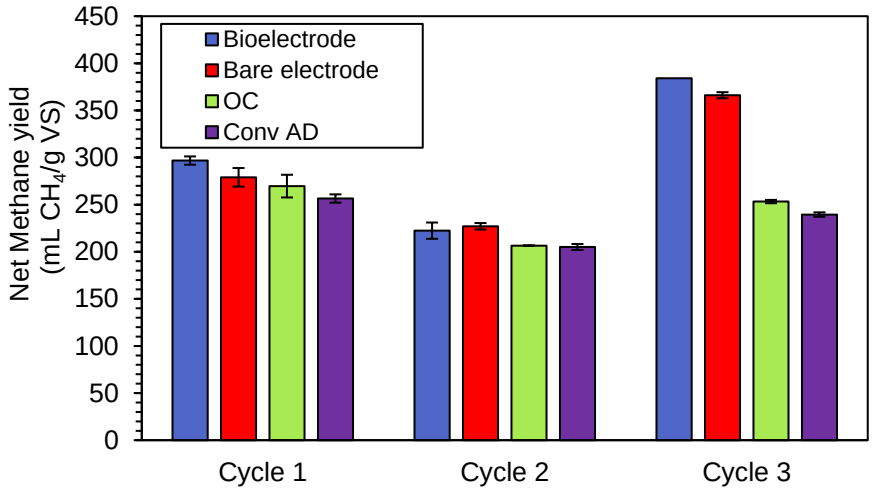

Figure 4.7. Net CH_4 yield of the reactors in Set 1

There is a decrease in the net methane yield of Conv AD in both Cycle 2 and Cycle 3 in comparison to Cycle 1 (Figure 4.7). This is due to the change of medium to 5 mM PBS, which had an inhibitory effect of 20% in Cycle 2 and 7% in Cycle 3. However, as described in the current uptake part, a conductive buffer medium is needed for biofilm formation during AD-MEC operation. When electrodes were introduced to the system without voltage application as in OC controls, CH_4 yield was increased by 5% in Cycle 1, 1% in Cycle 2, and 6% in Cycle 3. There are contradictory results in the literature and others reported that the implementation of electrodes can greatly improve CH_4 production without the use of voltage (Baek, Kim, et al., 2021; Baek, Saikaly, et al., 2021). However, the surface area of the electrodes in this study was smaller than in other studies, thus enhancement due to surface area was not significant in this study. Nevertheless, it makes more sense to evaluate the exact mechanisms involved in the enhancement of the AD-MEC system by comparing AD-MEC reactors to OC for CH_4 yield.

In cycle 1, biofilm on electrodes of the bare electrode could not develop due to no-PBS media; thus, CH_4 yields of bare electrode reactors (279 ± 9 mL CH_4/g VS) were similar to the yields of OC controls (270 ± 12 mL CH_4/g VS). Bioelectrode reactors promoted CH_4 production by 10% compared to OC in Cycle 1. When media changed to 5 mM PBS in Cycle 2, bioelectrode and bare electrode reactors had nearly equal

CH_4 yields as 222 ± 9 mL CH_4/g VS and 227 ± 3 mL CH_4/g VS, respectively. 8 – 10% enhancement was observed between AD-MEC reactors and OC reactors. This was similar to Cycle 1 indicating that independent of media usage, enhancement of methane production via the use of AD-MEC over conventional AD was limited under -0.9 V cathode potential. Therefore, in the third cycle, -1 V cathode potential was applied. Enhancement of CH_4 yields of bioelectrode (as 384 mL CH_4/g VS) and bare electrode (366 ± 3 mL CH_4/g VS) were 52% and 45% compared to OC, respectively. Moreover, voltage change from -0.9 V to -1 V increased CH_4 yield over 73% for bioelectrode and 61% for bare electrode compared to Cycle 2 bioelectrode and bare electrode reactors (Cycle 2 vs. Cycle 3). Similarly, Liu et al. (D. Liu et al., 2017) observed enhancement in CH_4 production with the increase of cathode potential from -0.8 V to -1.1 V and -1.3 V in MECs with graphite felt cathode. Comparing bare electrode and bioelectrode at Cycle 2, pre-biofilm formation did not have a significant improvement in CH_4 yield. When cathode potential increased to -1 V, the bioelectrode reactor showed only a 5% increase over the bare electrode reactor, which was not significant, indicating that bioelectrode usage does not offer a significant advantage in terms of CH_4 yield compared to the bare electrode as a start-up strategy.

In Set 1 H_2 production was also monitored during operation. The normalized cumulative H_2 production of the reactors is given in Figure 4.6B. No H_2 was detected in the control reactors. Under -0.9 V cathode potential, H_2 was not detected in AD-MEC reactors during Cycle 1 and Cycle 2. Although H_2 evolution on cathode may occur, H_2 may have been utilized simultaneously by hydrogenotrophic methanogens or homoacetogens (Q. Huang et al., 2020; Sasaki et al., 2013). Yet, H_2 production was recorded at -1 V cathode potential in AD-MEC reactors. Oxygen was not detected in the biogas for any of the reactors. It indicates that water electrolysis did not occur under these conditions. Maximum H_2 yield was 52 mL H_2/g VS and 33 mL H_2/g VS for bioelectrode and bare electrode, respectively in the first 2 days of cycle 3. H_2 was consumed after two days; however, after 7 days of operation, H_2 production increased again. It implies that H_2 production was faster than

consumption. Few studies reported H_2 production during AD-MEC operation (X. Guo et al., 2013; Hassanein et al., 2020; Hou et al., 2020). Guo et al. (X. Guo et al., 2013) observed 8 mL maximum H_2 production at 4 days of operation under 1.8 V applied voltage. Similar to this study, 1.4 and 1.8 V applied voltages resulted in a 1.7 – 5.2 times increase in hydrogen generation compared to control with no voltage application. (X. Guo et al., 2013). However, H_2 production was low compared to this study. These variations might result from differences in the microbial communities, MEC configuration, applied voltage, and substrates for H_2 production. Hassanein et al. (2020) investigated H_2 and CH_4 production from dairy manure in AD-MEC systems at an applied voltage of 1.2 V. Maximum H_2 production was reported as 0.16 m^3 $H_2/m^3/d$. In this study, maximum H_2 production was 0.24 m^3 $H_2/m^3/d$ for bioelectrode and 0.15 m^3 $H_2/m^3/d$ for bare electrode reactors, which is quite comparable to the study of Hassanein et al. (2020).

4.1.1.4 Methane Production Kinetics and Organic Removal

The modified Gompertz equation was used to calculate the kinetic parameters of CH_4 production. The parameters P, R_m, and were derived in relation to the comparison of experimental data to model simulation of VS normalized cumulative CH_4 production. Table 4.1 provides a summary of the parameters of the CH_4 fitted equation. The model and experimental plots are given in Appendix E. The correlation coefficients (R^2) were around 0.9922 – 0.9987 for all reactors, indicating a well–fitted model.

Table 4.1 Modified Gompertz kinetics of Set 1

	Reactors	VS removal (%)	P_∞* (mL CH_4/g VS)	R_m* (mL CH_4/g VS/d)	λ* (day)	R^2
Cycle 1	Conv AD	39.2 ± 3	250 ± 2	17.8 ± 0.1	1.23 ± 0.12	0.9961
	Open circuit	34.4 ± 1	264 ± 9 (6)	17.1 ± 1.2 (-)	1.19 ± 0.07 (3)	0.9943
	Bare electrode	32.8 ± 1	270 ± 11 (8)	18.9 ± 0.7 (6)	1.06 ± 0.15 (14)	0.9932
	Bioelectrode	35.9 ± 4	283 ± 16 (13)	20.9 ± 1.1 (17)	0.98 ± 0.15 (20)	0.9922
Cycle 2	Conv AD	28.7 ± 2	212 ± 4	14.5 ± 0.4	5.10 ± 0.61	0.9963
	Open circuit	31.5 ± 1	209 ± 1 (-)	14.1 ± 0.2 (-)	3.73 ± 0.09 (26)	0.9987
	Bare electrode	29.6 ± 1	227 ± 2 (3)	17.5 ± 0.1 (21)	3.44 ± 0.52 (33)	0.9975
	Bioelectrode	35.8 ± 5	227 ± 9 (3)	15.4 ± 0.6 (6)	4.85 ± 0.51 (5)	0.9979
Cycle 3	Conv AD	30.6 ± 1	231 ± 2	13.8 ± 0.2	6.15 ± 0.62	0.9963
	Open circuit	32.4 ± 1	243 ± 9 (5)	14.9 ± 0.3 (8)	6.09 ± 0.09 (1)	0.9951
	Bare electrode	32.0	364 (63)	15.4 (12)	5.34 (13)	0.9983
	Bioelectrode	31.8	382 (71)	15.6 (13)	4.40 (28)	0.9963

(P_∞: Maximum CH_4 yield potential as mL/g VS, R_m: Maximum CH_4 production rate as mL/g VS/d, λ: Lag phase as d, R^2: Coefficient of determination) and VS removal (%) of the reactors at 3 cycles

*Numbers in parentheses are the percent increase in CH_4 production rate and percent decrease in lag time compared to Conv AD in the respective cycles.

In Cycle 2 and Cycle 3, Conv AD reactors had similar CH_4 production rates (14.5 ± 0.4 mL/g VS/d and 13.8 ± 0.2 mL/g VS/d). However, the production rate in cycle 1 was higher (17.8 ± 0.1 mL/g VS/d) with no-PBS. These results are in agreement with the yield data and indicate that 5 mM PBS medium may have negatively affected the rate of methanogenesis during the AD process. On the other hand, Conv AD reactors had different lag times in the three cycles of Set 1. This discrepancy may be due to inoculum collection time (in relation to the activity of the inoculum), and operation time difference. Therefore, enhancement in AD-MEC reactors was assessed according to Conv AD in each respective cycle. OC reactors did not increase CH_4 in Cycle 1 and Cycle 2. However, an 8% increase was observed with OC reactors in Cycle 3. In contrast, the lag time of OC reactors was unaffected in Cycle 1 and Cycle 3 relative to Conv AD, while a 26% decrease was observed in Cycle 2. Therefore, adding electrodes to AD systems without applying voltage might not be efficient. Bioelectrode reactors increased production rate by 17% and 6% and decreased lag time by 20% and 5% in Cycle 1 and Cycle 2, respectively. Under -1 V, lag time decreased by 28% with the bioelectrode operation.

In the case of the bare electrode, performance was slightly impacted than that of the bioelectrode because biofilm and current were seen to be low in the first cycle. However, bare electrode usage increased the production rate by 21% and decreased lag time by 33% in Cycle 2, which was higher than the performance of bioelectrode reactors. Although CH_4 yields were nearly the same, rate and lag time were advantageous for bare electrode. The electroactive bacteria were well enriched and adapted in the reactor, as evidenced by the shortened lag time (An et al., 2020). Moreover, in Cycle 3 at -1 V cathode potential, the bare electrode showed a 12% increase in rate and a 13% decrease in lag time. Bioelectrode had a 13% increase in rate and a 28% decrease in lag time. At -1 V, Bioelectrode was more advantageous in terms of lag time. According to CH_4 production kinetics, the most beneficial start-up strategy is bare electrode usage under -0.9 V cathode potential due to the highest enhancement compared to Conv AD.

VS removal of the reactors in three cycles is also summarized in Table 4.1. 29.9 – 39.1% VS removal was observed in this Set. Among the reactors, there was no significant difference in organic removal. The complex and naturally polymeric cattle manure is made up of both soluble and insoluble organic compounds, including polysaccharides, lipids, and proteins (Nasir et al., 2012). The complex structure of these recalcitrant components of cattle manure (cellulose, hemicellulose, and lignin) may hinder the hydrolysis of cattle manure in AD (Y. Li et al., 2021; Nasir et al., 2012). Especially, lignin may only be degraded to a limited degree (Alvarez & Lidén, 2009). Similar VS removal efficiencies in the range of 28.2 - 37.1 were observed by Moset et al. (2015) with dairy cattle manure-fed reactors. Due to the composition of cattle manure, low VS removal compared to other substrates such as WAS were observed (Q. Huang et al., 2020; Zakaria & Dhar, 2019). The study measured only the organic removal at the end of the operation, and the results showed no significant difference in the ultimate VS removal between AD-MEC and conv. AD reactors. It is important to note that while AD-MEC operation may not impact the ultimate VS removal, it can potentially enhance the rate of organic decomposition. This increase in decomposition rate could, in turn, affect the rate of methane production.

4.1.1.5 Cyclic Voltammetry

The objective of CV was to analyze the electroactivity of the biofilm on the electrodes and how it altered under varied media and cathode potential. CV of anode and cathode at the start-up of AD-MEC and end of operation of three cycles are given in Figure 4.8. At the start-up (t=0), bioelectrode reactors had an oxidation peak in the anode CV and a reduction peak in the cathode CV indicating pre-biofilm formation (Figure 4.8A and Figure 4.8C). On the other hand, bare electrode reactors had zero peaks (Figure 4.8B and Figure 4.8D). In cycle 1 with no PBS, similar to current uptake data, bioelectrode continued to have electroactivity on electrodes. However, the Bare electrode reactor had similar CVs to bare electrodes at t=0, especially for the anode. It implies that there was no activity on the electrodes of bare electrode reactors with no-PBS media. Liang et al. (2015) showed that the bioanode of MECs with lower phosphate concentrations was not as electrochemically active as those with higher amounts, demonstrating that phosphate content is an important determinant in MEC performance. With 5 mM PBS media, biofilm formation, and activity were observed on the electrodes. Midpoint cathode potentials of bioelectrodes reactors were -0.46 V, -0.59 V, -0.5 V, and -0.4 V vs. Ag/AgCl for t=0, Cycles 1, 2, and 3, respectively. In the case of bare electrode, cathode midpoint potentials were -0.47 V for Cycle 2 and -0.4 V for cycle 3. Direct electron transfer might take place since midpoint potentials were close to -0.55 V (Fu et al., 2015).

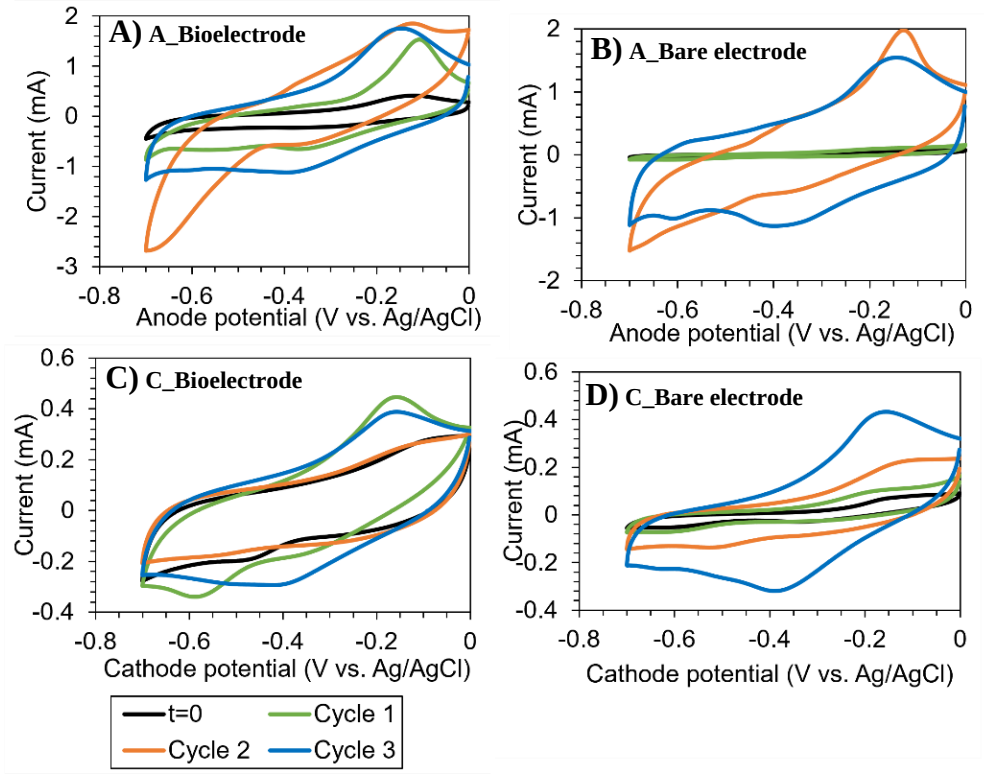

Figure 4.8. CV of A) anode of bioelectrode, B) anode of bare electrode, C) cathode of bioelectrode, and D) cathode of bare electrode AD-MEC reactors at the end of biofilm formation (t=0), Cycle 1, Cycle 2, and Cycle 3

4.1.1.6 Archaeal Communities

The samples were collected as described in Chapter 3.1.7. Genus level archaeal communities of electrodes of bioelectrode, bare electrode, and OC and suspended of Conv. AD reactors are given in Figure 4.9. *Methanosaeta* (64%) in suspended of Conv AD and (100%) on OC electrodes, *Methanobrevibacter* (61%) in the anode of the bare electrode, *Methanocorpusculum* (71%) on the anode of bioelectrode and (55%) cathode of bare electrode and *Methanoculleus* (54%) in cathode of bioelectrode genus were dominant. The microbial community of Conv. AD and OC electrodes were similar to each other with *Methanosaeta, an* acetoclastic methanogen that can utilize only acetate, dominancy. *Methanosaeta* is known for its ability to accept electrons from a syntrophic partner or conductive materials

performing direct interspecies electron transfer (DIET) (Cai, Liu, et al., 2016; J. H. Park et al., 2018). Thus, DIET might be performed on the surface of OC electrodes. Overall, acetoclastic methane generation may be the primary path for methane production in control reactors.

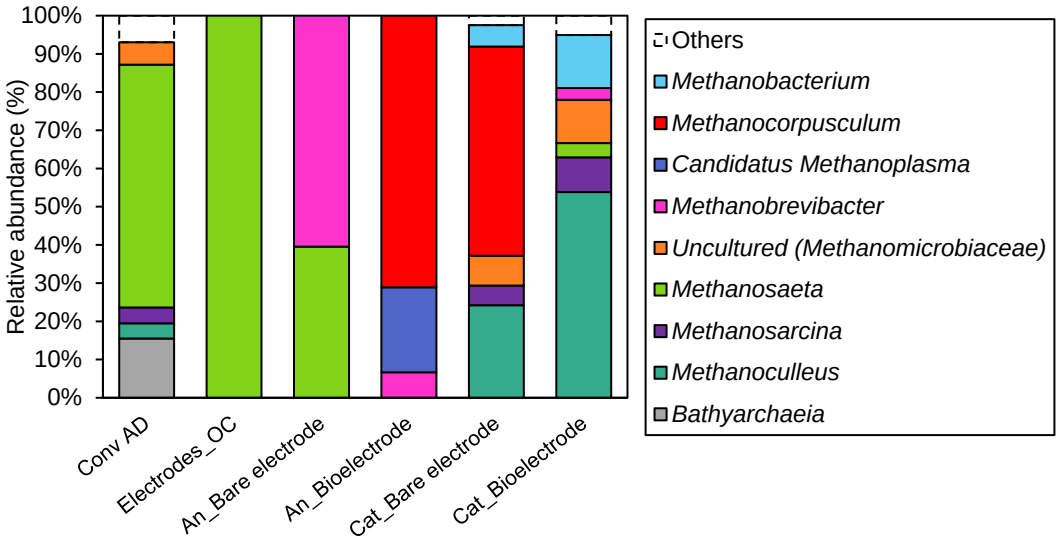

Figure 4.9. Set 1 - Relative abundance of archaeal communities at the genus level (The relative abundance of genus less than 3% of total composition was defined as others.)

In contrast, hydrogenotrophic methanogens, (*Methanocorpusculum*, *Methanoculleus*, *Methanobacterium*, and *Methanobrevibacter)* were dominant in AD-MEC reactors. Due to abiotic H_2 evolution on the cathode, hydrogenotrophic methanogens may be favored by applying voltage. It indicates that indirect transfer had a major role in AD-MEC operation rather than direct electron transfer (Sun et al., 2015). Similar observations were reported in a number of AD-MEC studies (Y. Li et al., 2016; Siegert et al., 2015; Siegert, Yates, et al., 2014; Z. Zhao et al., 2014). Moreover, hydrogenotrophic methanogens are less susceptible to unfavorable metabolic conditions, higher salt concentration or phosphate concentration may favor their growth in AD-MEC systems over acetoclastic ones (Florentino et al., 2019; D. Liu et al., 2016). Comparing the cathode biofilms of Bare electrode and Bioelectrode reactors, it was found that many of the methanogens were in the same

genus. The major difference was *Methanocorpusculum* and *Methanoculleus* dominancy in the cathode of bare electrode and bioelectrode, respectively. Lackner et al. (2020) showed that *Methanoculleus* was the dominant specie among phosphate-buffered samples. Moreover, Ghaderikia et al. (2023) reported that the first settlers resist the biofilm. It implies that the primary microbial community will remain on the electrodes and biofilm will not reshape entirely once the feed is changed. Considering these two studies, the use of 100 mM PBS during the biofilm development on the bioelectrode reactors was shown to be the explanation for the abundance of *Methanoculleus* over *Methanocorpusculum* between the cathodes of the bioelectrode and bare electrode.

When the anodes of AD-MEC reactors were compared, different hydrogenotrophic methanogens were observed. The anode of Bare electrode reactors was dominated by *Methanobrevibacter*. On the other hand, *Methanocorpusculum* was the dominant species in Bioelectrode reactors. Clearly, the archaeal communities in the Bioelectrode and Bare electrode reactors differed significantly. The alteration of environmental factors (controlled vs. uncontrolled environment) and media composition during biofilm formation and operation of the AD-MEC had a substantial impact on the archaeal community structure. Interestingly, despite these distinctions, there was not a significant difference in methane production between the two reactors. This indicates that methane production is not dependent solely on a single species, but rather on the synergistic interactions between multiple species. In addition, it is essential to observe that the operational conditions of the reactor systems played a significant role in shaping the microbial communities. Overall, these results emphasize the complexity of microbial interactions and the need to optimize methane production processes by considering environmental factors and operational conditions.

4.1.1.7 Bacterial Communities

Phylum-level bacterial communities of DNA collected from bioelectrode, bare electrode, and OC and suspended in Conv AD reactors are given in Figure 4.10A. Genus-level bacterial communities of the reactors are given in Figure 4.10B. It is interesting to note that the bacterial communities of the OC (open circuit), the anode of the bare electrode, and the anode of the bioelectrode were remarkably similar. Similarly, the cathode of the bioelectrode and the bare electrode showed similarities in their microbial communities as well. This similarity between microbial communities suggests that both the bare electrode and the bioelectrode supported the development and establishment of comparable bacterial populations. Thus, the bacterial community is not selective with respect to environmental conditions (controlled or uncontrolled) compared to the archaeal community.

Firmicutes was abundant phylum (13-50%) in all of the reactors. In the majority of manure digesters or co-digesters containing mixed substrates, *Firmicutes* predominates similar to this study (J. Li et al., 2015; F. H. Liu et al., 2009; St-Pierre & Wright, 2014). *Bacteroidota* (synonym *Bacteroidetes*) was another abundant phylum among 26% in suspended of Conv AD, 17% on electrodes of OC, 21% on the anode of the bare electrode, 18% on the anode of bioelectrode, 7% on the cathode of the bare electrode and 3% on the cathode of bioelectrode. *Bacteroidota* is a potential exoelectrogen that might interact with methanogens to enhance the performance of MEC by transferring electrons through the metabolism of organic substrates (H. J. Kang et al., 2021; S. Xu et al., 2015). Another dominant phylum was *Proteobacteria* 18% on electrodes of OC, 15% on the anode of bare electrode, 15% on the anode of bioelectrode, and 38% on the cathode of bioelectrode. Numerous bacteria that can give electrons outside of the cell are classified under *Proteobacteria* (L. Zhao et al., 2021). The bacterial populations at the phylum level were comparable between reactors and with several studies (Cerrillo et al., 2018; Lei et al., 2016; L. Zhao et al., 2021). Thus, biofilm formation on the anode was not selective in terms of the bacterial community. On the other hand, the dominant

phylum on the cathode of bioelectrode was *Desulfobacterota* which can use the extracellular electron transfer pathway (Ward et al., 2020). These results showed that exoelectrogens were abundant on electrodes of AD-MEC systems with a syntrophic relationship with methanogens performing DIET.

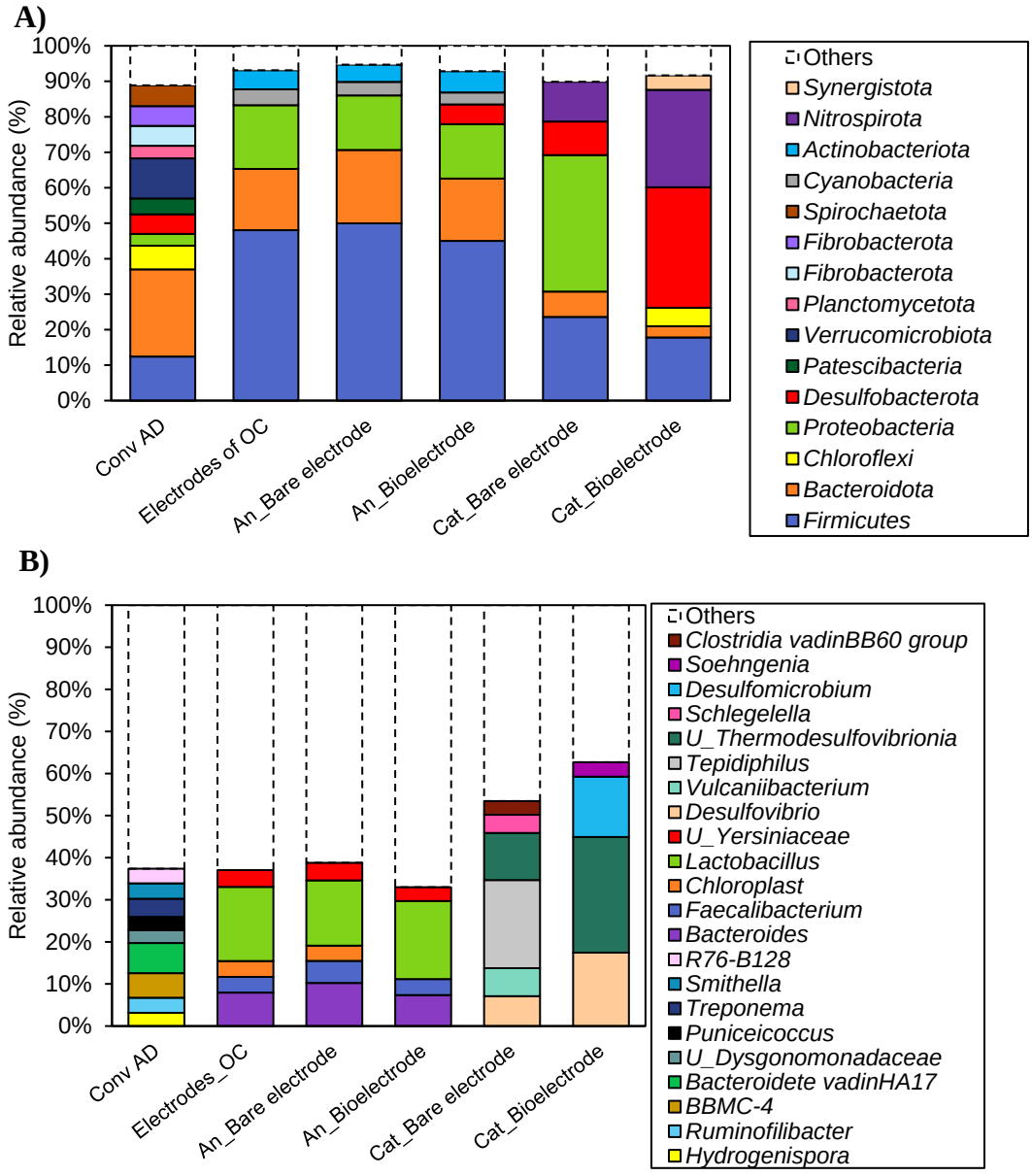

Figure 4.10. Set 1 - Relative abundance of bacterial communities A) at the phylum level, B) at the genus level

(The relative abundance of genus less than 3% of total composition was defined as others.) ("U_" means uncultured.)

The dominant genus in the reactors was *Bacterioidete* (7%) in suspended Conv AD, *Lactobacillus* (18%) on electrodes of OC, (15%) anode of the bare electrode, and (19%) anode of bioelectrode, *Tepidiphilus* (21%) on the cathode of the bare electrode, and uncultured *Thermodesulfovibrionia* (27%) on the cathode of bioelectrode. Sulfate-reducing bacteria (SBR) (*Thermodesulfovibrionia*, *Desulfovibrio,* and *Desulfomicrobium*) were dominant on the cathode of the AD-MEC reactors. These hydrogen-utilizing SRBs require acetate and CO_2 as carbon sources (Rabus et al., 2015; Umezawa et al., 2021). To date, sulfate reduction in biocathodes using hydrogen as the electron transfer mediator has been reported (Cordas et al., 2008). However, Su et al. (2012) showed that without electron shuttles or hydrogen production, sulfate-reducing biofilms are able to receive electrons directly from electrodes. Thus, as electroactive methanogens, SBR may be colonized on the cathode to receive electrons from the cathode surface or use hydrogen produced from cathode surface as electron shuffle (Yuan et al., 2020). SRB and methanogens use the same electron donor substrates and direct electrons from cathode (Hu et al., 2015). The utilization of acetate by SRB is thermodynamically more favorable than that by methanogens in terms of the standard Gibbs free energy (Muyzer & Stams, 2008). Due to their overlapping metabolic pathways and preferences for similar environmental conditions, SRB and methanogens could potentially compete in this research. The competition between these microbial groups can influence the overall AD and the production of methane, with the dominance of either SRB or methanogens influencing the distribution of electron flow and the composition of the final biogas. Yuan et al. (2020) showed that MEC enhanced the availability of substrates for anaerobic digestion, thereby increasing CH_4 production in the AD-MEC system under high-strength sulfate conditions. Similarly, AD-MEC may provide sufficient substrates to SRB and methanogens in this study.

4.1.2 Set 2: Cattle Manure Fed AD-MEC Using Graphite – Stainless Steel Electrodes

4.1.2.1 Biofilm Formation

Biofilm on the cathode was formed during 4 fed-batch cycles for 57 days. A new cycle started when the daily increase in methane production dropped below 10%. Cumulative CH_4 production is given in Figure 4.11A. The highest CH_4 production was observed in the third cycle with 28.9 mL. Inoculum decreased gradually among cycles. At the fourth cycle, no catholyte was left in the reactors as inoculum. At cycle 4, the bulk solution was composed of only media. Since no inoculum was added to the cathode chamber, CH_4 was produced only from methanogens on the cathode surface. This suggests that the biofilm grew successfully on the SS cathode.

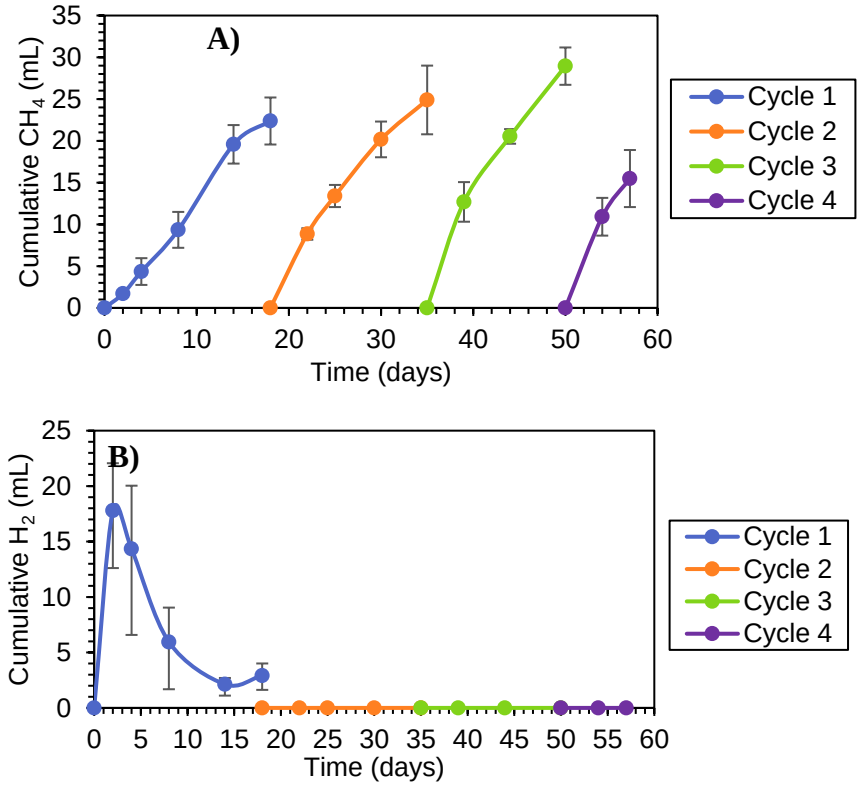

Figure 4.11. A) CH_4 production, and B) H_2 production during cathode biofilm formation in Set 2

In addition to CH_4, H_2 was observed during the first cycle of biofilm formation. Cumulative H_2 during cathode biofilm formation is given in Figure 4.11B. However, when graphite was used as a cathode in Set 1, H_2 was not detected at the same cathode potential. Similarly, Siegert et al. (2014) observed that SS cathode produced abiotic H_2 while H_2 was not produced with graphite block at -0.8 V vs. Ag/AgCl cathode potential. The highest H_2 was observed on day 2 with 17.8 mL. Then, H_2 is utilized by hydrogenotrophic methanogens. At other cycles, H_2 was not detected, indicating that any H_2 that is produced may have been simultaneously utilized by methanogens.

Compared to graphite cathode (Set 1), CH_4 production was higher in Cycle 2 and 3 with SS mesh cathode (Set 2). Due to increase hydrogen production with the use of SS mesh, hydrogenotrophic methane production may increase.

In addition to CH_4 and H_2 production, CV analysis was performed to monitor electro-active biofilm formation. As seen in Figure 4.12, no peaks were observed in the CV of bare SS. The peaks were observed in other cycles compared to bare SS, implying biofilm formation on the surface. CV plots obtained with SS were different than with graphite block electrodes. This difference may be due to the mesh-type electrode.

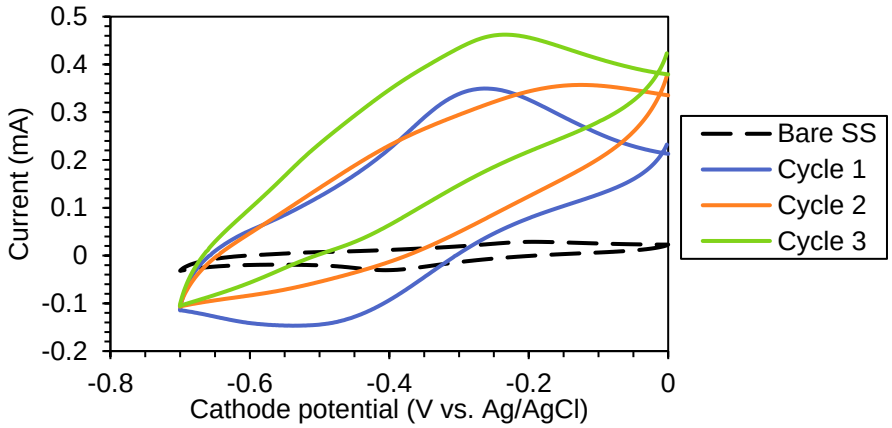

Figure 4.12. CV analyses during cathode biofilm formation in Set 2

Simultaneous with cathode biofilm formation, anode biofilm was formed in single-chamber MECs. The current density during anode biofilm formation is given in Figure 4.13A. Biofilm formation took a total of 23 days corresponding to 3 cycles.

The average peak current density was 0.678 ± 0.083 A/cm^2. The results were similar to Set 1 since the same electrode material, graphite, was used as anode. The stable current density was observed in Cycle 2 and Cycle 3. Observed current production suggested that exoelectrogens formed biofilm on the anode surface. This was also confirmed with CV analysis (Figure 4.13B). A distinctive oxidation peak was observed compared to the bare graphite anode. This implies the abundance of electro-active microorganisms on the anode surface.

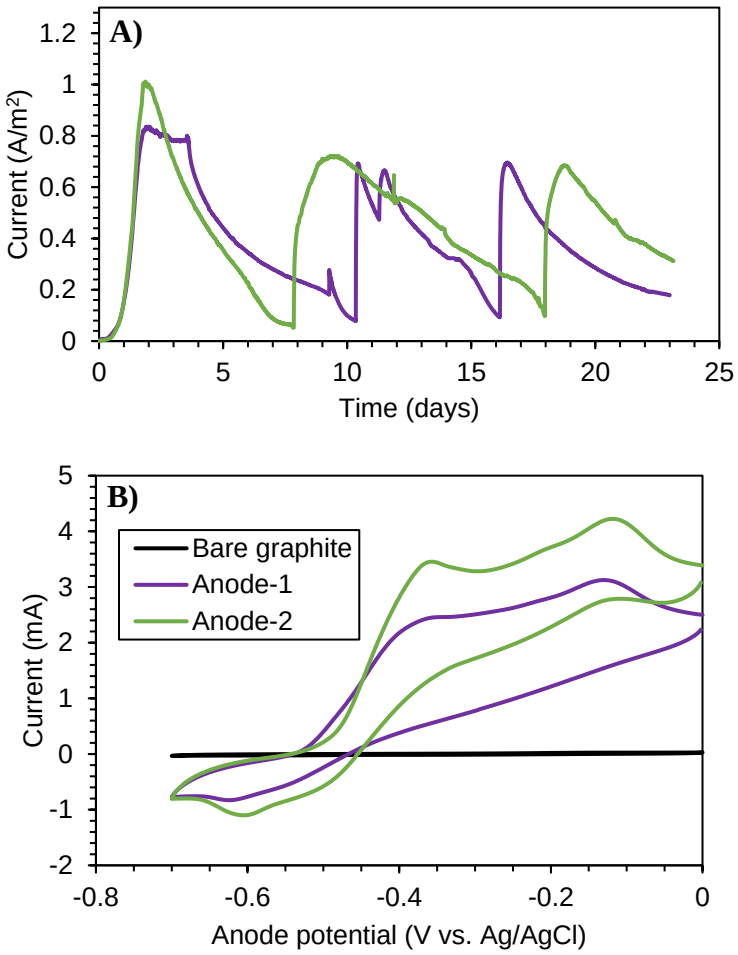

Figure 4.13. A) Current density graph, and B) CV analyses during anode biofilm formation of Set 2

4.1.2.2 Methane and Hydrogen Production

In AD-MEC operation, the reactors were operated in 3 cycles. The cathode potentials of -0.9 V, -1 V, and -0.95 V were applied in Cycle 1, Cycle 2, and Cycle 3, respectively. During the 3 cycles, CH_4 and H_2 production were monitored (Figure 4.14). At a cathode voltage of -0.9 V (Cycle 1), CH_4 productions of the Bioelectrode, and Bare electrode were similar until day 16 (Figure 4.14A). Nevertheless, the Bare electrode generated more CH_4 after day 16. Thus, prior biofilm growth did not affect CH_4 generation at -0.9 V potential. After 10 days, AD-MEC reactors began to surpass Conv. AD and OC controls.

As seen in Figure 4.14, applying a cathode potential of -1 V in Cycle 2 inhibited CH_4 production in voltage-applied reactors. Therefore, the CH_4 production in the AD-MEC was lower than in control reactors. Thus, the second cycle was operated for only 9 days due to the inhibition (Figure 4.14B). It has been reported in the literature that high H_2 partial pressure can inhibit methanogens (Deublein & Steinhauser, 2011). In the reactors, the H_2 partial pressure was calculated as given in Appendix F. The H_2 partial pressure was approximately 0.57 atm, which is exceedingly high compared to inhibitory levels (partial pressure $>10^{-4}$ atm) inhibits (Kutlar et al., 2022). This effect was not observed at -1 V cathode potential in Set 1 with graphite-graphite electrodes. The difference between the two sets was the cathode material, and the use of SS mesh as cathode increased H_2 production as expected (Ambler & Logan, 2011). Cycle 3 was operated by applying -0.95 V. As previously described in the experimental design, AD-MEC reactors of Set 2 were also operated with new bare electrodes starting from the second and third cycles. However, it seems that CH_4 production is very limited in New_Bare electrode reactors at -1 V. With higher cathode potentials, it might be challenging for biofilm to develop due to abiotic H_2 production on the cathode surface.

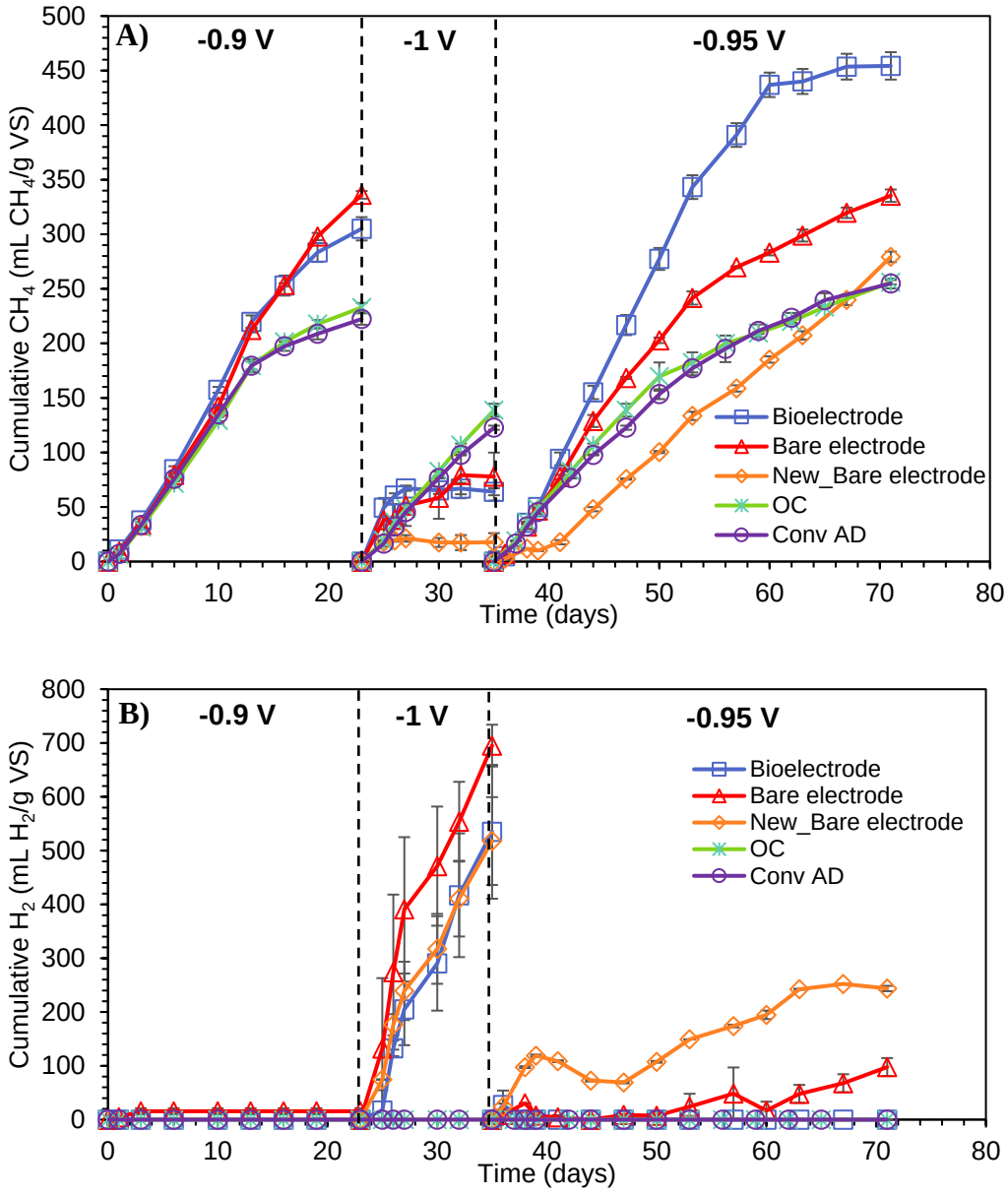

Figure 4.14. Cumulative A) CH_4 and B) H_2 production during AD-MEC operation in Set 3

In the 3rd cycle (-0.95 V cathode potential), the reactor with Bare electrode showed lower CH_4 production than the Bioelectrode reactors. After day 6, this difference increased gradually. New_Bare electrode reactors showed significantly lower performances than other reactors. After 30 days, the methane production was higher than control reactors. However, overall performance was lower than the other two

AD-MEC reactors (Bioelectrode and Bare electrode); since it could not catch up despite the long operating time (36 days). This may be due to inadequate biofilm colonization on the electrode surface, resulting in comparatively high H_2 generation (Figure 4.14B). Thus, no significant H_2 was observed in those reactors, except the New Bare electrode reactors. This suggests that hydrogenotrophic methanogens can consume H_2 that is produced abiotically on the cathode surface. In addition, Conv. AD and OC controls produced comparable amounts of CH_4 during each cycle. Consequently, adding electrodes without applying voltage had no effect on CH_4 generation. Although several studies have demonstrated that OC reactors may outperform AD-MEC reactors, the electrode surface area is a significant variable that may make a difference (Baek, Kim, et al., 2021; Baek, Saikaly, et al., 2021). Increasing the surface area further may alter the performance of OC compared to Conv. AD and AD-MEC reactors.

Although bare electrode reactors exhibited a higher yield at -0.9 V cathode potential, bioelectrode reactors produced significantly more CH_4 than bare electrode reactors at -0.95 V cathode potential. Although H_2 generation increases as the cathode potential rises, bioelectrode was used to simultaneously utilize the H_2; hence, no H_2 was observed at -0.95 V cathode potential. Nevertheless, Bare electrode reactors were unable to use the entire H_2 and produced less CH_4 than Bioelectrode. The abundance of hydrogenotrophic methanogens might be the explanation for this.

CH_4 yields provide a more straightforward comparison of the reactors' performance (Figure 4.15). The highest CH_4 was observed by the Bioelectrode reactors at – 0.95 V cathode potential (454 ± 13 mL CH_4/g VS). Compared to Conv. AD (222 ± 5 mL CH_4/g VS) reactors, there is an increase of 105%. It is followed by the Bare electrode at – 0.9 V cathode potential and the Bare electrode at – 0.95 V cathode potential. Although these reactors produced the same quantity of CH_4 in both cycles (Bare electrode at – 0.9 V: 336 ± 4 mL CH_4/g VS and Bare electrode at – 0.95 V: 335 ± 6 mL CH_4/g VS), they did so at varying rates. Moreover, the CH_4 production increased by 51% compared to the Conv. AD reactors. Bioelectrode reactors at -0.9 V cathode potential (305 ± 11 mL CH_4/g VS) increased CH_4 production by 37% compared to

Conv. AD reactors. OC reactors (233 ± 4 mL CH_4/g VS) increased CH_4 yield by 5% compared to Conv. AD. The increased surface area due to the electrodes did not cause a significant increase unless voltage was applied. The increase between the OC and AD-MEC reactors proved that the AD-MEC system works efficiently.

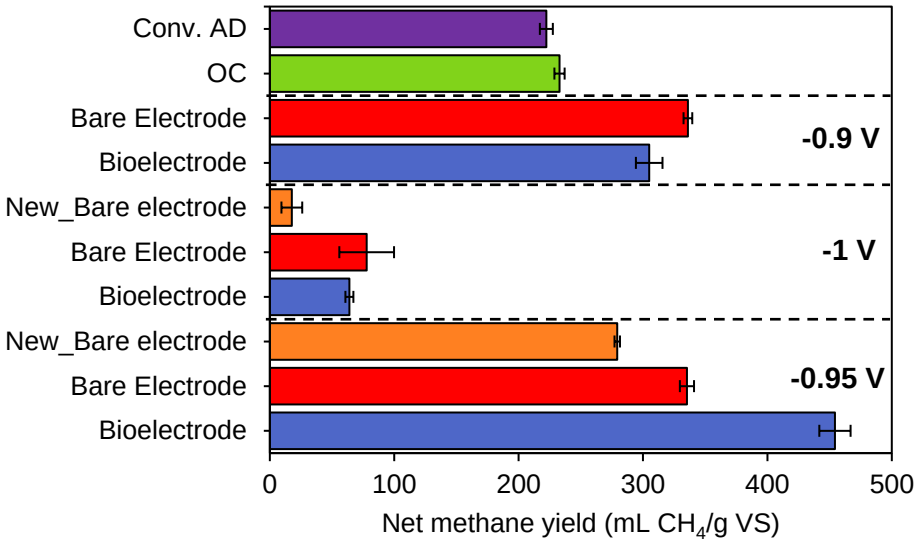

Figure 4.15. Net CH_4 yield of the reactors in Set 2

4.1.2.3 Current Uptake

During AD-MEC operation current uptake was monitored as seen in Figure 4.16. Replicates of the reactors are given in Appendix G. At cathode potential -0.9 V, Bioelectrode and Bare electrode reactors showed very similar current densities with averages of -0.58 ± 0.18 A/m^2 and -0.69 ± 0.25 A/m^2, respectively. The current densities did not change significantly over time for 22 days of operation. After 22 days, the first cycle was completed, and fresh seed, substrate, and media were put in the reactors. The cathode potential was increased to -1 V. The highest current density was observed at -1 V cathode potential. At -1 V, a new pair of bare electrodes was set at the start of the operation. The average current densities were -1.92 ± 1.16 A/m^2, -2.7± 1.1 A/m^2, and -1.6 ± 0.5 A/m^2 for Bioelectrode, Bare electrode and New_Bare electrode, respectively. Also, during the 9 days of operation, current densities varied

significantly. Although current uptake was the highest, CH_4 production was significantly low compared to other cycles. As discussed by Liang et al. (2015), even though greater applied voltage results in higher current, it is not advantageous for preserving the exoelectrogenic bacterial population in the microbial community of the bioanode. At the third cycle, the cathode potential was set - 0.95 V. The average current densities for Bioelectrode, Bare electrode, and New_Bare electrode were -0.69 ± 0.19 A/m^2, -1.27 ± 0.46 A/m^2, and -0.72 ± 0.32 A/m^2, respectively. The findings show that current increases along with cathode potential. Choi et al. (Choi et al., 2017) made comparable observations. As the cathode potential changed from -0.7 V to -1.01 V, the current considerably increased. Yet, increasing the cathode potential further decreases the current, which was not investigated in this study.

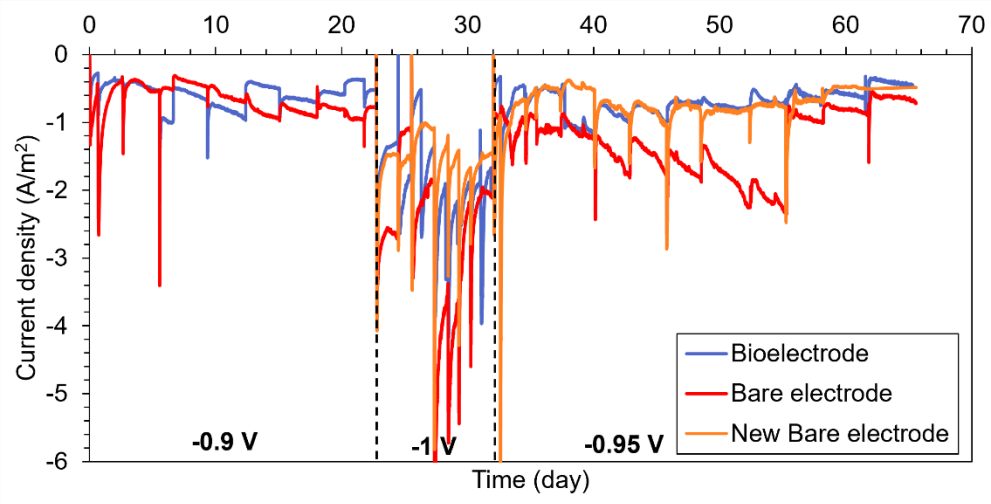

Figure 4.16. Average current uptake graph during AD-MEC operation in Set 2

4.1.2.4 Methane Production Kinetics and Organic Removal

The cumulative CH_4 yield plots were fitted by the modified Gompertz model. Kinetic parameter summaries are given in Table 4.2. The agreement between the model and experimental data was evaluated by the coefficient of determination (R^2) (Table 4.2) and model fit (Appendix H). The closer the R^2 value is to 1, the greater the agreement between the model and experimental data (Gurkok et al., 2011). R^2 values of all

reactors are higher than 0.995. Since the -1 V cathode potential inhibited CH_4 production, the kinetic data is not given for Cycle 2. In addition to the increase in CH_4 yield, the kinetics of CH_4 production may affect the implementation of AD-MEC systems compared to AD (Zakaria & Dhar, 2019). Thus, this implies that AD-MEC may handle more waste and generate more CH_4 in less time.

Table 4.2 Kinetic parameters from the modified Gompertz model and VS removal for Set 2

	Reactors	P_∞ (mL CH_4/g VS)	R_m (mL CH_4/g VS/d)	λ (day)	R^2
	Conv AD	228 ± 5	17.2 ± 1.0	1.7 ± 0.01	0.9983
	Open circuit	245 ± 5 (7)[a]	16.9 ± 0.5 (-)	1.9 ± 0.02 (-)	0.9982
-0.9 V	Bare electrode	394 ± 11 (73)	20.0 ± 0.3 (17)	2.6 ± 0.25 (-)	0.9983
-0.9 V	Bioelectrode	330 ± 17 (45)	20.5 ± 1.0 (19)	2.0 ± 0.12 (-)	0.9988
-0.95 V	New_Bare electrode	347 ± 2 (52)	9.8 ± 0.1 (-)	5.4 ± 0.01 (-)	0.9950
-0.95 V	Bare electrode	334 ± 16 (46)	15.8 ± 0.5 (-)	1.5 ± 0.21 (12)	0.9980
-0.95 V	Bioelectrode	477 ± 16 (109)	24.2 ± 1.2 (41)	2.8 ± 0.06 (-)	0.9980

[a] Numbers in parentheses are the percent increase in CH_4 production rate and percent decrease in lag time compared to Conv AD in respective cycles.

It was observed that the Conv. AD and OC reactors had similar CH_4 production rates. In general, the AD-MEC systems increased the rate and did not decrease the reactor start-up time. The highest CH_4 production rate was observed for the Bioelectrode reactors at -0.95 V cathode potential (24.2 mL CH_4/g VS/d). This rate was 41% higher than Conv. AD reactors. On the other hand, the shortest lag time was observed with Bare electrode reactors at -0.95 V with a 12% decrease with respect to Conv. AD. For -0.9 V cathode potential, the CH_4 production kinetics of Bioelectrode was higher than Bare electrode. However, the overall CH_4 production potential of the Bare electrode was higher (73% higher than Conv. AD). This implies that biofilm formation on bare electrodes may extend the start-up time of the reactor and limit the CH_4 production rate. After biofilm formation, the performance of the Bare electrode suppressed Bioelectrode reactors under -0.9 V cathode potential.

In addition to CH_4 production kinetics, organic removal is an important parameter to evaluate the performance of degradation and CH_4 production. In Figure 4.17, VS removal performances of the reactors are shown. Since at -1 V cathode potential, inhibition was observed, the operation was stopped earlier. Thus, VS removal was very low at this cathode potential. Other than Bioelectrode reactors at -0.95 V cathode potential, other reactors had comparable VS removal performances. Compared to Conv. AD reactors, the VS reduction in bioelectrode reactors was 48.5% greater in Cycle 3. AD-MEC systems speed up the organic removal rate and degradation of VFA; hence CH_4 production increases (Z. Yu et al., 2018).

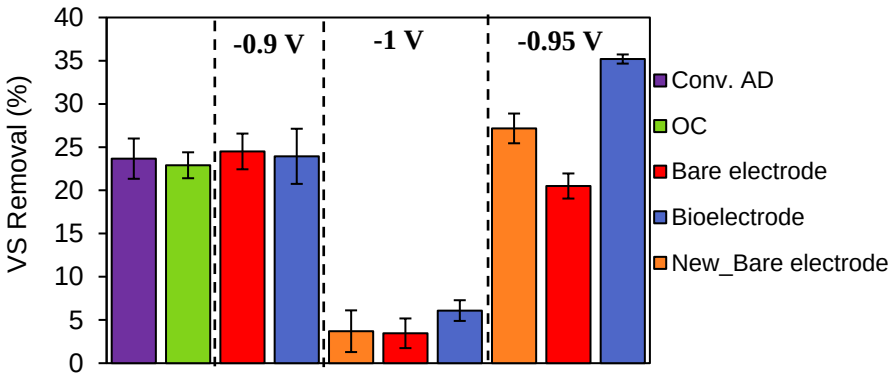

Figure 4.17. VS removal of the reactors

4.1.2.5 Cyclic Voltammetry

CV analyses were done weekly, beginning at t=0 to monitor the electroactivity of biofilm on electrodes and to explore its evolution over time. CV analyses for the three cycles are shown in Figure 4.18 – Figure 4.20. As seen in Figure 4.18, bioelectrode reactors had significant reduction and oxidation peaks at the initial CVs. On the other hand, bare electrodes had no electroactivity. In the first week, oxidation was observed for bare electrodes, implying the growth of electroactive biofilm (Figure 4.18A). The oxidation peak increases with the second week and is almost the same for the second and third weeks. Thus, exoelectrogens may require almost 15

days for bare electrode. On the other hand, the anode CV of bioelectrode showed relatively low peak oxidation compared to the initial (Figure 4.18B).

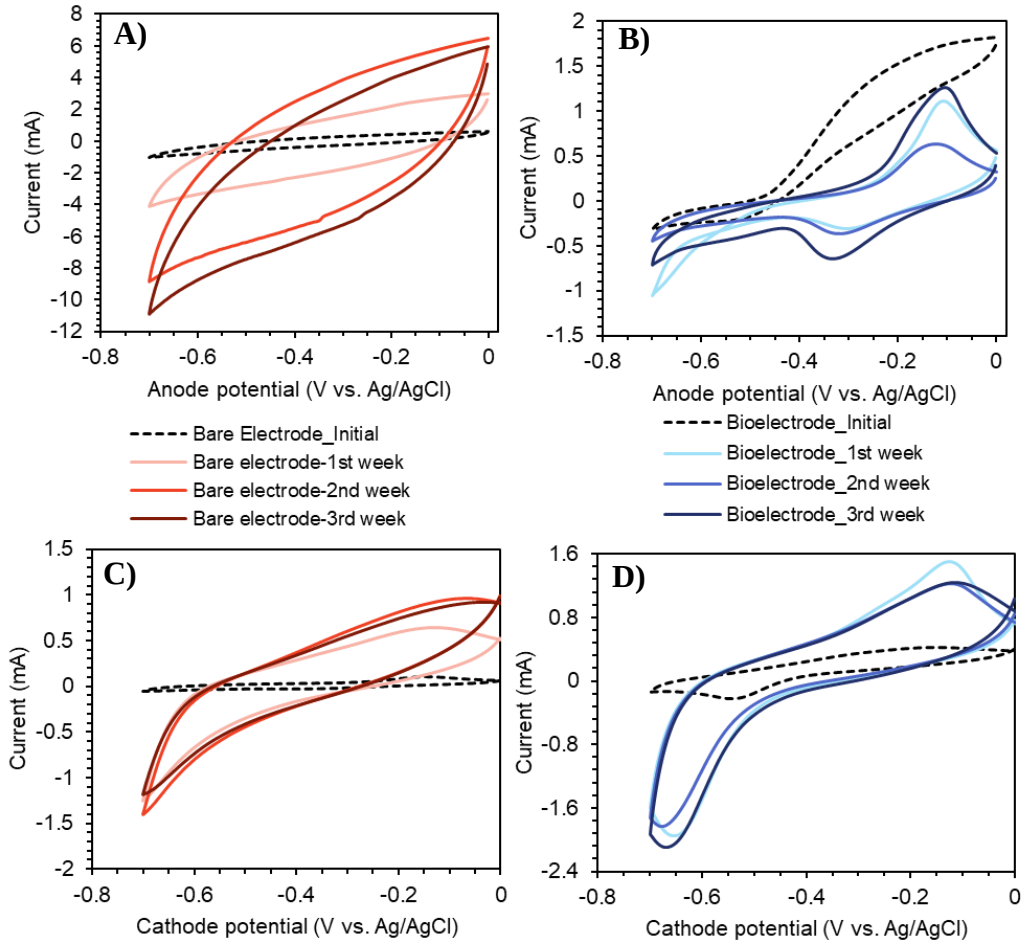

Figure 4.18. CV of the reactors at -0.9 V cathode potential, A) anode of Bare electrode, B) anode of Bioelectrode, C) cathode of Bare electrode, C) cathode of Bioelectrode reactors in Set 2

For the cathode, the oxidation peak increased significantly in the first week. The oxidation peak was found to be around -0.15 V, which is in the range of exoelectrogens that catalyze the bio-oxidation of volatile organic acids, such as *Geobacter* species (-0.46 V to 0 V) (Zhu et al., 2012). Moreover, the reduction peak at -0.44 V corresponded well with methanogenesis (E_0 values for $CO_2 \rightarrow CH_4$= -0.437 V vs. Ag/AgCl, and $CO_2 \rightarrow$ethanol: −0.51 V vs. Ag/AgCl) (K. Guo et al., 2014; F. Liu et al., 2012). When bare electrode and bioelectrode reactors were compared, the

peak point for oxidation was almost 4 times higher in the case of the bare electrode (Figure 4.18A and 4.18B). However, their shapes were significantly different. The shape of the CV depends on thermodynamic, kinetics, reversibility, and mass transfer properties (H. Wang et al., 2020). The bioelectrode reactors displayed distinct anode and cathode peaks, but the bare electrodes did not. Moreover, since the oxidation and the reduction did not take place at one potential, reactions were possibly quasireversible (H. Wang et al., 2020).

Due to inhibition at -1 V cathode potential, CV analyses are not given. In Cycle 3, cathode potential was decreased to -0.95 V. Corresponding CV analyses are given in Figure 4.19. When anode CV analyses were investigated, the highest oxidation point was observed with the Bare electrode (Figure 4.19B). It was followed by Bioelectrode and New_Bare electrode (Figure 4.19A and 4.19E). In the same way, cathode CV plots showed the same result. Bioelectrode showed a clear reduction peak (Figure 4.19F) since increased CH_4 generation may result from the high electroactivity of methanogens on the cathode for Bioelectrode. Moreover, over time, the New_Bare electrode exhibited a gradual increase in cathode reduction peaks, which coincided with an increase in methane production (Figure 4.19C). The peaks correspond well with exoelectrogens and methanogenesis (Figure 4.19A, 4.19B, and 4.19E).

As seen in Figure 4.19B, D, E, and F, CV plots of the first week were higher than CV plots of the remaining weeks. Peaks became lower over time for Bare electrode and Bioelectrode reactors. Bioelectrode formation and AD-MEC operation took 57 days and 71 days, respectively. This may cause maturation of the biofilm and a decrease in the electroactivity of the biofilm (J. Kang et al., 2012). A study conducted by J. Kang et al. (2012) showed that as the cell density increased, the current decreased in the CV graphs. This could be attributed to the reduced effective surface area of the electrodes due to bacterial cells covering a larger area, which interfered with the electrochemical reactions (J. Kang et al., 2012). As the biofilm matured and bacterial accumulation exponentially grew, the current of the colonized electrodes decreased compared to the uncolonized electrodes (J. Kang et al., 2012).

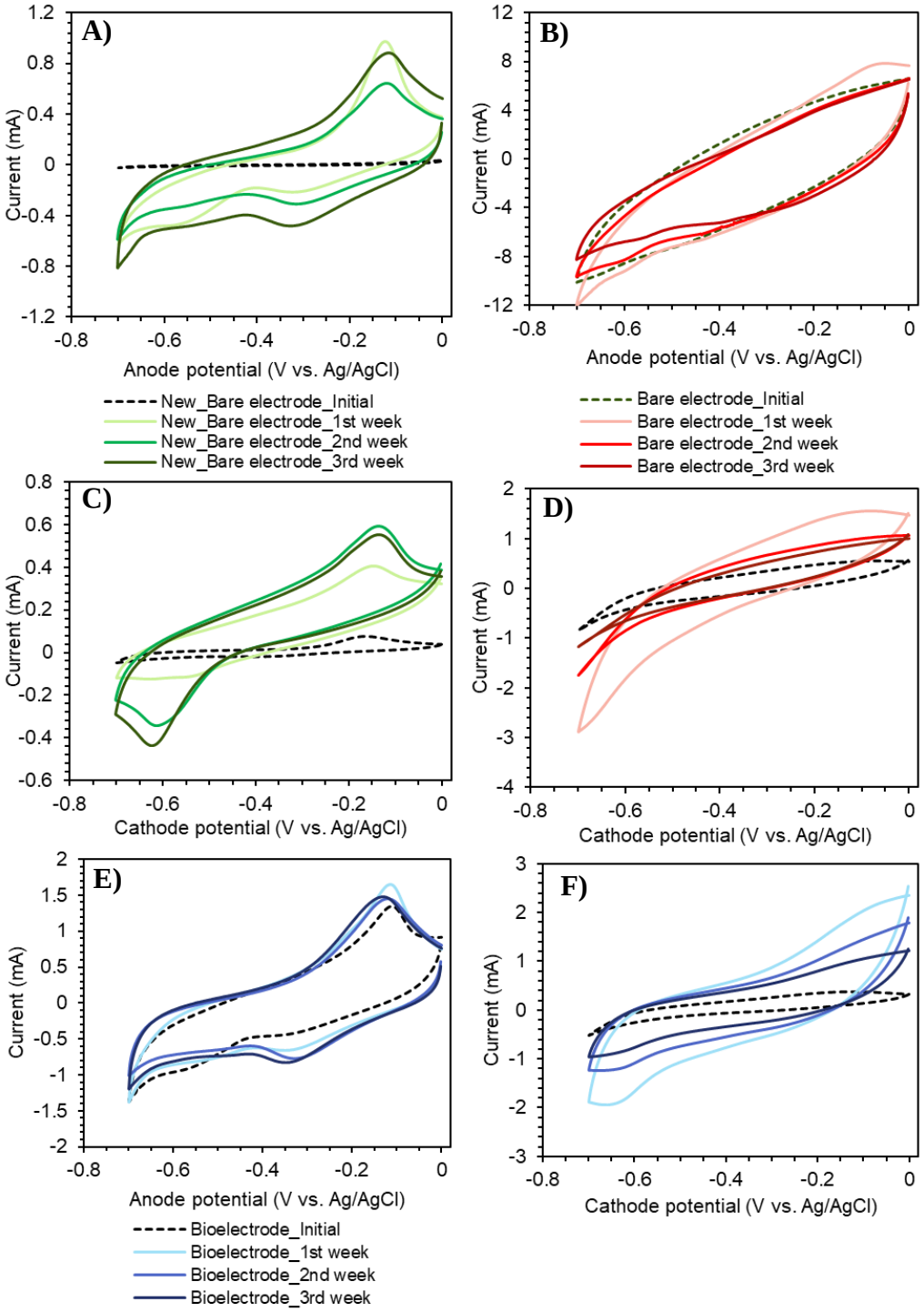

Figure 4.19. CV of the reactors at -0.95 V cathode potential, A) Anode of New_Bare electrode, B) anode of Bare electrode, C) cathode of New_Bare electrode, D) cathode of Bare electrode, E) anode of Bioelectrode, and F) cathode of Bioelectrode reactors in Set 2

4.1.3 Set 3: WBS Fed AD-MEC Using Graphite – Graphite Electrodes

4.1.3.1 Biofilm Formation on GAC

Three concentrations (25, 35, and 45 g/L) were tested during biofilm formation on GAC. In Test 1, bare GAC particles were amended to the reactors. CH_4 production of the tests is given in Figure 4.20 and Figure 4.21. The graph shows that bare GACs did not significantly increase CH_4 production (Figure 4.20). For these reasons, it was chosen to employ biofilm-developed GAC (BioGAC) particles rather than GAC without biofilm in AD-MEC operation. BioGACs were collected from the effluent of Test 1 reactors. In order to decide on the best concentration of BioGAC to use in the AD-MEC system, reactor operation was performed with the BioGAC as Test 2. Cumulative CH_4 productions are given in Figure 4.21. BioGAC_35 and BioGAC_45 produced almost the same CH_4 corresponding to a 9% increase compared to Conv. AD.

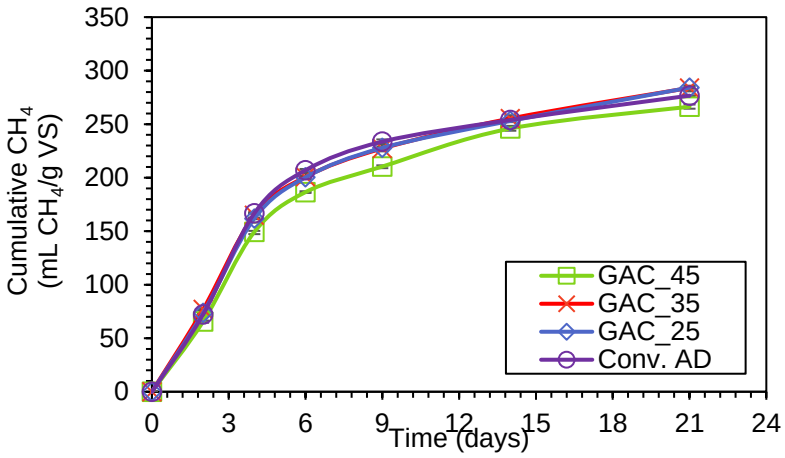

Figure 4.20. Cumulative CH_4 production of the reactors during Test 1 (GAC)

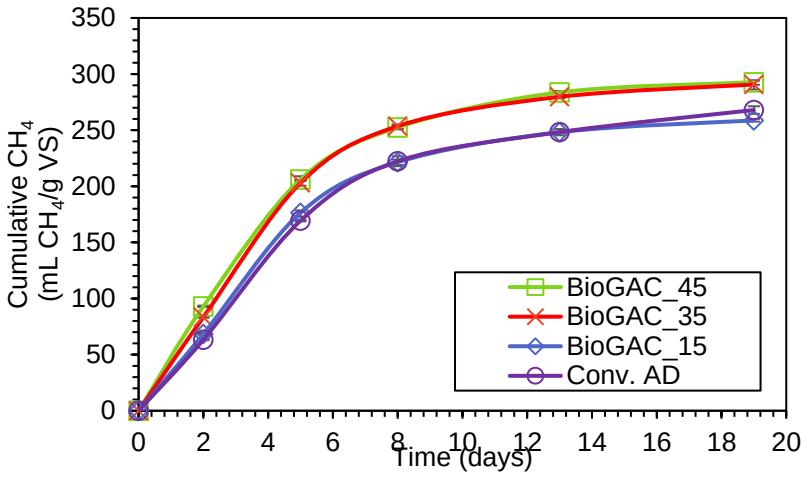

Figure 4.21. Cumulative CH_4 production of the reactors during Test 2 (BioGAC)

Upon analysis of the results, it was observed that BioGAC_35 and BioGAC_45 exhibited comparable outcomes. Nevertheless, the utilization of a higher concentration of GAC entails increased process costs. Consequently, the BioGAC_35 reactors were chosen for operation in the AD-MEC system, considering the balance between performance and cost-effectiveness.

4.1.3.2 Biofilm formation on Electrodes

The cathode biofilm was developed in four cycles, like the previous sets. A new cycle started when the daily increase in methane production dropped below 10%. Cumulative CH_4 production during 4 cycles is given in Figure 4.22. In the first two cycles, CH_4 is produced at a similar rate. As the inoculum was reduced repeatedly between cycles, the production of CH_4 will decline due to a decrease in background CH_4 production. In the fourth cycle, CH_4 synthesis is only possible through the cathode biofilm since no catholyte was left in the reactor. This demonstrates that the cathode biofilm was formed successfully. To make sure that the biofilm on the electrode surface was active, the fourth cycle was not completed.

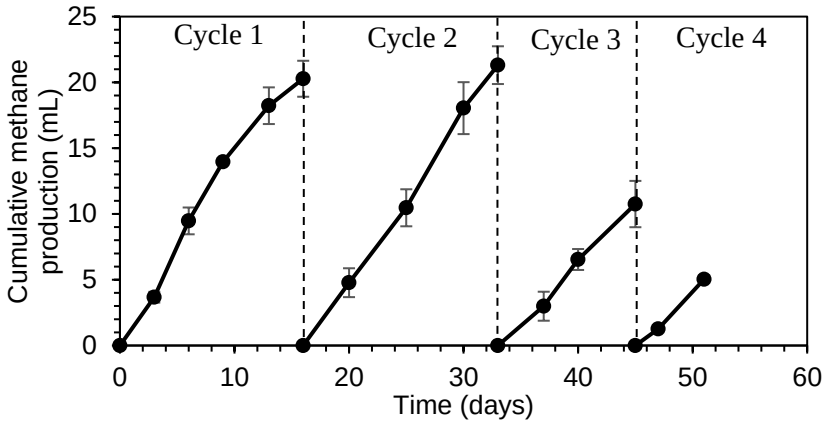

Figure 4.22. Cumulative CH_4 production during cathode biofilm development in Set 3

Biofilm growth during each cycle was verified with CV analysis in addition to CH_4 production. CV peaks of bare graphite and cathodes in each cycle were compared to one another to investigate the electroactivity of the biofilm (Figure 4.23). The CV graph of bare graphite did not exhibit a reduction peak. On the other hand, a clear reduction peak was observed in Cycle 3 (Figure 4.23). Thus, cathodic biofilm was successfully developed.

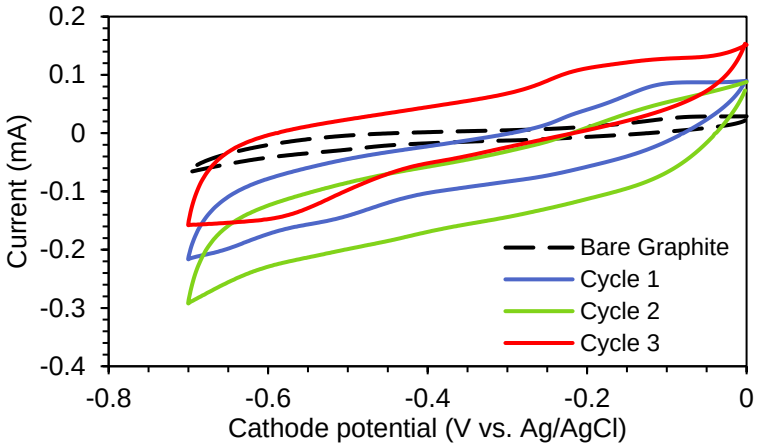

Figure 4.23. CV during cathode biofilm development in Set 3

The anode biofilm on graphite was formed at the same time as the cathode biofilm. The identical process as with the prior sets was used during anode biofilm formation. The system received a new injection of acetate when the current decreased to 0.15

A/m^2. Eight cycles were completed to form a biofilm (Figure 4.24A). It is observed that the current has decreased with time. The activity of the biofilm was confirmed with CV analysis. At the end of the anodic biofilm formation, CV was performed. The activity was observed with the clear oxidation peak in CV analysis (Figure 4.24B).

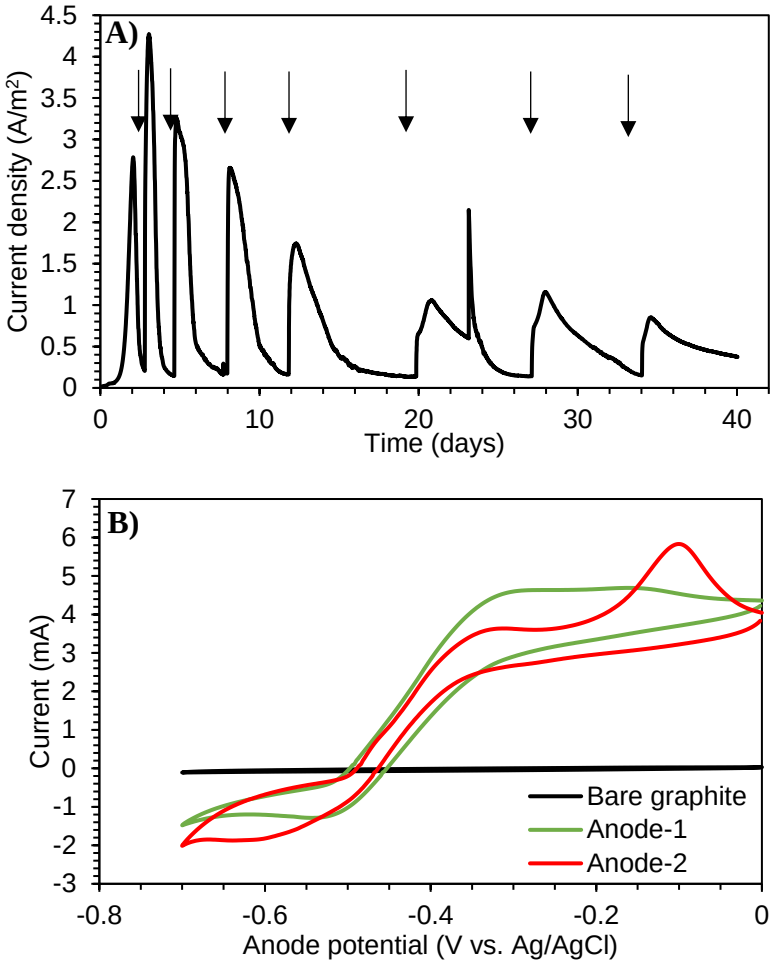

Figure 4.24. A) Current generation (Arrows represent new acetate injection.), B) CV during anode biofilm formation in Set 3

The generated bioelectrodes were then placed in AD-MEC single-chamber reactors.

4.1.3.3 Methane and Hydrogen Production

The total net CH_4 production is shown in Figure 4.25A. A cathode potential of -0.9 V and -1 V was applied during Cycle 1 and Cycle 2, respectively. The reactors generally produced equal amounts of CH_4 up until Day 12. The Bioel-BioGAC reactors started to produce more CH_4 than the other reactors after Day 12. Except for Bioel-BioGAC, all reactors produced the same amount of CH_4 on Day 23, at the end of Cycle 1. Bare el reactors showed a delay from day 2 to 10. Since at the start of the operation Bare el reactors had no biofilm, removed VS, and applied energy may be used for biofilm formation rather than CH_4 production. Moreover, H_2 was not detected during -0.9 V cathode potential.

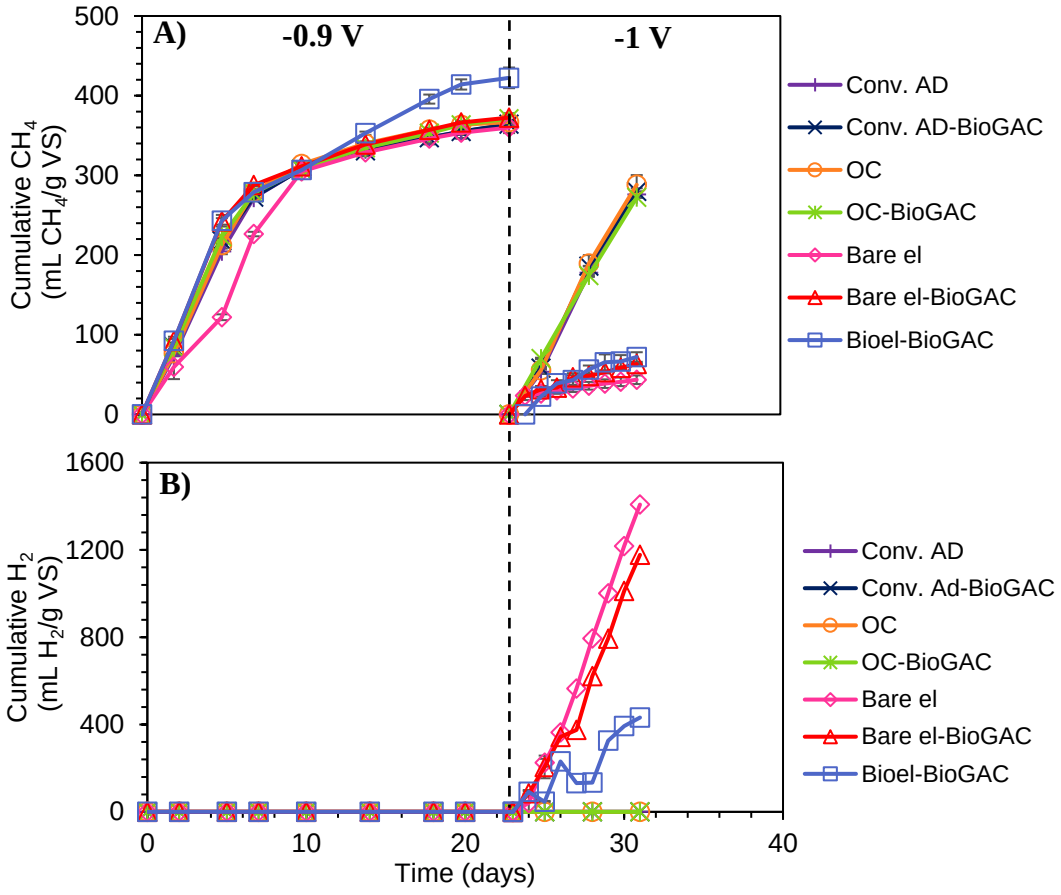

Figure 4.25. Cumulative A) CH_4, and B) H_2 production of reactors in Set 3

The cathode potential was raised to -1 V in Cycle 2. Due to significant H_2 production (Figure 4.25B), the AD-MEC reactors (Bare el, Bare el-BioGAC, Bioel-BioGAC) produced less CH_4 than the control reactors. At -1 V cathode potential, CH_4 production was inhibited since a significant amount of H_2 was created. A high H_2 partial pressure has been linked to methanogen inhibition in the literature (Deublein & Steinhauser, 2011). In the reactors, the H_2 partial pressure was approximately 0.46 atm, which is exceedingly high compared to inhibitory levels (partial pressure $>10^{-4}$ atm) inhibits (Kutlar et al., 2022). The calculation of the H_2 partial pressure was given in Appendix F. Cattle manure set with graphite-graphite electrodes enhanced CH_4 production at -1 V cathode potential; however, with WBS, this was not observed. Thus, on day 8, inhibition was verified, and the set was stopped.

Additionally, the CH_4 yields of the reactors at -0.9 V cathode potential are given in Figure 4.26. The highest CH_4 yield was observed with Bioel-BioGAC reactors with 422 ± 13 mL CH_4/g VS. Similar CH_4 yields were obtained in other reactors, with an average of 366 ± 5 mL CH_4/g VS. Implementation of AD-MEC integration with bioelectrodes and BioGAC increased the CH_4 yield by 16% compared to conventional AD system. When pairs of reactors such as Conv AD and Conv.AD-BioGAC, OC and OC-BioGAC, and Bare el and Bare el-BioGAC were compared, it can be concluded that the sole addition of BioGAC was not sufficient to boost CH_4 yield. Therefore, using both BioGAC and bioelectrodes had a synergistic effect on CH_4 production with AD-MEC systems fed with WBS.

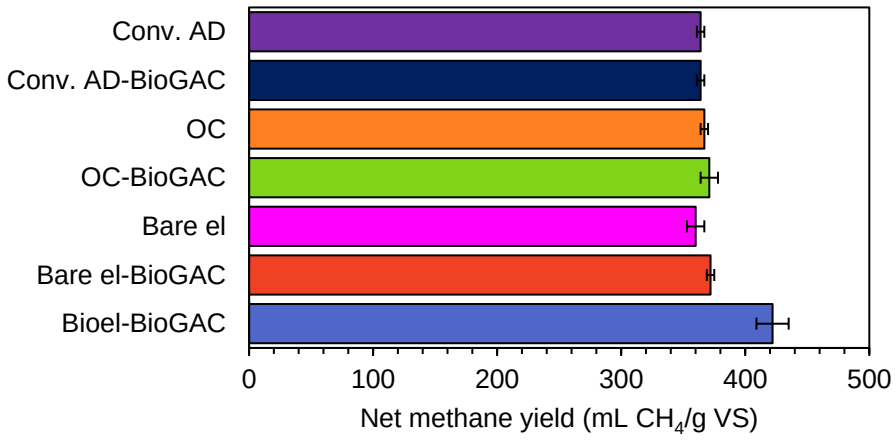

Figure 4.26. Net CH_4 yield of the reactors at -0.9 V cathode potential in Set 3

4.1.3.4 Current Uptake

Figure 4.27 shows the current density graphs for the two cycles of Set 3. Replicates of the reactors are given in Appendix I. The maximum current at -0.9 V cathode potential is produced by Bioel-BioGAC, with a peak current density of 3 A/m^2. The Bare el-BioGAC reactors had a peak current of 0.34 A/m^2, while the Bare el reactors recorded 1.6 A/m^2. The Bioel-BioGAC reactor's high current uptake and the excess CH_4 output may be related. The current in the Bare el reactors started to decrease after the fifth day of operation. Following that, the current densities in the Bare el and Bare el-BioGAC reactors were comparable. Compared to the first cycle, the current in the second cycle is extremely high at -1 V cathode potential. Peak current densities for Bare el, Bare el-BioGAC, and Bioel-BioGAC are -10.5 A/m^2, -9.5 A/m^2, and -4.4 A/m^2, respectively. The current density is shown to increase along with the cathode voltage. Moreover, an increase in current density is seen as a result of the increased H_2 production. More current, however, implies more energy is used.

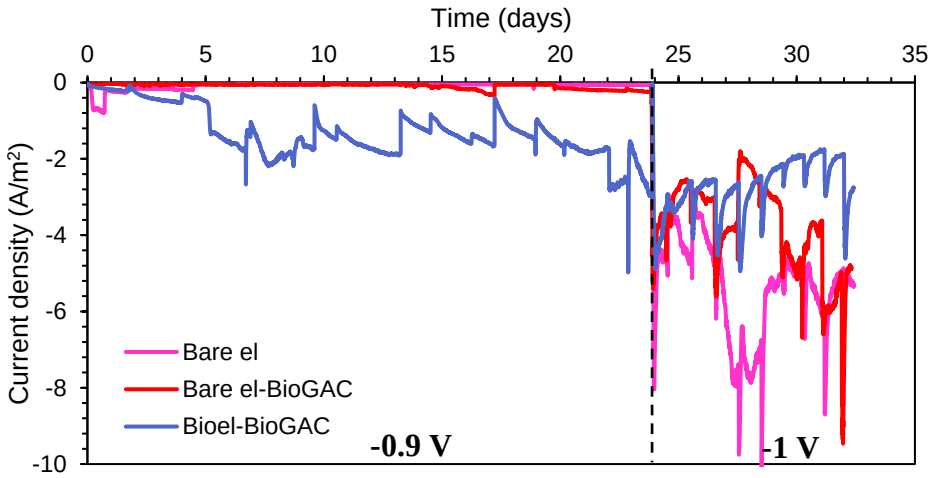

Figure 4.27. Current uptake of the AD-MEC reactors during 2 cycles

4.1.3.5 Methane Production Kinetics and Organic Removal

Modified Gompertz modeling was used to derive the kinetic parameters of the methane production in the reactors. Only kinetic data of reactors at -0.9 V cathode potential is given in Table 4.3 due to inhibition in Cycle 2. The model and experimental plots are given in Appendix J.

Table 4.3 Kinetic parameters and VS removal of the Set 3 reactors at -0.9 V cathode potential

Reactors	**VS removal (%)**	**P_∞ (mL CH_4/g VS)**	**R_m (mL CH_4/g VS/d)**	**λ (day)**	**R^2**
Conv.AD	19.8 ± 3.6	351 ± 10	45.9 ± 1.1	0.5 ± 0.01	0.9953
Conv. AD-BioGAC	28.9 ± 2.2	350 ± 6 (-)	46.0 ± 0.1 (-)	0.3 ± 0.05 (40)	0.9934
OC	14.7 ± 1.9	358 ± 4 (2)	47.5 ± 1.3 (3)	0.5 ± 0.05 (-)	0.9959
OC-BioGAC	26.3 ± 1.6	355 ± 9 (1)	46.7 ± 0.4 (2)	0.3 ± 0.11 (40)	0.9914
Bare el	14.8 ± 3.6	358 ± 12 (2)	39.2 ± 3.4 (-)	1.3 ± 0.48 (-)	0.9905
Bare el-BioGAC	21.9 ± 3.2	356 ± 5 (1)	50.8 ± 0.5 (11)	0.3 ± 0.15 (40)	0.9892
Bioel-BioGAC	21.8 ± 0.4	401 ± 9 (14)	42.3 ± 1.3 (-)	0 (100)	0.9718

The highest rate was observed in Bare el-BioGAC reactors with an 11% increase compared to Conv. AD (50.8 ± 0.5 mL CH_4/g VS/d). Although the methane yield of Bare el-BioGAC did not differ with Conv. AD reactors, the rate of the process increased with the use of Bare el-BioGAC.

It is clear that the Conv. AD reactors fed with WBS produce CH_4 at a high rate compared to cattle manure-fed reactors. BioGAC-added reactors decreased lag time by 40% in all cases. Bioelectrode implementation caused even an absence of a lag time. Thus, the BioGAC additive was the most significant factor when the reactor in terms of the start-up time.

While other reactors had an average VS reduction of 16.4 ± 2.9%, BioGAC reactors had a mean VS removal of 24.7 ± 3.5%. VS removal of BioGAC reactors was significantly high compared to the reactors without BioGAC. According to the results, the main factor affecting VS removal is the presence of BioGAC.

AD systems fed with WBS are already very effective compared to cattle manure-fed AD systems. By applying AD-MEC integration on a system that was already effective, possible improvements are limited. This improvement was made possible by combining the AD-MEC and BioGAC options. The results showed that using bioelectrodes together with BioGAC for WBS rather than bare electrodes had better outcomes. By speeding up a start-up, increasing organic removal from the reactor and CH_4 yield were successfully boosted. The production of CH_4 was also significantly reduced by the high cathode potential. This needs to be taken into account by WBS-fed systems.

4.1.3.6 Cyclic Voltammetry

In Figure 4.28, CV plots of the reactors are given. Since inhibition was observed with a -1 V cathode potential, CV data was not given. When the initial CV of Bare el and Bare el-BioGAC reactors were compared, BioGAC reactors had slight electro-activity compared to Bare el reactors. The BioGAC particles may cause a difference in CV because the cathode had contact with them.

In the first week, both anodic and cathodic peaks were observed. For cathode biofilm, the reduction peaks of Bare el and Bare el BioGAC were around -0.7 V – -0.6 V vs. Ag/AgCl. Similarly, the initial CV of Bioel-BioGAC showed a reduction peak around these values. However, the reduction peaks of the following weeks were around -0.3 V – -0.2 V vs. Ag/AgCl. This shows the changing biofilm to exoelectrogens like the *Geobacter* species that accelerate the bio-oxidation of volatile organic acids (He et al., 2021).

Moreover, the presence of a biocatalyst able to transport electrons extracellularly to the electrode was evidenced by the appearance of distinct oxidation peaks and reduction peaks in the CV curves of anodic biofilms (Qin et al., 2021).

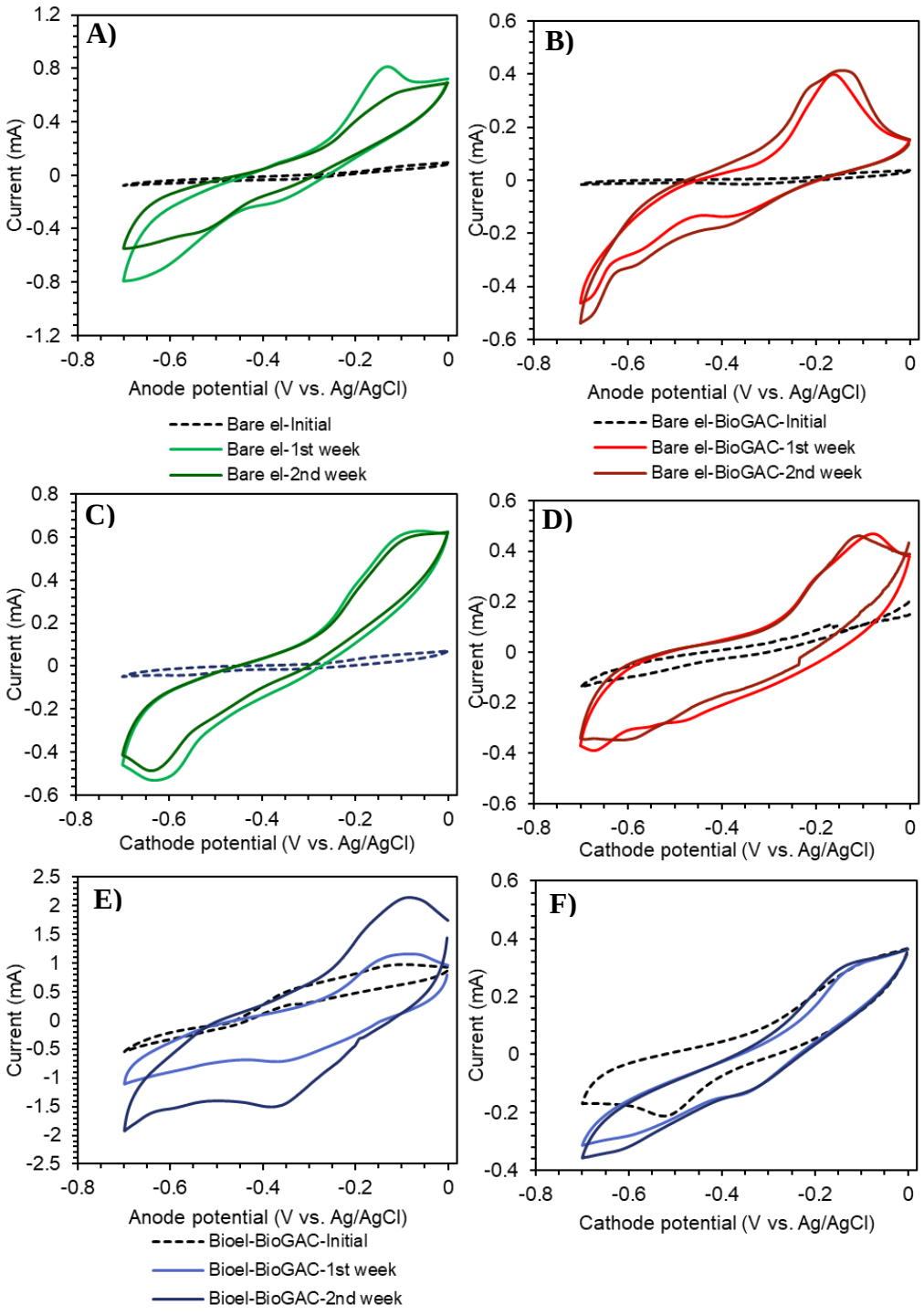

Figure 4.28. CV plots for A) anode of Bare el, B) anode of Bare el-BioGAC, C) cathode of Bare el, D) cathode of Bare el-BioGAC, E) anode of Bioel-BioGAC, and F) cathode of Bioel-BioGAC at -0.9 V cathode potential in Set 3

4.1.4 Comparison of AD-MEC Sets

The application of AD-MEC increased CH_4 production compared to conventional AD systems. CH_4 production and kinetics are unaffected by the addition of electrodes to a system without the application of voltage (*i.e.*, an increase in surface area). This is confirmed by the inclusion of OC controls in each set. Additionally, buffer media is essential for AD-MEC systems. Biofilm formation was not observed in electrode reactors without PBS media. After the media was replaced with 5 mM PBS, the formation of biofilm was monitored by current and CV. Therefore, AD-MEC systems require a conductive medium for effective electron transfer. Overall, bioelectrodes and bare electrodes demonstrated comparable efficacy, despite their distinct microbial communities. Controlled biofilm formation did not result in a significant improvement over the use of bare electrodes expect graphite-SS bioelectrode AD-MEC fed with cattle manure at -0.95 V cathode potential which produced the highest CH_4. Since energy is required for the formation of biofilm on bioelectrodes while increasing operational costs, it is suggested, to begin with bare electrodes.

All CH_4 yield values obtained from this study are summarized in Table 4.4. Among all reactors, graphite-SS bioelectrode AD-MEC fed with cattle manure at -0.95 V cathode potential produced the highest CH_4 yield (454 ± 13 mL CH_4/g VS). It was followed by WBS-fed reactors. WBS shows better CH_4 yield potential than cattle manure and this is due to the different characteristics of these feedstocks. Control reactors (OC and Conv. AD) fed by WBS are already quite efficient systems. Thus, a further increase may not be feasible with AD-MEC integration. By combining BioGAC and bioelectrodes, a 13% increase was accomplished. However, this limited increase may not be feasible considering the increase in capital and operational costs. Thus, cattle manure is a better option considering AD-MEC integration systems.

Obviously, to accomplish these CH_4 yields, the AD-MEC systems require a certain amount of energy. In order to calculate energy consumption in AD-MEC systems, it is necessary to measure the potential difference between the anode and cathode.

However, this measurement could not be performed in this study due to technical limitations. Nevertheless, because of the uneven distribution of applied potential within a large electrode, controlling the working electrode potential is not a viable option for commercial reactors, *i.e.*, a potentiostat may not be used in the field. Therefore, this study is preliminary research about AD-MEC systems investigating different substrates, cathode potential, and start-up strategies.

Table 4.4 CH_4 yields from all data sets of this study

Sets	Conditions	Reactors	Methane yield (mL CH_4/g VS)
Set 1: Cattle manure Gr-Gr	No PBS	Conv. AD_noPBS	257 ± 4
		OC_noPBS	270 ± 12
	No PBS, -0.9 V	Bareel_noPBS	279 ± 10
		Bioel_noPBS	297 ± 4
	5 mM PBS	Conv. AD	239 ± 2
		OC	253 ± 2
	5 mM PBS, -0.9 V	Bareel_5mMPBS	227 ± 3
		Bioel_5mMPBS	222 ± 9
	5 mM PBS	Conv. AD	205 ± 3
		OC	207 ± 1
	5 mM PBS, -1 V	Bareel_5mMPBS	366 ± 3
		Bioel_5mMPBS	384
Set 2: Cattle manure Gr-SS	5 mM PBS	Conv. AD	222 ± 5
		OC	233 ± 4
	5 mM PBS -0.9 V	Bare electrode	336 ± 4
		Bioelectrode	305 ± 11
	5 mM PBS -0.95 V	New_Bare electrode	279± 2
		Bare electrode	335 ± 6
		Bioelectrode	454 ± 13
Set 3: WBS-Gr-Gr	5 mM PBS	Conv. AD	364 ± 3
		Conv. AD-BioGAC	364 ± 3
		OC	367 ± 3
		OC-BioGAC	371 ± 7
	5 mM PBS -0.9 V	Bare el	360 ± 7
		Bareel-BioGAC	372 ± 3
		Bioel-BioGAC	422 ± 13

Table 4.5 and Table 4.6 and Table 4.7 presents theoretical calculations based on the produced current and the removal of VS for Set 1 (Cattle manure Gr-Gr), Set 2 (Cattle manure Gr-SS) and Set 3 (WBS-Gr-Gr), respectively. The calculations in the tables are given in Chapter 3.1.5. These calculations provide an estimation of the

expected outcomes in terms of various parameters. For Set 1 (Cattle manure Gr-Gr), the absence of PBS resulted in low current and unreliable CCE. While the uptake of current may not directly contribute to increased CH_4 production, its application potentially facilitated the conversion of intermediate products into CH_4. The current application also influenced the suspended sludge in the reactors, may enable DIET and fostering syntrophic relationships among microorganisms, leading to enhancement. (Kutlar et al., 2022; Şanlı, 2022) Moreover, the presence of electrodes increased the surface area, could potentially promote a higher cell density of methanogens and increased methanogenic activity.

In Set 1, the replicates of the bioelectrode and bare electrode showed variations, but they both produced the same amount of CH_4 as the OC. This suggests a high deviation in CCE. Interestingly, the Bare electrode generated more current, but this increased current was not effectively converted into CH_4 production. On the other hand, the Bioelectrode removed more VS compared to other reactors, indicating a higher removal efficiency. However, despite this enhanced VS removal, the conversion efficiency of the Bioelectrode reactor was similar to the expected or theoretical values. For Cycle 1 and Cycle 2, CO_2 levels were lower for Bioelectrode reactors compared to other ones. The enhancement in CH_4 may be due to CO_2 conversion to CH_4.

Under a cathode potential of -1 V, the presence of H_2 was detected. When calculating CCE, H_2 production was also taken into account. However, the current generated was significantly higher compared to the amount of CH_4 or H_2 produced, resulting in a low CCE. CCE calculation only considers use of electrons while production of CH_4 or H_2, however, there may be other reduced products such as acetate or the electrons may be used by other microorganisms rather than methanogenic electrotrophs such as SRB. Therefore, lower than 100% CCE is reasonable. Additionally, since H_2 was consumed by other microorganisms, the reliability of CCE calculations may be compromised. When investigating the conversion of VS to CH_4, the AD-MEC demonstrated an increase in OCE. In some cases, the conversion

efficiency was reported to be higher than 100%, which is attributed to rough estimations made by taking the ratio of the initial VS to COD of cattle manure sample fed to the reactors.

In Set 2 (Gr-SS Cattle manure), the CCE values were lower than 100%. This could be attributed to the fact that SS may consume more energy due to corrosion. Furthermore, the Bare electrode exhibited a higher CCE than the Bioelectrode in Set 1, resulting in a greater production of CH_4 by the Bare electrode.

When using a cathode potential of -1 V in Cycle 2, if the current measured is significantly higher than the amount of H_2 produced, it could be attributed to factors such as corrosion. Corrosion can lead to additional current flow due to the degradation of electrode materials (Azri et al., 2023; Cristiani et al., 2021). These factors can result in higher currents being observed compared to the actual H_2 production. Due to inhibition in Cycle 2, OCE values were not calculated.

At a cathode potential of -0.95 V, the bioelectrode exhibited the highest CCE value compared to the other electrodes. This higher CCE value is the main reason for the increase in CH_4 yield observed in the Bioelectrode reactor. Additionally, VS to CH_4 production in the Bioelectrode reactor was closer to the theoretical value, indicating a more efficient conversion process. Moreover, the Bioelectrode reactors showed a greater removal of VS, indicating a higher degradation of organic matter and potentially contributing to the increased CH_4 production.

Among Set 3 (Gr-Gr WBS), only the Bioel-BioGAC reactor produced more CH_4 compared to the OC. Consequently, CCE was calculated only for this reactor. The CCE of this reactor was lower than 100%.This indicates that some of the currents might have been utilized for other electrochemical reactions or processes rather than CH_4 production such as SRB activities.

Table 4.5 Theoretical calculations on AD-MEC for Set 1 (Cattle manure Gr-Gr)

Conditions	Reactors	CH_4 yield (mL CH_4/g VS)	VS Removal (%)	CO_2 Content (%)	Current to CH_4 (mL)	ΔCH_4 * (mL)	CCE (%)	Removed VS to CH_4 (mL)	Actual CH_4 (mL)	OCE (%)
No PBS	Conv. AD	257 ± 4	39.2 ± 3	39	NA	NA	NA	286	212	74
	OC	270 ± 12	34.4 ± 1	42	NA	NA	NA	250	220	88
No PBS, -0.9 V	Bare electrode	279 ± 10	32.8 ± 1	42	0.4	6.7	3111 ± 4112	239	227	95
	Bioelectrode	297 ± 4	35.9 ± 4	37	6.8	18.4	265 ± 47	262	238	91
5 mM PBS	Conv. AD	239 ± 2	28.7 ± 2	45	NA	NA	NA	163	162	99
	OC	253 ± 2	31.5 ± 1	45	NA	NA	NA	188	174	93
5 mM PBS, -0.9 V	Bare electrode	227 ± 3	29.6 ± 1	48	4.5	3	21 ± 30	167	176.2	106
	Bioelectrode	222 ± 9	35.8 ± 5	43	3.7	5.1	128 ± 181	207	179.1	86
5 mM PBS	Conv. AD	205 ± 3	30.6 ± 1	44	NA	NA	NA	179	170	95
	OC	207 ± 1	32.4 ± 1	42	NA	NA	NA	190	178	94
5 mM PBS, -1 V	Bare electrode	366 ± 3	32	38	111	67.4	62	187	246	131
	Bioelectrode	384	31.8	43	121	78.2	74	186	256	138

* $\Delta CH4 = CH_{4AD\text{-}MEC} - CH_{4OC}$
NA: Not applicable

Table 4.6 Theoretical calculations on AD-MEC for Set 2 (Cattle manure Gr-SS)

Conditions	Reactors	CH_4 yield ($mL\ CH_4/g\ VS$)	VS Removal (%)	CO_2 Content (%)	Current to CH_4 (mL)	ΔCH_4 (mL)	CCE (%)	Removed VS to CH_4 (mL)	Actual CH_4 (mL)	OCE (%)
5 mM PBS	Conv. AD	222 ± 5	23.7 ± 2.3	42	NA	NA	NA	181	157	87
	OC	233 ± 4	22.9 ± 1.5	43	NA	NA	NA	176	163	93
5 mM PBS -0.9 V	Bare electrode	336 ± 4	24.5 ± 2.1	42	53	53	91 ± 6	188	216	115
	Bioelectrode	305 ± 11	23.9 ± 3.2	46	57	37	70 ± 12	184	200	109
5 mM PBS -1 V	New_Bare electrode	-	-	-	67	-	35 ± 1	-	-	-
	Bare electrode	-	-	-	110	-	28 ± 1	-	-	-
	Bioelectrode	-	-	-	78	-	31 ± 3	-	-	-
5 mM PBS -0.95 V	New_Bare electrode	279± 2	27.2 ± 1.7	37	119	12	27 ± 1	237	186	78
	Bare electrode	335 ± 6	20.5 ± 1.5	40	187	41	28 ± 4	179	215	120
	Bioelectrode	454 ± 13	35.2 ± 0.5	44	64	103	167 ± 3	303	277	91

* $\Delta CH4 = CH_{4AD\text{-}MEC} - CH_{4OC}$
NA: Not applicable.
-: It is not given due to inhibition.

Table 4.7 Theoretical calculations on AD-MEC for Set 3 (WBS Gr-Gr)

Conditions	Reactors	CH_4 yield (mL CH_4/ g VS)	VS Removal (%)	CO_2 Content (%)	Current to CH_4 (mL)	ΔCH_4 (mL)	CCE (%)	Removed VS to CH_4 (mL)	Actual CH_4 (mL)	OCE (%)
5 mM PBS	Conv. AD	364 ± 3	19.8 ± 3.6	24	NA	NA	NA	140	151	109
	Conv. AD-BioGAC	364 ± 3	28.9 ± 2.2	19	NA	NA	NA	143	151	106
	OC	367 ± 3	14.7 ± 1.9	23	NA	NA	NA	142	152	107
	OC-BioGAC	371 ± 7	26.3 ± 1.6	21	NA	NA	NA	135	153	110
5 mM PBS -0.9 V	Bare el	360 ± 7	14.8 ± 3.6	21	18.7	-3	NA	73	149	204
	Bareel-BioGAC	372 ± 3	21.9 ± 3.2	21	2.8	2	NA	108	154	142
	Bioel-BioGAC	422 ± 13	21.8 ± 0.4	34	60.3	20	29 ± 8	108	172	160

* $\Delta CH4 = CH_{4AD\text{-}MEC} - CH_{4OC}$
NA: Not applicable.

4.2 Struvite Precipitation

4.2.1 RSM for the Optimization of Struvite Crystallization Process

BBD was applied to optimize performance parameters to maximize the NH_4-N, PO_4-P, and Mg^{2+} recovery. BBD provided 15 different experiments; within these, there were 12 different designs and 3 repetitions of the center point. Second-order regression equations related to the NH_4-N recovery (NR) and PO_4-P recovery (PR) and Mg^{2+} recovery (MR) are described as given in Eq. 4.1 – 4.3:

$\hat{Y}_{NR}$ = -420 + 61.2 pH + 99.5 Mg:N + 158.7 P:N - 2.07 pH*pH - 25.11 Mg:N*Mg:N - 26.55 P:N*P:N - 2.70 pH*Mg:N - 10.86 pH*P:N + 16.94 Mg:N*P:N (Eq. 4.1)

$\hat{Y}_{PR}$ = -1451 + 339.0 pH - 37.0 Mg:N + 142.9 P:N - 19.24 pH*pH + 0.05 Mg:N*Mg:N - 38.55 P:N*P:N + 3.08 pH*Mg:N - 7.97 pH*P:N + 16.45 Mg:N*P:N (Eq. 4.2)

$\hat{Y}_{MR}$ = 1177 - 220.9 pH - 32.0 Mg:N - 142.2 P:N + 11.08 pH*pH - 6.86 Mg:N*Mg:N - 10.21 P:N*P:N + 1.94 pH*Mg:N + 17.95 pH*P:N + 18.52 Mg:N*P:N (Eq. 4.3)

Experimental results demonstrated that NH_4-N recovery range between 78.45% ± 0.53% and 96.89% ± 0.64%. PO_4-P and Mg^{2+} recovery range between 69.2% ± 5.0% – 96.3% ± 1.3% and 99.9% ± 0.1% – 75.1% ± 0.3%, respectively (Table 4.8). The residual concentrations of the NH_4^+, PO_4^{3-}, and Mg^{2+} corresponding to each run are given in Table 4.8. The actual and predicted values plots showed significant consistency (R^2 = 0.8404 for NR, R^2 = 0.8739 for PR, and R^2 = 0.9187 for MR) (Figure 4.29). Further, as the R^2 value approaches 1.0, the model has a high correlation (Gurkok et al., 2011). Obtained R^2 value here demonstrated that the model fit the data with sufficient accuracy. Lower than 1.0 R^2 values, on the other hand, may be due to the impurities present in the additives. Also, there was no collinearity among variables (variable inflation factor (VIF) < 10) (Appendix K)

(Niu et al., 2019). Estimations of regression coefficients and results of statistical tests are given in Appendix K.

Table 4.8 The Box-Behnken design, experimental and predicted results for the NH_4-N recovery, residual PO_4-P concentration, and residual concentration of the NH_4^+, PO_4^{3-} and Mg^{2+}

Factors				Responses (%)			Residual mM		
Run	**pH**	**Mg:N**	**P:N**	**NH_4-N Recovery**	**PO_4-P Recovery**	**Mg^{2+} Recovery**	**NH_4^+**	**PO_4^{3-}**	**Mg^{2+}**
1	8.0	1.5	1.6	82.9 ± 0.4	81.7 ± 1.1	97.9 ± 0.3	17.1	30.3	3.2
2	9.0	1.5	1.6	85.3 ± 0.4	84.5 ± 3.0	99.9 ± 0.1	15.2	26.9	0.07
3	8.0	2.3	1.6	96.6 ± 0.6	87.7 ± 2.1	89.1 ± 0.2	3.7	23.0	29.0
4	9.0	2.3	1.6	96.9 ± 0.6	92.9 ± 1.6	92.7 ± 0.5	3.6	14.2	19.5
5	8.0	1.9	1.2	80.2 ± 0.4	84.9 ± 0.4	96.0 ± 0.1	11.3	18.4	40.2
6	9.0	1.9	1.2	90.0 ± 0.3	94.1 ± 0.8	85.9 ± 0.4	5.32	8.1	30.8
7	8.0	1.9	2	94.7 ± 0.3	70.2 ± 2.4	95.7 ± 0.1	5.1	60.0	8.0
8	9.0	1.9	2	95.8 ± 0.1	73.0 ± 0.3	99.9 ± 0.1	4.4	53.3	0.04
9	8.5	1.5	1.2	83.3 ± 0.7	83.6 ± 1.1	92.1 ± 0.6	19.5	23.1	14.1
10	8.5	2.3	1.2	78.5 ± 0.4	96.3 ± 1.3	75.1 ± 0.3	23.4	5.6	62.7
11	8.5	1.5	2	89.5 ± 0.4	69.2 ± 5.0	99.9 ± 0.1	10.8	63.7	0.05
12	8.5	2.3	2	95.4 ± 0.3	92.3 ± 1.0	94.8 ± 0.8	4.4	14.4	10.1
13	8.5	1.9	1.6	92.1 ± 0.5	89.7 ± 0.5	94.2 ± 0.6	8.6	17.7	15.3
14	8.5	1.9	1.6	96.3 ± 0.2	93.8 ± 0.7	92.8 ± 0.2	4.4	15.4	12.2
15	8.5	1.9	1.6	96.4 ± 0.3	91.1 ± 0.7	92.5 ± 0.3	4.3	14.0	16.0

Even though substitutes such as WMP and BM that are heterogeneous in nature have been used in this study, in nine out of fifteen experimental runs, NH_4-N recoveries were greater than 90%, with a maximum of 97%. NH_4-N recoveries attained in this study are higher than the performances reported in the literature. For example, Huang et al. (H. Huang et al., 2014) investigated the effect of low-cost MgO and waste phosphoric acid in struvite precipitation from landfill leachate. The maximum NH_4-N removal was observed as 83% with a 3:1:1 Mg:N:P molar ratio (H. Huang et al., 2014). The reason for higher NH_4-N recoveries in this work may be due to the pre-treatment (acidic dissolution process) that is applied to WMP, which may enhance the availability of WMP for a chemical reaction. Another factor influencing NH_4-N recovery could be the P:N ratio, which was kept higher than 1:1 in this work for all

experimental runs. Yet, accordingly, a higher residual PO_4-P concentration was observed in this study. In another work, 96% NH_4-N removal was observed using BM as a P source and seawater bittern as a Mg source for struvite precipitation from leachate by Siciliano (2016). Further, with pure chemical $MgCl_2$, only up to 65% NH_4-N recovery was observed previously when poultry manure-fed biogas plant digestate was subjected to an acidic dissolution process (Yilmazel & Demirer, 2011).

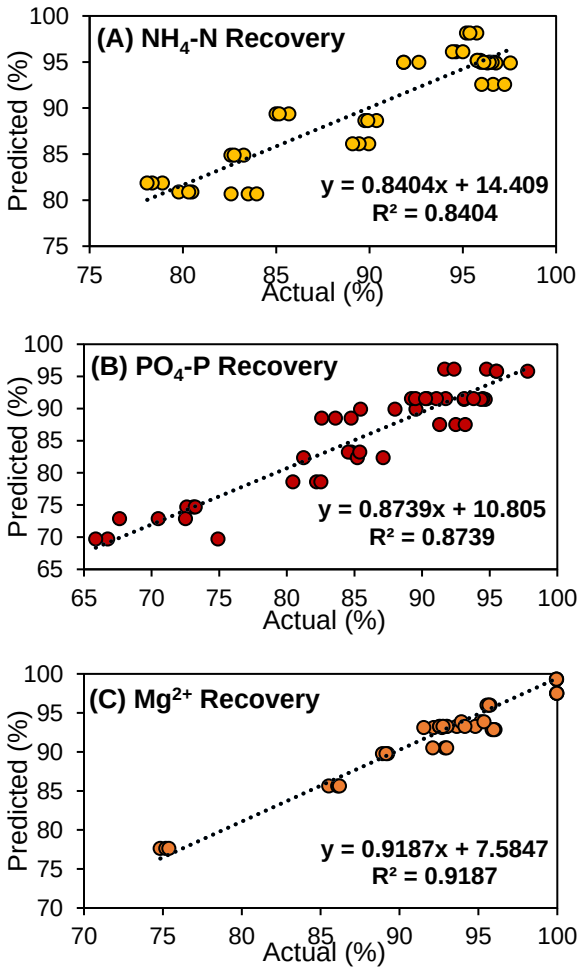

Figure 4.29. Scatter diagram of predicted vs. experimental response values for the (A) NH_4-N recovery (B) PO_4-P recovery, and (C) Mg^{2+} recovery (%)

The precision and significance of derived model parameters were examined using the analysis of variance (ANOVA). ANOVA results for the response surface quadratic model for the responses are given in Table 4.9. The regression analysis of

NH_4-N recovery indicated that all three factors (pH, Mg:N, and P:N) had significant effects ($P< 0.05$) on NH_4-N recovery. Among them, the P:N molar ratio was the most significant factor, with an *F*-value of 84.8, followed by the Mg:N molar ratio, with an *F*-value of 31.3. Clearly, the amount of added P has a significant role in N recovery because large amounts of Ca^{2+} and Mg^{2+} that may come from BM and/or WMP may compete against struvite for PO_4^{-3} to produce $Mg_3(PO_4)_2$ and $Ca_3(PO_4)_2$ (Song et al., 2018). This competition would decrease available PO_4^{-3} for struvite precipitation and may lower NH_4-N recovery (Song et al., 2018). Because the selected pH range (8 – 9) was suitable for struvite precipitation, it had a less significant effect on the model. Quadratic effects of Mg:N and P:N showed a significant effect ($P< 0.05$) on NH_4-N recovery. However, the quadratic effect of pH was insignificant ($P> 0$ .05). Besides, among the interaction effects, only pH x Mg:N was insignificant (Table 4.9).

The regression analysis of the PO_4-P recovery indicated that all three of the factors (pH, Mg:N, and P:N) had a significant effect ($P< 0.05$) on the PO_4-P recovery. Similar to NH_4-N recovery, the P:N molar ratio was the most significant factor. Thus, adding PO_4-P concentration with BM is directly related to the PO_4-P recovery. Regarding their quadratic effects, pH x pH and P:N x P:N has a significant impact ($P< 0.05$) on the PO_4-P recovery. On the other hand, the quadratic effect of Mg:N x Mg:N was insignificant. All interaction effects were insignificant ($P> 0.05$) (Table 4.9).

Similarly, Table 4.9 shows the ANOVA results for Mg^{2+} recovery. In comparison to the other responses, the residual Mg^{2+} concentration provided the greatest correlation between the experimental and model results ($R^2 = 0.9187$, $F = 43.93$). P:N and Mg:N were the two most crucial variables affecting the response. pH was insignificant affecting Mg^{2+} recovery since the selected pH range as it is changed within the optimal struvite precipitation pH levels. Similar to PO_4-P recovery, Mg:N and P:N molar ratios are the most significant factors over linear, square, and 2-way interactions.

Table 4.9 ANOVA results for the NH_4-N, PO_4-P, and Mg^{2+} recovery

Source	DF	Adj SS	Adj MS	F-Value	P-Value
NH_4-N recovery (%)					
Model	9	1540.00	171.11	20.47	0.000
Linear	3	1040.11	346.70	41.48	0.000
pH	1	69.68	69.68	8.34	0.007
Mg:N	1	261.72	261.72	31.32	0.000
P:N	1	708.70	708.70	84.80	0.000
Square	3	351.63	117.21	14.02	0.000
pH*pH	1	2.98	2.98	0.36	0.554
Mg:N*Mg:N	1	178.74	178.73	21.39	0.000
P:N*P:N	1	199.83	199.83	23.91	0.000
2-Way Interaction	3	148.27	49.42	5.91	0.002
pH*Mg:N	1	3.50	3.50	0.42	0.522
pH*P:N	1	56.64	56.64	6.78	0.013
Mg:N*P:N	1	88.13	88.13	10.54	0.003
R^2= 0.8404		$R^2_{(adj)}$ = 0.7993		$R^2_{(pred)}$ = 0.7266	
PO_4-P Recovery (%)					
Model	9	2949.26	327.7	26.94	0.000
Linear	3	2193.18	731.06	60.11	0.000
pH	1	149.75	149.75	12.31	0.001
Mg:N	1	942.64	942.64	77.51	0.000
P:N	1	1100.79	1100.79	90.51	0.000
Square	3	637.89	212.63	17.48	0.000
pH*pH	1	256.26	256.26	21.07	0.000
Mg:N*Mg:N	1	0	0	0	0.994
P:N*P:N	1	421.43	421.43	34.65	0.000
2-Way Interaction	3	118.19	39.4	3.24	0.034
pH*Mg:N	1	4.55	4.55	0.37	0.545
pH*P:N	1	30.5	30.5	2.51	0.122
Mg:N*P:N	1	83.14	83.14	6.84	0.013
R^2= 0.8739		$R^2_{(adj)}$ = 0.8414		$R^2_{(pred)}$ = 0.7802	
Mg^{2+} Recovery (%)					
Model	9	1587.91	176.435	43.93	0.000
Linear	3	1187.55	395.849	98.57	0.000
pH	1	0.01	0.009	0	0.963
Mg:N	1	549.56	549.565	136.84	0.000
P:N	1	637.97	637.973	158.85	0.000
Square	3	138.61	46.202	11.5	0.000
pH*pH	1	85.05	85.053	21.18	0.000
Mg:N*Mg:N	1	13.35	13.353	3.32	0.077
P:N*P:N	1	29.54	29.54	7.36	0.010
2-Way Interaction	3	261.76	87.252	21.73	0.000
pH*Mg:N	1	1.81	1.806	0.45	0.507
pH*P:N	1	154.59	154.593	38.49	0.000
Mg:N*P:N	1	105.36	105.359	26.23	0.000
R^2= 0.9187		$R^2_{(adj)}$ = 0.8978		$R^2_{(pred)}$ = 0.8569	

4.2.2 Response Surface Analysis

The interaction effects of variables can be visualized on response surface plots while the other factors are held constant. 3D response surface plots are given in Figure 4.30 for the NH_4-N, PO_4-P, and Mg^{2+} recovery. From the surface plots of NH_4-N in Figure 4.30A, it was indicated that increasing the P:N ratio from 1.2 to 2 and raising Mg:N ratio from 1.5 to 2.3 resulted in the highest NH_4-N recovery. It showed that the potential of NH_4^+ removal increases with the presence of Mg^{2+} and PO_4^{3-} ions. On the other hand, an increase in Mg:N ratio from 1.9 to 2.3 resulted in lower NH_4-N recovery at 1.2-1.5 P:N ratio. Figure 4.30B shows the interaction effect of pH x P:N on NH_4-N recovery. A response surface plot's slope indicates how significantly an input variable influences a response variable. Thus, P:N is more influential on NH_4-N recovery rather than pH change. Since the slope of Figure 4.30A is greater than Figure 4.30B and Figure 4.30C, it is clear that the interaction impact of Mg:N x P:N is more significant than the others on the NH_4-N recovery. Also, these results are consistent with the ANOVA outputs given in Table 4.9.

The significant effect of P:N on NH_4-N recovery may be explained by the fact that increasing P:N enables particle size increase of the precipitates; thus, a higher amount of struvite is produced at the same reaction time (Zhou et al., 2021). Besides, an increase of pH from 8 to 9 caused an increase in the NH_4-N recovery, which may be a result of a decrease in the H^+ concentration and, thus, increasing HPO_4^{-2} concentration. This could improve struvite production and accelerate the recovery of ammonia nitrogen (Song et al., 2018). Similar results were obtained in another recent study, where BBD was applied to increase ammonia nitrogen recovery during struvite precipitation (Zhou et al., 2021). In their study, Zhou and others (2021) changed pH between 9 and 10; thus, it was reported that pH x P:N significantly affected the recovery of ammonia nitrogen.

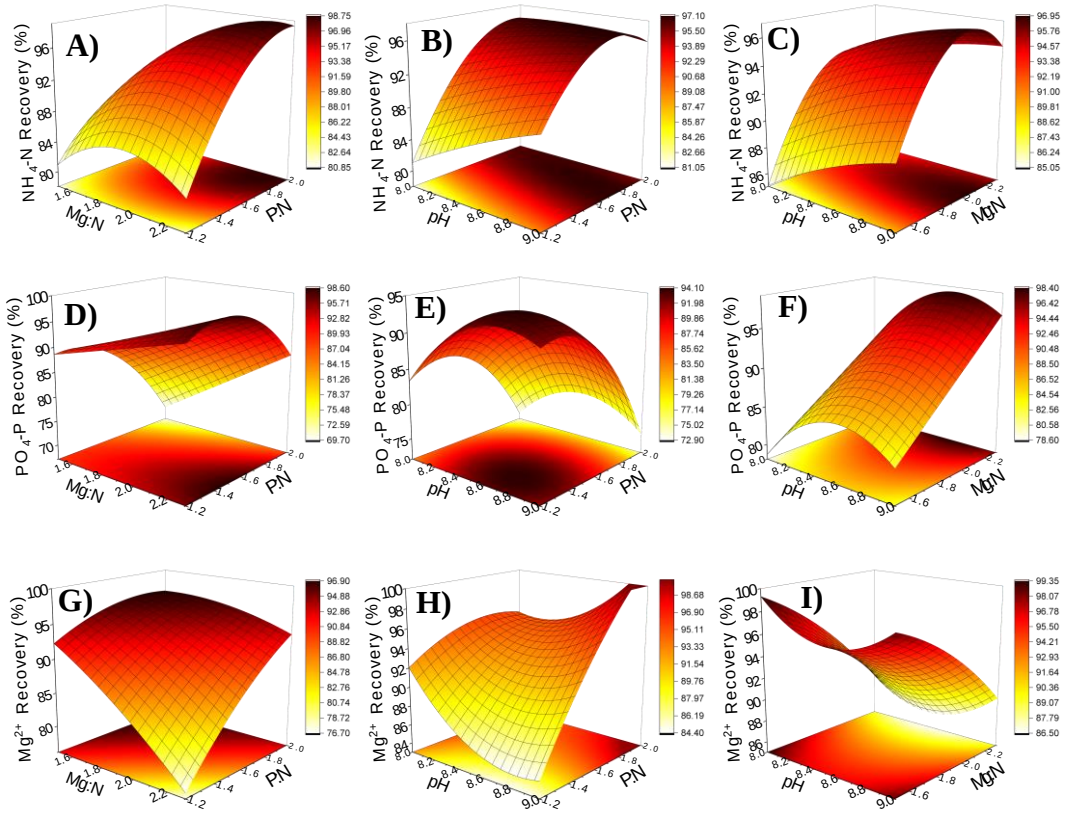

Figure 4.30. 3D surface and contour plots for NH_4-N (A)-(C), PO_4-P (D)-(F), and Mg^{2+} (G)-(I) showing the interaction of pH (8.0-9.0), Mg:N (1.5-2.3) and P:N (1.2-2.0) by fixing one factor at a time (pH = 8.5, Mg:N = 1.9, or P:N = 1.6)

The interaction effects of process variables on the PO_4-P recovery are given in Figure 4.30D-F. Considering the slope of the graphs, the P:N molar ratio was the most significant variable, and the findings match the ANOVA outputs (Table 4.9). High P:N molar ratio resulted in high residual PO_4-P concentration, indicating low PO_4-P recovery. It means that PO_4^{3-} concentration was in excess amounts compared to Mg^{+} and NH_4^{+} as well as other ions that may form precipitates with PO_4^{3-}; hence, PO_4^{3-} remained in the solution instead of precipitation (Table 4.8). Especially when the P:N ratio was higher than Mg:N ratio, the remaining PO_4-P concentration was highest among the other two ions. Moreover, PO_4-P recovery increases along with an increase in the Mg:N ratio (Figure 4.30D and Figure 4.30F). Similarly to this, Zin

et al. (2020) stated that the molar ratio of Mg^{2+} to PO_4-P should be greater to accomplish over 90% PO_4-P removal.

3D surface plots are given in Figure 4.30G-I for Mg^{2+} recovery. Figure 4.30G showed that Mg:N and P:N molar ratio has the opposite effect on Mg^{2+} recovery. For example, the highest recovery was achieved at 1.5 Mg:N and 2.0 P:N molar ratio. Siciliano and De Rosa (2014) showed that when the amount of magnesium was increased, where the recovery for Mg^{2+} lowered from 99% to 81.3%, which is similar to this study. Among parameters, the pH x P:N ratio has the highest significance on Mg^{2+} recovery as the slope of Figure 4.30H. The remaining Mg^{2+} may precipitate with PO_4^{3-} to create other precipitates, such as $Mg_3(PO_4)_2$, after PO_4^{3-} was recovered as struvite (Zin et al., 2020). Therefore, a high P:N ratio results in cause high Mg^{2+} recovery.

4.2.3 Verification of the Optimum Conditions

The process was optimized to determine a particular condition at which the NH_4-N, PO_4-P, and Mg^{2+} recovery efficiency would be high. From the model, optimum conditions were obtained as pH of 9.0, Mg:N molar ratio of 2.2, and P:N molar ratio of 1.8 with corresponding responses of 97.4% (95% prediction interval (PI): 90.95 – 100) NH_4-N recovery, 90.2% (95% PI: 82.44 – 98.03) PO_4-P recovery, and 96.8% (95% PI: 92.30 – 100) Mg^{2+} recovery. The tests were conducted under the model-provided optimal conditions to assess the dissimilarity between the experimental value and the optimum value estimated by the model. The experimental results were as follows: 97.8 ± 0.1% NH_4-N recovery and 96.6 ± 0.31% PO_4-P recovery and 84.4 ± 0.9% Mg^{2+} recovery. The experimental findings and predicted response values agree with a dissimilarity of 0.4%, 6.9%, and 14.3% for the NH_4-N, PO_4-P, and Mg^{2+} recovery, respectively. Since the predicted value was quite close to the experimental result, the model helps estimate the NH_4-N recovery under different conditions. For PO_4-P recovery, the result was within PI. On the other hand, there was a considerable discrepancy between the predicted and experimental results for Mg^{2+}. The remaining

concentration of the ions was 2.1 ± 0.07 mM, 5.8 ± 0.53 mM, and 33.3 ± 1.95 mM for the NH_4-N, PO_4-P, and Mg^{2+} ions. This indicates that NH_4-N and PO_4-P limit the precipitation and excess Mg^{2+} remains in the solution. Higher PO_4-P recovery and less available PO_4^{3-} ions compared to the predicted value result in the high dissimilarity of Mg^{2+} recovery. By decreasing the Mg:N or P:N molar ratio closer or below 1, more removal of Mg^{2+} and PO_4^{3-} can be accomplished, which can be studied deeper. However, it may result in high NH_4^+ effluent concentration. Regardless, the constructed model could identify the optimum conditions for nutrient recovery via the use of WMP and BM as additives. Considering the initial characteristics of P-enriched digestate, all struvite-formed ions had significantly lower concentrations. This work provides insight into simultaneous NH_4-N and PO_4-P recovery/removal as well since the majority of the struvite precipitation studies in the literature only focused on PO_4-P recovery/removal.

4.2.4 Product Purity and Characterization

The dried precipitates from 15 runs of BBD experiments, as well as a precipitate from the verification experiment, were all subjected to XRD analysis to determine if the obtained precipitates were struvite. The XRD patterns of the products are given in Figure 4.31. The intensity and positions of the XRD patterns match only with the reference struvite pattern (JCPDS file No.15–0762); hence it was confirmed that all the samples contained only struvite crystals. Since amorphous substances might potentially have precipitated together, it could not be said that the entire recovered precipitate was a struvite (Zin et al., 2020). In another study by Siciliano (2016), amorphous phases, strong magnesium phosphate, and potassium metaphosphate peaks were also observed in XRD results when BM and seawater bittern were used as P and Mg sources, respectively. Although WMP and highly heterogenous BM were used in this study, XRD patterns matched with struvite crystal. Additionally, Figure 4.31. shows that the mineralized products were preferentially oriented along the [010] direction because the products had significantly strong (020) and (040)

diffractions due to the use of BM and WMP (H. Li et al., 2015). Determining the crystal orientation of struvite is essential for comprehending its crystal structure, predicting its growth habit, identifying its mechanical properties and defects, and customizing its crystallographic texture for a variety of applications.

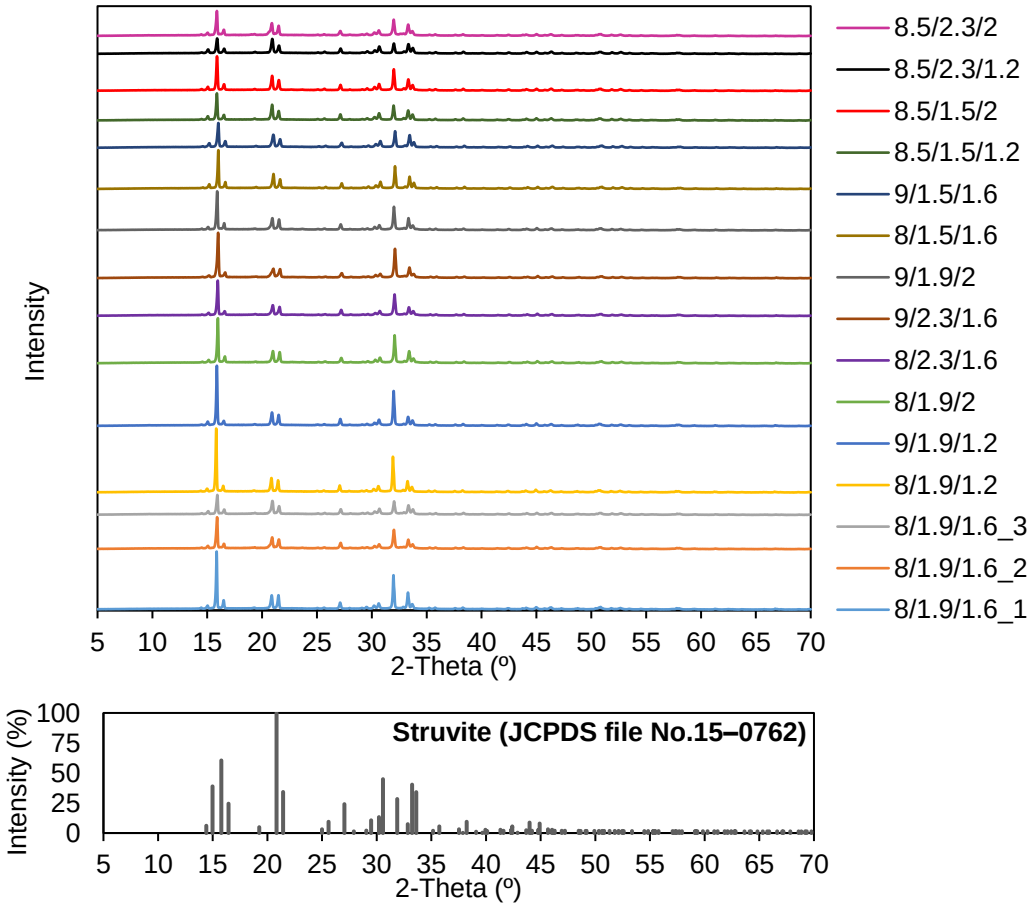

Figure 4.31. The XRD results of the precipitates obtained from experimental runs compared with the peaks of reference struvite (JCPDS file No.15–0762) (Conditions are given as pH/Mg:N/P:N)

The XRD pattern of the product formed at the optimal conditions (pH of 9.0, Mg:N of 2.2, and P:N of 1.8) is shown in Fig. 4. Also, this product was subjected to SEM analysis to assess the structure and morphology of the product (Figure 4.32.). There was no sign of any other crystalline compounds in the produced precipitate's X-ray diffractogram, indicating that impurities are in amorphous form. (Figure 4.32). SEM images showed that the precipitates have irregular prismatic orthorhombic crystals.

The structure was consistent with the literature, where rectangular platelet, prismatic, needle, and pyramidal shape crystals have been observed in different studies (Le Corre et al., 2009; Song et al., 2018). The SEM images of the product showed clearly defined crystals with some amorphous material depositions on their surface as XRD results. Moreover, the crystal size of the struvite has been reported between 10-40 µm (Siciliano & De Rosa, 2014). The crystal size of the product under optimum conditions is around 25 µm, which is consistent with the literature. The molar ratio of the ions, crystal growth conditions like mixing, and temperature can all be used to explain the various morphologies of struvite (Le Corre et al., 2009).

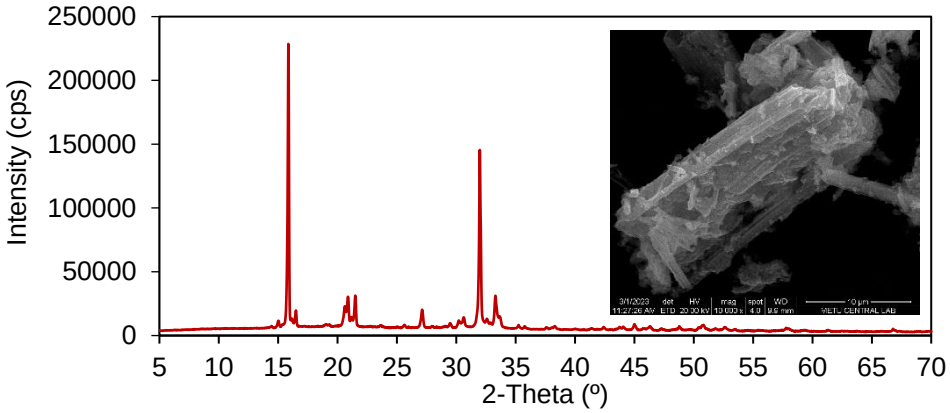

Figure 4.32. The XRD spectra and SEM images at 6000x magnification of the product under optimum condition (pH = 9.0, Mg:N = 2.2, P:N = 1.8)

To assess the product quality with amorphous depositions, the elemental composition of the dried product was examined. The mass of the product obtained at optimum condition was 0.12 ± 0.01 g product/mL digestate sample. Since other precipitates may be present in the product, purity is an important parameter to consider for the future economic viability of the process. The elemental composition of the product is given in Table 4.10. The impurities present in the BM and WMP may cause co-precipitates within the amorphous phase that decrease the purity of the product. Moreover, the highest impurity was Na due to NaOH addition. Thus, aeration may be used for pH increase in further studies. The obtained product was composed of 49% struvite. Investigations that have focused on product purity is quite limited. For example, similar digestate sample was used by Cerillo et al. (2015).

After struvite precipitation from pig slurry, purity was analyzed (Cerrillo et al., 2015). The purity was 48% and 44% at 100 rpm and 200 rpm mixing velocities, respectively (Cerrillo et al., 2015). Also, the study indicated that the obtained struvite is appropriate for use as an agricultural fertilizer (Cerrillo et al., 2015).

Moreover, the heavy metal content of the product was assessed. As a result, the heavy metal composition of the product was lower compared to Turkey's regulations (Appendix L).

Table 4.10 Elemental composition of the product

Macro elements		**Microelements**	
Element	**%**	**Element**	**%**
P	15.25	Al	0.083
Mg	6.7	Mn	0.066
H	4.7	Zn	0.04
Na	4.27	Ni	0.006
C	4.05	B	0.002
N	2.8	Ba	0.001
K	1.42	Co	0.001
S	1.39	Ti	0.001
Fe	1.22	V	0.001
Ca	0.875	Cr	0.001
		Cu	0.0004
		As	0.0002
		Li	0.0001
		Cd	0.00002
		Se	0.00002
		Pb	0.000001

4.2.5 Conclusion on Struvite Precipitation

This study used BM and WMP as sustainable substitutes for pure P and Mg sources for struvite precipitation from cattle manure digestate. BBD was applied to determine optimum conditions of process parameters of pH, Mg:N, and P:N molar ratio, and a model was developed to predict the recovery performance. ANOVA revealed that the model had been satisfactorily fitted to the experimental data. Additionally, 3D surface plots provided a visual insight into the different factors' combined effects on

the responses selected as NH_4-N, PO_4-P, and Mg^{2+} recovery. Among the parameters, the P:N molar ratio was the most significant factor for all responses. During the verification experiments, 97.8 ± 0.1% NH_4-N recovery and 96.6 ± 0.31% PO_4-P recovery, and 84.4 ± 0.9% Mg^{2+} recovery were attained under the optimum conditions (pH = 9.0, Mg:N = 2.2, P:N = 1.8). The verification experiment product quality was analyzed through purity measurement, XRD, and SEM. Even though waste material (WMP) and industrial by-product (BM) have been used as additives in this process, almost complete NH_4-N and PO_4-P recovery were recorded under optimum conditions with fairly high product purity (~49 %). However, Mg^{2+} concentration was higher compared to most digestate samples to achieve such higher NH_4-N and PO_4-P recovery. This should be taken into consideration. Moreover, struvite should be used in combination with other fertilizers for optimal results (Kataki et al., 2016). Fertilizer companies use struvite as an additive or a substitute raw material in standard fertilizer production technology (Kataki et al., 2016).

BM and WMP have a significant potential to be used partially or entirely as additives for the industrial recovery of nutrients since they are waste or by-product materials. These results are promising and illustrate a powerful example of industrial symbiosis between the meat, magnesite, and biogas industries. The findings of this study will stimulate more efforts to create sustainable strategies for resource recovery.

CHAPTER 5

CONCLUSIONS

Two novel technologies were investigated to enhance the application of AD technology in this thesis. As a new configuration, AD-MEC systems were combined. The results showed that AD-MEC systems produced more CH_4 per VS added into the reactors, increased the rate of the production and organic removal, decrease the start-up time and increase the stability of the process. AD-MEC reactors were compared to conventional AD reactors (Conv. AD) to assess the enhancement in CH4 production. Graphite cathode AD-MEC fed with cattle manure operation enhanced CH4 production by 10% with Bioelectrode and by 8% with Bare electrode under -0.9 V cathode potential. When the cathode potential was increased to -1 V, Bioelectrode and Bare electrode increased CH_4 production by 52% and 45%, respectively. When the cathode was changed to SS mesh, Bioelectrode increased CH4 production by 37%; however, the Bare electrode increased by 51% under -0.9 V cathode potential. On the contrary, when the cathode potential was -0.95 V, the Bare electrode increased CH_4 production by 51%, and Bioelectrode increased by 105%. For WBS-fed AD-MEC reactors, the enhancement was limited to 16% with Bioel-BioGAC reactors. The findings revealed that the formation of biofilms in a controlled setting led to alterations in microbial communities and system performance. The enhancements observed in the reactors were specific to each case and closely tied to the material and potential of the cathode. Notably, bioelectrodes and bare electrodes exhibited comparable performance, except for the graphite-SS bioelectrode AD-MEC fed with cattle manure at a cathode potential of -0.95 V. Allowing biofilms to develop on the bare electrodes during operation is a viable approach, and there is no significant advantage of prior cultivation of the biofilm in a controlled environment.

As a sustainable post-treatment option, struvite precipitation with low-cost materials was investigated in this thesis. BM and WMP were employed to precipitate struvite from cattle manure digestate as sustainable alternatives to pure P and Mg. NH_4-N, PO_4-P, and Mg^{2+} recovery range between 78.45% – 96.89% , 69.2% – 96.3%, and 99.9% – 75.1%, respectively. The actual and predicted values showed significant consistency, indicating that the model is satisfactory. Under optimum conditions (pH = 9.0, Mg:N = 2.2, and P:N = 1.8), 97.8 ± 0.1% NH_4-N recovery and 96.6 ± 0.31% PO_4-P recovery and 84.4 ± 0.9% Mg^{2+} recovery were attained. The XRD results confirmed the sole presence of struvite crystals. SEM images showed irregular prismatic orthorhombic crystals and amorphous material depositions on precipitates with ~25 μm crystal size. The product was 49% struvite with 15.25% P content. The heavy metal content was lower than regulatory limits. These encouraging findings demonstrate industrial synergy between the meat, magnesite, and biogas sectors. This study will spur sustainable resource recovery initiatives.

This study showed that both methods are promising to enhance the AD system. These systems may have an impact on mitigating climate change, depletion of nutrients, and achieving sustainable development goals. Research into the next generation of biogas technology should focus commercialization of the processes.

CHAPTER 6

RECOMMENDATIONS

The outcomes of this initiative have also created fresh opportunities, ideas, and research areas. In conclusion,

- The AD and AD-MEC systems are both significantly impacted by the buffer media. Finding the best buffer option to enhance the AD-MEC system requires evaluating performance from both the CH_4 and current production viewpoints.
- Future research should focus on evaluating the AD-MEC system's performance using complex waste streams similar to cattle manure in larger-scale reactors, with the ultimate goal of implementing large-scale or pilot systems utilizing such waste materials.
- Multiple electrodes and high surface area materials such as brush-like electrodes may be used to enhance biofilm attachment. Since methanogens develop slower than exoelectrogens, the anode-to-cathode ratio should be adjusted for maximal CH_4 generation.
- A detailed cost analysis should be conducted to reveal the change in the operational costs when sustainable substitutes are used for struvite precipitation.
- In addition to Mg, and P, the use of NaOH can be eliminated in struvite precipitation. Nutrient recovery via microbial electrolysis cells is a novel technology, which can be further investigated.

REFERENCES

Aage, H. K., Andersen, B. L., Blom, A., & Jensen, I. (1997). The solubility of struvite. *Journal of Radioanalytical and Nuclear Chemistry*, *223*(1–2), 213–215. https://doi.org/10.1007/BF02223387

Acelas, N. Y., Flórez, E., & López, D. (2015). Phosphorus recovery through struvite precipitation from wastewater: effect of the competitive ions. *Desalination and Water Treatment*, *54*(9), 2468–2479. https://doi.org/10.1080/19443994.2014.902337

Adekunle, K. F., & Okolie, J. A. (2015). A Review of Biochemical Process of Anaerobic Digestion. *Advances in Bioscience and Biotechnology*, *06*(03), 205–212. https://doi.org/10.4236/abb.2015.63020

Aguado, D., Barat, R., Bouzas, A., Seco, A., & Ferrer, J. (2019). P-recovery in a pilot-scale struvite crystallisation reactor for source separated urine systems using seawater and magnesium chloride as magnesium sources. *Science of the Total Environment*, *672*, 88–96. https://doi.org/10.1016/j.scitotenv.2019.03.485

Ahiler Development Agency. (2021). *Bone meal production plant pre-feasibility in Kırıkkale*. https://www.yatirimadestek.gov.tr/pdf/assets/upload/fizibiliteler/kirikkale-ili-kemik-unu-uretim-tesisi-on-fizibilite-raporu-2021.pdf

Ahn, Y., Im, S., & Chung, J. W. (2017). Optimizing the operating temperature for microbial electrolysis cell treating sewage sludge. *International Journal of Hydrogen Energy*, *42*(45), 27784–27791. https://doi.org/10.1016/j.ijhydene.2017.05.139

Ahn, Y., & Logan, B. E. (2013). Saline catholytes as alternatives to phosphate buffers in microbial fuel cells. *Bioresource Technology*, *132*, 436–439.

https://doi.org/10.1016/j.biortech.2013.01.113

Al-Mallahi, J., Sürmeli, R. Ö., & Çalli, B. (2020). Recovery of phosphorus from liquid digestate using waste magnesite dust. *Journal of Cleaner Production*, *272*. https://doi.org/10.1016/j.jclepro.2020.122616

Almatouq, A., & Babatunde, A. O. (2017). Concurrent hydrogen production and phosphorus recovery in dual chamber microbial electrolysis cell. *Bioresource Technology*, *237*, 193–203. https://doi.org/10.1016/j.biortech.2017.02.043

Alvarez, R., & Lidén, G. (2009). Low temperature anaerobic digestion of mixtures of llama, cow and sheep manure for improved methane production. *Biomass and Bioenergy*, *33*(3), 527–533. https://doi.org/10.1016/j.biombioe.2008.08.012

Ambler, J. R., & Logan, B. E. (2011). Evaluation of stainless steel cathodes and a bicarbonate buffer for hydrogen production in microbial electrolysis cells using a new method for measuring gas production. *International Journal of Hydrogen Energy*, *36*(1), 160–166. https://doi.org/10.1016/j.ijhydene.2010.09.044

An, Z., Feng, Q., Zhao, R., & Wang, X. (2020). Bioelectrochemical methane production from food waste in anaerobic digestion using a carbon-modified copper foam electrode. *Processes*, *8*(4). https://doi.org/10.3390/PR8040416

APHA, AWWA, & WPCF. (2017). Standard Methods for the Examination of Water and Wastewater. In *Am. Public Heal. Assoc.* https://doi.org/10.1016/B978-0-12-382165-2.00237-3

Ariyanto, E., Ang, H. M., & Sen, T. K. (2014). Impact of various physico-chemical parameters on spontaneous nucleation of struvite (MgNH4PO4.6H2O) formation in a wastewater treatment plant: kinetic and nucleation mechanism. *Desalination and Water Treatment*, *52*(34–36), 6620–6631. https://doi.org/10.1080/19443994.2013.821042

Astals, S., Martínez-Martorell, M., Huete-Hernández, S., Aguilar-Pozo, V. B., Dosta, J., & Chimenos, J. M. (2021). Nitrogen recovery from pig slurry by struvite precipitation using a low-cost magnesium oxide. *Science of the Total Environment*, *768*, 144284. https://doi.org/10.1016/j.scitotenv.2020.144284

Asztalos, J. R., & Kim, Y. (2015). Enhanced digestion of waste activated sludge using microbial electrolysis cells at ambient temperature. *Water Research*, *87*, 503–512. https://doi.org/10.1016/j.watres.2015.05.045

Azri, Y. M., Tou, I., & Sadi, M. (2023). Electrodes materials evaluation in plant microbial fuel cells: a comparison of graphite and stainless steels. *Biofuels*, *0*(0), 1–10. https://doi.org/10.1080/17597269.2023.2212987

Baek, G., Kim, J., Lee, S., & Lee, C. (2017). Development of biocathode during repeated cycles of bioelectrochemical conversion of carbon dioxide to methane. *Bioresource Technology*, *241*, 1201–1207. https://doi.org/10.1016/j.biortech.2017.06.125

Baek, G., Kim, K. Y., & Logan, B. E. (2021). Impact of surface area and current generation of microbial electrolysis cell electrodes inserted into anaerobic digesters. *Chemical Engineering Journal*, *426*(May), 131281. https://doi.org/10.1016/j.cej.2021.131281

Baek, G., Saikaly, P. E., & Logan, B. E. (2021). Addition of a carbon fiber brush improves anaerobic digestion compared to external voltage application. *Water Research*, *188*, 116575. https://doi.org/10.1016/j.watres.2020.116575

Bao, H., Yang, H., Zhang, H., Liu, Y., Su, H., & Shen, M. (2020). Improving methane productivity of waste activated sludge by ultrasound and alkali pretreatment in microbial electrolysis cell and anaerobic digestion coupled system. *Environmental Research*, *180*(August 2019), 108863. https://doi.org/10.1016/j.envres.2019.108863

Battistoni, P., Boccadoro, R., Fatone, F., & Pavan, P. (2005). Auto-nucleation and crystal growth of struvite in a demonstrative fluidized bed reactor (FBR).

Environmental Technology, *26*(9), 975–982. https://doi.org/10.1080/09593332608618486

Ben Moussa, S., Tlili, M. M., Batis, N., & Amor, M. Ben. (2011). Influence of temperature on Struvite precipitation by CO 2-deagassing method. *Crystal Research and Technology*, *46*(3), 255–260. https://doi.org/10.1002/crat.201000571

Bhuiyan, M. I. H., Mavinic, D. S., & Koch, F. A. (2008). Phosphorus recovery from wastewater through struvite formation in fluidized bed reactors: A sustainable approach. *Water Science and Technology*, *57*(2), 175–181. https://doi.org/10.2166/wst.2008.002

Bo, T., Zhu, X., Zhang, L., Tao, Y., He, X., Li, D., & Yan, Z. (2014). A new upgraded biogas production process: Coupling microbial electrolysis cell and anaerobic digestion in single-chamber, barrel-shape stainless steel reactor. *Electrochemistry Communications*, *45*, 67–70. https://doi.org/10.1016/j.elecom.2014.05.026

Borole, A. P., Hamilton, C. Y., Vishnivetskaya, T., Leak, D., & Andras, C. (2009). Improving power production in acetate-fed microbial fuel cells via enrichment of exoelectrogenic organisms in flow-through systems. *Biochemical Engineering Journal*, *48*(1), 71–80. https://doi.org/10.1016/j.bej.2009.08.008

Borole, A. P., Reguera, G., Ringeisen, B., Wang, Z. W., Feng, Y., & Kim, B. H. (2011). Electroactive biofilms: Current status and future research needs. *Energy and Environmental Science*, *4*(12), 4813–4834. https://doi.org/10.1039/c1ee02511b

Cai, W., Han, T., Guo, Z., Varrone, C., Wang, A., & Liu, W. (2016). Methane production enhancement by an independent cathode in integrated anaerobic reactor with microbial electrolysis. *Bioresource Technology*, *208*, 13–18. https://doi.org/10.1016/j.biortech.2016.02.028

Cai, W., Liu, W., Yang, C., Wang, L., Liang, B., Thangavel, S., Guo, Z., & Wang,

A. (2016). Biocathodic Methanogenic Community in an Integrated Anaerobic Digestion and Microbial Electrolysis System for Enhancement of Methane Production from Waste Sludge. *ACS Sustainable Chemistry and Engineering*, *4*(9), 4913–4921. https://doi.org/10.1021/acssuschemeng.6b01221

Call, D., & Logan, B. E. (2008). Hydrogen production in a single chamber microbial electrolysis cell lacking a membrane. *Environmental Science and Technology*, *42*(9), 3401–3406. https://doi.org/10.1021/es8001822

Carliell-Marquet, C. M., & Wheatley, A. D. (2002). Measuring metal and phosphorus speciation in P-rich anaerobic digesters. *Water Science and Technology : A Journal of the International Association on Water Pollution Research*, *45*(10), 305–312. https://doi.org/10.2166/wst.2002.0360

Cascarosa, E., Gea, G., & Arauzo, J. (2012). Thermochemical processing of meat and bone meal: A review. *Renewable and Sustainable Energy Reviews*, *16*(1), 942–957. https://doi.org/10.1016/j.rser.2011.09.015

Cerrillo, M., Palatsi, J., Comas, J., Vicens, J., & Bonmatí, A. (2015). Struvite precipitation as a technology to be integrated in a manure anaerobic digestion treatment plant - removal efficiency, crystal characterization and agricultural assessment. *Journal of Chemical Technology and Biotechnology*, *90*(6), 1135–1143. https://doi.org/10.1002/jctb.4459

Cerrillo, M., Viñas, M., & Bonmatí, A. (2018). Anaerobic digestion and electromethanogenic microbial electrolysis cell integrated system: Increased stability and recovery of ammonia and methane. *Renewable Energy*, *120*, 178–189. https://doi.org/10.1016/j.renene.2017.12.062

Chen, Y., Yu, B., Yin, C., Zhang, C., Dai, X., Yuan, H., & Zhu, N. (2016). Biostimulation by direct voltage to enhance anaerobic digestion of waste activated sludge. *RSC Advances*, *6*(2), 1581–1588. https://doi.org/10.1039/c5ra24134k

Cheng, S., & Logan, B. E. (2007). Sustainable and efficient biohydrogen

production via electrohydrogenesis. *Proceedings of the National Academy of Sciences of the United States of America*, *104*(47), 18871–18873. https://doi.org/10.1073/pnas.0706379104

Cheng, S., Xing, D., Call, D. F., & Logan, B. E. (2009). Direct biological conversion of electrical current into methane by electromethanogenesis. *Environmental Science and Technology*, *43*(10), 3953–3958. https://doi.org/10.1021/es803531g

Chimenos, J. M., Fernández, A. I., Villalba, G., Segarra, M., Urruticoechea, A., Artaza, B., & Espiell, F. (2003). Removal of ammonium and phosphates from wastewater resulting from the process of cochineal extraction using MgO-containing by-product. *Water Research*, *37*(7), 1601–1607. https://doi.org/10.1016/S0043-1354(02)00526-2

Choi, K. S., Kondaveeti, S., & Min, B. (2017). Bioelectrochemical methane (CH4) production in anaerobic digestion at different supplemental voltages. *Bioresource Technology*, *245*(July), 826–832. https://doi.org/10.1016/j.biortech.2017.09.057

Cordas, C. M., Guerra, L. T., & Xavier, C. (2008). Electroactive biofilms of sulphate reducing bacteria. *Electrochimica Acta*, *54*, 29–34. https://doi.org/10.1016/j.electacta.2008.02.041

Coutand, M., Cyr, M., Deydier, E., Guilet, R., & Clastres, P. (2008). Characteristics of industrial and laboratory meat and bone meal ashes and their potential applications. *Journal of Hazardous Materials*, *150*(3), 522–532. https://doi.org/10.1016/j.jhazmat.2007.04.133

Cristiani, L., Zeppilli, M., Villano, M., & Majone, M. (2021). Role of the organic loading rate and the electrodes' potential control strategy on the performance of a micro pilot tubular microbial electrolysis cell for biogas upgrading. *Chemical Engineering Journal*, *426*(August), 131909. https://doi.org/10.1016/j.cej.2021.131909

Cruz Viggi, C., Rossetti, S., Fazi, S., Paiano, P., Majone, M., & Aulenta, F. (2014). *Magnetite Particles Triggering a Faster and More Robust Syntrophic Pathway of Methanogenic Propionate Degradation*.

Cusick, R. D., & Logan, B. E. (2012). Phosphate recovery as struvite within a single chamber microbial electrolysis cell. *Bioresource Technology*, *107*, 110–115. https://doi.org/10.1016/j.biortech.2011.12.038

Cusick, R. D., Ullery, M. L., Dempsey, B. A., & Logan, B. E. (2014). Electrochemical struvite precipitation from digestate with a fluidized bed cathode microbial electrolysis cell. *Water Research*, *54*, 297–306. https://doi.org/10.1016/j.watres.2014.01.051

Dadrasnia, A., de Bona Muñoz, I., Yáñez, E. H., Lamkaddam, I. U., Mora, M., Ponsá, S., Ahmed, M., Argelaguet, L. L., Williams, P. M., & Oatley-Radcliffe, D. L. (2021). Sustainable nutrient recovery from animal manure: A review of current best practice technology and the potential for freeze concentration. *Journal of Cleaner Production*, *315*. https://doi.org/10.1016/j.jclepro.2021.128106

Daneshgar, S., Callegari, A., Capodaglio, A. G., & Vaccari, D. (2018). The potential phosphorus crisis: Resource conservation and possible escape technologies: A review. *Resources*, *7*(2). https://doi.org/10.3390/resources7020037

Darwish, M., Aris, A., Puteh, M. H., Jusoh, M. N. H., & Abdul Kadir, A. (2017). Waste bones ash as an alternative source of P for struvite precipitation. *Journal of Environmental Management*, *203*, 861–866. https://doi.org/10.1016/j.jenvman.2016.02.033

de Ridder, M., de Jong, S., Polchar, J., & Lingemann, S. (2012). *Risks and opportunities in the global phosphate rock market*. The Hague Centre for Strategic Studies. https://www.phosphorusplatform.eu/images/download/HCSS_17_12_12_Phos

phate.pdf

Desmidt, E., Ghyselbrecht, K., Zhang, Y., Pinoy, L., Van Der Bruggen, B., Verstraete, W., Rabaey, K., & Meesschaert, B. (2015). Global phosphorus scarcity and full-scale P-recovery techniques: A review. *Critical Reviews in Environmental Science and Technology*, *45*(4), 336–384. https://doi.org/10.1080/10643389.2013.866531

Deublein, D., & Steinhauser, A. (2011). Biogas from Waste and Renewable Resources: An Introduction. In *Industrial Biotechnology* (2nd ed.). WILEY-VCH Verlag GmbH & Co. KGaA, Boschstr. 12, 69469.

Deydier, E., Guilet, R., Sarda, S., & Sharrock, P. (2005). Physical and chemical characterisation of crude meat and bone meal combustion residue: "Waste or raw material?" *Journal of Hazardous Materials*, *121*(1–3), 141–148. https://doi.org/10.1016/j.jhazmat.2005.02.003

Di Iaconi, C., Pagano, M., Ramadori, R., & Lopez, A. (2010). Nitrogen recovery from a stabilized municipal landfill leachate. *Bioresource Technology*, *101*(6), 1732–1736. https://doi.org/10.1016/j.biortech.2009.10.013

Ditzig, J., Liu, H., & Logan, B. E. (2007). Production of hydrogen from domestic wastewater using a bioelectrochemically assisted microbial reactor (BEAMR). *International Journal of Hydrogen Energy*, *32*(13), 2296–2304. https://doi.org/10.1016/j.ijhydene.2007.02.035

Dogan, S., Aygun, A., Argun, M. E., & Esmeray, E. (2018). Optimization of struvite precipitation for landfill leachate treatment. *Uludağ University Journal of The Faculty of Engineering*, *23*(1), 65–76. https://doi.org/10.17482/uumfd.373302

EBA. (2018). EBA Statistical Report. In *European Biogas Association*. http://european-biogas.eu/2017/12/14/eba-statistical-report-2017-published-soon/

Engin, I. K., Cekmecelioglu, D., Meral, A., & Oktem, H. A. (2018). Enhancement of Heterotrophic Biomass Production. *Waste and Biomass Valorization*, *9*(5), 811–820. https://doi.org/10.1007/s12649-017-9846-8

EPDK. (2022). *Nihai Yenilenebilir Enerji Kaynakları (YEK) Listesi*. https://www.epdk.gov.tr/Detay/DownloadDocument?id=4ETVkLvlwO0=

Erdogan, N. (2013). Recycling of waste magnesite powders. *Ekoloji*, *86*, 75–83. https://doi.org/10.5053/ekoloji.2013.869

Fan, Y., Hu, H., & Liu, H. (2007). Sustainable Power Generation in Microbial Fuel Cells Using Bicarbonate Buffer and Proton Transfer Mechanisms. *Environmental Science and Technology*, *41*(23), 8154–8158.

Fattah, K. P., Sabrina, N., Mavinic, D. S., & Koch, F. A. (2008). Reducing operating costs for struvite formation with a carbon dioxide stripper. *Water Science and Technology*, *58*(4), 957–962. https://doi.org/10.2166/wst.2008.722

Feng, Q., Song, Y. C., & Bae, B. U. (2016). Influence of applied voltage on the performance of bioelectrochemical anaerobic digestion of sewage sludge and planktonic microbial communities at ambient temperature. *Bioresource Technology*, *220*, 500–508. https://doi.org/10.1016/j.biortech.2016.08.085

Feng, Y., Zhang, Y., Chen, S., & Quan, X. (2015). Enhanced production of methane from waste activated sludge by the combination of high-solid anaerobic digestion and microbial electrolysis cell with iron-graphite electrode. *Chemical Engineering Journal*, *259*, 787–794. https://doi.org/10.1016/j.cej.2014.08.048

Filer, J., Ding, H. H., & Chang, S. (2019). Biochemical methane potential (BMP) assay method for anaerobic digestion research. *Water (Switzerland)*, *11*(5). https://doi.org/10.3390/w11050921

Florentino, A. P., Sharaf, A., Zhang, L., & Liu, Y. (2019). Overcoming ammonia

inhibition in anaerobic blackwater treatment with granular activated carbon: The role of electroactive microorganisms. *Environmental Science: Water Research and Technology*, *5*(2), 383–396. https://doi.org/10.1039/c8ew00599k

Fu, Q., Kuramochi, Y., Fukushima, N., Maeda, H., Sato, K., & Kobayashi, H. (2015). Bioelectrochemical analyses of the development of a thermophilic biocathode catalyzing electromethanogenesis. *Environmental Science and Technology*, *49*(2), 1225–1232. https://doi.org/10.1021/es5052233

Gajaraj, S., Huang, Y., Zheng, P., & Hu, Z. (2017). Methane production improvement and associated methanogenic assemblages in bioelectrochemically assisted anaerobic digestion. *Biochemical Engineering Journal*, *117*, 105–112. https://doi.org/10.1016/j.bej.2016.11.003

Gao, Y., Sun, D., Dang, Y., Lei, Y., Ji, J., Lv, T., Bian, R., Xiao, Z., Yan, L., & Holmes, D. E. (2017). Enhancing biomethanogenic treatment of fresh incineration leachate using single chambered microbial electrolysis cells. *Bioresource Technology*, *231*, 129–137. https://doi.org/10.1016/j.biortech.2017.02.024

Gerardo, M. L., Aljohani, N. H. M., Oatley-Radcliffe, D. L., & Lovitt, R. W. (2015). Moving towards sustainable resources: Recovery and fractionation of nutrients from dairy manure digestate using membranes. *Water Research*, *80*, 80–89. https://doi.org/10.1016/j.watres.2015.05.016

Ghaderikia, A. (2022). *Start-Up Strategies for Enhanced Methane Production from Cattle Manure in Bioelectrochemical Systems*. Middle East Technical University.

Ghaderikia, A., Taskin, B., & Yilmazel, Y. D. (2023). Start-up strategies of electromethanogenic reactors for methane production from cattle manure. *Waste Management*, *159*(February), 27–38. https://doi.org/10.1016/j.wasman.2023.01.027

Gunay, A., Karadag, D., Tosun, I., & Ozturk, M. (2008). Use of magnesit as a magnesium source for ammonium removal from leachate. *Journal of Hazardous Materials*, *156*(1–3), 619–623. https://doi.org/10.1016/j.jhazmat.2007.12.067

Guo, F., Babauta, J. T., & Beyenal, H. (2021). The effect of additional salinity on performance of a phosphate buffer saline buffered three-electrode bioelectrochemical system inoculated with wastewater. *Bioresource Technology*, *320*(October 2020).

Guo, K., Donose, B. C., Soeriyadi, A. H., Prévoteau, A., Patil, S. A., Freguia, S., Gooding, J. J., & Rabaey, K. (2014). Flame oxidation of stainless steel felt enhances anodic biofilm formation and current output in bioelectrochemical systems. *Environmental Science and Technology*, *48*(12), 7151–7156. https://doi.org/10.1021/es500720g

Guo, X., Liu, J., & Xiao, B. (2013). Bioelectrochemical enhancement of hydrogen and methane production from the anaerobic digestion of sewage sludge in single-chamber membrane-free microbial electrolysis cells. *International Journal of Hydrogen Energy*, *38*(3), 1342–1347. https://doi.org/10.1016/j.ijhydene.2012.11.087

Guo, Z., Thangavel, S., Wang, L., He, Z., Cai, W., Wang, A., & Liu, W. (2017). Efficient Methane Production from Beer Wastewater in a Membraneless Microbial Electrolysis Cell with a Stacked Cathode : The Eff ect of the Cathode / Anode Ratio on Bioenergy Recovery. *Energy & Fuels*. https://doi.org/10.1021/acs.energyfuels.6b02375

Gurkok, S., Cekmecelioglu, D., & Ogel, Z. B. (2011). Optimization of culture conditions for Aspergillus sojae expressing an Aspergillus fumigatus α-galactosidase. *Bioresource Technology*, *102*(7), 4925–4929. https://doi.org/10.1016/j.biortech.2011.01.036

Hao, J., & Wang, H. (2015). Volatile fatty acids productions by mesophilic and

thermophilic sludge fermentation: Biological responses to fermentation temperature. *Bioresource Technology*, *175*, 367–373. https://doi.org/10.1016/j.biortech.2014.10.106

Hao, X., Wang, C., Van Loosdrecht, M. C. M., & Hu, Y. (2013). Looking beyond struvite for P-recovery. *Environmental Science and Technology*, *47*(10), 4965–4966. https://doi.org/10.1021/es401140s

Harnisch, F., & Freguia, S. (2012). A basic tutorial on cyclic voltammetry for the investigation of electroactive microbial biofilms. *Chemistry - An Asian Journal*, *7*(3), 466–475. https://doi.org/10.1002/asia.201100740

Hassanein, A., Witarsa, F., Guo, X., Yong, L., Lansing, S., & Qiu, L. (2017). Next generation digestion: Complementing anaerobic digestion (AD) with a novel microbial electrolysis cell (MEC) design. *International Journal of Hydrogen Energy*, *42*(48), 28681–28689. https://doi.org/10.1016/j.ijhydene.2017.10.003

Hassanein, A., Witarsa, F., Lansing, S., Qiu, L., & Liang, Y. (2020). Bio-electrochemical enhancement of hydrogen and methane production in a combined anaerobic digester (AD) and microbial electrolysis cell (MEC) from dairy manure. *Sustainability (Switzerland)*, *12*(20), 1–12. https://doi.org/10.3390/su12208491

He, C., Zhang, B., Jiang, Y., Liu, H., & Zhao, H. P. (2021). Microbial electrolysis cell produced biogas as sustainable electron donor for microbial chromate reduction. *Chemical Engineering Journal*, *403*(June 2020), 126429. https://doi.org/10.1016/j.cej.2020.126429

Hjorth, M., Christensen, K. V., Christensen, M. L., & Sommer, S. G. (2009). Solid-liquid separation of animal slurry in theory and practice. *Sustainable Agriculture*, *2*, 953–986. https://doi.org/10.1007/978-94-007-0394-0_43

Holm-Nielsen, J. B., Al Seadi, T., & Oleskowicz-Popiel, P. (2009). The future of anaerobic digestion and biogas utilization. *Bioresource Technology*, *100*(22), 5478–5484. https://doi.org/10.1016/j.biortech.2008.12.046

Hou, H., Li, Z., Liu, B., Liang, S., Xiao, K., Zhu, Q., Hu, S., Yang, J., & Hu, J. (2020). Biogas and phosphorus recovery from waste activated sludge with protocatechuic acid enhanced Fenton pretreatment, anaerobic digestion and microbial electrolysis cell. *Science of the Total Environment*, *704*, 135274. https://doi.org/10.1016/j.scitotenv.2019.135274

Hu, Y., Jing, Z., Sudo, Y., Niu, Q., Du, J., Wu, J., & Li, Y. (2015). Effect of influent COD / SO 2 4 ratios on UASB treatment of a synthetic sulfate-containing wastewater. *Chemosphere*, *130*, 24–33. https://doi.org/10.1016/j.chemosphere.2015.02.019

Huang, H., Mavinic, D. S., Lo, K. V, & Koch, F. A. (2006). Production and Basic Morphology of Struvite Crystals from a Pilot-Scale Crystallization Process. *Environmental Technology*, *3330*(May), 233–245. https://doi.org/10.1080/09593332708618637

Huang, H., Xiao, D., Zhang, Q., & Ding, L. (2014). Removal of ammonia from landfill leachate by struvite precipitation with the use of low-cost phosphate and magnesium sources. *Journal of Environmental Management*, *145*, 191–198. https://doi.org/10.1016/j.jenvman.2014.06.021

Huang, H., Zhang, D. D., Li, J., Guo, G., & Tang, S. (2017). Phosphate recovery from swine wastewater using plant ash in chemical crystallization. *Journal of Cleaner Production*, *168*, 338–345. https://doi.org/10.1016/j.jclepro.2017.09.042

Huang, Q., Liu, Y., & Dhar, B. R. (2020). A critical review of microbial electrolysis cells coupled with anaerobic digester for enhanced biomethane recovery from high-strength feedstocks. *Critical Reviews in Environmental Science and Technology*, *0*(0), 1–40. https://doi.org/10.1080/10643389.2020.1813065

IPCC. (2018). Special Report on Global Warming of 1.5°C Technical Summary. *Intergovernmental Panel on Climate Change*, *October 2018*, 1–6.

https://www.ipcc.ch/site/assets/uploads/sites/2/2019/05/SR15_TS_High_Res.pdf

Iqbal, M., Bhuiyan, H., & Mavinic, D. S. (2008). Assessing struvite precipitation in a pilot-scale fluidized bed crystallizer. *Environmental Technology*, *29*(11), 1157–1167. https://doi.org/10.1080/09593330802075452

Jaffer, Y., Clark, T. A., Pearce, P., & Parsons, S. A. (2002). Potential phosphorus recovery by struvite formation. *Water Research*, *36*(7), 1834–1842. https://doi.org/10.1016/S0043-1354(01)00391-8

Jiao, Y., Yuan, Y., He, C., Liu, L., Pan, X., & Li, P. (2022). Enrichment culture combined with microbial electrochemical enhanced low-temperature anaerobic digestion of cow dung. *Bioresource Technology*, *360*(May), 127636. https://doi.org/10.1016/j.biortech.2022.127636

Kadier, A., Al-Shorgani, N. K. N., Jadhav, D. A., Sonawane, J. M., Mathuriya, A. S., Kalil, M. S., Hasan, H. A., & Khulood Fahad Saud Alabbosh. (2020). Microbial Electrolysis Cell (MEC): An Innovative Waste to Bioenergy and Value-Added-By-product Technology. In *Bioelectrosynthesis: Principles and Technologies for Value-Added Products*.

Kadier, A., Simayi, Y., Abdeshahian, P., Azman, N. F., Chandrasekhar, K., & Kalil, M. S. (2016). A comprehensive review of microbial electrolysis cells (MEC) reactor designs and configurations for sustainable hydrogen gas production. *Alexandria Engineering Journal*, *55*(1), 427–443. https://doi.org/10.1016/j.aej.2015.10.008

Kampen, W. H. (2014). Nutritional Requirements in Fermentation Processes. In *Fermentation and Biochemical Engineering Handbook: Principles, Process Design, and Equipment: Third Edition* (Third Edit). Elsevier Inc. https://doi.org/10.1016/B978-1-4557-2553-3.00004-0

Kang, H. J., Lee, S. H., Lim, T. G., Park, J. H., Kim, B., Buffière, P., & Park, H. D. (2021). Recent advances in methanogenesis through direct interspecies

electron transfer via conductive materials: A molecular microbiological perspective. *Bioresource Technology*, *322*(October 2020). https://doi.org/10.1016/j.biortech.2020.124587

Kang, J., Kim, T., Tak, Y., Lee, J. H., & Yoon, J. (2012). Cyclic voltammetry for monitoring bacterial attachment and biofilm formation. *Journal of Industrial and Engineering Chemistry*, *18*(2), 800–807. https://doi.org/10.1016/j.jiec.2011.10.002

Karthikeyan, R., Cheng, K. Y., Selvam, A., Bose, A., & Wong, J. W. C. (2017). Bioelectrohydrogenesis and inhibition of methanogenic activity in microbial electrolysis cells - A review. *Biotechnology Advances*, *35*(6), 758–771. https://doi.org/10.1016/j.biotechadv.2017.07.004

Kataki, S., West, H., Clarke, M., & Baruah, D. C. (2016). Phosphorus recovery as struvite: Recent concerns for use of seed, alternative Mg source, nitrogen conservation and fertilizer potential. *Resources, Conservation and Recycling*, *107*, 142–156. https://doi.org/10.1016/j.resconrec.2015.12.009

Kotsyurbenko, O. R., Chin, K., Glagolev, M. V, Stubner, S., Simankova, M. V, Nozhevnikova, A. N., & Conrad, R. (2004). *Acetoclastic and hydrogenotrophic methane production and methanogenic populations in an acidic West-Siberian peat bog*. *6*, 1159–1173. https://doi.org/10.1111/j.1462-2920.2004.00634.x

Krähenbühl, M., Etter, B., & Udert, K. M. (2016). Pretreated magnesite as a source of low-cost magnesium for producing struvite from urine in Nepal. *Science of the Total Environment*, *542*, 1155–1161. https://doi.org/10.1016/j.scitotenv.2015.08.060

Kutlar, F. E., Tunca, B., & Yilmazel, Y. D. (2022). Carbon-based conductive materials enhance biomethane recovery from organic wastes: A review of the impacts on anaerobic treatment. *Chemosphere*, *290*(September 2021), 133247. https://doi.org/10.1016/j.chemosphere.2021.133247

LaBarge, N., Yilmazel, Y. D., Hong, P. Y., & Logan, B. E. (2017). Effect of pre-acclimation of granular activated carbon on microbial electrolysis cell startup and performance. *Bioelectrochemistry*, *113*, 20–25. https://doi.org/10.1016/j.bioelechem.2016.08.003

Lackner, N., Wagner, A. O., Markt, R., & Illmer, P. (2020). Ph and phosphate induced shifts in carbon flow and microbial community during thermophilic anaerobic digestion. *Microorganisms*, *8*(2). https://doi.org/10.3390/microorganisms8020286

Le Corre, K. S., Valsami-Jones, E., Hobbs, P., & Parsons, S. A. (2007). Impact of reactor operation on success of struvite precipitation from synthetic liquors. *Environmental Technology*, *28*(11), 1245–1256. https://doi.org/10.1080/09593332808618885

Le Corre, K. S., Valsami-Jones, E., Hobbs, P., & Parsons, S. A. (2009). Phosphorus recovery from wastewater by struvite crystallization: A review. *Critical Reviews in Environmental Science and Technology*, *39*(6), 433–477. https://doi.org/10.1080/10643380701640573

Ledda, C., Schievano, A., Salati, S., & Adani, F. (2013). Nitrogen and water recovery from animal slurries by a new integrated ultrafiltration, reverse osmosis and cold stripping process: A case study. *Water Research*, *47*(16), 6157–6166. https://doi.org/10.1016/j.watres.2013.07.037

Lee, M. E., Steiman, M. W., & St. Angelo, S. K. (2021). Biogas digestate as a renewable fertilizer: Effects of digestate application on crop growth and nutrient composition. *Renewable Agriculture and Food Systems*, *36*(2), 173–181. https://doi.org/10.1017/S1742170520000186

Lee, S. I., Weon, S. Y., Lee, C. W., & Koopman, B. (2003). Removal of nitrogen and phosphate from wastewater by addition of bittern. *Chemosphere*, *51*(4), 265–271. https://doi.org/10.1016/S0045-6535(02)00807-X

Lei, Y., Sun, D., Dang, Y., Chen, H., Zhao, Z., Zhang, Y., & Holmes, D. E. (2016).

Stimulation of methanogenesis in anaerobic digesters treating leachate from a municipal solid waste incineration plant with carbon cloth. *Bioresource Technology*, *222*, 270–276. https://doi.org/10.1016/j.biortech.2016.10.007

Li, B., Boiarkina, I., Young, B., & Yu, W. (2016). Quantification and mitigation of the negative impact of calcium on struvite purity. *Advanced Powder Technology*, *27*(6), 2354–2362. https://doi.org/10.1016/j.apt.2016.10.003

Li, B., Boiarkina, I., Yu, W., Huang, H. M., Munir, T., Wang, G. Q., & Young, B. R. (2019). Phosphorous recovery through struvite crystallization: Challenges for future design. In *Science of the Total Environment*. https://doi.org/10.1016/j.scitotenv.2018.07.166

Li, H., Yao, Q. Z., Wang, Y. Y., Li, Y. L., & Zhou, G. T. (2015). Biomimetic synthesis of struvite with biogenic morphology and implication for pathological biomineralization. *Scientific Reports*, *5*, 1–8. https://doi.org/10.1038/srep07718

Li, J., Rui, J., Yao, M., Zhang, S., Yan, X., Wang, Y., Yan, Z., & Li, X. (2015). Substrate type and free ammonia determine bacterial community structure in full-scale mesophilic anaerobic digesters treating cattle or swine manure. *Frontiers in Microbiology*, *6*(NOV), 1–10. https://doi.org/10.3389/fmicb.2015.01337

Li, S., Zeng, W., Xu, H., Jia, Z., & Peng, Y. (2020). Performance investigation of struvite high-efficiency precipitation from wastewater using silicon-doped magnesium oxide. *Environmental Science and Pollution Research*, *27*(13), 15463–15474. https://doi.org/10.1007/s11356-019-07589-3

Li, Y., Zhang, Y., Liu, Y., Zhao, Z., Zhao, Z., Liu, S., Zhao, H., & Quan, X. (2016). Enhancement of anaerobic methanogenesis at a short hydraulic retention time via bioelectrochemical enrichment of hydrogenotrophic methanogens. *Bioresource Technology*, *218*, 505–511. https://doi.org/10.1016/j.biortech.2016.06.112

Li, Y., Zhao, J., Krooneman, J., & Euverink, G. J. W. (2021). Strategies to boost anaerobic digestion performance of cow manure: Laboratory achievements and their full-scale application potential. *Science of the Total Environment*, *755*. https://doi.org/10.1016/j.scitotenv.2020.142940

Liang, D., Xu, W., Liu, Y., Peng, S., Xie, B., Lu, S., Xiang, Y., & Liu, H. (2015). Can bicarbonate replace phosphate to improve the sustainability of bioelectrochemical systems for H2. *RSC Advances*, 27082–27086. https://doi.org/10.1039/c5ra00702j

Lin, R., Cheng, J., Zhang, J., Zhou, J., Cen, K., & Murphy, J. D. (2017). Boosting biomethane yield and production rate with graphene: The potential of direct interspecies electron transfer in anaerobic digestion. *Bioresource Technology*, *239*, 345–352. https://doi.org/10.1016/j.biortech.2017.05.017

Liu, B., Giannis, A., Zhang, J., Chang, V. W. C., & Wang, J. Y. (2013). Characterization of induced struvite formation from source-separated urine using seawater and brine as magnesium sources. *Chemosphere*, *93*(11), 2738–2747. https://doi.org/10.1016/j.chemosphere.2013.09.025

Liu, D., Zhang, L., Chen, S., Buisman, C., & Ter Heijne, A. (2016). Bioelectrochemical enhancement of methane production in low temperature anaerobic digestion at 10 °C. *Water Research*, *99*, 281–287. https://doi.org/10.1016/j.watres.2016.04.020

Liu, D., Zheng, T., Buisman, C., Heijne, A., & Ter Heijne, A. (2017). Heat-Treated Stainless Steel Felt as a New Cathode Material in a Methane-Producing Bioelectrochemical System. *ACS Sustainable Chemistry and Engineering*, *5*(12), 11346–11353. https://doi.org/10.1021/acssuschemeng.7b02367

Liu, F. H., Wang, S. B., Zhang, J. S., Zhang, J., Yan, X., Zhou, H. K., Zhao, G. P., & Zhou, Z. H. (2009). The structure of the bacterial and archaeal community in a biogas digester as revealed by denaturing gradient gel electrophoresis and 16S rDNA sequencing analysis. *Journal of Applied Microbiology*, *106*(3),

952–966. https://doi.org/10.1111/j.1365-2672.2008.04064.x

Liu, F., Rotaru, A. E., Shrestha, P. M., Malvankar, N. S., Nevin, K. P., & Lovley, D. R. (2012). Promoting direct interspecies electron transfer with activated carbon. *Energy and Environmental Science*, *5*(10), 8982–8989. https://doi.org/10.1039/c2ee22459c

Liu, W., Cai, W., Guo, Z., Wang, L., Yang, C., Varrone, C., & Wang, A. (2016). Microbial electrolysis contribution to anaerobic digestion of waste activated sludge, leading to accelerated methane production. *Renewable Energy*, *91*, 334–339. https://doi.org/10.1016/j.renene.2016.01.082

Liu, X., Hu, Z., Mu, J., Zang, H., & Liu, L. (2014). Phosphorus recovery from urine with different magnesium resources in an air-agitated reactor. *Environmental Technology (United Kingdom)*, *35*(22), 2781–2787. https://doi.org/10.1080/09593330.2014.921732

Logan, B. E. (2009). Exoelectrogenic bacteria that power microbial fuel cells. *Nature Reviews Microbiology*, *7*(5), 375–381. https://doi.org/10.1038/nrmicro2113

Logan, B. E., Call, D., Cheng, S., Hamelers, H. V. M., Sleutels, T. H. J. A., Jeremiasse, A. W., & Rozendal, R. A. (2008). Microbial electrolysis cells for high yield hydrogen gas production from organic matter. *Environmental Science and Technology*, *42*(23), 8630–8640. https://doi.org/10.1021/es801553z

Lovley, D. R. (2017). *Happy together : microbial communities that hook up to swap electrons*. 327–336. https://doi.org/10.1038/ismej.2016.136

Luo, W., Hai, F. I., Price, W. E., Guo, W., Ngo, H. H., Yamamoto, K., & Nghiem, L. D. (2016). Phosphorus and water recovery by a novel osmotic membrane bioreactor-reverse osmosis system. *Bioresource Technology*, *200*, 297–304. https://doi.org/10.1016/j.biortech.2015.10.029

Mancipe-Jiménez, D. C., Costa, C., & Márquez, M. C. (2017). Methanogenesis inhibition by phosphorus in anaerobic liquid waste treatment. *Waste Treatment and Recovery*, *2*(1), 1–8. https://doi.org/10.1515/lwr-2017-0001

Marone, A., Carmona-Martínez, A. A., Sire, Y., Meudec, E., Steyer, J. P., Bernet, N., & Trably, E. (2016). Bioelectrochemical treatment of table olive brine processing wastewater for biogas production and phenolic compounds removal. *Water Research*, *100*, 316–325. https://doi.org/10.1016/j.watres.2016.05.008

Martins, G., Salvador, A. F., Pereira, L., & Alves, M. M. (2018). Methane Production and Conductive Materials: A Critical Review. *Environmental Science and Technology*, *52*(18), 10241–10253. https://doi.org/10.1021/acs.est.8b01913

Merlin Christy, P., Gopinath, L. R., & Divya, D. (2014). A review on anaerobic decomposition and enhancement of biogas production through enzymes and microorganisms. *Renewable and Sustainable Energy Reviews*, *34*, 167–173. https://doi.org/10.1016/j.rser.2014.03.010

Molino, A., Nanna, F., Ding, Y., Bikson, B., & Braccio, G. (2013). Biomethane production by anaerobic digestion of organic waste. *Fuel*, *103*, 1003–1009. https://doi.org/10.1016/j.fuel.2012.07.070

Moset, V., Poulsen, M., Wahid, R., Højberg, O., & Møller, H. B. (2015). Mesophilic versus thermophilic anaerobic digestion of cattle manure: Methane productivity and microbial ecology. *Microbial Biotechnology*, *8*(5), 787–800. https://doi.org/10.1111/1751-7915.12271

Muyzer, G., & Stams, A. J. M. (2008). The ecology and biotechnology of sulphate-reducing bacteria. *Nature Reviews Microbiology*, *6*(june). https://doi.org/10.1038/nrmicro1892

Nasir, I. M., Mohd Ghazi, T. I., & Omar, R. (2012). Anaerobic digestion technology in livestock manure treatment for biogas production: A review.

Engineering in Life Sciences, *12*(3), 258–269. https://doi.org/10.1002/elsc.201100150

Niu, K., Wu, J., Qi, L., & Niu, Q. (2019). Energy intensity of wastewater treatment plants and influencing factors in China. *Science of the Total Environment*, *670*(12), 961–970. https://doi.org/10.1016/j.scitotenv.2019.03.159

Numviyimana, C., Warchoł, J., Izydorczyk, G., Baśladyńska, S., & Chojnacka, K. (2020). Struvite production from dairy processing wastewater: Optimizing reaction conditions and effects of foreign ions through multi-response experimental models. *Journal of the Taiwan Institute of Chemical Engineers*, *117*, 182–189. https://doi.org/10.1016/j.jtice.2020.11.031

Odabaş, Y. (2022). *Enhancement of biomethane production from cattle manure digestion via granular activated carbon amendment*. Middle East Technical University.

Ohlinger, K. N., Young, T. M., & Schroeder, E. D. (2014). Postdigestion struvite precipitation using a fluidized bed reactor. *Journal of Environmental Engineering*, *126*(April), 1–9. https://doi.org/https://doi.org/10.1061/(ASCE)0733-9372(2000)126:4(361)

Park, J. H., Kang, H. J., Park, K. H., & Park, H. D. (2018). Direct interspecies electron transfer via conductive materials: A perspective for anaerobic digestion applications. *Bioresource Technology*, *254*(January), 300–311. https://doi.org/10.1016/j.biortech.2018.01.095

Park, J., Lee, B., Tian, D., & Jun, H. (2018). Bioelectrochemical enhancement of methane production from highly concentrated food waste in a combined anaerobic digester and microbial electrolysis cell. *Bioresource Technology*, *247*(September 2017), 226–233. https://doi.org/10.1016/j.biortech.2017.09.021

Pastor, L., Mangin, D., Ferrer, J., & Seco, A. (2010). Struvite formation from the supernatants of an anaerobic digestion pilot plant. *Bioresource Technology*,

101(1), 118–125. https://doi.org/10.1016/j.biortech.2009.08.002

Pawar, A. A., Karthic, A., Lee, S., Pandit, S., & Jung, S. P. (2020). Microbial electrolysis cells for electromethanogenesis: Materials, configurations and operations. *Environmental Engineering Research*, *27*(1), 200484–0. https://doi.org/10.4491/eer.2020.484

Polat, S., & Sayan, P. (2019). Application of response surface methodology with a Box–Behnken design for struvite precipitation. *Advanced Powder Technology*, *30*(10), 2396–2407. https://doi.org/10.1016/j.apt.2019.07.022

Qin, X., Lu, X., Cai, T., Niu, C., Han, Y., Zhang, Z., Zhu, X., & Zhen, G. (2021). Magnetite-enhanced bioelectrochemical stimulation for biodegradation and biomethane production of waste activated sludge. *Science of the Total Environment*, *789*, 147859. https://doi.org/10.1016/j.scitotenv.2021.147859

Quintana, M., Colmenarejo, M. F., Barrera, J. J. Ä. S., García, G., García, E., Bustos, A., Garci Äa, G., Garci Äa, E., & Bustos, A. (2004). Use of a Byproduct of Magnesium Oxide Production To Precipitate Phosphorus and Nitrogen as Struvite from Wastewater Treatment Liquors. *Journal of Agricultural and Food Chemistry*, *52*(2), 294–299. https://doi.org/10.1021/jf0303870

Rabus, R., Venceslau, S. S., Wöhlbrand, L., Voordouw, G., Wall, J. D., & Pereira, I. A. C. (2015). A Post-Genomic View of the Ecophysiology , Catabolism and Biotechnological Relevance of Sulphate-Reducing Prokaryotes. In *Advances in Microbial Physiology* (Vol. 66). https://doi.org/10.1016/bs.ampbs.2015.05.002

Rahaman, M. S., Mavinic, D. S., Meikleham, A., & Ellis, N. (2014). Modeling phosphorus removal and recovery from anaerobic digester supernatant through struvite crystallization in a fluidized bed reactor. *Water Research*, *51*, 1–10. https://doi.org/10.1016/j.watres.2013.11.048

Raposo, F., Fernández-Cegrí, V., de la Rubia, M. A., Borja, R., Béline, F.,

Cavinato, C., Demirer, G., Fernández, B., Fernández-Polanco, M., Frigon, J. C., Ganesh, R., Kaparaju, P., Koubova, J., Méndez, R., Menin, G., Peene, A., Scherer, P., Torrijos, M., Uellendahl, H., … de Wilde, V. (2011). Biochemical methane potential (BMP) of solid organic substrates: Evaluation of anaerobic biodegradability using data from an international interlaboratory study. *Journal of Chemical Technology and Biotechnology*, *86*(8), 1088–1098. https://doi.org/10.1002/jctb.2622

Ray, S., Kuppam, C., Pandit, S., & Kumar, P. (2023). Biogas Upgrading by Hydrogenotrophic Methanogens : An Overview. *Waste and Biomass Valorization*, *14*(2), 537–552. https://doi.org/10.1007/s12649-022-01888-6

Romero-Güiza, M. S., Astals, S., Mata-Alvarez, J., & Chimenos, J. M. (2015). Feasibility of coupling anaerobic digestion and struvite precipitation in the same reactor: Evaluation of different magnesium sources. *Chemical Engineering Journal*, *270*, 542–548. https://doi.org/10.1016/j.cej.2015.02.057

Rout, P. R., Bhunia, P., & Dash, R. R. (2017). Evaluation of kinetic and statistical models for predicting breakthrough curves of phosphate removal using dolochar-packed columns. *Journal of Water Process Engineering*, *17*(February), 168–180. https://doi.org/10.1016/j.jwpe.2017.04.003

Rubio-Rincón, F. J., Lopez-Vazquez, C. M., Ronteltap, M., & Brdjanovic, D. (2014). Seawater for phosphorus recovery from urine. *Desalination*, *348*, 49–56. https://doi.org/10.1016/j.desal.2014.06.005

Ryu, H. D., Lim, D. Y., Kim, S. J., Baek, U. Il, Chung, E. G., Kim, K., & Lee, J. K. (2020). Struvite precipitation for sustainable recovery of nitrogen and phosphorus from anaerobic digestion effluents of swine manure. *Sustainability (Switzerland)*, *12*(20), 1–15. https://doi.org/10.3390/su12208574

Sakthivel, S. R., Tilley, E., & Udert, K. M. (2012). Wood ash as a magnesium source for phosphorus recovery from source-separated urine. *Science of the Total Environment*, *419*, 68–75.

https://doi.org/10.1016/j.scitotenv.2011.12.065

Şanlı, M. (2022). *Impact Of Process Conditions on Methane Production in Anaerobic Digestion and Microbial Electrolysis Cell (AD-MEC) Integrated Systems*. Middle East Technical University.

Sasaki, D., Sasaki, K., Watanabe, A., Morita, M., Matsumoto, N., Igarashi, Y., & Ohmura, N. (2013). Operation of a cylindrical bioelectrochemical reactor containing carbon fiber fabric for efficient methane fermentation from thickened sewage sludge. *Bioresource Technology*, *129*, 366–373. https://doi.org/10.1016/j.biortech.2012.11.048

Sena, M., Seib, M., Noguera, D. R., & Hicks, A. (2021). Environmental impacts of phosphorus recovery through struvite precipitation in wastewater treatment. *Journal of Cleaner Production*, *280*, 124222. https://doi.org/10.1016/j.jclepro.2020.124222

Shi, L., Simplicio, W. S., Wu, G., Hu, Z., Hu, H., & Zhan, X. (2018). Nutrient Recovery from Digestate of Anaerobic Digestion of Livestock Manure: a Review. *Current Pollution Reports*, *4*(2), 74–83. https://doi.org/10.1007/s40726-018-0082-z

Siciliano, A. (2016). Assessment of fertilizer potential of the struvite produced from the treatment of methanogenic landfill leachate using low-cost reagents. *Environmental Science and Pollution Research*, *23*(6), 5949–5959. https://doi.org/10.1007/s11356-015-5846-z

Siciliano, A., & De Rosa, S. (2014). Recovery of ammonia in digestates of calf manure through a struvite precipitation process using unconventional reagents. *Environmental Technology (United Kingdom)*, *35*(7), 841–850. https://doi.org/10.1080/09593330.2013.853088

Siciliano, A., Limonti, C., Curcio, G. M., & Molinari, R. (2020). Advances in struvite precipitation technologies for nutrients removal and recovery from aqueous waste and wastewater. *Sustainability (Switzerland)*, *12*(18).

https://doi.org/10.3390/su12187538

Siciliano, A., Ruggiero, C., & De Rosa, S. (2013). A new integrated treatment for the reduction of organic and nitrogen loads in methanogenic landfill leachates. *Process Safety and Environmental Protection*, *91*(4), 311–320. https://doi.org/10.1016/j.psep.2012.06.008

Siegert, M., Li, X. F., Yates, M. D., & Logan, B. E. (2014). The presence of hydrogenotrophic methanogens in the inoculum improves methane gas production in microbial electrolysis cells. *Frontiers in Microbiology*, *5*(DEC), 1–12. https://doi.org/10.3389/fmicb.2014.00778

Siegert, M., Yates, M. D., Call, D. F., Zhu, X., Spormann, A., & Logan, B. E. (2014). Comparison of nonprecious metal cathode materials for methane production by electromethanogenesis. *ACS Sustainable Chemistry and Engineering*, *2*(4), 910–917. https://doi.org/10.1021/sc400520x

Siegert, M., Yates, M. D., Spormann, A. M., & Logan, B. E. (2015). Methanobacterium Dominates Biocathodic Archaeal Communities in Methanogenic Microbial Electrolysis Cells. *ACS Sustainable Chemistry and Engineering*, *3*, 1668–1676. https://doi.org/10.1021/acssuschemeng.5b00367

Sondergaard, M., Jensen, J. P., Jeppesen, E., & M. Sondergaard, J.P. Jensen, E. J. (2003). Role of sediment and internal loading of phosphorus in shallow lakes. *Hydrobiologia*, *506*(509), 135–145.

Song, W., Li, Z., Liu, F., Ding, Y., Qi, P., You, H., & Jin, C. (2018). Effective removal of ammonia nitrogen from waste seawater using crystal seed enhanced struvite precipitation technology with response surface methodology for process optimization. *Environmental Science and Pollution Research*, *25*(1), 628–638. https://doi.org/10.1007/s11356-017-0441-0

St-Pierre, B., & Wright, A. D. G. (2014). Comparative metagenomic analysis of bacterial populations in three full-scale mesophilic anaerobic manure digesters. *Applied Microbiology and Biotechnology*, *98*(6), 2709–2717.

https://doi.org/10.1007/s00253-013-5220-3

Stams, A. J. M., & Plugge, C. M. (2009). Electron transfer in syntrophic communities of anaerobic bacteria and archaea. *Nature Publishing Group*, *7*(auguST). https://doi.org/10.1038/nrmicro2166

Stratful, I., Scrimshaw, M. D., & Lester, J. N. (2004). Removal of Struvite to Prevent Problems Associated with its Accumulation in Wastewater Treatment Works. *Water Environment Research*, *76*(5), 437–443. https://doi.org/10.2175/106143004x151491

Su, W., Zhang, L., Tao, Y., Zhan, G., Li, D., & Li, D. (2012). Electrochemistry Communications Sulfate reduction with electrons directly derived from electrodes in bioelectrochemical systems. *Electrochemistry Communications*, *22*, 37–40. https://doi.org/10.1016/j.elecom.2012.04.030

Sun, R., Zhou, A., Jia, J., Liang, Q., Liu, Q., Xing, D., & Ren, N. (2015). Characterization of methane production and microbial community shifts during waste activated sludge degradation in microbial electrolysis cells. *Bioresource Technology*, *175*, 68–74. https://doi.org/10.1016/j.biortech.2014.10.052

TURKSTAT. (2022). *Turkish statistical institute*. https://data.tuik.gov.tr/Bulten/Index?p=Kirmizi-Et-Uretim-Istatistikleri-2020-2021-45671

Umezawa, K., Kojima, H., Kato, Y., & Fukui, M. (2021). Dissulfurispira thermophila gen. nov., sp. nov., a thermophilic chemolithoautotroph growing by sulfur disproportionation, and proposal of novel taxa in the phylum Nitrospirota to reclassify the genus Thermodesulfovibrio. *Systematic and Applied Microbiology*, *44*(2), 126184. https://doi.org/10.1016/j.syapm.2021.126184

Uysal, A., Yilmazel, Y. D., & Demirer, G. N. (2010). The determination of fertilizer quality of the formed struvite from effluent of a sewage sludge

anaerobic digester. *Journal of Hazardous Materials*, *181*(1–3), 248–254. https://doi.org/10.1016/j.jhazmat.2010.05.004

Vaneeckhaute, C., Lebuf, V., Michels, E., Belia, E., Vanrolleghem, P. A., Tack, F. M. G., & Meers, E. (2017). Nutrient Recovery from Digestate: Systematic Technology Review and Product Classification. *Waste and Biomass Valorization*, *8*(1), 21–40. https://doi.org/10.1007/s12649-016-9642-x

Varanasi, J. L., Veerubhotla, R., Pandit, S., & Das, D. (2018). Biohydrogen production using microbial electrolysis cell: Recent advances and future prospects. In *Biomass, Biofuels, Biochemicals: Microbial Electrochemical Technology: Sustainable Platform for Fuels, Chemicals and Remediation*. Elsevier B.V. https://doi.org/10.1016/B978-0-444-64052-9.00035-2

Wang, H., Liu, Y., Du, H., Zhu, J., Peng, L., Yang, C., & Luo, F. (2021). Exploring the effect of voltage on biogas production performance and the methanogenic pathway of microbial electrosynthesis. *Biochemical Engineering Journal*, *171*(January), 108028. https://doi.org/10.1016/j.bej.2021.108028

Wang, H., Sayed, S. Y., Luber, E. J., Olsen, B. C., Shirurkar, S. M., Venkatakrishnan, S., Tefashe, U. M., Farquhar, A. K., Smotkin, E. S., McCreery, R. L., & Buriak, J. M. (2020). Redox Flow Batteries: How to Determine Electrochemical Kinetic Parameters. *ACS Nano*, *14*(3), 2575–2584. https://doi.org/10.1021/acsnano.0c01281

Wang, J., Burken, J. G., Zhang, X. (Jackie), & Surampalli, R. (2005). Engineered Struvite Precipitation: Impacts of Component-Ion Molar Ratios and pH. *Journal of Environmental Engineering*, *131*(10), 1433–1440. https://doi.org/10.1061/(asce)0733-9372(2005)131:10(1433)

Wang, R., Li, Y., Wang, W., Chen, Y., & Vanrolleghem, P. A. (2015). Effect of high orthophosphate concentration on mesophilic anaerobic sludge digestion and its modeling. *Chemical Engineering Journal*, *260*, 791–800. https://doi.org/10.1016/j.cej.2014.09.050

Wang, X. T., Zhang, Y. F., Wang, B., Wang, S., Xing, X., Xu, X. J., Liu, W. Z., Ren, N. Q., Lee, D. J., & Chen, C. (2022). Enhancement of methane production from waste activated sludge using hybrid microbial electrolysis cells-anaerobic digestion (MEC-AD) process – A review. *Bioresource Technology*, *346*(December 2021), 126641. https://doi.org/10.1016/j.biortech.2021.126641

Ward, L. M., Bertran, E., & Johnston, D. T. (2020). Genomic sequence analysis of Dissulfurirhabdus thermomarina SH388 and proposed reassignment to Dissulfurirhabdaceae fam. nov. *Microbial Genomics*, *6*(7), 2–6. https://doi.org/10.1099/mgen.0.000390

WBA. (2019). Global potential of biogas. In *World Biogas Association*.

Xavier, L. D., Cammarota, M. C., Yokoyama, L., & Volschan, I. (2014). Study of the recovery of phosphorus from struvite precipitation in supernatant line from anaerobic digesters of sludge. *Water Science and Technology*, *69*(7), 1546–1551. https://doi.org/10.2166/wst.2014.033

Xiao, B., Chen, X., Han, Y., Liu, J., & Guo, X. (2018). Bioelectrochemical enhancement of the anaerobic digestion of thermal-alkaline pretreated sludge in microbial electrolysis cells. *Renewable Energy*, *115*, 1177–1183. https://doi.org/10.1016/j.renene.2017.06.043

Xing, T., Yun, S., Li, B., Wang, K., Chen, J., Jia, B., Ke, T., & An, J. (2021). Coconut-shell-derived bio-based carbon enhanced microbial electrolysis cells for upgrading anaerobic co-digestion of cow manure and aloe peel waste. *Bioresource Technology*, *338*(May), 125520. https://doi.org/10.1016/j.biortech.2021.125520

Xu, N., Li, Y., Zheng, L., Gao, Y., Yin, H., Zhao, J., Chen, Z., Chen, J., & Chen, M. (2014). Synthesis and application of magnesium amorphous calcium carbonate for removal of high concentration of phosphate. *Chemical Engineering Journal*, *251*, 102–110. https://doi.org/10.1016/j.cej.2014.04.037

Xu, S., He, C., Luo, L., Lü, F., He, P., & Cui, L. (2015). Comparing activated carbon of different particle sizes on enhancing methane generation in upflow anaerobic digester. *Bioresource Technology*, *196*, 606–612. https://doi.org/10.1016/j.biortech.2015.08.018

Yenigün, O., & Demirel, B. (2013). Ammonia inhibition in anaerobic digestion: A review. *Process Biochemistry*, *48*(5–6), 901–911. https://doi.org/10.1016/j.procbio.2013.04.012

Yetilmezsoy, K., Kocak, E., Akbin, H. M., & Özçimen, D. (2020). Utilization of struvite recovered from high-strength ammonium-containing simulated wastewater as slow-release fertilizer and fire-retardant barrier. *Environmental Technology (United Kingdom)*, *41*(2), 153–170. https://doi.org/10.1080/09593330.2018.1491642

Yilmazel, Y. D., & Demirer, G. N. (2011). Removal and recovery of nutrients as struvite from anaerobic digestion residues of poultry manure. *Environmental Technology*, *32*(7), 783–794. https://doi.org/10.1080/09593330.2010.512925

Yilmazel, Y. D., & Demirer, G. N. (2013). Nitrogen and phosphorus recovery from anaerobic co-digestion residues of poultry manure and maize silage via struvite precipitation. *Waste Management and Research*, *31*(8), 792–804. https://doi.org/10.1177/0734242X13492005

Yu, J., Kim, S., & Kwon, O. S. (2019). Effect of applied voltage and temperature on methane production and microbial community in microbial electrochemical anaerobic digestion systems treating swine manure. *Journal of Industrial Microbiology and Biotechnology*, *46*(7), 911–923. https://doi.org/10.1007/s10295-019-02182-6

Yu, Z., Leng, X., Zhao, S., Ji, J., Zhou, T., Khan, A., Kakde, A., Liu, P., & Li, X. (2018). A review on the applications of microbial electrolysis cells in anaerobic digestion. *Bioresource Technology*, *255*(February), 340–348. https://doi.org/10.1016/j.biortech.2018.02.003

Yuan, Y., Cheng, H., Chen, F., Zhang, Y., Xu, X., Huang, C., & Chen, C. (2020). Enhanced methane production by alleviating sul fi de inhibition with a microbial electrolysis coupled anaerobic digestion reactor. *Environment International*, *136*(January), 105503. https://doi.org/10.1016/j.envint.2020.105503

Zakaria, B. S., & Dhar, B. R. (2019). Progress towards catalyzing electro-methanogenesis in anaerobic digestion process: Fundamentals, process optimization, design and scale-up considerations. *Bioresource Technology*, *289*(May), 121738. https://doi.org/10.1016/j.biortech.2019.121738

Zakaria, B. S., & Ranjan Dhar, B. (2021). An intermittent power supply scheme to minimize electrical energy input in a microbial electrolysis cell assisted anaerobic digester. *Bioresource Technology*, *319*(July 2020), 124109. https://doi.org/10.1016/j.biortech.2020.124109

Zarebska, A., Romero Nieto, D., Christensen, K. V., Fjerbæk Søtoft, L., & Norddahl, B. (2015). Ammonium fertilizers production from manure: A critical review. *Critical Reviews in Environmental Science and Technology*, *45*(14), 1469–1521. https://doi.org/10.1080/10643389.2014.955630

Zhang, T., Ding, L., Ren, H., & Xiong, X. (2009). Ammonium nitrogen removal from coking wastewater by chemical precipitation recycle technology. *Water Research*, *43*(20), 5209–5215. https://doi.org/10.1016/j.watres.2009.08.054

Zhang, W., Dixon, M. B., Saint, C. P., Teng, K. S., & Furumai, H. (2018). Electrochemical biosensing of algal toxins in water : The current state-of-art Electrochemical biosensing of algal toxins in water : The current. *ACS Sensors*, *3*, 1233–1245. https://doi.org/10.1021/acssensors.8b00359

Zhang, Y., & Angelidaki, I. (2014). Microbial electrolysis cells turning to be versatile technology: Recent advances and future challenges. *Water Research*, *56*, 11–25. https://doi.org/10.1016/j.watres.2014.02.031

Zhang, Y., Merrill, M. D., & Logan, B. E. (2010). The use and optimization of

stainless steel mesh cathodes in microbial electrolysis cells. *International Journal of Hydrogen Energy*, *35*(21), 12020–12028. https://doi.org/10.1016/j.ijhydene.2010.08.064

Zhao, L., Wang, X. T., Chen, K. Y., Wang, Z. H., Xu, X. J., Zhou, X., Xing, D. F., Ren, N. Q., Lee, D. J., & Chen, C. (2021). The underlying mechanism of enhanced methane production using microbial electrolysis cell assisted anaerobic digestion (MEC-AD) of proteins. *Water Research*, *201*(May), 117325. https://doi.org/10.1016/j.watres.2021.117325

Zhao, Z., Zhang, Y., Chen, S., Quan, X., & Yu, Q. (2014). Bioelectrochemical enhancement of anaerobic methanogenesis for high organic load rate wastewater treatment in a up-flow anaerobic sludge blanket (UASB) reactor. *Scientific Reports*, *4*, 1–8. https://doi.org/10.1038/srep06658

Zhao, Z., Zhang, Y., Ma, W., Sun, J., Sun, S., & Quan, X. (2016). Enriching functional microbes with electrode to accelerate the decomposition of complex substrates during anaerobic digestion of municipal sludge. *Biochemical Engineering Journal*, *111*, 1–9. https://doi.org/10.1016/j.bej.2016.03.002

Zhao, Z., Zhang, Y., Quan, X., & Zhao, H. (2016). Evaluation on direct interspecies electron transfer in anaerobic sludge digestion of microbial electrolysis cell. *Bioresource Technology*, *200*, 235–244. https://doi.org/10.1016/j.biortech.2015.10.021

Zhao, Z., Zhang, Y., Wang, L., & Quan, X. (2015). Potential for direct interspecies electron transfer in an electric-anaerobic system to increase methane production from sludge digestion. *Scientific Reports*, *5*(June), 1–12. https://doi.org/10.1038/srep11094

Zhen, G., Lu, X., Kobayashi, T., Kumar, G., & Xu, K. (2016). Promoted electromethanosynthesis in a two-chamber microbial electrolysis cells (MECs) containing a hybrid biocathode covered with graphite felt (GF). *Chemical*

Engineering Journal, *284*, 1146–1155. https://doi.org/10.1016/j.cej.2015.09.071

Zhen, G., Lu, X., Kobayashi, T., Li, Y. Y., Xu, K., & Zhao, Y. (2015). Mesophilic anaerobic co-digestion of waste activated sludge and Egeria densa: Performance assessment and kinetic analysis. *Applied Energy*, *148*, 78–86. https://doi.org/10.1016/j.apenergy.2015.03.038

Zhou, S., Dong, M., Ding, X., Xue, X., & Yang, H. (2021). Application of RSM to optimize the recovery of ammonia nitrogen from high chromium effluent produced in vanadium industry using struvite precipitation. *Journal of Environmental Chemical Engineering*, *9*(6), 106318. https://doi.org/10.1016/j.jece.2021.106318

Zhu, X., Yates, M. D., & Logan, B. E. (2012). Set potential regulation reveals additional oxidation peaks of Geobacter sulfurreducens anodic biofilms. *Electrochemistry Communications*, *22*(1), 116–119. https://doi.org/10.1016/j.elecom.2012.06.013

Zin, M. M. T., Tiwari, D., & Kim, D. J. (2020). Maximizing ammonium and phosphate recovery from food wastewater and incinerated sewage sludge ash by optimal Mg dose with RSM. *Journal of Industrial and Engineering Chemistry*, *86*, 136–143. https://doi.org/10.1016/j.jiec.2020.02.020

APPENDICES

A. Set 2 – Inoculum preparation and specific methanogenic activity of the seed

For inoculum preparation, the fed-batch operation was employed with a 1.8 L active volume reactor. HRT was 16 days. The organic loading rate was 5 kg VS/m^3.day. After 26 days, production stabilized. Then, the seed was used for AD-MEC operation.

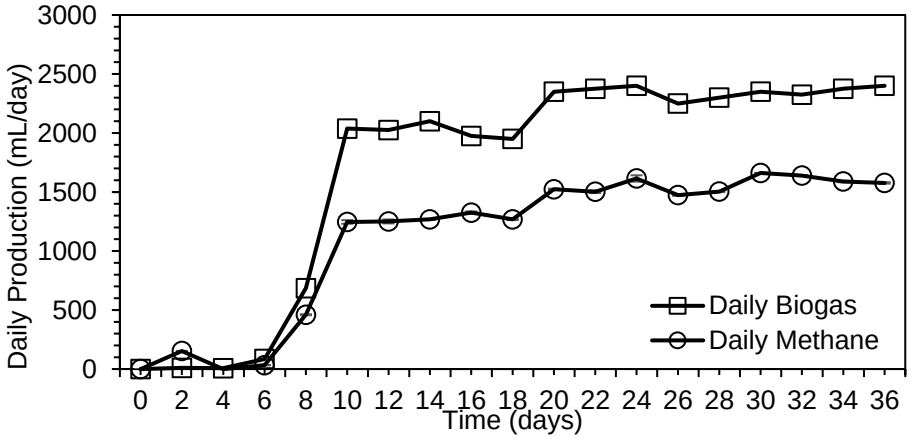

Figure A.1. Daily CH_4 production in the seed reactor

The seed was subjected to specific methanogenic activity (SMA) test before use. 88.75 mL CH_4 was the theoretical value. 81.1% of activity was observed for the inoculum.

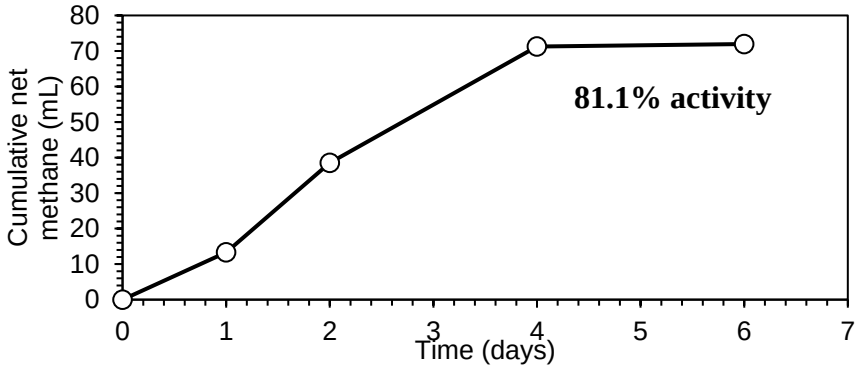

Figure A.2. SMA of seed

B. Example calculations

Modified Gompertz kinetic parameter calculations (provide a reference):

$$P = P_{\infty}.\exp\left\{-\exp\left[\frac{R_m.e}{P_{\infty}}(\lambda - t) + 1\right]\right\}$$

P_{∞}: Maximum CH_4 yield potential as mL CH_4/g VS

R_m: Maximum CH_4 production rate as mL CH_4/g VS /d

λ: Lag phase as d,

R^2: Coefficient of determination

For each sample, the expected CH_4 production was estimated using the modified Gompertz formula. The following is a formula for summing the squared differences between observed and projected CH_4 levels across all samples.

$$SRR = \sum_{n}(P_{Predicted} - P_{actual})^2$$

Using the Excel solver, the minimal SSR value with a starting value of 1 for P, R_m, and λ was computed. Later, the R^2 value was determined for each reactor to determine the relationship between expected and actual CH_4.

C. AD-MEC operation with 100 mM PBS media

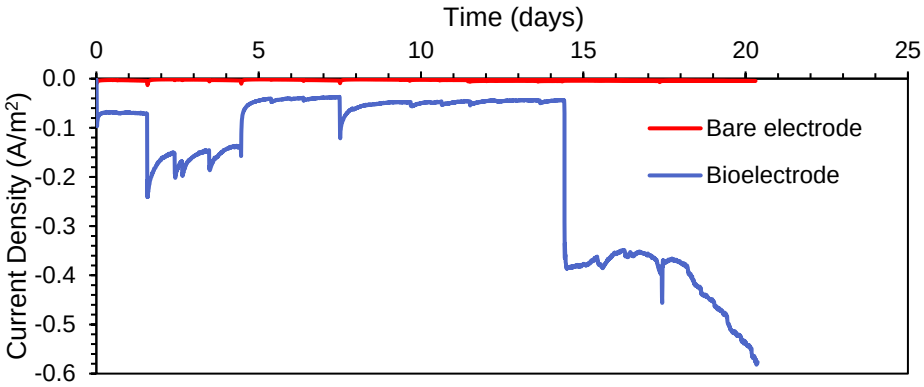

Figure C.1. Current density of AD-MEC operation with 100 mM PBS

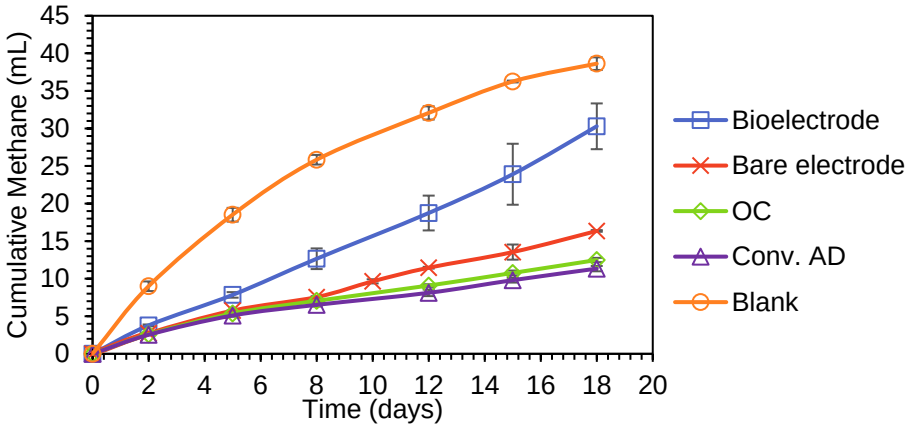

Figure C.2. Cumulative CH4 of AD-MEC operation with 100 mM PBS

D. Current density of the replicate AD-MEC reactors in Set 1

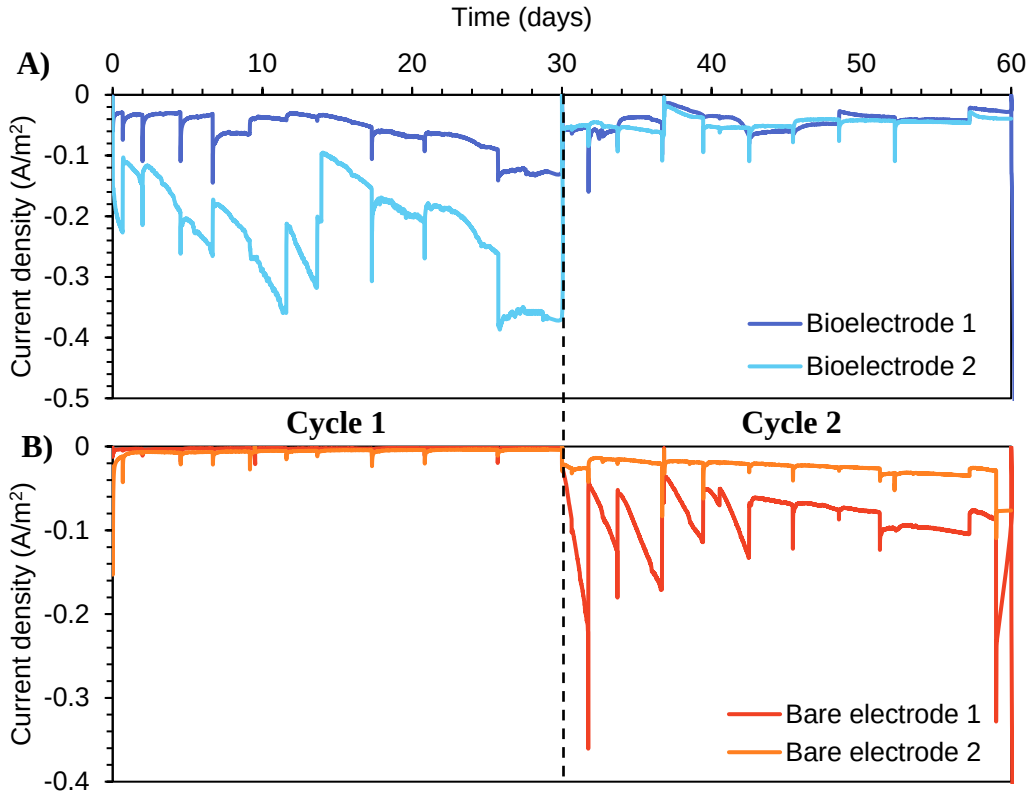

Figure D.1. Current Density of the replicate A) Bioelectrode, B) Bare electrode AD-MEC reactors in Set 1 during Cycle 1 and Cycle 2

E. The modified Gompertz models of Set 1

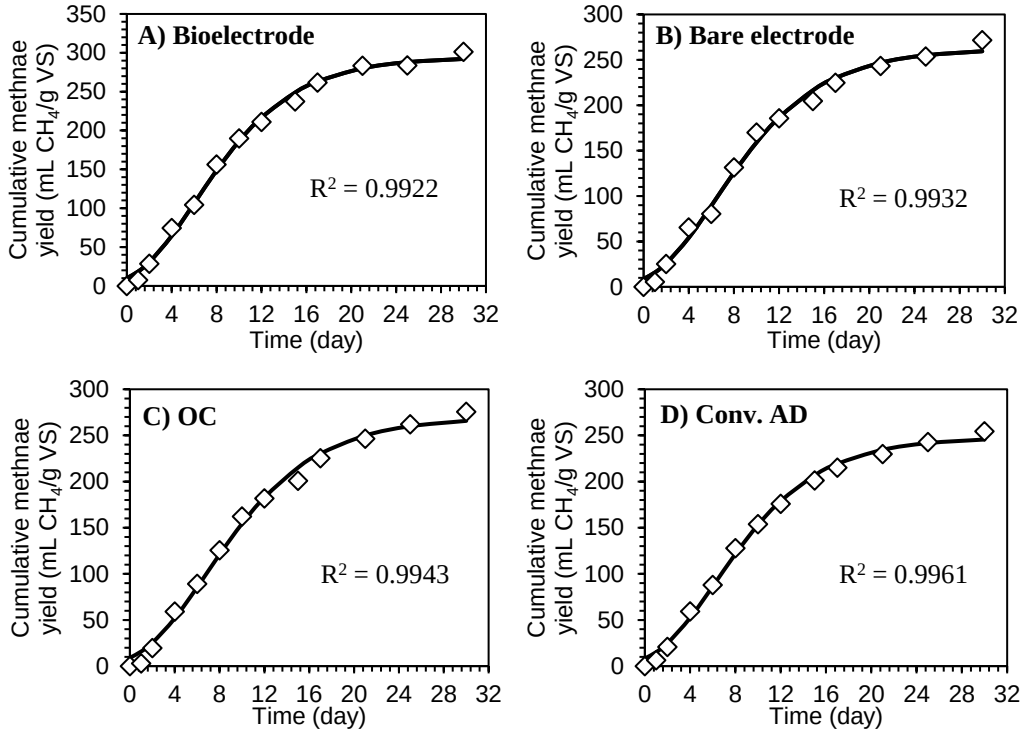

Figure E.1. The modified Gompertz model for cycle 1 (No-PBS, -0.9 V cathode potential) of reactors A) Bioelectrode, B) Bare electrode, C) OC, and D) Conv. AD (Dots: experimental data, Solid line: model data)

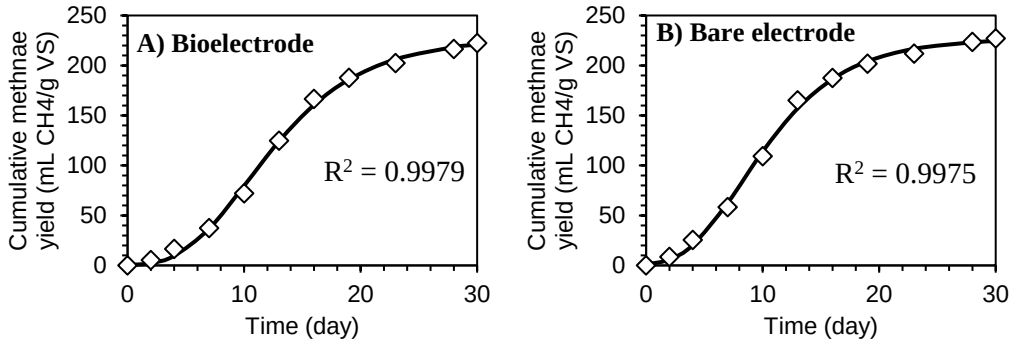

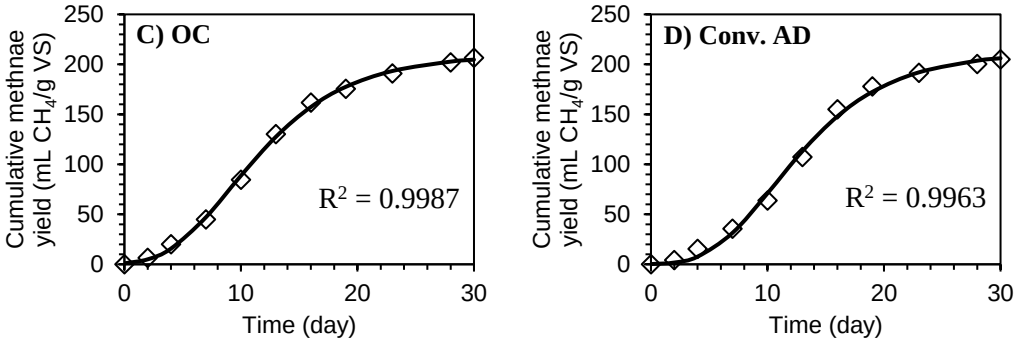

Figure E.2. The modified Gompertz model for cycle 2 (5 mM, PBS, -0.9 V cathode potential) of reactors A) Bioelectrode, B) Bare electrode, C) OC, and D) Conv. AD (Dots: experimental data, Solid line: model data)

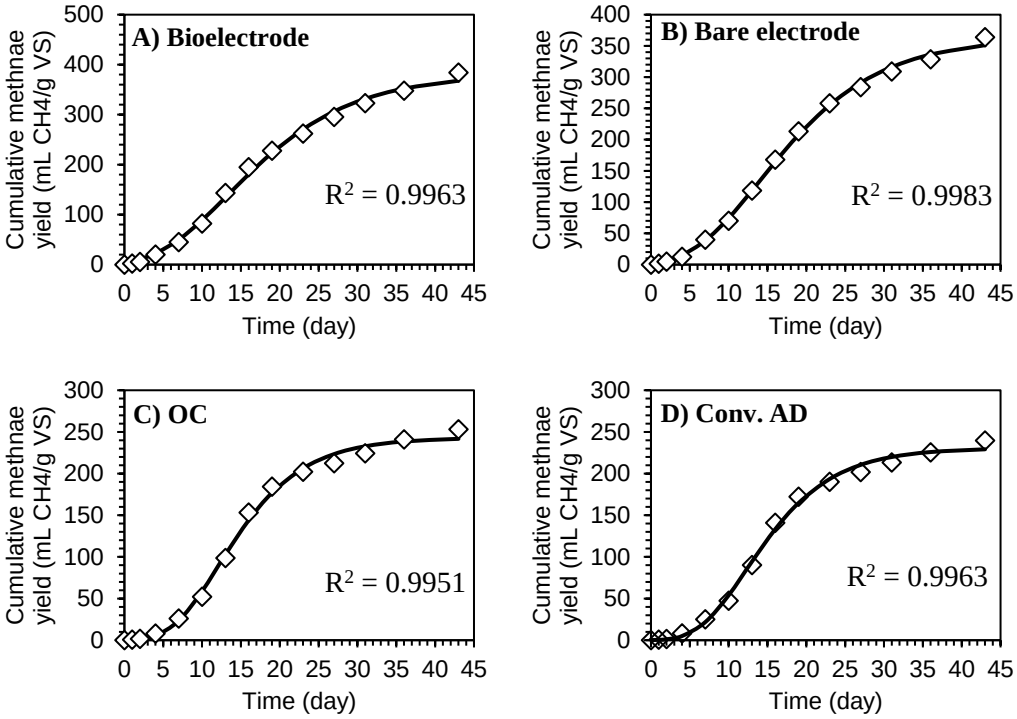

Figure E.3. The modified Gompertz model for cycle 3 (5 mM, PBS, -1 V cathode potential) of reactors A) Bioelectrode, B) Bare electrode, C) OC, and D) Conv. AD (Dots: experimental data, Solid line: model data)

F. H_2 partial pressure calculation

In calculations, water vapor pressure was considered since reactors were operated at 35 °C. According to Neubert et al. (2021), absolute humidity (AH) was calculated:

$$AH = \frac{m_{H2O}}{V_{biogas}} = \frac{P_{H2O,sat}}{T_{biogas} . R_{H2O}}$$

where R_{H2O} = 461.52 J/kg.K

$$P_s\ (Pa) = \frac{\exp\left(34.494 - \frac{4924.99}{T+237.1}\right)}{(T+105)^{1.57}} \quad \text{(unit of Pa)}$$

T = 35 °C

The water vapor pressure is 5629 Pa at 35 °C.

$$AH = \frac{m_{H2O}}{V_{biogas}} = \frac{P_{H2O,sat}}{T_{biogas} . R_{H2O}}$$

Example calculation for the Bioelectrode reactor in Set 2 Cattle manure Gr-SS at -1 V cathode potential:

$$\frac{m_{H2O}}{0.418\ L} = \frac{5629\ Pa}{308\ K\ .461.52 \frac{J}{kg.K}}$$

m_{H2O} = 0.017 g

Then, using ideal gas law,

P.V = n.R.T

$$v = \frac{n.R.T}{p.M} = \frac{(0.017\ g)\left(8.314 \frac{J}{mol.K}\right)(308\ K) x 1000 \frac{m3}{L}}{(99000\ Pa)(18.02 \frac{g}{mol})} = 0.023\ L$$

where M is the molecular weight of the water.

Then, to find the v_{biogas}^{dry}:

$$v_{biogas}^{total} = v_{biogas}^{dry} + v_{H2O}$$

v_{biogas}^{dry}=0.418 L - 0.023 L = 0.39 L

$\frac{v_{H2}}{v_{total\ biogas}}$=0.56 ($H_2$ content of the reactor)

$$\frac{P_{H2}}{P_{total\ biogas}} = \frac{P_{H2}}{101.325\ kPa} = 0.56$$

P_{H2} = 57.45 kPa = 0.57 atm

Reference:

Neubert, K., Kretzschmar, J., dos Santos, T. R., Härtig, C., & Harnisch, F. (2021). Making sense of gas measurements: quantification of multicomponent gas mixtures in biological and chemical laboratory experiments. ChemTexts, 7, 1-25.

G. The current density of the replicates of AD-MEC reactors in Set 2

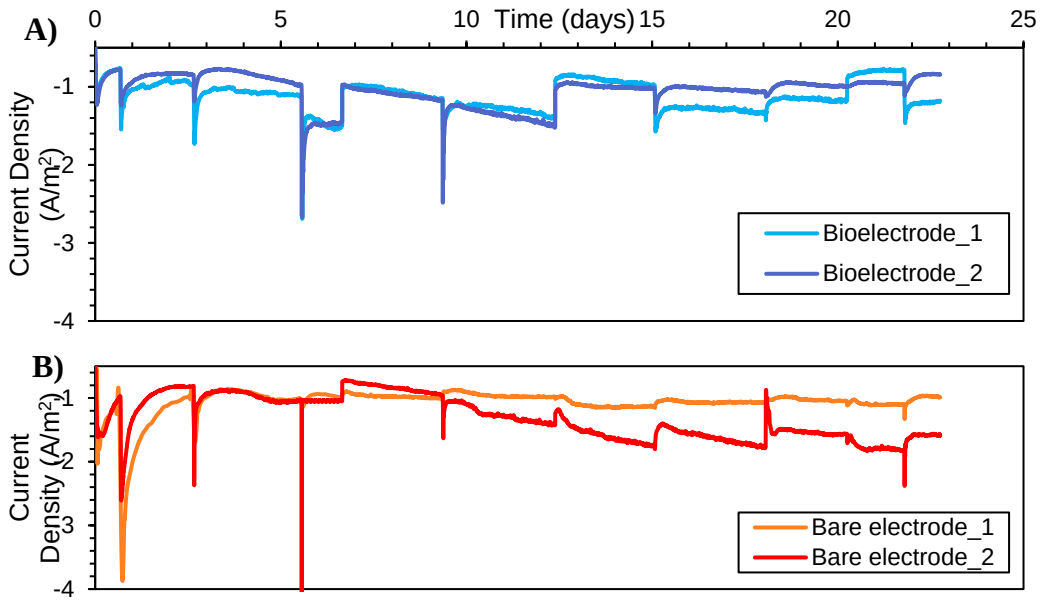

Figure G.1. Current Density of the replicate A) Bioelectrode and B) Bare electrode AD-MEC reactors under -0.9 V cathode potential in Cycle 1

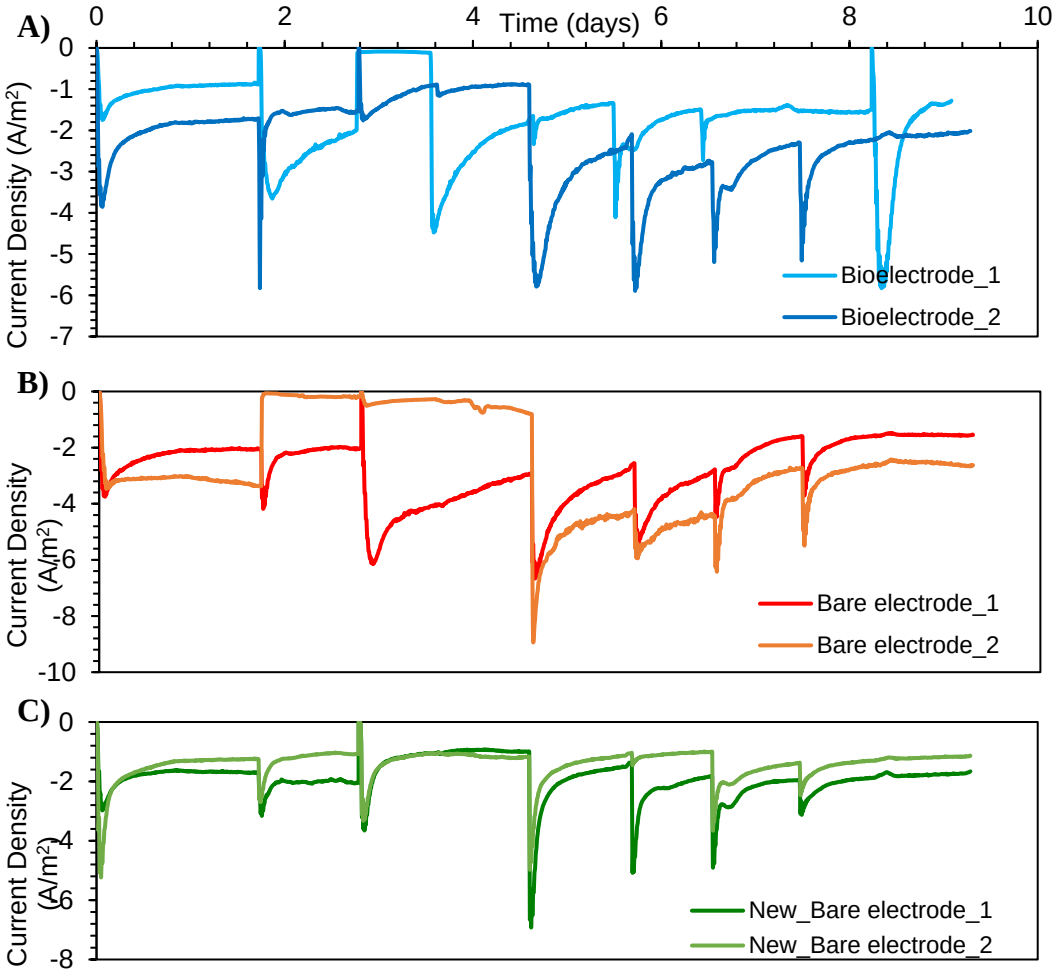

Figure G.2. Current Density of the replicate A) Bioelectrode, B) Bare electrode, and C) New_Bare electrode AD-MEC reactors under -1 V cathode potential in Cycle 2

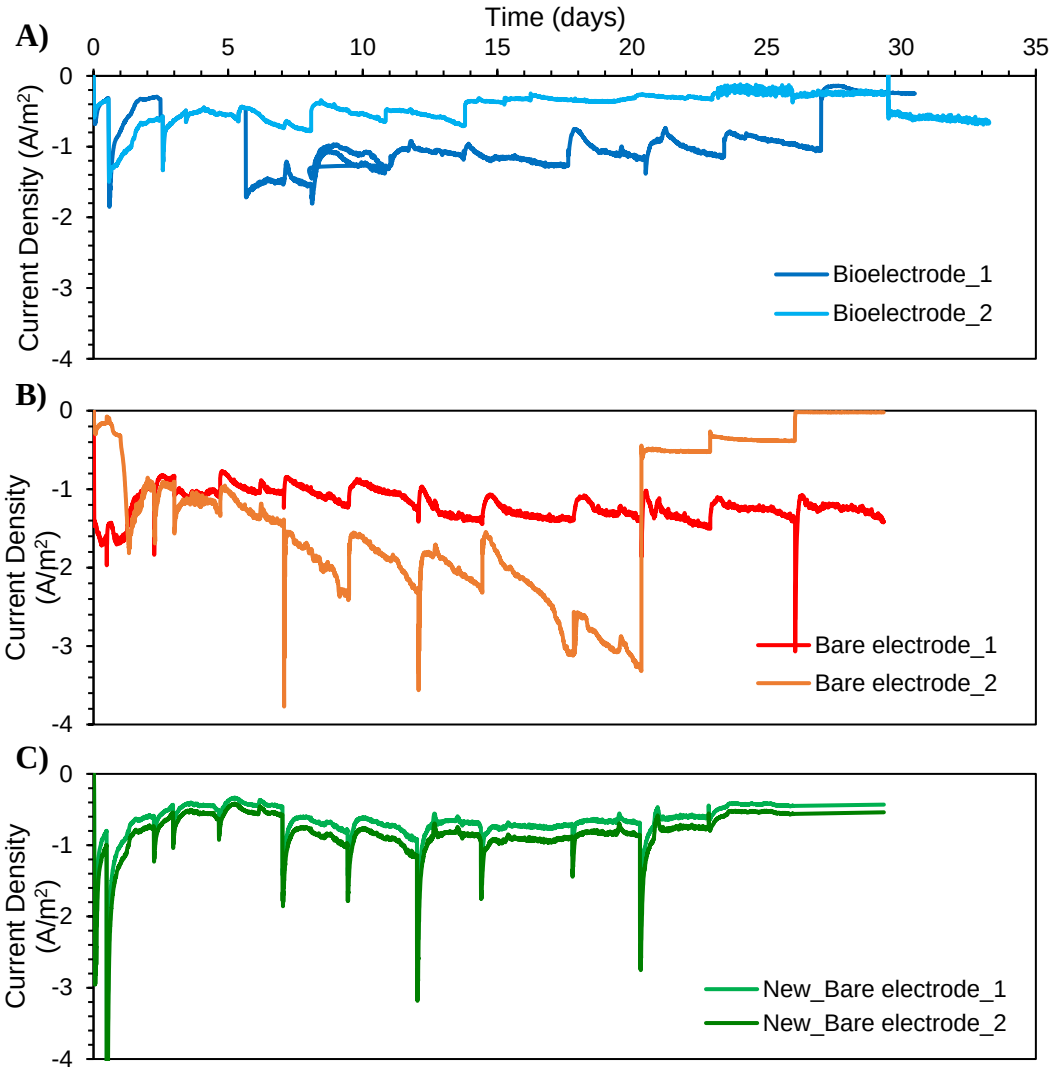

Figure G.3. Current Density of the replicate A) Bioelectrode, B) Bare electrode, and C) New_Bare electrode AD-MEC reactors under -0.95 V cathode potential

H. The modified Gompertz models for Set 2

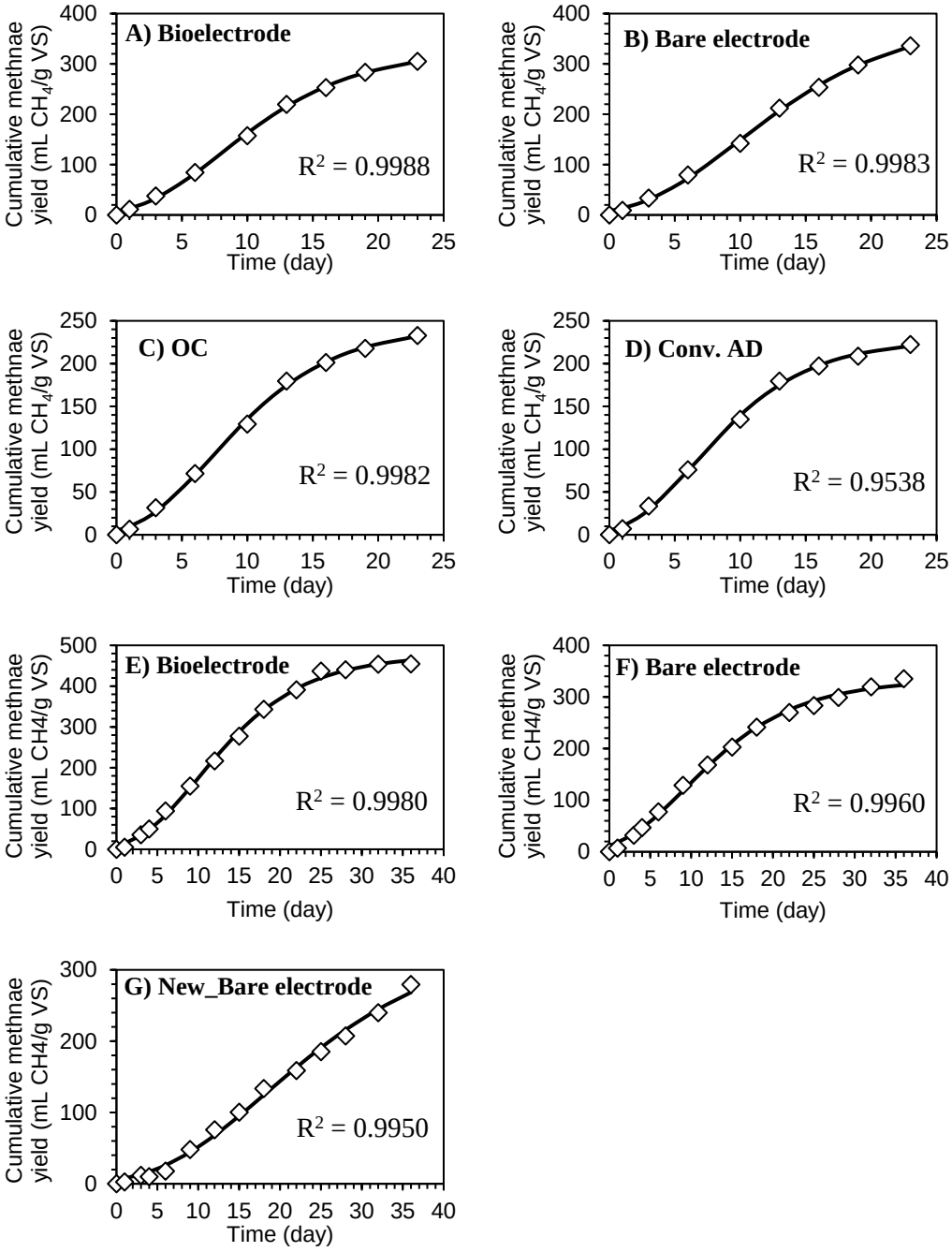

Figure H.1. The modified Gompertz model A) Bioelectrode, B) Bare electrode, C) OC, and D) Conv. AD under -0.9 V cathode potential, E) Bioelectrode, F) Bare electrode, and G) New_Bare electrode under -0.95 V cathode potential (Dots: experimental data, Solid line: model data)

I. The current density of the replicates of AD-MEC reactors in Set 3

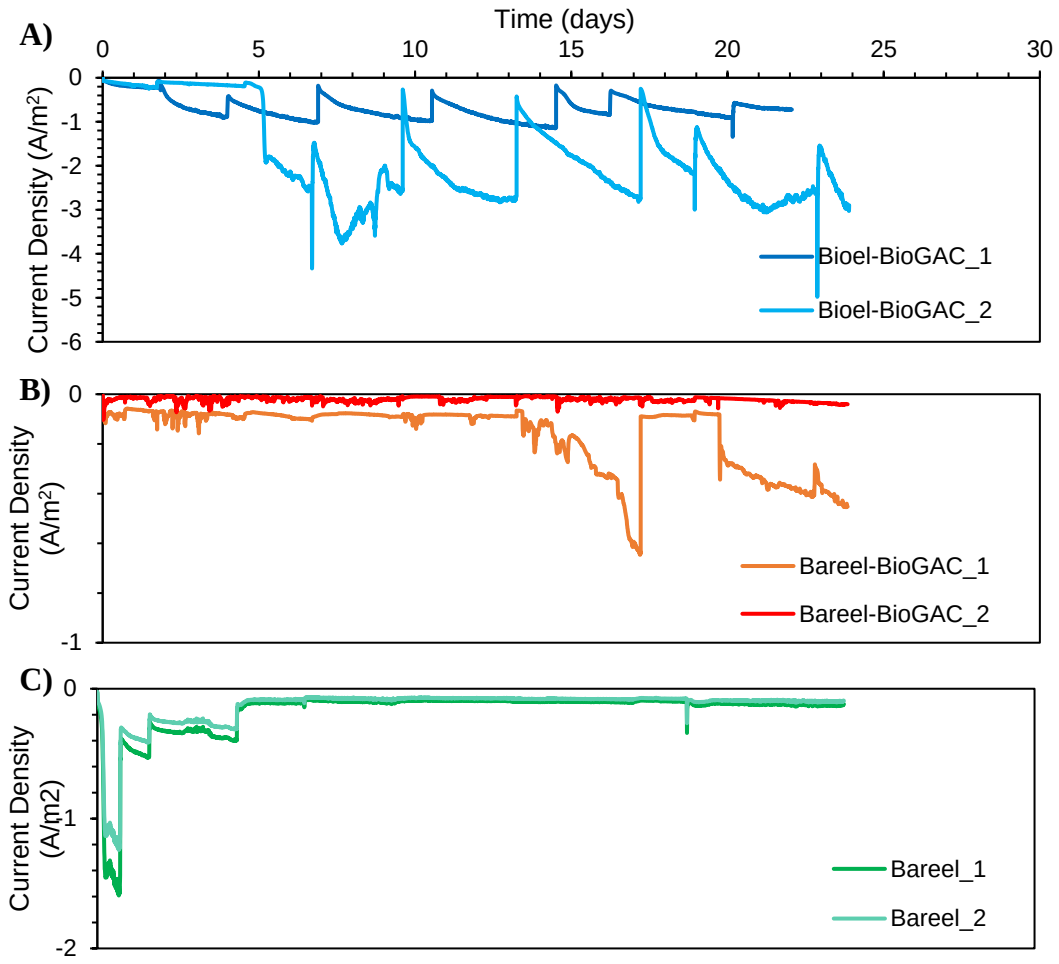

Figure I.1. Current Density of the replicate A) Bioel-BioGAC, B) Bareel-BioGAC, and C) Bareel AD-MEC reactors under -0.9 V cathode potential in Cycle 1

J. The modified Gompertz models for Set 3

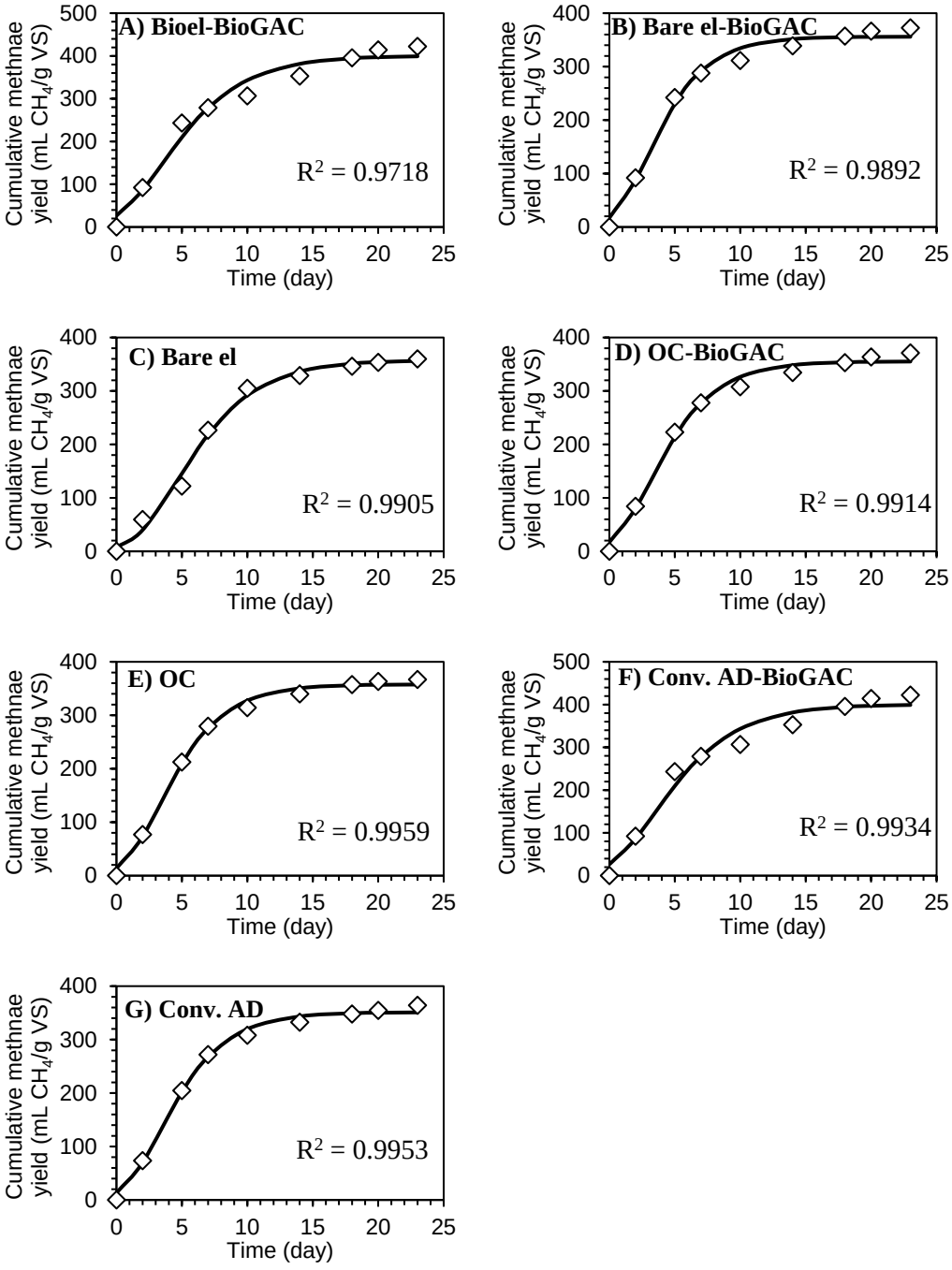

Figure J.1. The modified Gompertz model A) Bioel-BioGAC, B) Bare el-BioGAC, C) Bare el, D) OC-BioGAC, E) OC, F) Conv. AD-BioGAC G) Conv. AD under -0.9 V cathode potential (Dots: experimental data, Solid line: model data)

K. Estimations of regression coefficients and results of statistical tests

Table K.1. Estimations of regression for NH_4-N Recovery

Coded Coefficients					
Term	**Coef**	**SE Coef**	**T-Value**	**P-Value**	**VIF**
Constant	94.952	0.964	98.53	0	
pH	1.704	0.59	2.89	0.007	1
Mg:N	3.302	0.59	5.6	0	1
P:N	5.434	0.59	9.21	0	1
pH*pH	-0.519	0.869	-0.6	0.554	1.01
Mg:N*Mg:N	-4.017	0.869	-4.62	0	1.01
P:N*P:N	-4.247	0.869	-4.89	0	1.01
pH*Mg:N	-0.54	0.835	-0.65	0.522	1
pH*P:N	-2.173	0.835	-2.6	0.013	1
Mg:N*P:N	2.71	0.835	3.25	0.003	1

Table K.2. Estimations of regression for PO_4-P Recovery

Coded Coefficients					
Term	**Coef**	**SE Coef**	**T-Value**	**P-Value**	**VIF**
Constant	91.52	1.16	78.73	0	
pH	2.498	0.712	3.51	0.001	1
Mg:N	6.267	0.712	8.8	0	1
P:N	-6.772	0.712	-9.51	0	1
pH*pH	-4.81	1.05	-4.59	0	1.01
Mg:N*Mg:N	0.01	1.05	0.01	0.994	1.01
P:N*P:N	-6.17	1.05	-5.89	0	1.01
pH*Mg:N	0.62	1.01	0.61	0.545	1
pH*P:N	-1.59	1.01	-1.58	0.122	1
Mg:N*P:N	2.63	1.01	2.61	0.013	1

Table K.3. Estimations of regression for Mg^{2+} Recovery

Coded Coefficients					
Term	**Coef**	**SE Coef**	**T-Value**	**P-Value**	**VIF**
Constant	93.246	0.668	139.59	0	
pH	-0.019	0.409	-0.05	0.963	1
Mg:N	-4.785	0.409	-11.7	0	1
P:N	5.156	0.409	12.6	0	1
pH*pH	2.771	0.602	4.6	0	1.01
Mg:N*Mg:N	-1.098	0.602	-1.82	0.077	1.01
P:N*P:N	-1.633	0.602	-2.71	0.01	1.01
pH*Mg:N	0.388	0.579	0.67	0.507	1
pH*P:N	3.589	0.579	6.2	0	1
Mg:N*P:N	2.963	0.579	5.12	0	1

L. Comparison of the product heavy metal content with regulations

Table L.1. The heavy metal content of the product and Turkey regulations' limit value

Heavy Metal Compound	Limit value (%)	The product (%)
Cd	0.0003	0.00002
Cu	0.045	0.0004
Ni	0.012	0.006
Pb	0.015	0.000001
Zn	0.11	0.04
Hg	0.0005	-
Cr	0.035	0.001